OVERCOMING TRANSPORT BARRIERS TO NANOPARTICLE-BASED CHEMOTHERAPY

SUBMITTED TO THE FACULTY OF THE UNIVERSITY OF MINNESOTA BY

AMEYA RAJEEV KIRTANE

IN PARTIAL FULFILLMENT OF THE REQUIREMENTS FOR THE DEGREE OF

DOCTOR OF PHILOSOPHY

JAYANTH PANYAM
(ADVISER)

AUGUST 2015

Acknowledgements

The past five years were a tremendous learning experience. Several people have contributed selflessly to my growth as a scientist, and I take this opportunity to thank them.

I cannot thank my adviser, Dr. Jayanth Panyam, enough for his guidance and support during my graduate studies. His enthusiasm for science was a constant source of inspiration for me. I thank him for teaching me the nuances of drug delivery and cancer. The freedom he gave me, in terms of the projects I could pursue and my approach to those projects, helped me excel. His faith in me encouraged me to move outside my comfort zone and produce some of my best work.

Dr. Ron Siegel contributed invaluable input towards the pharmacokinetic model described in this thesis. What started off as a project for a final exam was translated into a thought experiment for me. My discussions with him made me critically think about the EPR effect. He helped me move from the laborious Stella model to a high throughput Matlab model. My thesis and, more importantly, my PhD experience would not have been as rewarding without him.

I would also like to forward my sincere thanks to Drs. Elmquist, Wiedmann, McCarthy and Wang. Their input and critical evaluation of my thesis have significantly improved the quality of this work.

I would like to thank past and present members of the Panyam lab for making the past five years an enjoyable experience. I would especially thank Dr. Suresh

Swaminathan for the countless discussions we have had about science. His work with CD133 targeted nanoparticles was a fantastic reference for me and has greatly influenced my work. I owe most of my lab skills to Dr. Tanmoy Sadhukha. He guided me from the day I started working in the lab, and has been a tremendous resource for me ever since. My *mantra* has been 'whenever in doubt, go to Tanmoy', and I have never been disappointed. I am grateful for all the efforts he put into making me a better scientist.

I am extremely thankful to the Pharmaceutics department. The five seminars I presented during my residence were humbling experiences with a steep learning slope. The input of the faculty and students helped me refine my presentation skills. This work wouldn't have been possible without the administrative assistance of Candy McDermott, Erica Flynn, Jody Tracy, and Jeanene Noll.

I have had the opportunity to work with several of Dr. Panyam's collaborators. This has enriched my PhD experience. I would particularly thank Drs. Henry Wong and Jung Min Song for the opportunity to work with them, and learn vital techniques.

I also appreciate the help offered by Brenda Koniar. Her training and assistance with the animal studies allowed me to undertake tedious and challenging experiments. Thanks also to Josh Parker, Jim Fisher, John Oja, Guillermo Marques and Peter Villalta for their technical assistance.

Financial support from National Institute of Health, Committee for Pharmaceutical Development (U of MN), Department of Pharmaceutics (U of MN), and the Graduate school (U of MN) is gratefully acknowledged.

A very special thanks to my friends: Ravindra, Charuta, Shreyas, Satyajeet, Sanika, Manan, Pallavi, Gargee, Maya, Kanchan, Renuk, Amruta, and Balaji. They had more faith in me than I had in myself. A huge thank you to Suril Shah for keeping me grounded through good times and sticking with me through the difficult ones.

I am extremely grateful to Eileen Huttlin for her immense support and patience. I thank her for helping me believe in my abilities, and reminding me of the final goal of my research, which is to help people.

I am indebted to my high school teacher, Mrs. Ujwala Ranade. She sparked my interest in science. Many of the questions encountered during my PhD had their answers rooted in what she taught me in high school. If it wasn't for her, I would not have been here.

I would also acknowledge my family for helping me, both financially and spiritually, through my masters and PhD. They have been a constant source of support and encouragement for me.

Most importantly, it is my parents who deserve the credit for my academic endeavors. They imbibed in me an appreciation for the power of knowledge and hard work. It is because of this, that in spite of my limited intellectual ability, I believe I can fulfill my goals.

Dedication

This work is dedicated to my parents and teachers

Abstract

Targeted delivery of drugs to tumors is critical for optimal implementation of chemotherapy. Targeted drug delivery can be achieved by encapsulating drugs in nanometer-sized drug carriers. Consequently, a significant amount of preclinical research is focused on the development of nanoparticle-based chemotherapeutics. In spite of many key advances, these systems still have some major limitations. These stem from extensive distribution of nanoparticles to off-target sites, and the presence of several resistance mechanisms within the tumor. The goal of this thesis was to investigate, and potentially improve, the various steps involved in the delivery of nanoparticles to solid tumors.

Using a pharmacokinetic modeling approach, the effect of physicochemical properties of nanoparticles and vascular permeability of the tumor on the systemic distribution of nanoparticles was studied. Transport across compartments was calculated using equations for transvascular convection and diffusion of nanoparticles. The results of the modeling studies suggested that optimal drug targeting would be observed only in an intermediate particle size range. At a particle size below the vascular pore size of the toxicity compartment, nanoparticles extensively accumulated in that compartment. This reduced the fraction available for deposition into the tumor. At a particle size above the vascular pore size of the tumor, accumulation of nanoparticles in the tumor was not possible. Most of the drug was either eliminated in the form of nanoparticles or released in the central compartment. Hence, the lower and upper bounds of the optimal particle size range were determined by the vascular pore size of the toxicity

and target compartments, respectively. With a decrease in drug release rate, the average number of visits of the drug in the target compartment increased. Hence, decreasing the rate of drug release could favorably affect the drug targeting index. Maximal benefit with this strategy was also experienced in an intermediate particle size range, which was dictated by vascular pore sizes of the toxicity and target compartments.

Due to leaky tumor blood vessels and prothrombogenic tumor microenvironment, fibrinogen gets deposited in the tumor and is converted to cross-linked fibrin. Using a series of immunohistochemistry analysis and *in vitro* diffusion studies, it was established that most human solid tumors are characterized by the deposition of a significant amount of fibrin and that the presence of fibrin retarded the mobility of nanoparticles. However, no previous studies have analyzed the influence of fibrin on the intratumoral distribution of nanoparticles. The central hypothesis of this chapter was that degrading fibrin using a fibrinolytic enzyme [tissue plasminogen activator (tPA)] will improve the intratumoral distribution of nanoparticles and their chemotherapeutic efficacy. In an A549 orthotopic lung cancer model, co-administration of tPA improved the anti-cancer efficacy of paclitaxel nanoparticles ($p<0.05$, on Day 73 after commencement of treatment). In this chronic study, the average tumor bioluminescence in animals treated with the combination therapy was lower than the other groups for >2 months. In a B16F10 mouse melanoma model the combination therapy reduced the rate of tumor growth by ~1.5 fold relative to that with just paclitaxel nanoparticles ($p=0.08$). Further, immunohistochemistry

revealed that administration of tPA resulted in the decompression of tumor blood vessels. Using Power Doppler ultrasound, we established that treatment with tPA led to a 3-4 fold improvement in tumor perfusion ($p<0.05$, after second dose). All these results suggest that fibrinolytic therapy may lead to an enhanced intratumoral distribution of nanoparticles.

Tylocrebrine is a potent anti-cancer drug but has a narrow therapeutic index. Extensive distribution to the central nervous system and reduced cell uptake in the acidic tumor microenvironment limited the clinical translation of the drug. To address both issues, tylocrebrine was encapsulated in polymeric nanoparticles targeted to the epidermal growth factor receptor (EGFR). *In vitro* studies in human cancer cell lines showed that decrease in the extracellular pH led to a 3-fold decrease in drug uptake ($p<0.05$) and ~2-10 fold reduction in drug potency. However, when encapsulated in targeted nanoparticles, its potency was less affected by extracellular pH. Pharmacokinetic studies in mice revealed that the drug rapidly accumulated in the brain, and brain accumulation could be reduced by encapsulation in nanoparticles (~2-fold; $p<0.05$, compared to free drug at 0.5 h post dose). When delivered in targeted nanoparticles, the tumor accumulation and retention of the drug was also improved ($p<0.05$, compared to free drug at 4h post dose). In a xenograft mouse model of human epidermoid cancer, treatment with tylocrebrine solution retarded tumor growth. However, tumor inhibition was found to be more significant with EGFR targeted nanoparticles ($p<0.05$, compared to saline and non-targeted nanoparticle treated animals). This effect was likely due to the improved tumor accumulation and higher potency of targeted nanoparticles.

In conclusion, this thesis presents an analysis of the three steps of nanoparticle transport from the site of administration to the site of action. These steps include systemic distribution, intratumoral distribution and cell uptake. Improving the efficiency of each of these steps can improve the overall efficacy of chemotherapy.

Table of Contents

List of Figures

List of Tables

List of Abbreviations

ABC	ATP-binding cassette
AUC	Area under the curve
BBB	Blood brain barrier
BCA	Bicinchoninic acid assay
BCRP	Breast cancer resistant protein
CMC	Critical micellar concentration
CNS	Central nervous system
CSC	Cancer stem cell
DMEM	Dulbecco's Minimum Essential Media
DTI	Drug targeting index
ECM	Extracellular matrix
EDC	1-ethyl-3-[3-dimethylaminopropyl] carbodiimide hydrochloride
EGFR	Epidermal growth factor receptor
EMT	Epithelial to mesenchymal transition
EPR	Enhanced permeability and retention effect
GFP	Green fluorescent protein
HBD	Hydrogen bond donors
HIF1a	Hypoxia inducible factor 1a
HPMA	*N*-(2-hydroxypropyl) methacrylamide
HRE	Hypoxia responsive element

IAASF	Interfacial activity assisted surface functionalization
ID	Injected dose
IFP	Interstitial fluid pressure
MDR	Multidrug resistance
MDR1	Multidrug resistant protein
MPS	Mononuclear phagocyte system
MRP1	Multidrug resistance associated protein
NBD	Nucleotide binding domain
NHS	N-hydroxysuccinimide
NPs	Nanoparticles
PBS	Phosphate buffered saline
PEG	Poly(ethylene glycol)
PEO-PbAE	poly(ethylene oxide)-modified poly(beta-amino ester)
PEO-PCL	poly(ethylene oxide)-modified poly(epsilon-caprolactone)
P-gp	P-glycoprotein
PI3K	Phosphoinositol 3 kinase
PLA	Poly(lactide)
PLGA	poly(lactide-co-glycolide)
RIPA	Radioimmunoprecipitation assay
RPMI	Roswell Park Memorial Institute
TGFβ	Transforming growth factor β
TMD	Transmembrane domain
tPA	Tissue plasminogen activator

VEGF	Vascular endothelial growth factor

Chapter 1 Exploiting Nanotechnology to Overcome Tumor Drug Resistance: Challenges and Opportunities[1]

[1] Parts of this chapter are published elsewhere [460]. Reproduced with permission.

1.1 Summary

Tumor cells develop resistance to chemotherapeutic drugs through multiple mechanisms. Overexpression of efflux transporters is an important source of drug resistance. Efflux transporters such as P-glycoprotein reduce intracellular drug accumulation and compromise drug efficacy. Various nanoparticle-based approaches have been investigated to overcome efflux-mediated resistance. These include the use of formulation excipients that inhibit transporter activity and co-delivery of the anticancer drug with a specific inhibitor of transporter function or expression. The effectiveness of nanoparticles and other colloidal drug carriers can be diminished by poor transport in the tumor tissue. Hence, adjunct therapies that improve the intratumoral distribution of nanoparticles may be vital to the successful application of nanotechnology to overcome tumor drug resistance. This review discusses the mechanisms of tumor drug resistance and highlights the opportunities and challenges in the use of nanoparticles to improve the efficacy of anticancer drugs against resistant tumors.

1.2 Introduction

Despite major advances in cancer diagnosis and therapy, development of drug resistance and tumor relapse are frequent occurrences [2, 3]. While tumor cells evade death through multiple mechanisms [4], overexpression of efflux transporters is an important source of drug resistance. Tumor cells either inherently express efflux transporters or upregulate their expression in response to chemotherapy. Efflux transporters are capable of actively clearing a wide variety of substrates out of the cells. This results in sub-optimal intracellular drug concentrations and lack of efficacy [5]. Several efforts have been directed at inhibiting efflux transporters in tumors. Many small molecule efflux inhibitors have been tested in combination with chemotherapeutics in the clinic. However, unfavorable pharmacokinetics and significant dose-limiting toxicities have hampered their progress [6-8]. Co-administration of the chemotherapeutic and efflux inhibitor in nanoparticles (NPs) may allow temporal co-localization of these molecules, limit their non-specific distribution, and hence their toxicities [9]. In addition, several studies have shown that some of the excipients used in the construction of NPs are capable of inhibiting efflux transporters [10]. Taken together, nanotechnology offers a promising approach for overcoming efflux pump-based drug resistance **(Figure 1-1)**.

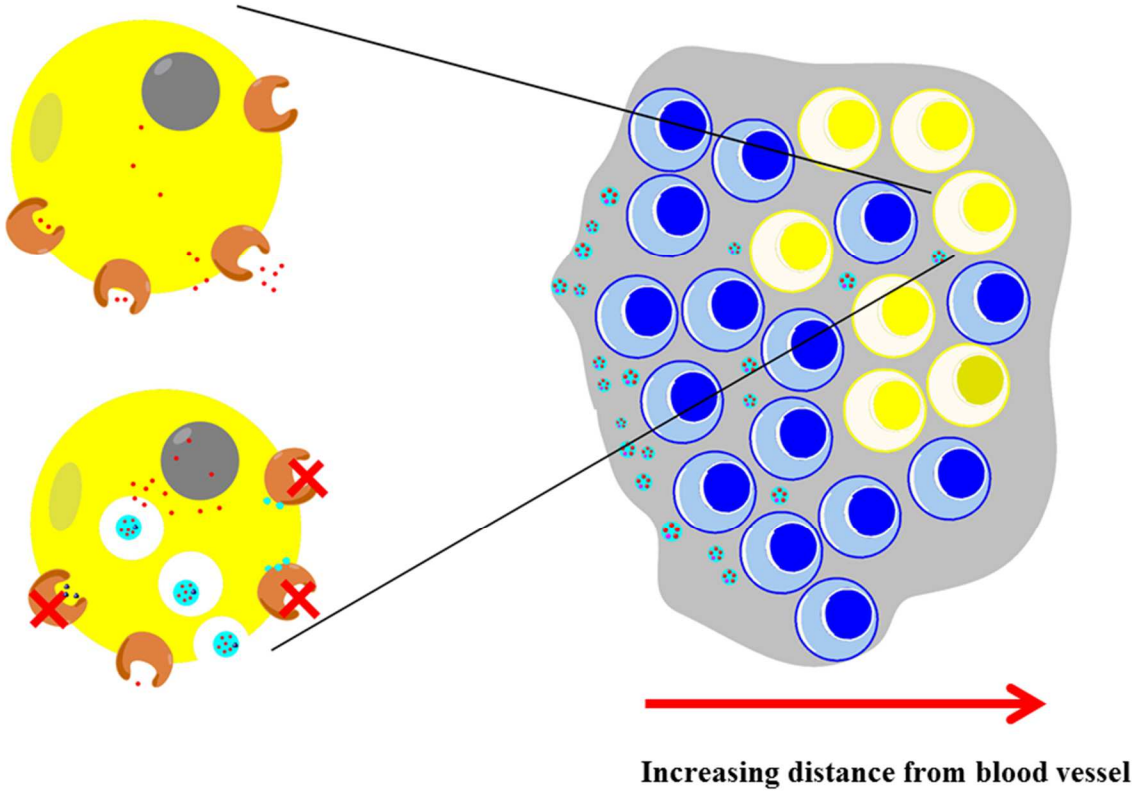

Figure 1-1. Opportunities and challenges in utilizing nanotechnology to overcome drug resistance.

Nanoparticles can inhibit drug efflux through (i) altered cellular distribution of the encapsulated drug (ii) use of specific excipients and (iii) co-delivery of agents that can inhibit efflux transporters. The drug resistant cells are often located farther away from blood vessels. High transport resistance within tumors limits NPs to regions adjacent to the blood vessels. It is critical that NPs reach areas distant from the blood vessels in order to effectively overcome drug resistance. Key: Blue cells—drug sensitive cells; yellow cells—resistant cells; grey area—tumor ECM; light blue circles—nanoparticle excipients; red dots—chemotherapeutic drug; blue triangles—efflux pump inhibitor.

In order for NP-based therapies to be successful, however, it is essential that NPs are transported efficiently to the tumor cells. Tumors are characterized by inadequate blood supply and elevated interstitial fluid pressure (IFP) [11]. As a result, transport in the tumor is highly hindered. Several approaches have been proposed for improving intratumoral transport of macromolecules and drug carriers [11]. These include the use of anti-angiogenics [12] and modification of the tumor stroma [13].

In this review, we will focus on these two important issues: (1) the use of nanotechnology to overcome efflux activity in tumor cells and (2) inefficient transport of drugs and drug carriers within the tumor tissue. We will provide a mechanistic perspective of why nanotechnology has the potential to overcome drug resistance and why the use of adjunct therapies to improve transport may be critical to the success of nanotechnology-based anticancer therapies.

1.3 Mechanisms of tumor drug resistance

1.3.1 Efflux transporters

A majority of chemotherapeutics have intracellular targets. Thus, to kill the tumor cell, many anticancer drugs have to accumulate inside the cell at sufficient concentrations. A major hurdle to achieving adequate intracellular drug concentrations is the presence of efflux proteins on the tumor cell membrane [14, 15]. Drug efflux pumps belong to a family of transporters called the ATP-binding cassette (ABC) transporters. ABC transporters are one of the largest superfamily of proteins. The human genome encodes for 48 ABC proteins. These include 20

transporter proteins, further divided into 7 sub-families, ABC A-G [16]. Some of the important and well-studied transporters include ABCB 1 [P-glycoprotein (P-gp), multidrug resistance protein 1 (MDR1)], ABCC 1-3 [multidrug resistance associated protein (MRP) 1-3], and ABCG 2 [breast cancer resistance protein (BCRP)]. P-gp was the first discovered efflux transporter [17, 18]. In 1983, Kartner and coworkers first demonstrated the correlation between increased expression of P-gp in tumor cells with the development of drug resistance [19]. This was followed by Chen and others, who described the sequence of the *MDR1* cDNA and its homology to two bacterial transporters, thereby defining the first member of the ABC transporter family [20]. Ueda and coworkers demonstrated that expression of a full length cDNA for the human *MDR1* gene confers drug resistance in tumor cells, confirming the role of *MDR1* gene in drug resistance [21]. It was later discovered that some tumor cells that did not have upregulated P-gp levels could also actively efflux drugs. This led to the discovery of MRP 1 [22]. Since then, additional transporters have been identified and their roles in drug transport have been investigated [16]. Of these, P-gp is one of the most consistently over-expressed transporters in drug-resistant tumors [23].

Even under normal physiological conditions, efflux transporters are widely expressed in the body (reviewed in [24]). Some organs show a particularly high expression of these transporters. For example, P-gp, BCRP and MRP 2 are highly expressed on the apical sides of the lung, testis, placenta, and brain. On the other hand, MRP 1 is highly expressed on the basolateral side of these organs [4, 25-30]. These transporters create a formidable barrier that protects important organs

from toxic xenobiotics. Consequently, these transporters play a key role in altering the absorption, distribution, metabolism, and excretion of drugs [31-33].

1.3.1.1 Structure and mechanism of P-gp

P-gp is a 170 kDa protein with broad substrate specificity [34]. Structurally, it comprises 2 transmembrane domains (TMDs) and 2 nucleotide binding domains (NBDs). The TMDs are hydrophobic domains consisting of 6 transmembrane segments, while NBDs are hydrophilic intracellular domains [35]. NBDs provide a docking site for the ATP molecules. While the exact mechanism by which P-gp interacts with its substrate is not fully understood, it is thought that binding of a substrate to the high-affinity binding site results in ATP hydrolysis, causing a conformational change that shifts the substrate to a lower affinity binding site and then into the extracellular space or outer leaflet of the membrane [36-38]. Whether P-gp extracts its substrate from the cytoplasm [39] or from within the membrane ('vacuum cleaner' hypothesis) is not clear, but evidence suggests that substrates diffuse from the lipid bilayer into the drug-binding pocket located in a hydrophobic environment [40, 41]. Studies from our laboratory suggest that drug released into the cytoplasm from NPs is susceptible to P-gp mediated efflux [42]. P-gp overexpression also confers resistance to drugs through mechanisms not directly related to transport. For example, overexpression of P-gp confers resistance to complement-mediated cytotoxicity due to delayed deposition of complement on the plasma membrane [43, 44]. Also, P-gp over-expressing cells are less sensitive to multiple forms of caspase-dependent cell death, including those mediated by Fas ligand [45] and serum withdrawal [46]. Some of the transport-independent

effects of P-gp may be explained by the fact that over-expressed P-gp can constitute an important part of the plasma membrane. In Chinese hamster ovary (CHO) cells, P-gp alone accounted for about 20% of the total plasma membrane proteins [47]. This degree of overexpression could affect the activity of other membrane proteins.

1.3.1.2 Acquired and intrinsic resistance

In vitro studies have shown that the expression of efflux pumps increases in response to chemotherapy. These changes arise from copy number alterations of the gene or increased expression of these genes [48-51]. This change in efflux transporters in response to chemotherapy is evident in clinical studies as well [52]. Abolhoda *et al.* tested the effect of doxorubicin treatment on five patients with lung metastasis [53]. The authors found that after a 20-minute chemoperfusion, there was a 6-7 fold increase in *MDR1* gene expression in these tumors. This phenomenon of upregulation of efflux transporters in response to drug treatment is termed as acquired resistance. Interestingly, Levchenko *et al.* reported the intercellular transfer of functional P-gp protein from P-gp positive cells to P-gp negative cells both *in vitro* and *in vivo* [54]. The transfer occurred between different cell types, and allowed the recipient drug-sensitive cells to survive toxic drug concentrations, leading to increased tumor resistance. This mechanism could explain how some sensitive cells acquire drug resistance.

Another striking feature of efflux transporters is the wide range of substrate specificity [34, 35]. Weakly basic and neutral compounds have been found to be the most vulnerable to these pumps [35, 55, 56]. However, some reports suggest

that even acidic compounds can be subject to efflux [57, 58]. A rare common feature is that most compounds transported by these pumps are amphiphilic in nature [35]. The broad substrate specificity and upregulation in response to chemotherapy have serious consequences. Resistance arising from one drug can lead to cross-resistance to other chemotherapeutics that are substrates of the same transporter. Such a resistance is termed as multidrug resistance (MDR). Because of this phenomenon, sequential chemotherapy or switching to a different drug class may not be useful once a patient develops resistance to one drug class.

A fraction of tumor cells intrinsically have a higher expression of efflux transporters even before exposure to chemotherapy [5]. This phenotype may be a manifestation of tumor microenvironmental conditions, tissue of origin, and/or rampant genetic mutations characteristic of cancer cells [4]. This phenomenon is termed as intrinsic resistance.

Acquired and intrinsic resistances may stem from mechanisms not involving efflux transporters as well. This is especially evident with drugs classified as ‘targeted therapies’ [59]. These drugs target specific aberrant cellular pathways that are essential for the survival of cancer cells. For example, the epidermal growth factor receptor (EGFR) is upregulated in multiple cancers. Activation of EGFR results in the activation of multiple kinases that aid in tumor growth and survival. Hence, antagonists that block EGFR signaling are of considerable interest [60]. However, this enthusiasm has been dampened by the appearance of intrinsic and acquired resistances (reviewed in [61]). Upon continued exposure to EGFR antagonists, tumor cells resort to alternate pathways that enable survival and

proliferation independent of EGFR activation [62]. Thus, in spite of EGFR inhibition, there is no effect on the tumor cell viability. On the other hand, some tumors do not rely on EGFR signaling at all. These tumors are intrinsically resistant to EGFR-targeted therapies.

Intracellular detoxification is another mechanism of drug resistance. Such mechanisms enable faster elimination of the drug from within the cell and hence reduce their intracellular concentration [63]. Glutathione conjugation is an example of the detoxification strategy employed by tumor cells [64, 65]. Mellish *et al.* showed that this mechanism can be upregulated in response to sustained exposure to chemotherapeutics [66]. The authors isolated a human ovarian carcinoma cell line from untreated patients. This cell line was exposed to increasing concentrations of cisplatin for 18 months. The resultant cell line was less susceptible to cell death induced by cisplatin and other platinum containing drugs. The authors found that the resistant cell line had higher levels of glutathione and correspondingly lower intracellular drug concentration [66].

Several anti-cancer agents induce DNA damage to bring about cell death. However, cancer cells can develop mechanisms to increase DNA repair and thereby develop resistance to these drugs. The mechanisms of DNA repair and drug resistance have been reviewed in detail elsewhere [67-69].

1.3.1.3 Efflux transporters and cancer stem cells

According to the consensus definition, cancer stem cells (CSCs) are minority cells that are capable of potentially unlimited self-renewal owing to asymmetric cell division, and have the ability to produce multiple differentiated cell

types that constitute solid tumors [70]. Although not fully established, the origins of CSCs could theoretically arise from oncogene activation in normal adult tissue stem cells or through the acquisition of stem cell-like properties via microenvironmentally triggered phenotypic changes in cancer cells. CSCs possess a number of intrinsic properties that contribute to therapy resistance and ultimately disease recurrence [71]. Similar to normal stem cells, CSCs have protective mechanisms against external insults from cytotoxic chemotherapy, which include alterations in the intrinsic apoptotic pathway, DNA repair, and most notably, overexpression of efflux transporters [72].

From the perspective of drug resistance, selective pressures within the tumor microenvironment can result in the generation of intrinsically resistant cells. In addition, standard therapeutic regimens, if ineffective in eradicating tumor cell burden, can result in a residual population of cells displaying acquired resistance. Both resistance mechanisms would ultimately result in the expansion of the CSC fraction within the tumor. These therapy-resistant cells, now considered the CSC population, are known to overexpress ABC transporters [73]. This principle is frequently exploited for their isolation. Rhodamine and Hoechst 33342 fluorescent dyes, substrates of both ABCG2 and ABCB1, are used in the analysis of the so-called side population of cells displaying low dye retention, via flow cytometric techniques. These side population cells display the ability to actively efflux ABC transporter substrates, as well as additional properties ascribed to CSCs, including tumor seeding at limiting dilution, a heightened anti-apoptotic state, relative

proliferative quiescence, and resistance to conventional chemotherapy upon sorting these cells from the bulk population [74].

To demonstrate the role of CSCs in acquired resistance, numerous reports document a selective enrichment of the CSC fraction following conventional chemotherapy treatment *in vitro*. The ovarian cancer cell lines OVCA 433 and HEY, when treated with cisplatin and paclitaxel *in vitro*, result in cells with increased sphere forming efficiency, CSC marker gene expression, and tumor seeding efficiency *in vivo* [75]. Immortalized mammary epithelial (HMLE) cells induced to passage through epithelial to mesenchymal transition (EMT) have been shown to display the properties of CSCs. When these cells are spiked into non-CSC enriched HMLE cells and treated with paclitaxel *in vitro*, the CSCs selectively survive treatment, providing direct evidence for the role of CSCs in acquired drug resistance [76].

Another key reason for the therapeutic resistance of CSCs is their quiescent nature [77]. A number of chemotherapeutic agents are effective only against actively dividing cells. CSCs, like normal stem cells, divide infrequently and produce transient amplifying cells which populate the tumor. Hence, chemotherapy may be effective in eradicating the bulk of the tumor but may lack efficacy against the quiescent stem cell population [71].

1.3.1.4 Elevated levels of efflux transporters and poor prognosis

There is considerable evidence linking the presence of MDR cells with poor prognosis in cancer [78, 79]. Evidence for the role of P-gp in clinical tumor resistance was first provided by Trock and co-workers, who demonstrated P-gp

expression in about 40% of breast cancer samples and its correlation with decreased treatment response [80]. Additional studies [4, 81, 82] further confirm this observation, and suggest that pretreatment P-gp expression is a strong predictor for clinical response to drug therapy [83]. Karaszi *et al.* examined the response to therapy of 93 acute leukemia patients [84]. These patients were treated with various therapies depending on the disease subtype. Based on a calcein efflux assay, these patients were then classified into MDR^+ or MDR^- groups. It was found that 72% of the MDR^- patients responded to therapy, while only 31% of MDR^+ patients did. Consequently, there was a three-fold difference in median patient survival. Similar results were reported by Leith *et al.,* who found that elderly leukemic patients responded poorly to treatment in comparison to younger patients because of elevated P-gp expression [85].

1.3.2 Sequestration in acidic organelles

In addition to efflux pumps, sequestration in acidic organelles can reduce the bioavailability of anticancer drugs at their intracellular site of action [86]. Anthracyclines such as doxorubicin and daunorubicin accumulate in the nucleus (its site of action) in sensitive cells. In drug resistant cells, these weakly basic drugs are primarily distributed into acidic organelles such as late endosomes and lysosomes [87]. The elevated activity of the vacuolar H^+-ATPase pump in drug resistant cells leads to highly acidified pH of these organelles [88, 89]. Basic drugs are expected to be highly ionized under these conditions. This results in their trapping within these organelles and loss of activity. The trapped drug is likely extruded out of the cell by exocytosis [90].

1.3.3 Resistance to transport of macromolecules and drug carriers

In addition to the tumor cells, the tumor extracellular matrix (ECM) is a source of resistance to chemotherapy. Transport of drug into and within the tumor is extremely inefficient [91, 92]. This leads to regions of high and low drug concentrations in the tumor [93]. The regions receiving lower drug concentrations often harbor the more aggressive and tumorigenic cells [94]. Thus, it is extremely important to achieve therapeutic drug concentrations in these under-supplied regions.

In order to address the issue of inefficient drug distribution, it is essential to understand the processes governing drug transport in the tumor. In the following sections, we provide a brief description of the physiological factors governing intratumoral drug transport.

1.3.3.1 Transport process in normal tissues

Exchange of fluid and nutrients (as well as drugs) between blood vessels and tissue is governed by several parameters, and this relationship is defined quantitatively by Starling's law **(Figure 1-2)** [95, 96]. There are two components that drive the outward flow of soluble drug molecules into the tissue: the hydrostatic pressure head (arising from convection in the capillaries) and osmotic pressure head (arising from a difference in concentration of solutes). In normal tissues, this net pressure is directed towards the tissue and allows a convenient exchange of nutrients with the vascular compartment. The excess fluid draining into the tissues is cleared by the lymphatic system. As a result, a net negative pressure is maintained [13, 97]. Additionally, each cell in the body is only a few cell-diameters

away from the nearest blood vessel. This restricts the distance a solute has to travel in the interstitium to encounter the farthest cell from the blood vessel [98]. Thus, the negative pressure difference and short interstitial distances allow efficient solute transport in normal tissues.

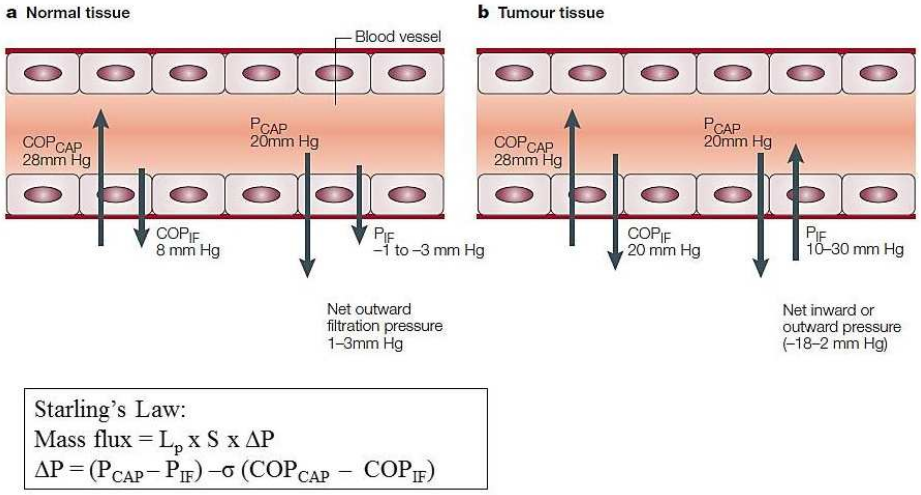

Starling's Law:
Mass flux = L_p x S x ΔP
$\Delta P = (P_{CAP} - P_{IF}) - \sigma (COP_{CAP} - COP_{IF})$

Figure 1-2. Forces that regulate transcapillary transport in tissues.

The figure shows the hydrostatic and colloid osmotic pressures in capillaries (P_{CAP} and COP_{CAP}, respectively) and the surrounding interstitium (P_{IF} and COP_{IF}, respectively) in normal tissues (a) and tumor tissues (b). It should be noted that values are approximate. (a) In normal human capillaries, the COP_{CAP} is about 28 mm Hg, which tends to keep fluid in the capillaries. The forces that tend to move fluid out from the capillaries are the P_{CAP} (about 20 mm Hg), the COP_{IF} (about 8 mm Hg) and the P_{IF}, which is normally negative (−1 to−3 mm Hg). So there is normally a net outward filtration pressure from the capillaries in tissues of 1–3 mmHg. This outward pressure assures a flow of fluid out from the vessels and through the interstitium, and contributes to transport of molecules to and from cells. (b) In tumor tissues, the COP_{IF} is increased to about 20 mm Hg and the PIF is increased to 10–30 mm Hg, resulting in some tumors in a net outward pressure of about 2 mm Hg (which is similar to that of normal tissues), but in other tumors in a net inward pressure of up to 18 mm Hg. Reprinted with permission from [13]. The equation describes Starling's law. Mass flux across the capillaries is governed by the hydraulic conductivity (Lp), blood vessel surface area (S), and pressure difference (ΔP). σ indicates the reflection co-efficient.

1.3.3.2 Transport process in the tumor

Differences in tumor and normal tissue physiologies give rise to major obstacles to drug delivery to and within the tumor [99, 100]. The direction and magnitude of the driving force for drug transport is not constant throughout the tumor. This inconsistency in the driving force arises from the differences in the functionality of the lymphatic system. The advancing edge of the tumor exhibits normal lymphatic drainage. As a result, the fluid entering the tumor from the blood vessels is cleared normally [101]. This helps maintain a negative pressure gradient in this part of the tumor, similar to that in normal tissues [102]. However, the core of the tumor experiences no such driving force for drug transport. The lymphatic vessels are usually collapsed and show minimal hydraulic conductivity in the center of the tumor. As a result, excess fluid entering the tumor is not drained from this central core [101, 103]. Hence, the pressure differential in the core of the tumor is often in the opposite direction, i.e., from the tumor towards the blood vessels [13]. Additionally, the core of the tumor is characterized by poor vessel coverage [104-106]. Consequently, drug transport to the core of the tumor is reliant on the diffusion of the drug from well-perfused peripheral regions [107]. These disparities in normal and tumor physiologies arise from two major factors: angiogenesis and tumor microenvironment.

1.3.3.3 Angiogenesis

Tumor cells divide more rapidly than normal cells. As the tumor grows larger, it can no longer survive on the pre-existing blood vessels of the surrounding normal tissue. Tumors produce potent growth factors such as vascular endothelial growth factor (VEGF), which enable the sprouting of new blood vessels from

existing ones. This process is known as angiogenesis [108, 109]. In normal tissues, this process is tightly regulated and involves a balance between pro- and anti-angiogenic factors, leading to well-formed blood vessels with a hierarchical architecture. In contrast, tumors are characterized by a pro-angiogenic environment. This results in poorly developed vascular anatomy (lack of pericyte coverage and leakiness) and architecture (dead ends and irregular flow patterns) [110-112].

The leakiness of tumor blood vessels leads to expulsion of vascular components including excess fluid into the tumor interstitium. The lack of lymphatic drainage restricts the removal of fluids and other vascular components from the tumor microenvironment. Presence of these vascular components in the limited ECM space results in elevated IFP [100, 102, 113-115] and prevents the entry of drugs into the tumor [116]. Elevated IFP has been shown to correlate with poor response to chemotherapy and immunotherapy [117]. A study by Curti and coworkers followed the response of 6 non-Hodgkin's lymphoma patients to chemotherapy. The patients received a chemotherapy combination consisting of either ProMACE CytaBOM (cyclophosphamide, doxorubicin, etoposide cytozar, bleomycin, vincristine, methotrexate and prednisone) or EPOCH (etoposide, prednisolone, vincristine, doxorubicin and cyclophosphamide). Tumor IFPs were monitored before and after treatment. The authors found that the responders showed a lower pre-treatment IFP as compared to the non-responders. Additionally, the tumor IFPs of the responders decreased with treatment while that of the non-responders increased. This study also monitored the IFP of 10

melanoma patients treated with interleukin-1 and 2 based immunotherapy. The melanoma nodules that responded to immunotherapy showed a lower IFP than those that did not respond to immunotherapy. These results show that elevated IFP can significantly decrease therapeutic efficacy of multiple treatment modalities.

1.3.3.4 Reactive tumor microenvironment

Overexpression of cross-linking agents such as lysyl oxidase in tumors leads to a higher degree of polymerization of biopolymers like collagen and hyaluronic acid [118, 119]. Moreover, fibroblasts in the tumor microenvironment are in an activated state. Activated fibroblasts, or myofibroblasts, secrete copious amounts of ECM components. Additionally, myofibroblasts use specialized receptors on their cell surface to engage these biopolymers and increase the overall ECM rigidity [120, 121]. All these factors contribute to a reactive tumor microenvironment and an increased resistance to diffusional drug transport within the tumor ECM [122].

It should be noted, however, the rigidity of tumor ECM is likely heterogeneous. Overexpression of matrix metalloproteinases is a hallmark of many tumors and is associated with increased tumor invasiveness [123]. The expression of this enzyme brings about proteolysis of the collagen fibrils in the tumor [123], and should thus reduce matrix stiffness. However, this reduction in matrix stiffness may be spatially and temporally limited. Tumor cells present on the periphery are more likely to migrate [124]. Hence the stiffness of the bulk of the tumor may not be affected by the expression of the protease.

1.3.3.4.1 Presence of fibrin in tumors

An important feature distinguishing normal tissues from tumors is the presence of fibrin in the ECM. Fibrin is the key ingredient of the blood clot and is deposited at sites of pathological damage, inflammation and in tumors.

1.3.3.4.1.1 Source of fibrin in tumors

Fibrinogen, a soluble blood protein, exists as a dimer and consists of 3 peptide chains, viz. Aα, Bβ and γ. Upon thrombin-mediated cleavage of N-terminus peptides from the A and B chains, fibrinogen is converted to insoluble fibrin. Further action by Factor XIIIa leads to the covalent cross-linking of the α and γ chains [125]. This cross linked product resembles fibrin found in tumors. This product can be characterized by the presence of γ dimers and its insolubility in urea [126].

Tumor blood vessels are hyperpermeable due to proangiogenic tumor microenvironment. As a result, fibrinogen gets deposited within the tumor [127]. Additionally, tumor cells express significant amount of thrombin and tissue factor [128]. This leads to the conversion of fibrinogen to cross-linked fibrin.

Early studies utilized immunohistochemistry or immunofluorescence techniques to detect fibrin in tumors [129]. However, antibodies used for these purposes could not distinguish between fibrinogen and fibrin. Key evidence for accumulation of cross-linked fibrin in tumors was provided by Dvorak and colleagues. In these experiments, ^{125}I-labeled fibrinogen was injected in guinea pigs bearing bile duct carcinomas [130]. A few minutes after injection, animals were sacrificed and tumors were collected. Radioactivity in urea-soluble and urea-

insoluble fractions of the tumor were measured. The radioactivity in the urea soluble fraction (representing fibrinogen, fibrinogen-degradation products and insoluble but non-cross linked fibrin) of the tumor was found to be 5-6 fold higher than surrounding normal tissues. This supported previous studies suggesting extravasation of fibrinogen in tumors. More interestingly, the radioactivity in the urea-insoluble fraction of the tumor (denoting cross-linked fibrin) was ~10-20 fold higher than the surrounding normal tissues. This provided strong evidence supporting the presence of fibrin, and not just fibrinogen, in tumors. Half of the radioactive product present in these tumors was in the form of fibrin. Similar results were obtained in different mouse tumor models as well [131].

The two factors responsible for fibrin deposition in tumors are hyperpermeability of blood vessels and high activity of coagulation factors. Studies in healthy eyes and muscles of guinea pigs have revealed that increasing the permeability of blood vessels by local administration of VEGF and histamine can cause accumulation of cross-linked fibrin in these tissues [132]. This suggests that most cells do possess a certain level of thrombogenic activity. However, normal tissues do not accumulate significant fibrin due to the poor extravasation of fibrinogen from the blood vessels. Some studies in renal cell carcinomas have shown that the level of VEGF secretion (and hence hyperpermeability) may predict fibrin deposition in tumors [133].

1.3.3.4.1.2 Function of fibrin in tumors

Fibrin serves an important function in tumor growth [134, 135]. As one of the earliest events in tumor development [135], fibrin provides a scaffold for the tumor

cells to attach. As time progresses the fibrin scaffold is first replaced by an undifferentiated tissue, and finally by ECM components such as collagen [136]. Consequently, fibrin expression is often found to be most around the growing edges of the tumor.

In addition to providing a scaffold for tumor cells, fibrin plays an important role in modulating the activity of fibroblasts and macrophages. It was shown that fibroblasts migrated efficiently in fibrin matrices prepared from cross-linked fibrin [137]. On the other hand, macrophage mobility was dramatically reduced in cross-linked fibrin [138]. Presence of fibronectins or glycosamoniglycans in the fibrin matrix (as found in tumor matrices) further decreased the migration of macrophages. This opposite effect of cross-linked fibrin on the mobility of fibroblasts and macrophages is interesting. Fibroblasts play an important role in the synthesis, organization and maturation of the ECM in tumors [139], while, in certain conditions, macrophages can potentially inhibit tumor growth [140]. Hence, these studies provide some evidence to the protective and nurturing role of fibrin in tumor growth. It is interesting to note that tissue remodeling and inhibition of inflammation are physiological functions of fibrin during wound healing [141]. This mechanism is hijacked by tumors to support its growth.

Finally, fibrin turnover is rapid in tumors [142]. This leads to generation of large amounts of fibrin degradation products. In their experiments with chick chorioallantoic membrane, Thompson *et al.* showed that fibrin degradation products led to angiogenesis [143]. This provides further evidence to the patho-physiologic roles of fibrin in tumors.

1.3.3.4.1.3 Effect of fibrin on tumor drug delivery

Due to the high expression of fibrin in tumors and a limited expression in normal tissues, it can be a good target for drug delivery. However, very few literature reports make use of this strategy.

Bale *et al.* used an antibody targeted to fibrin for the tumor specific delivery of radioactive I^{131} [144]. In a variety of rat tumors, accumulation of fibrin-targeted antibody was found to be 5-6-fold higher than the control antibody. Treatment with the targeted antibody labeled with I^{131} resulted in complete regression of tumors with no relapse. While control animals treated with non-targeted radiation therapy responded to the treatment, almost all tumors relapsed within a week.

In another report, Nishikawa *et al.* presented an elegant use of platelets for drug targeting [145]. The envelope of Sendai virus is known to generate an anti-tumor immune response. Unfortunately, systemic administration of the viral envelope causes haemagglutination. Platelets are known to engulf several particulate matter *in vivo*. Moreover, they have the property to home to the site of fibrin accumulation. Hence, platelets can act as suitable carriers to minimize systemic toxicity and maximize tumor homing of the viral envelope. Encapsulation of the viral envelope in platelets decreased its systemic toxicities. Importantly, in a B16F10 melanoma model, platelets were found to co-localize with fibrin within the tumor. This led to a significant suppression of tumor growth as compared to the untreated controls [145].

Fibrin accumulation in the tumor has also been used for an interesting ‘amplification’ strategy. Simberg and colleagues reported the discovery of CREKA

peptide that binds fibrin [146]. Conjugation of the peptide to the surface of liposomes and iron oxide nanoparticles improved their delivery of B16F1 tumors. Microscopy studies showed the colocalization of nanoparticles with fibrin in tumors. Interestingly, the authors found that the peptide promoted clotting within tumors. Increase in fibrin levels led to an amplification in signal available for successive dose of nanoparticles. In another report, von Maltzahn *et al.* showed that gold nanoparticle-mediated hyperthermia or delivery of tumor specific tissue factor can also increase fibrin accumulation in tumors [147]. Increase in fibrin accumulation in tumors can further improve the tumor delivery of fibrin homing nanoparticles. It is interesting to note that the intravascular clotting caused by the CREKA peptide led to the arrest of nanoparticles inside tumor blood vessels. This provides initial evidence that fibrin may occlude drug delivery to tumors.

These studies suggest that fibrin can act as a viable target for drug delivery. However, the role of fibrin in mediating solid stress or its effect on the intratumoral distribution of drugs has not been yet studied.

1.3.4 Acidic and hypoxic microenvironment

Limited solute distribution within the tumor ECM also means reduced transport of oxygen to the tumor cells. This leads to regions within the tumor that are hypoxic [148, 149]. Hypoxia can directly and indirectly affect the effectiveness of chemotherapy (reviewed in [150]). Many cytotoxics (eg.bleomycin) and photosensitizers (eg. porphyrin) rely on the production of free radicals for their activity [151, 152]. The activity of these drugs is compromised under hypoxia.

Additionally, hypoxia reduces cell proliferation [153]. Since a number of anti-cancer drugs selectively kill rapidly dividing cells, these drugs are relatively ineffective in these regions.

Hypoxia leads to stabilization of an otherwise labile transcriptional factor called hypoxia inducible factor 1α (HIF1α) [154, 155]. This leads to the activation of several genes associated with the hypoxia responsive element (HRE). *MDR1* gene is one of those genes regulated by HRE [156]. As discussed before, upregulation of *MDR1* gene leads to resistance to drug therapy. It is thus conceivable that the hypoxic regions are rich in cells expressing the efflux transporters.

Tumor cells rely on glycolysis for energy production. This phenomenon is termed as the Warburg effect [157, 158]. Excess glycolysis, leads to the generation of lactic acid. Poor transport of nutrients in tumors is coupled with poor drainage of waste products as well. Thus, lactic acid is not cleared from the tumor efficiently, resulting in a drop in local pH. The acidic microenvironmental pH leads to ionization of weakly basic drugs such as doxorubicin in the tumor ECM. Since ionized drugs do not cross cell membranes efficiently, the acidic microenvironment limits intracellular drug accumulation and can, thus, lead to a loss in therapeutic efficacy [159].

1.4 Approaches to overcome tumor drug resistance

Upregulation of efflux transporters is correlated with poor prognosis in a number of cancers [78]. Consequently, a significant body of research has been directed towards overcoming drug resistance by inhibiting or circumventing these

transport processes. Many of these efforts have involved the use of NPs [160]. In the following sections, we provide the rationale for the use of NPs for drug delivery to tumors. We also outline the various mechanisms by which NPs can be used to overcome efflux transport mediated drug resistance.

1.4.1 Enhanced permeability and retention (EPR) effect

The task of delivering drugs selectively to tumors is extremely challenging. Several strategies have been developed to maximize drug delivery to solid tumors. These include conjugation of drugs to antibodies or antibody fragments that bind to tumor cells [161-163], conversion to non-toxic prodrugs that are activated in the tumor [164-166], conjugation to hydrophilic polymers [167-169] and encapsulation in nanocarriers [170-172]. The rationale driving the use of macromolecules and nanoparticles for tumor-targeted drug delivery is summarized as the EPR effect [173]. Proposed by Matsumura and Maeda almost three decades ago [174], the EPR effect states that colloidal carriers have a greater tendency to enter tumors than normal tissues. Additionally, their elimination from tumors is delayed. This can result in greater drug exposure in tumors than in normal tissues.

Unfortunately, very few literature reports have analyzed the pharmacokinetics underlying the EPR effect from a mechanistic perspective [175, 176]. Additionally, expectations from the nanoparticle-based therapy are often unrealistic [177, 178], which can adversely affect the future development of these technologies. In the following sections, we summarize the fundamentals of drug transport across tumor blood vessels. We also discuss some features of nanoparticles and drug that

enable the existence of the EPR effect. We show here that several physiological features of the tumor and physicochemical properties of the drug as well as nanoparticles affect drug transport, making the EPR effect a specialized phenomenon. It will be clear that although only a small number of variables are considered in this discussion, drawing any general conclusions is challenging. This highlights the complexities of drug targeting to tumors.

1.4.1.1 Factors affecting drug concentration in the tumor

Upon IV administration, the rate of change of drug concentration in the tumor can be described using the following equation:

$$V_{tumor}\frac{dC_{tumor}}{dt} = Cl_{deposition}C_{plasma} - Cl_{elimination}C_{tumor}$$

Where C_{plasma} represents the concentration of drug in plasma, C_{tumor} represents drug concentration in the tumor. $Cl_{deposition}$ and $Cl_{elimination}$represent distributional clearances for drug deposition into the tumor and drug elimination from the tumor, respectively.

Higher drug concentration in the tumor can be achieved by altering any or all of the three parameters: increase in the deposition clearance $Cl_{deposition}$, increase in drug concentration in the central compartment C_{plasma} or decrease in elimination clearance from the tumor $Cl_{elimination}$. In the following sections, we analyze which of these parameters can be favorably affected by nanoencapsulation.

1.4.1.2 Deposition clearance into the tumor

Angiogenesis is a hallmark of most solid tumors [179]. Due to excessive secretion of pro-angiogenic factors, tumor blood vessels develop in a disorderly

manner. Consequently, they lack pericyte coverage and a well-developed basement membrane, and often have gaps between their endothelial cells. Hence, tumor blood vessels are considered porous in nature [110, 180].

As described extensively by Jain and colleagues, drug transport across porous blood vessels occurs by two processes, convection and diffusion [99, 107, 181, 182]. Convectional transport is driven by the pressure differential between the capillary and tumor interstitium, and is proportional to the reflection coefficient of nanoparticles. Diffusional transport arises from the concentration difference between the capillary and tumor tissue. Diffusional flux is directly proportional to the diffusion coefficient of nanoparticles. Due to the colloidal size of nanoparticles, diffusion is rather limited and convection is the major mode of transport [183] (at least in the peripheral regions of the tumor [102], where majority of drug exchange occurs [184]). On the other hand, transport of soluble drug molecules occurs predominantly by diffusion [183].

Several studies have analyzed the transvascular flux of macromolecules [176, 185, 186] and nanoparticles [1, 185, 186]. Generally, with an increase in particle size, transvascular flux (and hence deposition clearance) decreases [1]. Studies comparing the transvascular flux of nanoparticles to soluble drug molecules have not been conducted. Hence, providing experimental evidence to compare deposition clearance of nanoparticles and soluble drug molecules is not currently possible. However, some speculations can be made. For drugs with favorable tumor to plasma partition coefficients, distribution across tumor blood vessels is limited by blood flow. In this condition, molecular/particle size may be a good

predictor of transvascular flux, and the free drug should deposit within the tumor with much greater efficiency than nanoparticles. For drugs that have low tumor to plasma partition coefficients, drug transport is limited by their partition coefficient and size may not be a good predictor of transvascular flux. In such a case, deposition clearance of the soluble drug may or may not be higher than that of nanoparticles.

1.4.1.3 Drug concentration in the central compartment

Drug concentration in the central compartment is another important determinant of tumor concentration. The concentration-time profile of a drug in the central compartment after a single intravenous dose is determined by its systemic clearance and volume of distribution.

Drawing generalizations comparing the pharmacokinetics of a soluble drug to its nanoparticle formulation is obviously not possible without experiments. However, there is extensive work comparing the pharmacokinetics of doxorubicin and paclitaxel in soluble form and in various nanoparticle formulations. Some common trends are observed. Encapsulating paclitaxel in nanoparticles results in a reduction in systemic clearance [187-192] (as observed by the reduced terminal slope of the concentration-time profile) and a reduced volume of distribution [188, 190, 193] (as evidenced by the increase in the initial plasma concentration) of the drug. Similar results have also been reported for various formulations of doxorubicin [194-198]. Reduced drug clearance can be attributed to delayed release of the drug from the nanoparticles and resultant protection from hepatic enzymes and renal filtration. The altered distribution of the drug can be a result of

the limited ability of nanoparticles to extravasate across intact normal blood vessels. Regardless of the mechanism, an increase in plasma concentration of the drug increases the driving force for accumulation in the tumor. Not surprisingly, some reports show a near linear relationship between half-life of nanoparticles and tumor exposure [199, 200].

The ‘enhanced permeability’ component of the EPR effect is a complex and conditional phenomenon. The name ‘enhanced permeability’ gives an impression that nanoparticles may have a greater deposition clearance into the tumor than the free drug. However, that is likely to occur only under special circumstances. The more likely explanation (that is currently supported by experimental evidence) for the increased tumor entry of nanoparticles is the increased plasma concentration. In any case, ‘enhanced permeability’ should be characterized and justified on a case-by-case basis.

1.4.1.4 Elimination clearance of nanoparticles

Under normal physiological conditions, fluid entering tissues returns back into systemic circulation via lymphatic drainage. Due to increased solid stress, lymphatics in the core of the tumor are compressed and non-functional [201, 202]. As a result, convective forces, driving the movement of fluid out, are absent or minimal in the core of the tumor. Fluid exchange can still occur in the peripheral regions of the tumor. Hence, the limited convection and diffusion in the tumor periphery are the major routes of elimination from the tumor [181]. Several factors such as partition coefficient, concentration difference and size play an important role in determining the rate of transport. Hence, it is not possible to draw any

generalizations. However, if size was the only determining factor, nanoparticles are significantly larger than the soluble drug molecule. Consequently, the elimination clearance of nanoparticles from tumors would be lower than that of the free drug. The impaired pathophysiology of tumors enables a delayed retention of nanoparticles and encapsulated drug within the tumor [174].

Thus, the EPR effect is a highly specialized occurrence. The existence of this effect relies on several variables such as the type of tumor, type of drug, physicochemical properties of nanoparticles, pharmacokinetics of the drug and nanoparticles, and so on. Though a very limited number of variables were considered in the discussion above, making generalizations about the EPR effect is not possible.

Table 1-1. Tumor targets, ligands, and type of nanoparticles used for active targeting

Target	Type of ligand	Type of nanoparticle	Reference
αvβ3	Peptide	Perfluorocarbon	[203]
		Silica	[204]
		Polysaccharide	[205]
		Micelles	[206-208]
		Polymer	[209, 210]
		Quantum dots	[211]
		Iron oxide	[212, 213]
	Antibody	Perfluorocarbon	[214]
Biotin	Small molecule	Polymer	[9, 215]
CA125	Antibody	Liposomes	[216]
CD13	Peptide	Liposomes	[217]
CD133	Antibody	Polymer	[218]
CD19	Antibody	Liposomes	[219]
CD20	Antibody	Polymer	[220]
CD3	Antibody	Polymer	[221]
CD44	Glycosaminoglycan	Polymer	[222]
Claudin 4	Antibody	Silica	[223]
EGFR	scFv	Gold	[224]
		Quantum dots	[225]
	Peptide	Polymer	[226, 227]
		Iron oxide	[228]
	Antibody	Gold	[229-231]
		Polymer	[220]
		Iron oxide	[232-234]
Folate receptor	Small molecule	Polysaccharide	[235, 236]
		Iron oxide	[237]
		Polymer	[215, 238-241]
		Quantum dots	[242]
		Oligonucleotide	[243]
		Liposomes	[244]
		Micelles	[245]
Glucose transporter	Small molecule	Polymer	[246]
	Antibody	Liposomes	[247]
Lectin	Monosaccharide	Liposomes	[248]
LHRH-receptor	Protein	Protein	[249]

Tumor lymphatic vessel	Peptide	Polymer	[250]
Mesothelin	Antibody	Silica	[223]
Nucleolin	Peptide	Polymer	[251-253]
Nucleosome	Antibody	Liposomes	[254]
PSMA	Antibody Small molecule Aptamer	Quantum dots Quantum dots Polymer Polymer Polymer-Lipid Micelles	[255] [211] [256] [257, 258] [259] [260]
Sigma	Small molecule	Cyclodextrin Liposomes	[261] [262, 263]
SPARC	Peptide	Iron oxide	[264]
Transferrin receptor	Glycoprotein	Gold Cyclodextrin Polymer Silica Liposomes	[265] [266, 267] [268] [223] [269]
uPAR	Peptide	Iron oxide	[270, 271]

1.4.2 'Active' targeting

The expression of several cell surface receptors and transporters is upregulated in cancer cells [272]. Conjugating drugs to ligands that bind these receptors can potentially improve drug delivery to tumors. There are several research initiatives exploring the delivery of chemotherapeutics conjugated to antibodies or antibody fragments that bind to these cancer specific markers [273].

A similar targeting approach has been applied to improve the delivery of nanoparticles to solid tumors as well. This strategy is commonly labeled as 'active' targeting [274]. This field has matured tremendously, wherein elegant synthetic

techniques have been devised to maximize the benefits of active targeting [215, 256, 275]. A variety of targets have been explored. These include receptors overexpressed on the tumor cell surface [223, 240, 266], endothelial cells of angiogenic blood vessels [206, 209] and tumor lymphatic vessels [250]. Diverse types of ligands, ranging from small molecules to full length antibodies, have been immobilized on the nanoparticle surface for active targeting. A list of targets, ligands and the type of nanoparticles used for active targeting is summarized in **Table 1-1**. While this list is not exhaustive, it provides a good idea of the variety of ligands and targets used for active targeting. Other lists similar to this can be found in several review articles written about this subject [274, 276-279].

Recently some aspects of active targeting have been called into question. These include the cost effectiveness and translatability of this approach [280], or if it should even be called 'active' targeting. One very important question is whether ligand conjugation can significantly (dramatically) improve the tumor accumulation/efficacy of nanoparticles. If it does/does not, why? The answer to most of these questions may be rooted in fundamental mechanisms involved in cellular uptake and transport of drug and nanoparticles. Hence, we carefully analyze these mechanisms and attempt to address important questions in active targeting.

1.4.2.1 Mechanism of active targeting

Nanoparticles enter the tumor microenvironment by passing through the pores of the tumor blood vessels. Once in the vicinity of the cell, nanoparticles are taken up by the process of endocytosis. This process is accelerated if the nanoparticles

are conjugated to a ligand (henceforth referred to as targeted nanoparticles) that binds to cell surface receptors [281]. Binding of the ligand to the tumor cell surface receptor triggers endocytosis. This has been supported by mathematical models that show that the energy released upon binding of the ligand to the cell surface receptor accelerates wrapping of cell membrane around the nanoparticle, leading to the formation of the endocytic vesicles [282]. Hence, targeted nanoparticles can be taken up at a faster rate as compared to non-targeted nanoparticles [283]. This may lead to enhanced intracellular drug concentration.

Enhanced drug concentration in the tumor tissue can also be achieved because of enhanced retention of nanoparticles. According to this theory, targeted nanoparticles that are attached to the cell membrane are less likely to be eliminated from the tumor [284]. Consequently, they have a greater probability of entering the cells. Alternately, the exocytosis of targeted nanoparticles from tumor cells is also delayed as compared to that of non-targeted nanoparticles [285].

However, current pharmacokinetic studies cannot help determine which of these mechanisms is operational *in vivo*.

1.4.2.2 Active targeting vs. ligand mediated targeting

There is considerable debate over whether the process should be referred to as active targeting or ligand mediated targeting. As stated by Prof. Bae, the term ‘active targeting’ provides a false impression that the ligand is carrying the nanoparticle to the site of the tumor [286]. In fact, the ligand has no role to play in the targeting phenomenon until the nanoparticle is within a few nanometers of the tumor cell surface [276]. The term might have originated to differentiate this

phenomenon from the EPR effect, which is commonly referred to as passive targeting. However, even 'actively targeted' nanoparticles enter the tumor via the EPR effect. Also, similar to non-targeted nanoparticles [287], their cellular uptake is an energy-dependent, active process [283]. The only difference may be that their cellular uptake is triggered by the binding of the ligand to the cell surface receptor. Thus, it is well justified to change the terminology from active targeting to ligand mediated targeting.

1.4.2.3 Impact of ligand conjugation on the biodistribution of nanoparticles

It is often suggested that conjugation of a tumor targeting ligand may improve the selectivity of nanoparticles [177, 288, 289]. In other words, ligand conjugation may reduce the off-target accumulation of nanoparticles. In this section, we analyze if this is possible.

Most studies comparing targeted and non-targeted nanoparticles are carried out in mouse xenograft models [290-293]. Though this model is imperfect, there is lack of clinical data available to understand this phenomenon. Hence, we present some calculations with respect to this model. We should also note that the calculations described here are based on concentrations and not area under the curves (AUCs), and therefore do not provide a complete picture.

Pharmacokinetic experiments with the murine model are carried out when the tumor is ~100-400 mm^3 in volume. These tumors weigh ~0.1-0.4 g. The highest tumor concentration that is achieved is at best ~5-10% injected dose/g tissue. This indicates that ~1-4% of the injected dose is in the tumor at t_{max}. On the other hand, liver concentrations at t_{max} range from 10-50% injected dose/g tissue, and the liver

weighs ~1.5 g. This indicates that ~15-75% of the injected dose is in the liver at t_{max}. As is evident, a very small fraction of the dose accumulates in the tumor. Additionally, this small concentration is also transient and is lower before or after t_{max}. Increasing the tumor accumulation of nanoparticles by 2-4-fold through ligand mediated targeting (as is commonly observed with these systems [222, 225, 251, 293]) is unlikely to affect the overall biodistribution of nanoparticles in a favorable manner.

Interestingly, conjugation of the ligand to nanoparticles can, in some cases, increase the off-target accumulation of nanoparticles [294, 295]. Typically, a ligand is conjugated to the terminal end of the hydrophilic polymer [such as poly(ethylene glycol) (PEG)] used to prevent opsonization. Conjugation of the targeting ligand to the nanoparticle surface can reduce the fraction of the nanoparticle surface occupied by PEG. This can increase the rate of opsonization and clearance of nanoparticles by the mononuclear phagocyte system (MPS). This will lead to an increased accumulation in the MPS-associated organs such as liver and spleen.

Regardless of the mechanism, several studies have shown the beneficial effect of nano-encapsulation on the tumor accumulation of drugs. Additionally, many unique properties of nanomaterials enable them to overcome MDR, and improve the potency of the encapsulated drug. In the following sections, we discuss the various benefits of nano-encapsulation on treating MDR tumors.

1.4.3 Inhibition and evasion of drug efflux

1.4.3.1 Use of excipients that inhibit efflux transporters

NPs are multicomponent systems consisting of various excipients including polymers, lipids, and/or surfactants. While these materials have traditionally been considered inert, several studies have documented their ability to inhibit efflux activity.

1.4.3.1.1 Surfactants

Surfactants are amphiphilic molecules comprising both hydrophilic and hydrophobic groups. At concentrations above critical micellar concentration (CMC), surfactants self-assemble to form micelles. In aqueous solutions, the hydrophobic core of micelles can be used to solubilize lipophilic anti-cancer agents [296]. Surfactants are also used to stabilize the surface of polymeric or lipid NPs to form stable amphiphilic colloids in physiological fluids [228, 297, 298]. Thus, surfactants are arguably one of the most widely used excipients in nano drug delivery systems [299, 300].

The potential of surfactants to sensitize resistant cells to chemotherapeutics was first reported in drug-resistant CHO cells [301]. Since then, many groups have investigated the use of surfactants to inhibit efflux transporters [302]. Woodcock *et al.* showed that various surfactants were capable of overcoming drug resistance, with Cremophor® EL being the most potent [303]. Pre-treatment or concomitant treatment of MDR cells with Cremophor® EL significantly increased the cellular uptake and retention of daunorubicin. This effect resulted from enhanced membrane fluidity in the presence of the surfactant. Using fluorescence anisotropy,

the authors observed a progressive decrease in membrane viscosity with an increase in surfactant concentration [304]. However, the use of Cremophor® EL has been associated with several toxicities including hypersensitivity and peripheral neuropathy [305]. This has significantly limited the use of this excipient in clinical practice.

Pluronics are another class of surfactants that are extensively used in NP formulations [306, 307]. Pluronics are A-B-A type of block co-polymers consisting of poly(ethylene oxide) and poly(propylene oxide) blocks. They have been shown to inhibit efflux transporters in different MDR-cell types [308]. In fact, multiple mechanisms have been attributed to their activity **(Figure 1-3)** (reviewed in [10]). In their seminal mechanistic studies, Batrakova *et al.* showed that pluronic-85 brought about a concentration-dependent depletion in intracellular ATP levels [309]. This energy depletion led to a decline in the activity of efflux transporters. Using confocal microscopy, the same group later showed colocalization of fluorescently labeled pluronic-85 with mitotracker red, a fluorescent label for mitochondria [310]. This provided additional evidence supporting the role of pluronics in interfering with mitochondrial processes and cellular energetics. Similar to the studies with Cremophor® EL, pluronic-85 also showed an increase in cell membrane fluidization [310]. It is possible that the changes in membrane permeability induced by surfactants are relevant not only to the cell membrane but also to intracellular organelle membranes. This may cause a loss in polarity of mitochondrial membranes and a depletion of cellular ATP.

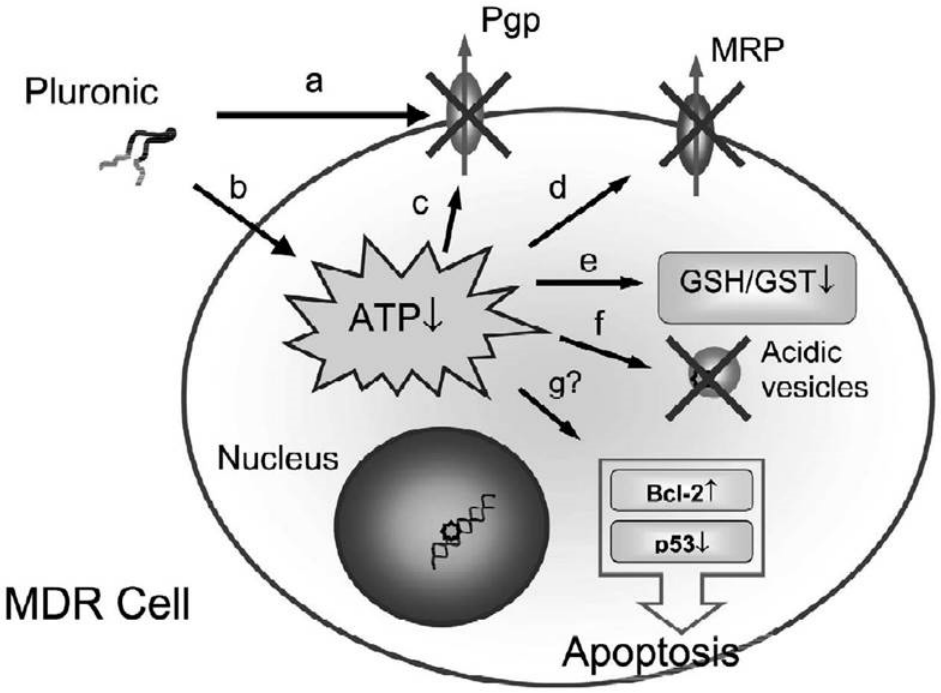

Figure 1-3. Schematic presenting multiple effects of Pluronic block copolymers displayed in MDR cell.

These effects include (a) decrease in membrane viscosity ('fluidization'); (b) ATP depletion; (c, d) inhibition of drug efflux transport systems; (e) reduction in GSH/GST detoxification activity; and (f) drug release from acidic vesicles in the cell. Effects of Pluronic block copolymers on apoptosis (g) are not sufficiently studied at present. Reprinted with permission from [10].

Based on pre-clinical efficacy data, a pluronic formulation of doxorubicin, SP1049C, is in clinical trials [311]. SP1049C contains a mixture of two pluronics,

L61 and F127. Results from a phase II clinical trial in patients with advanced adenocarcinoma of the esophagus and gastroesophageal junction were reported recently for this formulation [311]. These studies showed that the objective response rate in these patients was 47%. Previous clinical trials with doxorubicin have documented an objective response rate of ~20%. The improved response rate with SP1049C is highly promising and suggests that this formulation will likely have an impact on tumor drug resistance.

Other surfactants have shown comparable efficacy in preclinical studies [302]. For example, polyoxyl 15 hydroxystearate (solutol HS15) has shown potent activity in overcoming drug resistance. Coon *et al.* showed that treatment of drug resistant KB8-5-11 carcinoma epidermoid cells with solutol HS15 increased their sensitivity to doxorubicin [312]. Similarly, a recent study showed that paclitaxel encapsulated in lipid NPs stabilized with polyoxyethylene 20 stearyl ether (Brij® 78) had enhanced cellular uptake and efficacy. The authors confirmed that this action was due to ATP depletion caused by the surfactant [313, 314]. NPs stabilized with d-alpha tocopheryl polyethylene glycol 1000 succinate (Vitamin E TPGS) also showed a similar effect [315].

With a multitude of surfactants demonstrating efflux inhibition, some studies have attempted to identify structural features of the surfactant that are key to achieving maximal activity [316]. One such study focused on various esters of ethylene oxide and fatty acids. Two variables were evaluated: the type of fatty acid and the molar ratio of ethylene oxide to fatty acid. The unsaturated version of C18 fatty acid (oleic acid) resulted in better MDR modulation than the saturated C18

analog, stearic acid. In contrast to stearic acid, 12-hydroxy stearic acid did not show any effect on efflux transport [317]. Maximal efflux inhibition was found at a molar ratio of 20:1. This study shows that optimizing the ratio of the hydrophilic fraction (ethylene oxide) to hydrophobic fraction (fatty acid) is essential to maximizing the activity. In another study, Lo compared various surfactants ranging in HLB values from 4 to 40. A maximal inhibition of efflux transport was seen at HLB values between 10 and 17 [318]. Surfactants with different HLB values may vary in their ability to partition into the cell membrane, and this may explain the effect of HLB values on the MDR inhibitory activity of surfactants.

1.4.3.1.2 Polymers

Polymers lacking amphiphilic properties have also been shown to be useful in overcoming drug resistance. In particular, poly(alkyl cyanoacrylate) has been extensively studied for its ability to improve the intracellular transport of chemotherapeutics [319-321]. An interesting mechanism, distinct from the ones discussed before, was proposed by de Verdière *et al.* [322]. Doxorubicin, by itself, was ineffective against the drug-resistant P388-ADR leukemia cell line. However, NP-encapsulated drug showed a significantly higher toxicity. On further investigation, the authors found that NPs were not internalized effectively into cells, thus ruling out enhanced cellular uptake as a possible mechanism of improved efficacy. A degradation product of the polymer, poly(cyano acrylic acid), was found to form a complex with the cationic drug. This uncharged complex was transported into the cells much more efficiently than the charged drug molecule [322].

Another mechanism suggested by this research relates to saturation of efflux transport. NPs that rapidly release their entire payload near the cell membrane could achieve very high local drug concentration and thus saturate the efflux transporter. The authors showed that poly(isobutyl cyanoacrylate) NPs (showing rapid drug release) successfully overcame drug resistance through saturation of efflux activity. However poly(isohexyl cyanoacrylate) NPs (showing a slower drug release) were ineffective in saturating the efflux transporters. The proposed saturation mechanism is plausible *in vitro* where the concentration of the drug used was ~0.1-10 µg/mL [322]. However, such high local concentrations may not be achievable *in vivo*, potentially limiting the significance of this mechanism.

It was later shown that doxorubicin encapsulated in poly(isohexyl cyanoacrylate) NPs could successfully overcome tumor drug resistance *in vivo* [323]. In a chemo-resistant transgenic mouse model of hepatocellular adenocarcinoma, the authors found that free doxorubicin showed a modest cytotoxic effect. However, there was almost a 3-fold increase in the apoptotic index when doxorubicin was encapsulated in NPs [323]. This was likely due the formation of an uncharged complex between the drug and the degradation product of the polymer, leading to higher intracellular drug concentrations.

Another polymer with reported P-gp inhibitory potential is PEG [324-326]. PEG is extensively used in NP formulations to provide a hydrophilic corona, to stabilize carriers in physiological fluids, and to evade macrophage uptake [327]. In a rat intestinal model, Shen *et al.* showed that various molecular weights of PEG were capable of inhibiting the P-gp-mediated efflux of rhodamine-123 [328].

However, PEG was not very potent in inhibiting P-gp. For example, PEG 20,000 decreased the secretory transport of rat intestinal membrane by ~65% at a concentration of 5% w/w. In contrast, pluronic-85 showed a 50% depletion in ATP levels at a concentration as low as 0.00067% w/w [10]. Additionally, it remains to be seen if such an inhibition is capable of reversing drug resistance in tumor cells.

1.4.3.2 Efflux bypass by altering sub-cellular localization of drug

1.4.3.2.1 Endocytosis Vs. diffusion

Most drug molecules enter cells by diffusion across the cell membrane [329]. This unprotected passage of drug through the cell membrane makes it vulnerable to the action of efflux transporters [329]. NPs are too large for diffusion-mediated transport. NP-encapsulated drug is taken up through endoctytic vesicles, which deposit the drug in the perinuclear regions, away from the cell membrane and closer to its site of action [287, 330-332]. This can lead to a higher intracellular concentration of the drug and greater therapeutic activity **(Figure 1-4)**.

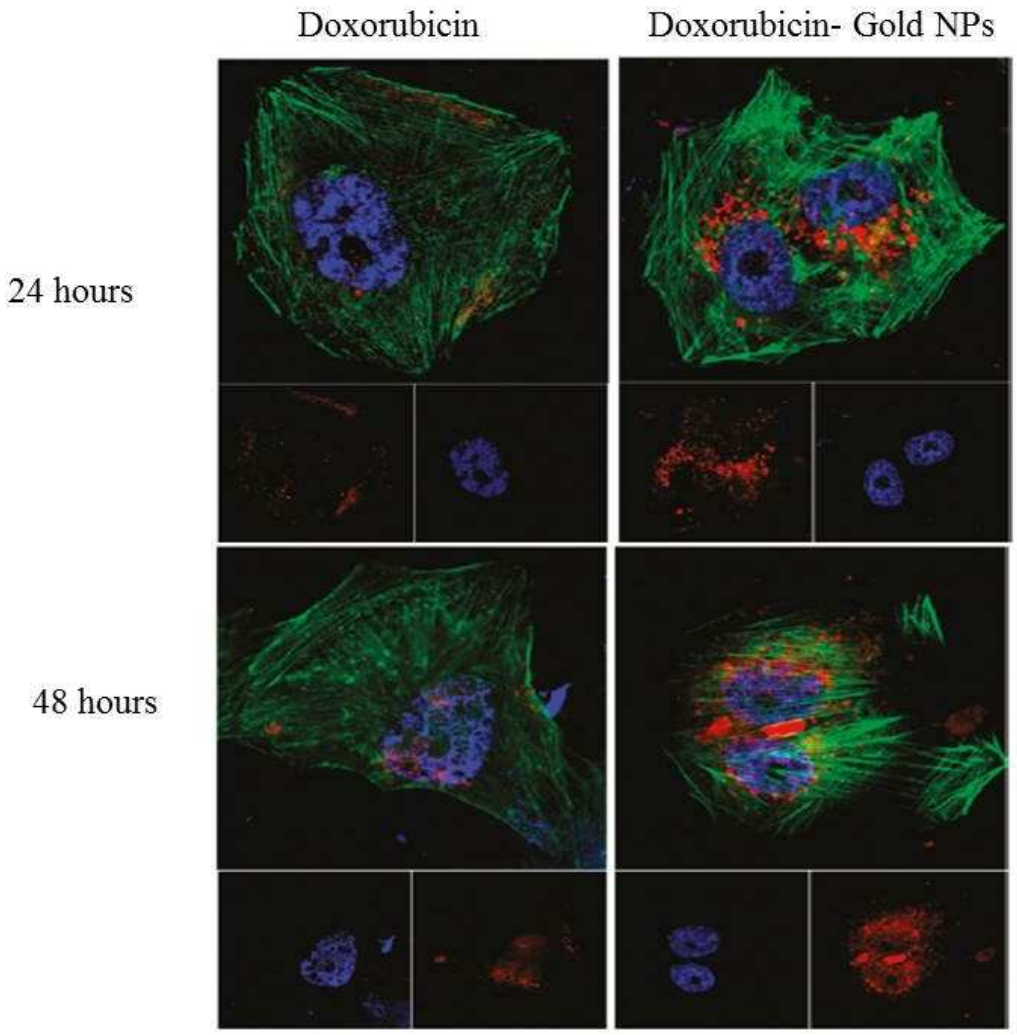

Figure 1-4. Different intracellular localization of NPs and free drug.

Confocal laser microscopic observation of MCF-7/ADR cells incubated with free doxorubicin (DOX) or DOX-tethered AuNPs for 24 and 48 h. The dose of doxorubicin or its equivalent was 5 μg mL1 in the cell culture. The cells were counterstained with DAPI (blue) for the cell nucleus and Alexa Fluor 488 phalloidin (green) for the cell membrane. Reprinted with permission from [333]. © 2011 American Chemical Society.

Though altered drug distribution was regarded as one of the mechanisms for NP-mediated MDR reversal, there was a lack of convincing evidence supporting this hypothesis [332, 334, 335]. Recently, a lipid-polymer NP system developed by Wong *et al.* offered some interesting insights [336]. The authors showed that the excipients used in the system did not have any effect on the efflux transport process [337]. Only encapsulation of the drug within this "hybrid" carrier resulted in a change in the sub-cellular distribution of the drug. This led to a reversal of drug resistance in a human cell line MDA435/LCC6/MDR1, and a mouse cell line, EMT6/AR1. This reversal was attributed to altered route of entry of the drug into the cells [336]. In another study, surfactant-polymer NPs loaded with doxorubicin were tested in NCI-ADR/RES cells [338]. The authors found that NP-encapsulated doxorubicin was significantly more cytotoxic than the free drug. Previous reports had shown that the polymer (alginate) used in these studies had no effect on drug efflux [319].While the surfactant used in the formulation (docusate sodium) may have P-gp inhibitory activity, the mechanism of efflux inhibition was not investigated. However, the intracellular localization of the drug was different when the drug was administered in the form of NPs.

Additional evidence for the role of altered intracellular distribution was provided by extensive work done in the field of polymer-drug conjugates. Polymer-drug conjugates, similar to NPs, are unable to enter the cell via diffusion. Omelyanenko *et al.* showed that the uptake of *N*-(2-hydroxypropyl) methacrylamide (HPMA) – adriamycin conjugate by endocytosis led to higher intracellular concentrations and higher potency in A2780/AD resistant ovarian

cancer cell line [329, 339]. Confocal laser scanning microscopy confirmed that the increased potency was due to an altered route of entry into the cells for the drug-polymer conjugate.

1.4.3.2.2 Triggered intracellular drug release

An inherent limitation of NP systems is the leakage of drug while the carrier is in systemic circulation. As a result, a fraction of the drug is still subject to efflux. This decreases the targeted bioavailability and hence the effectiveness of the drug. An interesting approach to overcome this limitation is to trigger drug release in response to specific intracellular cues. Upon endocytosis, NPs are trafficked into early and late endosomes, which eventually fuse with lysosomes. This exposes NPs to a gradually decreasing pH environment. Several groups have utilized this low pH as a trigger to release drug from NPs [340-343]. These systems ideally show no or limited drug release at physiological pH.

A detailed investigation of such a system was reported by Wang and coworkers [333]. This group used gold NPs covalently conjugated to doxorubicin using a PEG spacer. Conjugation of doxorubicin to PEG was done via either a pH-sensitive hydrazone bond or a pH-insensitive carbamate bond. When conjugated to the NP surface, the close proximity of gold and doxorubicin quenched the fluorescence of the drug. This allowed for evaluation of the intracellular drug release. In comparison to that with the free drug, the intracellular concentrations achieved with NP-conjugated drug were higher in the drug resistant MCF-ADR cells but not in drug sensitive MCF-7 cells. However, drug conjugated via the pH-sensitive hydrazone bond but not via the carbamate bond was successfully

released intracellularly. This resulted in a significant decrease in the IC50 values of doxorubicin encapsulated in the pH-sensitive formulation. In fact, the IC50 values of free drug and drug bound via the carbamate bond were identical. This report highlights two important properties a formulation should possess. First, it should be able to protect the drug from efflux pumps. Second, the formulation should be able to release the drug in the perinuclear regions, away from the efflux pumps and near the site of drug action [333].

A similar phenomenon has been shown by other groups using iron oxide nanoparticles [344], polymer micelles [345], and liposomes [346]. All these reports suggest the need to protect the drug from the environment until the drug reaches its target site of action.

1.4.3.2.3 Altering rate of drug release at the site of action

The rate of drug release has also been shown to play an important role in overcoming drug resistance. Gao *et al.* reported an elegant example of NP-engineering to improve drug delivery to resistant cancer cells [347]. This group synthesized doxorubicin loaded mesoporous silica NPs with varying pore sizes. With an increase in pore size, the rate of drug release from these particles increased. However, NPs showed drug release only under acidic conditions such as those found in late endosomes.

The authors found that free drug and NP-loaded drug were taken up to the same extent by sensitive MCF-7 cells. However, encapsulation in NPs resulted in a dramatic increase in the uptake of doxorubicin in resistant cells. On further investigation, the authors found that there was a significant difference in the

intracellular drug concentrations and cytotoxicity achieved by the different NP-formulations in resistant cells. NPs that showed rapid drug release resulted in the highest intracellular drug concentrations and hence highest potency. Faster release, following uptake, led to a rapid increase in intracellular concentrations and greater cytotoxicity *in vitro* [347]. It must be noted, however, that even under acidic conditions, NPs released only 30-35% of their cargo over 30 hours. Hence, a major portion of the drug would likely remain bound to NPs and be potentially unused.

1.4.3.3 Simultaneous delivery of drugs and efflux inhibitors

In addition to the serendipitous use of active excipients, multiple pharmacologically active agents have been used intentionally for inhibiting efflux transporters. Initial studies were performed with 'first generation' inhibitors such as cyclosporine and verapamil, which were already in use for other indications [348]. Clinical trials with these agents failed to prove the role of P-gp in drug resistance [349]. A number of factors such as absence of confirmation of P-gp expression in the tumors and unexpected dose-limiting toxicities of P-gp inhibitors could have contributed to this failure [6]. In 2001, List *et al.* published the long-term results of treatment of acute myelogenous leukemia with daunomycin in combination with the P-gp inhibitor cyclosporine [350]. These results were the first to indicate the survival advantage of the combination treatment. Second generation inhibitors (e.g., PSC 833, VX-710) were developed solely for the purpose of overcoming drug resistance [351]. These agents were tested in clinical trials in various malignancies for which there was evidence of P-gp expression or were associated with a poorer therapeutic outcome [352]. One major limitation of these trials, however, was the

reduction in anticancer drug doses that was required with concurrent administration of the inhibitor [7]. P-gp inhibitors increased the serum levels of the co-administered chemotherapeutic drug. Due to this pharmacokinetic interaction, the dose of the drug had to be reduced. A number of studies found that this reduction in dose led under-treatment of patients, which could have contributed to the failure of these combination treatments [7]. Pharmacokinetic interactions between the P-gp inhibitor and the drug could also result from inhibitors' ability to inhibit other proteins involved in drug metabolism such as cytochrome P450 [8]. Third-generation inhibitors (tariquidar, zosuquidar, laniquidar, and ONT-093) have high potency and greater specificity for P-gp.

A primary concern even with the third generation inhibitors is that these agents may increase the side effects of chemotherapy by blocking physiological anticancer drug efflux from normal cells [353]. This is a relevant concern, because P-gp plays important roles in the physiological regulation of endogenous compounds and xenobiotics in the body [354]. It is therefore important to limit the exposure of normal cells and tissues to the efflux inhibitor and anticancer drug combination. Secondly, the differences in physicochemical properties of the anticancer drug and efflux inhibitor may result in differences in the pharmacokinetics and tumor accumulation of the two agents. For optimal efficacy, both the drug and the inhibitor need to be temporally co-localized in the tumor cells.

Nano drug delivery platforms have the potential to overcome MDR by enabling simultaneous delivery of chemotherapeutics and efflux inhibitors. For example, administration of vincristine and verapamil in a single co-encapsulated

poly(lactic-co-glycolic acid) (PLGA) NPs was more effective means of reversing drug resistance in vitro, than either single agent in multiple MDR cell lines [355, 356]. Similarly PLGA NPs loaded with both paclitaxel and tariquidar were effective in inducing cytotoxicity in drug resistant cell lines JC and NCI/ADR cells in vitro and *in vivo* **(Figure 1-5)** [9]. Polymer-lipid nanoparticle systems containing tristearin and steric acid as lipid components, with pluronic F68 polymer, was able to efficiently coencapsulate doxorubicin and elacridar and overcome MDR in a drug-resistant breast cancer cell line [357].

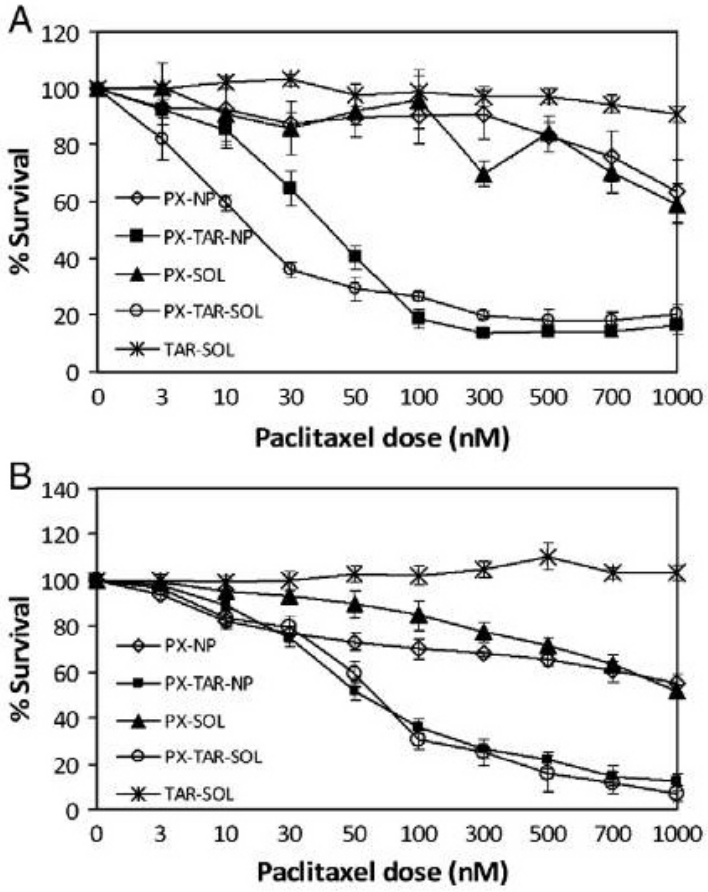

Figure 1-5. Enhanced cytotoxicity of dual agent nanoparticles in drug-resistant cell lines.

(a) JC and (b) NCI-ADR-RES cells were incubated with treatments for 24 h and the cell viability was determined by MTS assay. Legend: PX-NP—Nanoparticles containing paclitaxel; PXTAR-NP—Nanoparticles containing paclitaxel and tariquidar; PX-SOL—Paclitaxel in solution; PX-TAR-SOL—Paclitaxel and tariquidar in solution; and TAR-SOL—Tariquidar in solution. Data as mean ± S.D.; n = 10. Reprinted with permission from [9].

Another strategy involves the use of NPs containing both a chemotherapeutic agent and siRNA targeting the P-gp transcript. When using P-gp gene silencing to overcome drug resistance, the potential for kinetic differences in gene silencing and the availability of chemotherapeutic agents at the target site is a concern. Differences in size, biodistribution, and other physical characteristics of siRNA-transfection complexes and small molecule chemotherapeutics could give rise to differences in biodistribution. However, for optimum efficacy, the chemotherapeutic agent should be available at its target site when the gene is silenced. The use of mesoporous silica nanoparticles loaded with doxorubicin and siRNA targeting the P-gp transcript demonstrated synergistic inhibition of tumor growth than the single agent-loaded NPs in an orthotopic model of breast cancer [358]. In a similar study, poly(ethylene oxide)-modified poly(beta-amino ester) (PEO-PbAE) and PEO-modified poly(epsilon-caprolactone) (PEO-PCL) NPs were formulated to efficiently encapsulate *MDR1* silencing siRNA and paclitaxel. Combination of *MDR1* gene silencing and nanoparticle-mediated delivery significantly improved the cytotoxic activity of paclitaxel in SKOV3TR cells [359]. Active targeting of nanoparticles to cancer cells via biotin-functionalized PLGA NPs loaded with both P-gp-targeted siRNA and paclitaxel was able to overcome drug resistance in vitro as well as in vivo [360].

Encapsulation of efflux inhibitors in NPs can potentially limit the distribution of these agents and significantly limit their side effects. However, altered biodistribution of NP-encapsulated drug can have unintended consequences. As observed with Doxil, encapsulation of doxorubicin in liposomes was able to limit its

cardiotoxicity. However, new side effects such as hand-foot syndrome and mucositis were observed because of certain physicochemical properties of the formulation [361]. Hence, it is possible that the side effects of efflux inhibitors may not be completely eliminated with the use of nano-encapsulation. However, if these newer side effects are milder than the existing ones, nanotechnology may still be an attractive alternative.

1.4.4 Improving transport

The vast body of evidence supporting the reversal of drug resistance by NPs offers a promising strategy to overcome an important problem in cancer therapy. In order to maximize this potential, it is critical that NPs (or at least the released therapeutic agent) reach every tumor cell. However, NPs are often limited to regions immediately adjacent to the blood vessels [91, 93]. Paradoxically, it is the regions away from the blood vessels that are rich in drug-resistant and aggressive cells [94]. The ability of NPs to overcome MDR will hence be realized only if they reach these poorly-perfused regions. Thus, any discussion of the use of nanotechnology to overcome drug resistance is incomplete without considering the problem of transport resistance in tumors. Several adjunct therapies have been proposed to enhance the transport of molecules in the tumor ECM. We provide here a summary of the progress made in this field and their possible implications for overcoming MDR using nanotechnology.

1.4.4.1 Inhibition of angiogenesis to improve drug delivery to tumors

Jain and co-workers proposed that the delivery of drugs to tumors is limited because of a faulty “delivery system” [111]. This “delivery system” referred to the blood vessels supplying the tumor. The leakiness of tumor blood vessels contributes to elevated IFP in tumors [116]. Consequently, it was hypothesized that repairing the tumor vasculature could reverse the elevated IFP. This would, in turn, lead to improved drug delivery and penetration. This process of inhibiting tumor vasculature and restoration of a normal phenotype has been termed as vascular normalization [111]. Such normalization includes various characteristics such as increased pericyte coverage, decreased vessel diameter, decreased blood volume, establishment of vessel hierarchy and enhanced tissue coverage by the blood vessels.

However, literature reports have been somewhat equivocal about the utility of this technique [362-365]. Some studies show that decreasing vascular permeability improves the delivery of drugs to the tumors [366]. Others suggest that increasing vascular permeability may improve drug delivery [367, 368]. Some of these conflicting results can be attributed to differences in tumor models used, and the inherent heterogeneity between tumors. Some reports suggest that lack of techniques to monitor and characterize the phenomenon of vascular normalization limits our understanding [111]. Nevertheless, a huge body of research has established that inhibiting angiogenesis is a highly effective but a temporary method to improve drug delivery and penetration into solid tumors [363, 369, 370]. In the following sections, we will summarize the pre-clinical and clinical studies that have investigated different strategies for inhibiting tumor vasculature.

1.4.4.1.1 VEGF inhibitors

Amongst several pro-angiogenic factors, VEGF is one of the most potent [109, 371]. It acts through tyrosine kinase receptors VEGFR1 and VEGFR2 [372, 373]. Initial efforts to inhibit VEGF resulted in the discovery of bevacizumab, a humanized monoclonal antibody that binds to VEGF and prevents its activity [374]. It is the first anti-angiogenic approved by the FDA for multiple indications including colorectal, lung, renal cancers, and glioblastoma [374, 375]. Other VEGF inhibitors include pazopanib, sorafenib, sunitinib, and vandetanib. Although inhibitors of the VEGF pathway have shown only modest efficacy as a monotherapy [376, 377], they hold tremendous promise in improving the delivery of co-administered chemotherapeutics [378].

The initial motive behind using VEGF inhibitors for monotherapy was to inhibit angiogenesis and 'starve' the tumor [379, 380]. The redundancy of angiogenic pathways has limited the clinical utility of this approach [381, 382]. Yet, certain transient morphological and functional changes to vasculature in response to VEGF inhibition (vascular normalization) leads to decreased IFP and improved drug delivery [383].

Tong *et al.* showed that DC101 (VEGFR2 blocker) could cause vessel normalization in mouse xenograft models of small cell lung cancer and glioblastoma [384]. This resulted in a significant decrease in vascular permeability and IFP. The decrease in IFP led to improved penetration of macromolecules like albumin and lectin in these tumors. Using immunostaining, the authors determined that there was no change in the lymphatic drainage from the tumor, suggesting

that the decrease in tumor IFP was only due to the changes in the blood vessels [384].

1.4.4.1.2 Other targets for vascular normalization

Several other molecular targets have been explored for vessel normalization [13, 385]. The EGFR is upregulated in multiple cancers [386]. A consequence of EGFR activation is the increased secretion of VEGF. Thus, VEGF secretion can be decreased by inhibiting EGFR [387, 388]. In a recent report, Cerniglia and co-workers [389] showed that inhibiting the EGFR pathway could lead to vessel normalization. Treatment with erlotinib (an EGFR inhibitor) led to a decreased expression of VEGF, increased tumor perfusion and increased delivery of cisplatin. This resulted in enhanced therapeutic activity of cisplatin as compared to that with drug administration alone [389]. However, inhibiting the EGF pathway has resulted in a mixed response in clinical trials with no, moderate or good results [390-394].

Phosphoinositol-3-kinase (PI3K), like EGF, is another element upstream of VEGF. Qayum *et al.* showed that inhibiting PI3K leads to vessel normalization and improved therapeutic response to doxorubicin [395]. Similarly, selenium agents have been shown to have anti-angiogenic effects. They elicit their effects by down-regulating the expression of pro-angiogenic factors like cyclooxygenase-2 and nitric oxide synthase [396-398]. Bhattacharya *et al.* showed that treatment with methylselenocysteine led to an increased delivery of doxorubicin to human head and neck squamous carcinoma xenografts [399]. This effect was elicited through vessel maturation caused by methylselenocysteine [399].

The redundancy of angiogenic pathways can result in the development of resistance to therapies that rely on specific signaling pathways [373]. Escorcia and co-workers demonstrated that targeted radiation can be used to bring about vessel normalization [400]. The authors used a monoclonal antibody that identified specific epitopes on tumor neovasculature. This antibody was conjugated to actinium-225, which emits short range α particles. Pretreating tumors with targeted actinium 225 resulted in tumor vasculature normalization. This, in turn, led to an enhanced response to a combination treatment consisting of leucovorin and 5-fluorouracil [400].

1.4.4.1.3 Concentration and time dependency of vascular normalization

There has been considerable debate about the mechanism by which anti-angiogenic drugs improve the delivery of chemotherapeutics. Some reports suggest that inhibiting angiogenesis leads to decreased perfusion, while others have showed an increase. This has been complemented with data showing either decreased or increased drug delivery to the tumor [362].

The disparities in therapeutic response to anti-angiogenic therapies may be due to the concentration and time dependence of this technique. This dependence has been termed as the normalization window [111]. At sub-therapeutic concentrations of VEGF inhibitors, there may not be any effect on the blood vessels or on drug delivery. At very high concentrations, these therapies may completely destroy the vasculature. This will diminish drug delivery to the tumor [401]. Additionally, vessel normalization is highly transient. If the anti-angiogenic therapy is prolonged, the tumor vasculature could become inadequate for drug

delivery [402]. Dickson *et al.* showed that the duration of vessel normalization depends on the physicochemical properties of the anti-angiogenic therapy as well as the type and location of the tumor [363]. The time dependence of vessel normalization also means that additional imaging techniques will be required to determine the normalization window for drug delivery. This somewhat limits the use anti-angiogenics. However, in a very interesting report, Rolny *et al.* presented a novel strategy to induce vascular normalization [403]. The authors showed that histidine-rich glycoprotein (HRG) could inhibit angiogenesis both directly and by converting tumor associated macrophages to an M1-like phenotype. The latter effect resulted in a longer vascular normalization window [404]. Such strategies with sustained responses hold significant promise in improving the delivery of chemotherapeutics [404].

Another source of disparity in measuring the activity of anti-angiogenics may stem from the current methods of characterization. Anti-angiogenic drugs can alter two parameters associated with chemotherapeutics: drug deposition and drug penetration. When one measures drug deposition in the tumor, concentrations are assessed as a whole. These concentrations may be localized in particular foci within the tumor and may not be representative of the therapeutic activity. Drug deposition may be a function of blood supply and may decrease with declining perfusion. However, the presentation of drug to resistant and hypoxic cells (function of drug penetration) is governed by intratumoral transport, which increases in response to a decrease in IFP [405]. Therapeutic response to the drug is a combined effect of both drug deposition and drug penetration. Thus, in order

to comprehensively quantify the activity of anti-angiogenics, it is important to monitor both these parameters [405].

1.4.4.1.4 Suitability of anti-angiogenic therapy to improve NP transport

The use of anti-angiogenic drugs has been shown to have both positive and negative effects on the tumor delivery of nanomedicine. In a recent study, Vlahovic *et al.* found that pre-treatment with imatinib (a PDGFR-β inhibitor) led to enhanced accumulation of Doxil® in a mouse model of non-small cell lung cancer [406]. The same group later showed that treatment with pazopanib (inhibitor of VEGF and PDGF receptors) led to a decrease in the penetration of Doxil® in the same tumor model [407].

A recent study by Chauhan *et al.* offers some directions for the use of anti-angiogenics with nanotherapeutics [1]. The authors used DC101 as the VEGF blocker in combination with quantum dots of various sizes. In an orthotopic mouse mammary tumor model, the authors found that DC101 enhanced the penetration of NPs in a size-dependent manner. The advantage associated with the use of anti-angiogenic therapy was maximal for particles < 60 nm in size **(Figure 1-6)**. The authors also found that there was a significant benefit of using DC101 in combination with Abraxane® (~10 nm diameter) but not with Doxil® (~100 nm diameter). The size dependence of this advantage is yet to be measured in different tumor models [1]. If the degree of normalization is variable amongst tumors, it is likely that this size dependence will also show a similar trend.

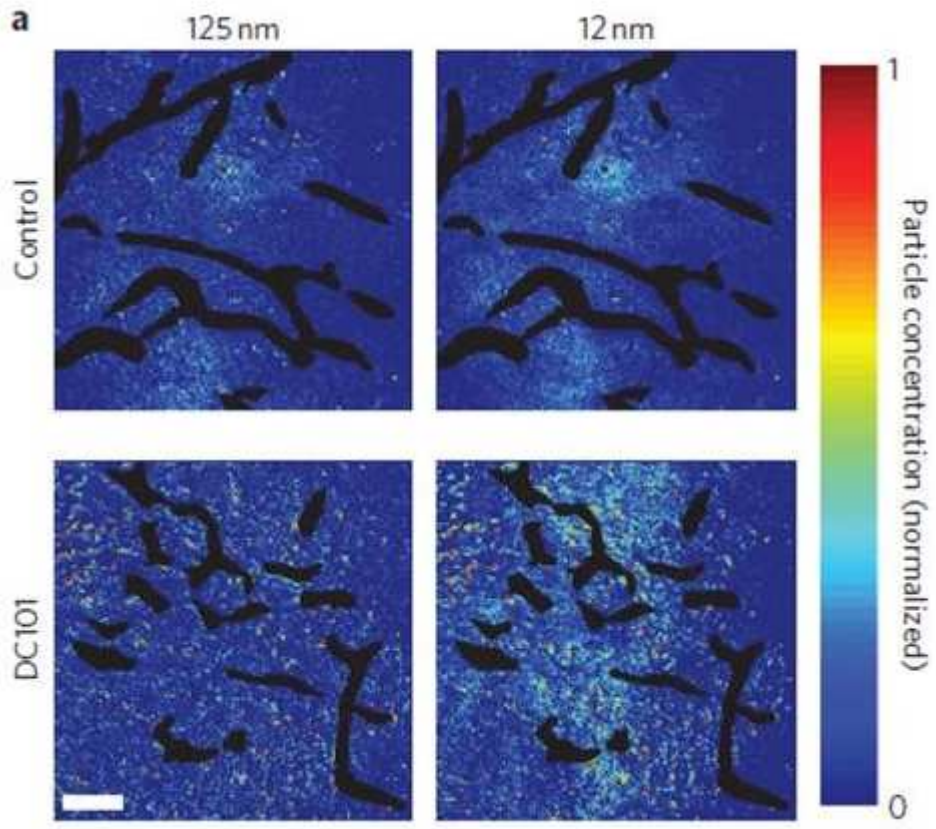

Figure 1-6. Effects of vascular normalization on nanoparticle delivery in tumors.

Nanoparticle penetration versus particle size in orthotopic 4T1 mammary tumors in response to normalizing therapy with DC101. Nanoparticle concentrations (denoted by pseudocolor) are relative to initial intravascular levels, with vessels shown in black. Normalization improves 12 nm particle penetration while not affecting 125 nm penetration. Scale bar, 100 mm. Reprinted with permission from [1].

1.4.4.2 Modifying tumor matrix to improve drug penetration

Tumor vessel normalization is an attractive strategy for enhancing the penetration of small molecules and macromolecules. Nonetheless, vascular normalization results in a reduction in the vascular pore size. To effectively utilize this technique for improving the delivery and penetration of NPs, the particle size of NPs has to be in the ~20 nm size range [408]. However, drug loading is severely compromised in such small particles, making these formulations impractical for *in vivo* use. Thus, alternative strategies to decrease IFP and to enhance intratumoral penetration of colloidal carriers are necessary. Altering the composition of the tumor ECM provides another route to improve the tumor tissue distribution of NPs. The tumor ECM can be modified by either using enzymes that degrade specific ECM components or by modifying the tumor-associated cells that directly affect the behavior of ECM components.

1.4.4.2.1 Tissue digesting enzymes

The tumor matrix is rich in collagen and hyaluronic acid [409], making them obvious targets for enhancing drug delivery. The effect of hyaluronic acid-digesting enzyme, hyaluronidase, was first reported by Maier *et al*. in patients with bladder cancer [410]. In their seminal studies, the authors found that co-administration of hyaluronidase with mitomycin-C significantly reduced the recurrence of bladder cancer in comparison to patients who received only the chemotherapeutic. Other groups later showed that the efficacy of chemotherapeutics could be enhanced by using hyaluronidase in multi-cellular spheroid models *in vitro* and in pre-clinical tumor models [411-414]. Brekken *et al.* were the first to show that intratumoral

injection of hyaluronidase decreased IFP in orthotopic osteosarcomas in mice without affecting the arterial pressure [415]. The resultant increase in transvascular gradient may have led to the observed enhancement in drug delivery. The same group later confirmed that periodic fluctuations in IFP brought about by hyaluronidase administration increased the delivery of antibodies [416]. Subsequently, the effect of hyaluronidase administration on the uptake and distribution of Caelyx^{TM} (pegylated liposomal doxorubicin hydrochloride) was measured [417]. Intratumoral administration of hyaluronidase led to an increase in tumor deposition of the formulation. More importantly, the distribution profile of the delivery system was altered. In the absence of the enzyme, liposomes were regionalized to the rim of the tumor. However co-administration of the enzyme led to increased penetration of the liposomes to the core of the tumor **(Figure 1-7)**. Recently, Provenzano *et al.* reported a novel mechanism that may operate in improving drug delivery in response to hyaluronidase administration [418]. The authors found that K-ras driven pancreatic tumors in genetically modified mice were nearly avascular. Systemic administration of pegylated hyaluronidase led to the opening up of previously dysfunctional blood vessels. This led to enhanced delivery and efficacy of co-administered gemcitabine. This is the first study to show that enzymatic ablation of tumor ECM can restore blood supply, leading to increased drug delivery [418].

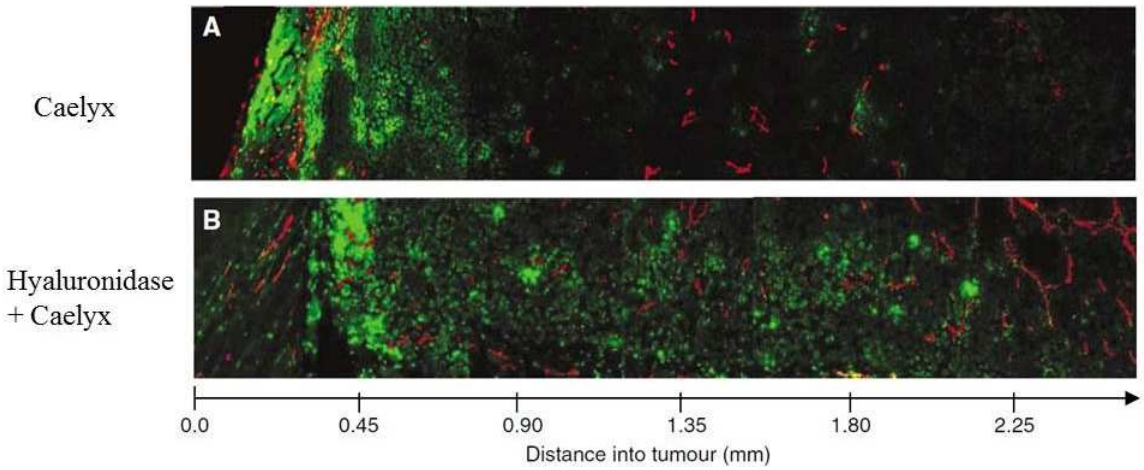

Figure 1-7. Distribution of liposomal doxorubicin in hyaluronidase treated osteosarcomas.

Distribution of liposomal doxorubicin in osteosarcoma xenografts treated with liposomal doxorubicin alone (16 mg kg^{-1}) (A) or liposomal doxorubicin combined with hyaluronidase (1500 U) (B). Representative images of doxorubicin (green) relative to capillaries (red) are presented from the rim to the center of the tumor sections. Reprinted with permission from [417].

The other ECM target for improving tumor penetration of chemotherapeutics is collagen. In an orthotopic osteosarcoma mouse model, Eikenes *et al.* showed that systemic administration of collagenase led to a rapid decline in tumor IFP, with only minor effects on the arterial blood pressure [419]. The resulting transcapillary gradient was maintained for nearly 24 hours. This led to enhanced delivery and penetration of a fluorescently-labeled antibody [419]. McKee *et al.* examined local injection of collagenase to improve the intratumoral distribution of an oncolytic virus [420]. Transfection of tumor cells with the virus was detected by expression of

green fluorescent protein (GFP). Without collagenase co-administration, the virus was localized in regions that lacked collagen. Consequently, GFP expression was found only in limited regions within the tumor. Co-injection of collagenase significantly improved the distribution of the virus. This was confirmed by extensive GFP expression over the entire tumor. It is interesting to note that the virus had a hydrodynamic diameter of 150 nm, a size comparable to that of many NP formulations reported in the literature. Zheng and co-workers reported similar results [421]. The authors found that intratumoral administration of collagenase led to improved distribution of Doxil® in head and neck tumor xenografts. Interestingly, collagenase activity was observed only following local injections [421].

The above study by Zheng *et al.* highlights some key issues [421]. First, the toxicity associated with the use of these tissue-degrading enzymes is an important issue. Both collagen and hyaluronic acid are ubiquitously expressed in the body [418]. They form important components of the ECM and are essential for the function of vital organs. Intratumoral administration of these enzymes may prevent systemic toxicity. However, many tumors that require chemotherapeutic intervention may not be accessible by such local treatment. Second, the improvements in drug transport achieved with ECM degradation are transient. Collagen and hyaluronic acid are replenished within 8-24 hours [419, 422]. Since NP accumulation in the tumor is a relatively rapid event (few hours), transient decrease in ECM levels will help improve NP delivery to tumors [215]. However, NP penetration within a tumor is a relatively slower event [423, 424]. Thus, the transient nature of this technique may not improve the tissue transport of NPs. One

possible strategy to overcome this problem is to immobilize the enzyme on the surface of NPs. This will ensure colocalization of NPs and the enzyme. Moreover, the passive targeting effect of NPs may limit the distribution and toxicity of the enzyme. An example of this approach was provided by Goodman *et al.*[425]. In that study, collagenase was physically adsorbed on the surface of polystyrene NPs. The adsorbed enzyme degraded collagen and improved the penetration of NPs in an *in vitro* multicellular spheroid model [425]. The study, however, did not examine the performance of this system *in vivo.* Rapid desorption of a physically adsorbed enzyme in the presence of plasma proteins may be a significant limitation of this approach. Covalent conjugation of the enzyme to the NP surface may overcome this limitation [426].

The choice of ECM component to be targeted for improving drug penetration is interesting. Collagenase administration has been unequivocally shown to increase drug penetration. However, there are conflicting reports regarding the utility of hyaluronidase for improving drug penetration [427]. In an interesting report, Netti *et al.* proposed that proteoglycans such as hyaluronic acid resemble “aqueous cages” [428]. These aqueous cages are passages through which the drug carrier can diffuse freely. Thus, eliminating these cages by degrading hyaluronic acid could hinder the transport of drug carriers. On the other hand, the solid collagen matrix may not offer a conducive environment for transport, and degrading collagen could, therefore, improve carrier distribution. The authors suggest that the amount of any ECM component does not dictate the magnitude of the effect it has

on transport resistance. The structural assembly and organization of the component could play a more important role [428].

1.4.4.2.2 Modifying stromal cells

In addition to degrading the tumor stroma, an interesting alternative is to inhibit the secretion of ECM components by the stromal cells. An elegant example of this hypothesis was shown by Olive *et al.* [429]. Using a genetically engineered mouse model, the authors determined that pancreatic cancers had very little vascular coverage and that drug delivery to these tumors was severely impeded. The hedgehog signaling pathway was constitutively active in tumor-associated stromal cells. This led to the secretion of large amounts of ECM components. The authors showed that concomitant administration of a hedgehog pathway inhibitor (IPI 926) greatly increased the delivery and therapeutic efficacy of gemcitabine. A very recent report showed the safety of the IPI 926 in phase I clinical trials [430].

In another study, treatment with losartan was shown to decrease collagen I synthesis by fibroblasts in carcinomas [431]. Those effects were brought about through inhibition of the activity of transforming growth factor β (TGF β). The decrease in collagen content was sustained for a period of two weeks in a dose-dependent manner. Decreased collagen content was associated with an increase in the tumor penetration of liposomal doxorubicin and an increased therapeutic response [431].

1.5 Conclusions

Development of resistance to multiple drugs is a key obstacle to achieving successful treatment outcomes in many cancers. Tumor cells overexpress efflux

transporters, which reduce intracellular drug accumulation and efficacy. NPs offer an attractive platform to overcome drug resistance. Many of the excipients used in fabricating NPs possess intrinsic efflux pump inhibitory activity. Intracellular distribution of NPs to specific loci in the cell, away from the activity of efflux pumps can also shield the encapsulated drug from transporters. An additional approach is to co-deliver specific inhibitors of transporter activity or function with the chemotherapeutic. However, poor intratumoral penetration of NPs limits their potential. Approaches that improve NP transport in tumors can significantly enhance their activity. Normalizing tumor vasculature has shown promising results with small molecules. Some NP formulations can also benefit from this approach. The field of ECM modification is relatively under-studied and holds tremendous potential for improving the therapeutic outcomes in hard-to-treat, avascular tumors.

1.6 Statement of the problem and hypothesis

Delivering chemotherapeutic agents in nano-sized carriers can potentially reduce the off-target distribution and increase the tumor accumulation of the drugs. However, the full potential of nanoparticle-based chemotherapy has not been realized yet. Several physiological barriers prevent the optimal performance of nanoparticles. In this thesis, we studied these barriers from the perspective of drug transport.

Transport of nanoparticles from the site of administration to the site of action can be considered to occur in three distinct steps: systemic distribution, intratumoral distribution and cell uptake. Inefficiencies in each step lead to

decreased accumulation of nanoparticles within tumor cells and compromised therapeutic efficacy. The goal of this research was to improve nanoparticle-based chemotherapy by enhancing the efficiency of each of these steps.

The specific aims for the thesis and their respective working hypotheses are as follows:

Specific aim 1: Examine the effect of vascular properties of tumors and physicochemical properties of nanoparticles on the drug targeting index of nanoparticles

We hypothesized that optimal drug targeting is achieved in a limited particle size range, and this particle size range depends on the vascular pore size of the tumor as well as of the site of toxicity. (*Chapter 2*)

Specific aim 2: Determine the effect of fibrinolytic therapy on anti-cancer efficacy of nanoparticles

We hypothesized that treatment with a fibrinolytic enzyme will improve the intratumoral distribution and anti-cancer efficacy of nanoparticles. (*Chapter 3*)

Specific aim 3: Evaluate the performance of tylocrebrine encapsulated in EGFR-targeted nanoparticles

The central hypothesis in this chapter was that encapsulation of tylocrebrine in EGFR-targeted nanoparticles will improve the drug targeting index by simultaneously enhancing the tumor cell uptake (and potency) and reducing the brain penetration of tylocrebrine. (*Chapter 4*)

Chapter 2 A Pharmacokinetic Model for Quantifying the Effect of Vascular Permeability on the Choice of Drug Carrier: A Framework for Personalized Nanomedicine[2]

[2] This chapter is published elsewhere [527]. Reproduced with permission.

2.1 Summary

Drug carriers in the ~100 nm size range are of considerable interest in the field of cancer therapy because of their ability to passively accumulate in tumors. Tailoring the physicochemical properties of these carriers to individual patient requirements will help exploit their full therapeutic potential. Here we present a pharmacokinetic model to explain how vascular physiology could be used to guide the optimal choice of specific formulation parameters. We find that in order to maximize the benefit-to-risk ratio, nano systems should be confined to a specific particle size range. The optimal particle size range is dictated by the vascular pore size of not only the tumor tissue but also of the normal organs. Additionally, the duration of drug release is a key variable that can be used to maximize the therapeutic benefit of nanomedicine. Our model further suggests that the enhanced permeability and retention (EPR) effect is not necessarily a universal outcome for every nano carrier in every tumor model but will only be observed for nanoparticles of a specific size range. This optimal size range, in turn, is governed by the vascular physiology of the tumor and of non-target organs.

2.2 Introduction

Cytotoxic anticancer therapies are often characterized by severe dose-limiting toxicities, resulting from their poor discrimination between tumor and normal tissues. These side effects can be significantly reduced by delivering these drugs in nano sized carriers [432]. Nanoparticles (NPs) primarily extravasate from porous blood vessels found in tumors, thereby reducing drug exposure to non-target tissues. Additionally, because of underdeveloped lymphatic drainage, NPs are not cleared quickly from the tumor. This phenomenon, known as the enhanced permeability and retention (EPR) effect [174], has become the principal basis for the use of nano drug delivery systems for anticancer therapies [433].

Recent studies suggest that, in addition to patient-specific tailoring of anticancer drugs and drug doses [434, 435], there is a need to develop personalized drug carriers [436, 437]. In much the same way that tumor cell signatures can dictate the choice of drug, characteristics of the tumor blood vessels can affect the choice of drug carrier. Multimodal imaging techniques enable noninvasive characterization of tumor and normal organ blood vessels [401, 438, 439]. Moreover, the availability of facile synthetic approaches allows tailoring of physicochemical properties of drug carriers for specific needs [440, 441]. However, there are currently no models available for guiding the selection of an optimal drug carrier based on particular tumor characteristics. The selection criterion for nano drug carriers is unique because it is expected that these systems not only enhance drug efficacy but also mitigate toxicity [442, 443]. Earlier efforts in this area have focused mainly on the deposition of NPs in the tumor and have

not considered their distribution in normal tissues where toxic effects may occur. Some normal organs including liver and spleen also have porous blood vessels (sinusoidal capillaries) that are permeable to NPs. Also, much of the previous modeling work has dealt with tracking only the NPs and not the free drug, whose release commences as soon as the NPs are introduced in systemic circulation [444-446].

We report here a semi-physiologically based pharmacokinetic model to describe the disposition of NPs as well as the released drug in tumors and in normal organs that also have porous blood vessels (**Figure 2-1**) [447-449]. We use a metric called the drug targeting index (DTI) to measure the performance of nano delivery systems [450]. The DTI considers both efficacy and toxicity, and enables a comparison of the pharmacokinetic performance of NPs with that of the free drug and of two different delivery systems. We find that two critical physicochemical properties of the drug carrier, viz. particle size and drug release rate, play an important role in determining the DTI of nano delivery systems. However, the optimal particle size and drug release rate are dictated by vascular characteristics of the tumor and normal organs. Thus, our work describes quantitatively how individual vascular physiology can impact the choice of the drug carrier. It is expected that the results of our modeling studies will provide a framework for the future development of personalized nano therapeutics.

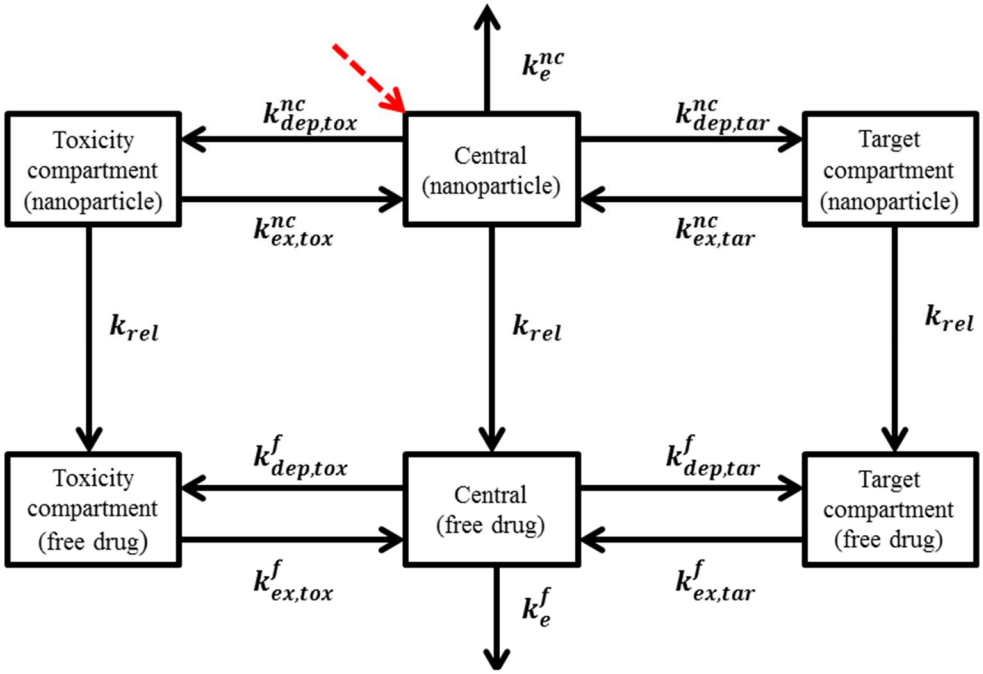

Figure 2-1. Construction of pharmacokinetic model

The model consists of 6 compartments, 3 compartments representing the nanoparticle-encapsulated drug and 3 compartments representing the free drug. The dose is administered in the central compartment and is shown by the red dotted arrow. The tumor is considered to be the target compartment and a normal organ is considered to be the toxicity compartment.

2.3 Methods

2.3.1 Drug targeting index

A nanoformulation can enhance the usefulness of a drug in two ways. First, it can increase the exposure of free drug to sites of action in target tissues following

release from the NPs, compared to the exposure that occurs when drug is administered in its free form. Second, the nanoformulation can reduce drug exposure to tissues associated with toxicity. A simple metric that combines these benefits is the drug targeting index, DTI, defined as[450]

$$DTI = \frac{\left(\frac{AUC_{tar}^{f}}{AUC_{tox}^{f}}\right)_{nano}}{\left(\frac{AUC_{tar}^{f}}{AUC_{tox}^{f}}\right)_{free}} \tag{1}$$

Where the subscripts *free* and *nano* refer to drug that is administered in its free form, and drug that is administered encapsulated in NPs, respectively

$$AUC_{i}^{f} = \int_{0}^{\tau} C_{i}^{f}\, dt \qquad i = tar, tox; \tag{2}$$

with C_i^f referring to the concentration of free drug in the target (*tar*) or toxicity associated (*tox*) tissues. NP associated drug is assumed to be non-active. The numerator in Eq. (1) corresponds to the drug administered as a NP formulation, while the denominator corresponds to drug administered in its free form. It is assumed without loss of generality that in either case, drug is administered as a bolus at time zero, and before that the body is void of drug. Provided pharmacokinetics are linear, the doses used under the two circumstances cancel out when ratios are taken and hence do not affect DTI.

2.3.2 Pharmacokinetic model

Only spherical monodisperse NPs are considered in the present work. We also assume that the shape, size and surface properties of the carrier remain constant while it is in circulation. Hence, the pharmacokinetic properties of the NPs are time independent. NPs are also assumed to release drug at the same first order rate within all compartments. Finally, we assume that exchange of free drug across porous capillaries is rapid and is rate-limited by perfusion to that compartment.

A six compartment pharmacokinetic model, illustrated in **Figure 2-1**, has been chosen to account for the pharmacokinetic behavior of NPs and free drug. The central compartment represents NPs or drug in the vasculature (plasma), while the peripheral compartments represent parenchyma in organs involved in drug response and toxicity. All compartments are assumed to be well stirred. While a more general multicompartmental model could be formulated, the results are insensitive to such detail. It is important however that the target and toxicity associated tissues be separate.

The concentration-time profiles of NPs in the central, target and toxicity compartments are generated using the mass balance equations listed below. NPs and drug are assumed to exchange between compartments with linear kinetics (constant clearance values), and with defined volume parameters for all compartments. Elimination of NPs and drug is assumed to be first order and from the central compartment. Free drug is assumed to be released by first order kinetics into the compartment in which its NP resides at the time.

The clearance and volume parameters for free drug are taken as given, since they would be assessed in independent pharmacokinetic studies. Since fluid flow into and out of organ parenchyma is generally the same, we may take the deposition and exit clearances of free drug to be equal. However, NPs tend to be blocked from flow through tissue parenchyma by the interstitial matrix, hence their deposition and exit clearances will differ.

Parameter definitions are listed in **Table 2-1**. In the following equations, the subscript "*i*" designates the compartment (*i*=*c*, *tar*, *tox* and *c, tar and tox* indicate the central, target and toxicity compartments, respectively). The superscripts "*nc*" and "*f*" signify NP-encapsulated drug and free drug, respectively. For nanoencapsulated drug, the mass balances are

$$\frac{dC_c^{nc}}{dt} = \frac{\sum_{i=tar,tox} Cl_{ex,i}^{nc}\, C_i^{nc}}{V_c^{nc}} - \frac{\sum_{i=tar,tox} Cl_{dep,i}^{nc}\, C_c^{nc}}{V_c^{nc}} - (k_{rel} + k_{elim}^{nc})C_c^{nc} \qquad (3)$$

$$\frac{dC_i^{nc}}{dt} = \frac{Cl_{dep,i}^{nc}}{V_i^{nc}}\, C_c^{nc} - \left(\frac{Cl_{ex,i}^{nc}}{V_i^{nc}} + k_{rel}\right) C_i^{nc}; \qquad i = tar, tox; \qquad (4)$$

The mass balances for free drug are given by

$$\frac{dC_c^{f}}{dt} = \frac{\sum_{i=tar,tox} Cl_i^f C_i^f}{V_c^f} - \frac{\sum_{i=tar,tox} Cl_i^f C_c^f}{V_c^f} + \left(\frac{k_{rel} V_c^{nc}}{V_c^f}\right) C_c^{nc} - \frac{Cl_{elim}^f}{V_c^f} C_c^f \qquad (5)$$

$$\frac{dC_i^{f}}{dt} = \frac{Cl_i^f}{V_i^f}\left(C_c^f - C_i^f\right) + \left(\frac{k_{rel} V_i^{nc}}{V_i^f}\right) C_i^{nc}; \qquad i = tar, tox; \qquad (6)$$

Because DTI is dose independent, the initial condition may be taken as $C_c^{nc}(0) = 1$ when drug is administered in NPs, or $C_c^f(0) = 1$ when drug is administered in its free form. All other compartments start with zero concentration.

2.3.3 Exchange between the central compartment and target and the toxicity compartments

The deposition and exit clearances of NPs into and out of well stirred compartments depend on blood flow, Q_i, and the corresponding intrinsic clearance values, according to[451]

$$Cl_{dep,i}^{nc} = \frac{Q_i Cl_{dep,i}^{int}}{Q_i + Cl_{dep,i}^{int}} \qquad i = tar, tox \qquad (7)$$

$$Cl_{ex,i}^{nc} = \frac{Q_i Cl_{ex,i}^{int}}{Q_i + Cl_{ex,i}^{int}} \qquad i = tar, tox \qquad (8)$$

Both blood flow and intrinsic clearance correspond to capillary beds perfusing the relevant tissues. Intrinsic clearances are determined using Starling's approximation, as described by Chauhan *et al.* [1] In that model, exchange of NPs between compartments occurs by convection and diffusion across porous capillary walls separating blood from parenchyma, with pores considered to be of constant radius, R_i, and length, L_i. The capillary surface area and porosity (#pores/area) are designated by S_i and γ_i respectively.

The effect of NP size on diffusion and convection in the pores depends on the NP's size and the pore radius [452]. For spherical NPs of uniform radius, *a*, the relevant parameter is

$$\lambda_i = \min\left(\frac{a}{R_i}, 1\right) \qquad i = tar, tox \tag{9}$$

which is bounded above by unity. Transport is not possible for NPs with larger diameter than the pores. In the following, we drop the subscript *i = tar, tox* for notational clarity, realizing that in calculations, parameter values are compartment specific and the subscripts must be restored. A nonzero value of λ indicates that transport of a NP across a pore will be hindered partially by frictional interactions between the particle and the pore wall. The hindrance factors *H(λ)* and *W(λ)* corresponding, respectively, to diffusion and convection are determined according to the recently published correlations [452]

$$H = 1 + \frac{9}{8}\,\lambda.\ln\lambda - 1.56034\lambda + 0.528155\,\lambda^2 + 1.91521\lambda^3 - 2.81903\lambda^4 + 0.270788\lambda^5 + 1.10115\lambda^6 - 0.435933\lambda^7 \tag{10}$$

$$W = (1-\lambda)^2\left(\frac{1 + 3.867\,\lambda - 1.907\lambda^2 - 0.834\lambda^3}{1 + 1.867\lambda - 0.741\lambda^2}\right) \tag{11}$$

The hindrance factor *H* is used in the following equation for diffusive permeability of the capillary wall:

$$K = \frac{\gamma HD}{L} \tag{12}$$

where

$$D = \frac{k_B T}{6\pi\mu a} \tag{13}$$

is the unhindered Stokes-Einstein diffusion coefficient of the NPs, In calculating *D*, k_B is the Boltzmann constant, *T* is absolute body temperature and *μ* is the viscosity of vascular fluid in the pores. Convective transport across the capillary in response to transwall pressure gradient is accounted for by taking the product of the hydraulic permeability of the vessel wall,

$$L_p = \frac{\gamma R^2}{8\mu L} \tag{14}$$

and the reflection coefficient, $\sigma = 1 - W$, which quantifies the selectivity of the pores against NP convection.

The relative importance of convection compared to diffusion of NPs across capillary walls for a given pressure gradient, $P_{cap} - P_{if}$, between the capillary lumen and the interstitial fluid, is determined by the Peclet number,

$$Pe = \frac{L_p(1-\sigma)(P_{cap} - P_{if})}{K} \tag{15}$$

Combining diffusive and convective transport of NPs, and considering the total surface area, *S*, of capillaries perfusing a compartment (tissues/organs), exchange clearance parameters between capillaries and interstitium of a compartment are given by

$$Cl_{dep}^{int} = \frac{L_p(1-\sigma)S(P_{cap} - P_{if})}{1 - e^{-Pe}} = \frac{PeKS}{1 - e^{-Pe}} \tag{16}$$

$$Cl_{ex}^{int} = \frac{L_p(1-\sigma)S(P_{cap} - P_{if})}{e^{Pe} - 1} = \frac{PeKS}{e^{Pe} - 1} \tag{17}$$

Evidently from Eqs. (7) - (17), compartmental clearances depend on physiological variables such as blood flow, vascular pore size, pore surface area, and pressure differences across the blood vessel wall, and on the size of the NPs. Calculated values of clearance are used as input functions in the rate equations of the pharmacokinetic model.

Notice that $Cl_{dep}^{int} = e^{Pe} Cl_{ex}^{int}$, which suggests that when pressure in the capillaries exceeds that in the tissue parenchyma such that *Pe* >> 0, convection dominates diffusion across the pore walls and deposition is strongly favored over exit, and the “ex” terms in Eqs. (3) and (4) can be dropped.

2.3.4 Further Assumptions

In the simulations carried out below, NPs were assumed to be administered to the central compartment, which was also assumed to contain the sites for free drug elimination. We fit values reported in literature for PEG (5000 Da)-functionalized, silica-coated CdSe quantum dots of various sizes [1] to a polynomial (**Figure 2-2**), which was used in the simulations. While elimination of NPs from circulation can generally be through renal filtration or macrophage uptake, the diameter of NPs studied here was above the renal filtration cutoff of 5.5 nm [453]. Hence, in this model, we assumed that elimination of NPs is only by uptake into macrophages.

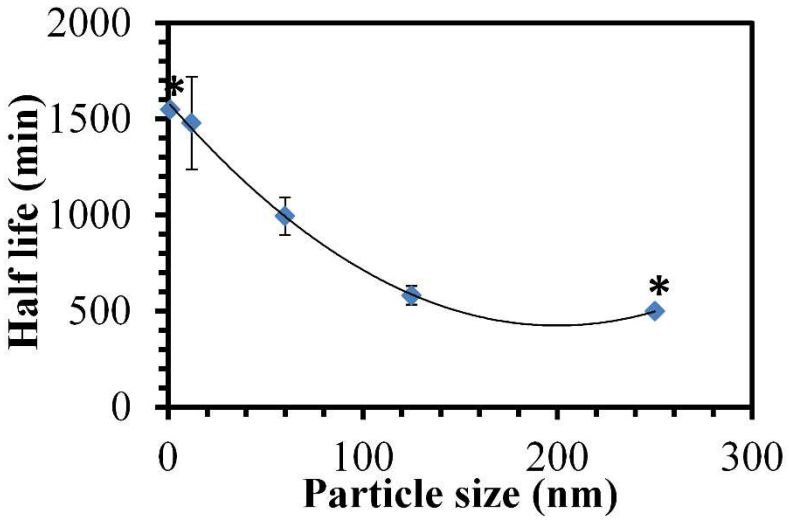

Figure 2-2.Half-life of nanoparticles in the central compartment as a function of particle size

The data points were extracted from previously reported values [1]. A curve was fitted to this data and the equation describing the curve is included in the list of equations. * indicates data points were extrapolated.

NPs that are phagocytosed by macrophages deposit in the liver [361]. However, a quantitative estimation of the NP deposition through this process is difficult. Therefore, we assumed that NPs that are taken up by the macrophages are eliminated from the body and do not deposit in the toxicity compartment. Deposition of NPs in the toxicity compartment was assumed to occur only through the capillary fenestrae.

2.3.5 Calculation of a closed loop solution of drug targeting index

In order to develop a quantitative relation between NP properties, physiological parameters and DTI, we solve the pharmacokinetic model and develop an expression for DTI involving only rate constants. We limit ourselves here to the case where deposition of NPs dominates exit of NPs, i.e. *Pe* >> 0 in both the target and toxicity compartments. Eqs. (3)-(6), with terms corresponding to NP exit from the target and toxicity compartments dropped, can be rewritten in terms of rate constants using the generic identification $k = CL/V$. The result is

$$\frac{dC_c^{nc}}{dt} = -\sum_{i=tar,tox} k_{dep,i}^{nc}\, C_c^{nc} - (k_{rel} + k_{elim}^{nc}) C_c^{nc} \tag{18}$$

$$\frac{dC_i^{nc}}{dt} = k_{dep,i}^{nc}\, C_c^{nc} - k_{rel} C_i^{nc}\,; \qquad i = tar, tox \tag{19}$$

$$\frac{dC_c^{f}}{dt} = \sum_{i=tar,tox} k_i^f \left(C_i^f - C_c^f\right) + \left(\frac{V_c^{nc}}{V_c^f}\right) k_{rel} C_c^{nc} - k_{elim}^f C_c^f \tag{20}$$

$$\frac{dC_i^f}{dt} = k_i^f \left(C_c^f - C_i^f\right) + \left(\frac{V_i^{nc}}{V_i^f}\right) k_{rel} C_i^{nc}; \qquad i = tar, tox \tag{21}$$

Integration of these equations, with proper initial conditions, will lead to a set of simultaneous equations for relevant AUCs, which can then be introduced into Eq. (1), with a resulting expression for DTI in terms of the system parameters. This route is tedious and not necessarily revealing. A more straightforward and intuitive procedure is to consider the average number (expected value) of visits that a drug molecule makes to the target and toxicity compartments when drug is administered free or in a nanocarrier. This average is proportional to the AUC of free drug in that compartment. Hence, we may replace Eq. (1) with

$$DTI = \frac{\left(\frac{< \#visits >_{tar}}{< \#visits >_{tox}}\right)_{nano}}{\left(\frac{< \#visits >_{tar}}{< \#visits >_{tox}}\right)_{free}} = \frac{(< \#visits >_{tar})_{nano} / (< \#visits >_{tar})_{free}}{(< \#visits >_{tox})_{nano} / (< \#visits >_{tox})_{free}} \tag{22}$$

To begin, we calculate the average numbers (expected values) of visits to the target and toxicity compartments for drug administered that is administered in its free form. We consider first the target compartment. Each visit to that compartment will be preceded by a visit to the central compartment. The probability that such a visit will occur without drug being eliminated first is $p = k_{dep,tar}^f / \left(k_{dep,tar}^f + k_{elim}^f\right)$, and the probability that there will be exactly *n* such

visits before elimination is $p^n(1-p)$. Thus the expected number of visits is given by

$$(< \#visits >_{tar})_{free} = (1-p)\sum_{n=1}^{\infty} np^n = \frac{p}{1-p} = \frac{k^f_{dep,tar}}{k^f_{elim}} \tag{23}$$

and by similar reasoning,

$$(< \#visits >_{tox})_{free} = \frac{k^f_{dep,tox}}{k^f_{elim}} \tag{24}$$

Now let F_{tar}, F_{tox} and F_c denote the fractions of drug that are released from the NPs into the target, toxicity and central compartments, respectively. Since drug is not removed from the toxicity compartment, drug molecules released from NPs into the central and toxicity compartments will look, to the target compartment, like drug administered in its free form, and these molecules will, on average, visit the target compartment $(< \#visits >_{tar})_{free}$ times. Drug released from NPs into the target compartment will visit that compartment once before returning to the central compartment, and thereafter it will return to the target compartment, on average, $(< \#visits >_{tox})_{free}$ times. We therefore assert that

$$(< \#visits >_{tar})_{nano} = F_{tar}\left[1 + (< \#visits >_{tar})_{free}\right] + (F_{tox} + F_c)(< \#visits >_{tar})_{free}$$

and by similar steps,

$$(< \#visits >_{tox})_{nano} = F_{tox}\left[1 + (< \#visits >_{tox})_{free}\right] + (F_{tar} + F_c)(< \#visits >_{tox})_{free}$$

Introducing these expressions into Eq. (A.5) and rearranging,

$$\mathrm{DTI} = \frac{1 + \left(\frac{F_{tar}}{F_{tar} + F_{tox} + F_c}\right)\frac{1}{(< \#visits >_{tar})_{free}}}{1 + \left(\frac{F_{tox}}{F_{tar} + F_{tox} + F_c}\right)(< \#visits >_{tox})_{free}} \tag{25}$$

We now derive expressions for F_{tar}, F_{tox}, and F_c. Here the assumption that NPs, once having entered the target (or toxicity) compartment remain there without back transfer to the central compartment (*Pe* >> 0), simplifies matters. Following injection at time 0, the fraction of NPs remaining in the central compartment at time *t* will be $\exp(-k_{tot}^{nc}t)$, where $k_{tot}^{nc} = k_{dep,tar}^{nc} + k_{dep,tox}^{nc} + k_{elim}^{nc}$. The fraction of drug remaining in these NPs at that time will be $\exp(-k_{rel}t)$. Since $\int_0^\infty k_{tot}^{nc}\exp(-k_{tot}^{nc}t)dt = 1$ accounts for the final disposition of of all the NPs, the fraction of NPs transferred to the target compartment will be $\int_0^\infty k_{dep,tar}^{nc}\exp(-k_{tot}^{nc}t)dt = k_{dep,tar}^{nc}/k_{tot}^{nc}$, and the fraction of drug released into the target compartment will be

$$F_{tar} = \int_0^\infty k_{dep,tar}^{nc}\,\mathrm{e}^{-k_{tot}^{nc}t}\,\mathrm{e}^{-k_{rel}t}dt = \frac{k_{dep,tar}^{nc}}{k_{tot}^{nc} + k_{rel}} \tag{26}$$

Similarly,

$$F_{tox} = \frac{k_{dep,tox}^{nc}}{k_{tot}^{nc} + k_{rel}} \tag{27}$$

At any time, the fraction of drug still remaining in the NPs in the central compartment that will be released will be

$$F_c = \frac{k_{rel}}{k_{tot}^{nc} + k_{rel}} \tag{28}$$

Combining Eqs. (25)-(28) and rearranging, we obtain Eq. (29). This relatively simple result relies in the assumed unidirectional transfer or NPs to the target and toxicity compartments from the central compartment, and the assumption that free drug is eliminated only from the central compartment.

$$DTI = \frac{1 + k_{elim}^{f}\left(\frac{k_{dep,tar}^{nc}/k_{dep,tar}^{f}}{k_{dep,tar}^{nc} + k_{dep,tox}^{nc} + k_{rel}}\right)}{1 + k_{elim}^{f}\left(\frac{k_{dep,tox}^{nc}/k_{dep,tox}^{f}}{k_{dep,tar}^{nc} + k_{dep,tox}^{nc} + k_{rel}}\right)} \tag{29}$$

Where $k_{dep,tar}^{f} = CL_{dep,tar}^{f}/V_c^{nc}$ and $k_{dep,tox}^{f} = CL_{dep,tox}^{f}/V_c^{nc}$ are rate constants associated with deposition on NPs into the target and toxicity compartments, respectively.

2.4 Results and discussion

2.4.1 Definition of DTI

The DTI, which quantifies the overall benefit of using a nanoformulation over free drug, is a ratio of ratios, which can be interpreted as a multiplier for the

therapeutic index of the drug due to nanoencapsulation [450]. A large DTI can result from improved targeting to the target compartment (here the tumor), reduced exposure of the toxicity compartment (here the "normal" organs), or both. For the model depicted in **Figure 2-1**, with all transfers assumed to be first order, and neglecting back transfers of NPs from the tumor and normal organs to blood, a closed form solution for DTI is obtained (shown in Eq. 29).

According to Eq. 29, DTI increases when NPs are more rapidly transferred to the tumor than to normal organs (increasing $k_{dep,tar}^{nc}/k_{dep,tox}^{nc}$), when free drug enters the normal tissues more rapidly than into tumor (increasing $k_{dep,tox}^{f}/k_{dep,tar}^{f}$), with increasing elimination rate of free drug (k_{elim}^{f}), and with decreasing rate of drug release from the NPs (k_{rel}).

2.4.2 Effect of vascular pore size and pore fraction of the target compartment

The EPR effect exists because of the porous nature of tumor vasculature. Porosity is highly heterogeneous and depends on the type, size and location of the tumor [454]. Inter- and intra-patient differences can have a significant impact on the tumor accumulation of NPs. To examine these effects, four different tumor vascular pore sizes (100, 200, 300 and 600 nm) were studied (the tumor vascular pore size in humans has not been studied rigorously; however, extensive work with mouse xenograft models of human tumors have shown that the tumor vascular pore size can vary from 100 nm-1 μm) [186, 454]. The pore size of the toxicity compartment (75 nm), rate constant for drug release from NPs ($8x10^{-5}$ s^{-1}), and

fraction of the tumor vasculature occupied by the pores (5%) were held constant. We used Starling's approximation to model the effect of the size of pores and pore fraction on the NPs' pharmacokinetics [1]. Although the interstitial fluid pressure can be affected by the difference in the blood vessel porosities [116], in our calculations we assumed that interstitial fluid pressures are independent of pore size. Detailed transport models for NPs can be refined within the framework of the general pharmacokinetic model of **Figure 2-1.**

We first determined the deposition clearance of NPs into the tumor as a function of particle size at various tumor vascular pore sizes (**Figure 2-3 A**). (Deposition clearance is converted to the deposition rate constant upon division by the central compartment volume.) Regardless of the pore size, the smallest NPs show the highest deposition clearance in the tumor. Also, the tumor deposition clearance of NPs increases with increasing vascular pore size. **Figure 2-3 B** shows the deposition clearance of NPs in the toxicity compartment. In our model, we assumed that the toxicity compartment, liver for example [455], is characterized by pores that are permissive to NP entry [447, 449]. However, the volume of this compartment and its blood supply are assumed to be larger than those of the tumor compartment. The deposition clearance for NPs in the toxicity compartment followed the same trend as those seen in the tumor.

Although deposition clearance provides vital mechanistic information about the ease of NP accumulation into the two peripheral compartments, this metric provides a very limited description of the overall pharmacokinetics of the drug carrier or the released drug. To assess the on-target exposure to the drug, we

calculated the area under the curve (AUC) of released drug in the target compartment (**Figure 2-3 C**). Though the deposition clearance of the smallest particles was the highest, this did not translate into the highest intratumoral AUC. For all pore sizes, the AUC was maximal at an intermediate particle size. This intermediate particle size (~70 nm) was close to the pore cutoff size of the toxicity compartment. The DTI profiles (**Figure 2-3 D**) show that in addition to maximal on-target accumulation, intermediate sized NPs also showed minimum off-target accumulation.

The larger toxicity compartment can strongly affect the deposition of NPs in the smaller target compartment. The availability of 20 nm NPs for deposition in the toxicity compartment and a higher blood supply to the toxicity compartment predisposes a large fraction of these NPs to be deposited in the toxicity compartment. Consequently, the fraction available for deposition in the tumor is low. On the other hand, the deposition clearance of 70-nm NPs in the toxicity compartment is close to zero, rendering a higher fraction available for deposition in the tumor. Thus, 70-nm NPs have a higher targeted bioavailability in the tumor as compared to the 20-nm NPs. This translates into greater deposition of 70 nm NPs in the tumor and a higher AUC for the free drug.

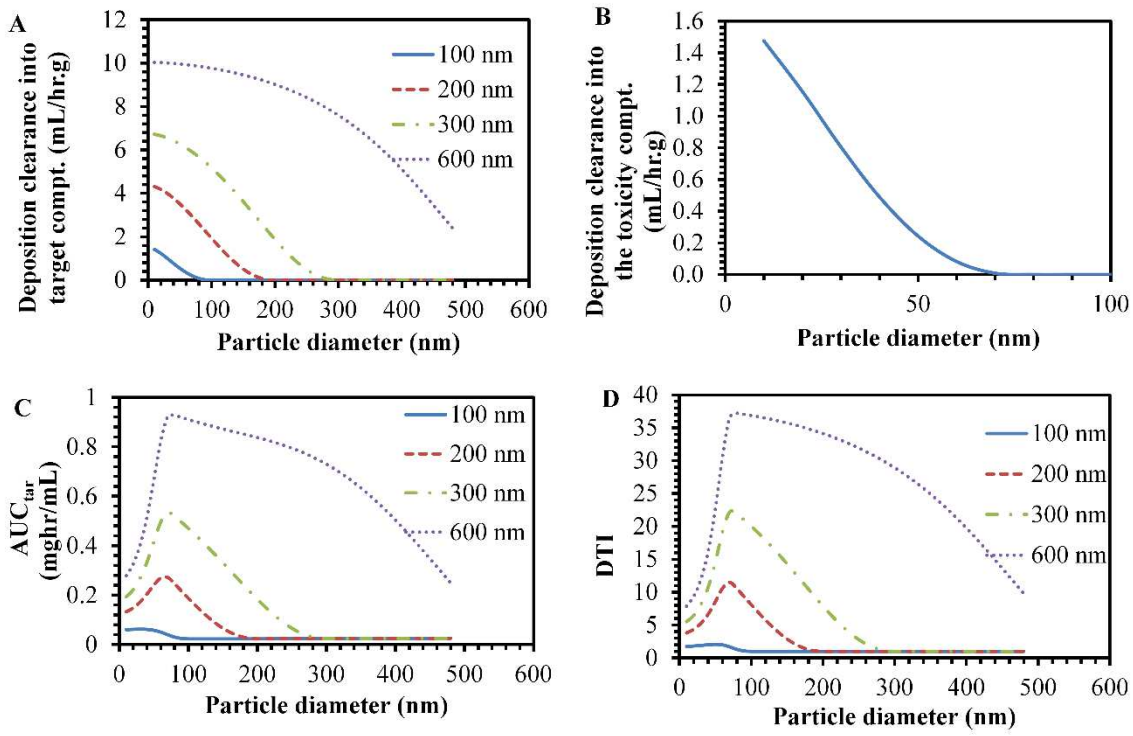

Figure 2-3. Effect of vascular pore size of the target compartment

(A) Deposition clearance of nanoparticles in the target compartment. (B) Deposition clearance of nanoparticles in the toxicity compartment. (C) AUC of the free drug in the target compartment. (D) DTI of nanoparticles of different sizes. The legend in A, C and D indicates the diameter of the pores in the tumor vasculature.

Longer retention and slower venous drainage of 70 nm NPs in comparison with 20 nm NPs can also result in a higher AUC. However, this is not likely. In our model, elimination clearance of NPs from the tumor compartment, though size-dependent, was very low. In fact, the decline in NP encapsulated drug concentration from the tumor compartment was due to release of the drug from NPs. This decrease is identical for all particle sizes (**Figures 2-4 A-D**).

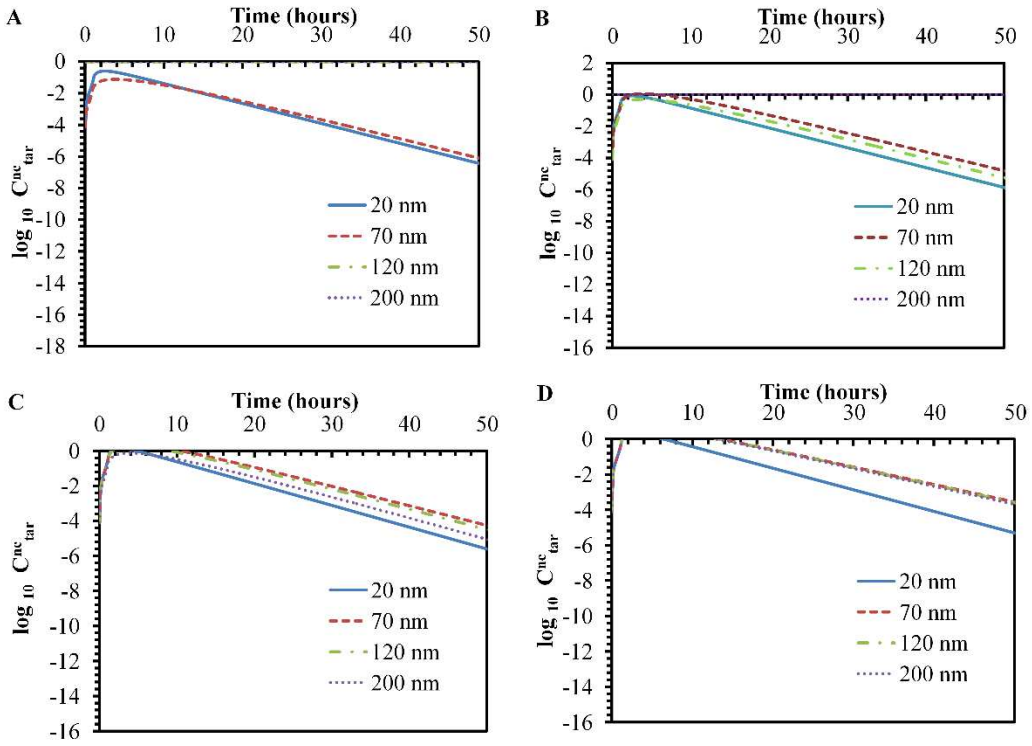

Figure 2-4. Concentration-time profiles of nanoparticles in the target compartment on a semi-log scale

The target compartment was assumed to have a pore size of (A) 100 nm, (B) 200 nm, (C) 300 nm, and (D) 600 nm. The figure legends indicate the size of nanoparticles.

Above a particle size of 70 nm, deposition clearance into the toxicity compartment is zero. On the other hand, deposition clearance into the target compartment either decreases or remains constant as the particle size increases. Above 70 nm, the deposition clearance and the circulation half life of NPs dictate NP accumulation in the target compartment. These differences are evident in the concentration-time profiles of different size NPs in tumors with different pore sizes.

For example, for a pore size of 300 nm (**Figure 2-5 A**), there is an appreciable difference in the concentration-time profile of 70 nm and 120 nm NPs. However, for a pore size of 600 nm (**Figure 2-5 B**), the concentration-time profiles of 70 and 120 nm NPs virtually overlap.

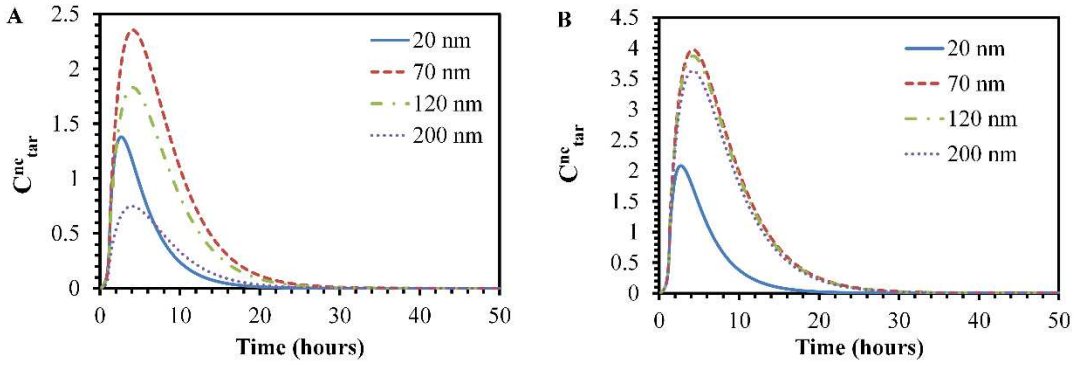

Figure 2-5. Concentration-time profiles of nanoparticles in the target compartment

The target compartment was assumed to have a pore size of (A) 300 nm and (B) 600 nm. The figure legends indicate the diameter of nanoparticles.

In addition to the vascular pore size, vascular pore fraction can also affect the degree of porosity. We modeled the effect of varying the vascular pore fraction of the target compartment. These results are summarized in **Figure 2-6 A-C**. The tumor AUC of the free drug and DTI increased with increasing pore fraction. However, similar to our previous results, the highest tumor AUC and DTI are achieved for NPs having a particle size that is close to the vascular pore size of the toxicity compartment.

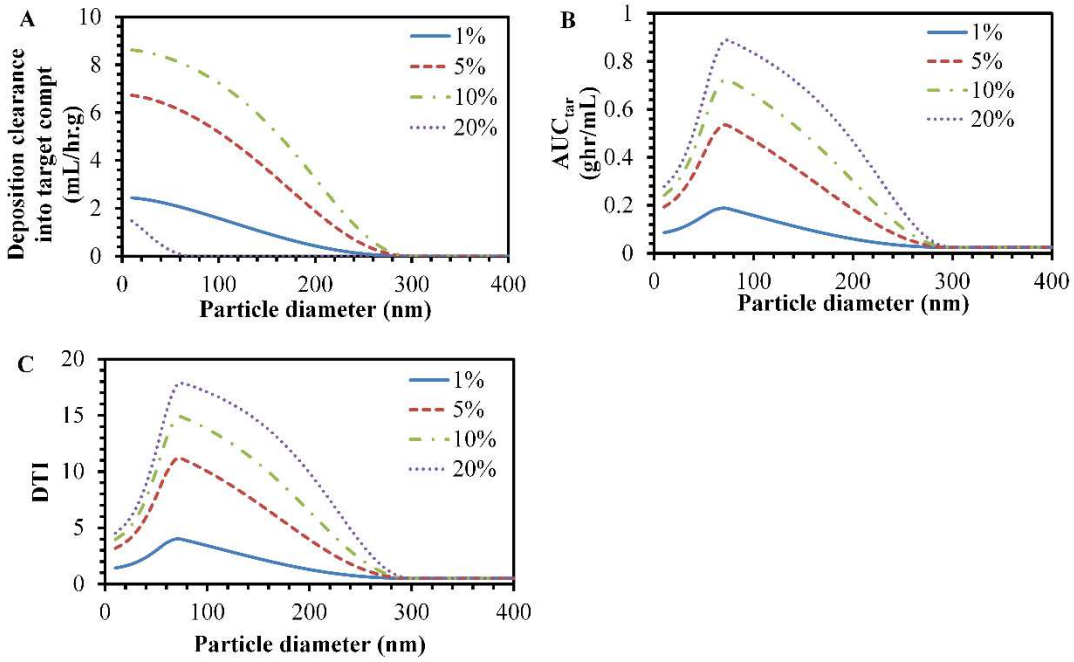

Figure 2-6. Effect of vascular pore fraction of the target compartment

(A) Deposition clearance of nanoparticles in the target compartment, (B) AUC of the free drug in the target compartment, (C) DTI of various sized nanoparticles. Figure legend indicates the fraction of the tumor blood vessel surface area occupied by pores.

Our data thus suggests that the optimal particle size depends on the vascular characteristics of both the toxicity and target compartments. In agreement with previous reports, a small particle size is desirable for maximal on-target effect [1, 424]. However, there is a lower limit to the particle size, and this is dictated by the pore size of the toxicity compartment. On the other hand, the highest particle size

at which the maximum on-target effect is maintained is a function of the pore size of the target compartment and the circulation half-life of the NPs. Thus, patients with highly porous tumors are better candidates for treatment with NPs. For tumors with smaller pore sizes or lower pore fractions, a careful consideration of the vascular pore size of the toxicity compartment(s) is necessary to minimize off-target toxicity.

2.4.3 Effect of the vascular pore size of the toxicity compartment

Results from the previous section show that the site of toxicity plays an important role in determining the optimal particle size range. The major site of toxicity differs from one drug class to another. Hence, the optimal particle size range for the nano-carrier also depends on the drug of interest. We modeled the effect of varying the vascular pore size of the toxicity compartment. We evaluated pore sizes of 20, 75, 150 and 300 nm. The pore size (300 nm) and pore fraction (5%) of the target compartment and the rate constant for drug release from NPs ($8x10^{-5}$ s^{-1}) were held constant.

NP deposition clearance into the tumor is unaffected by changes in pore size of the toxicity compartment (**Figure 2-7 A**). The deposition clearance of NPs in the toxicity compartment increases with increasing pore size (**Figure 2-7 B)**.

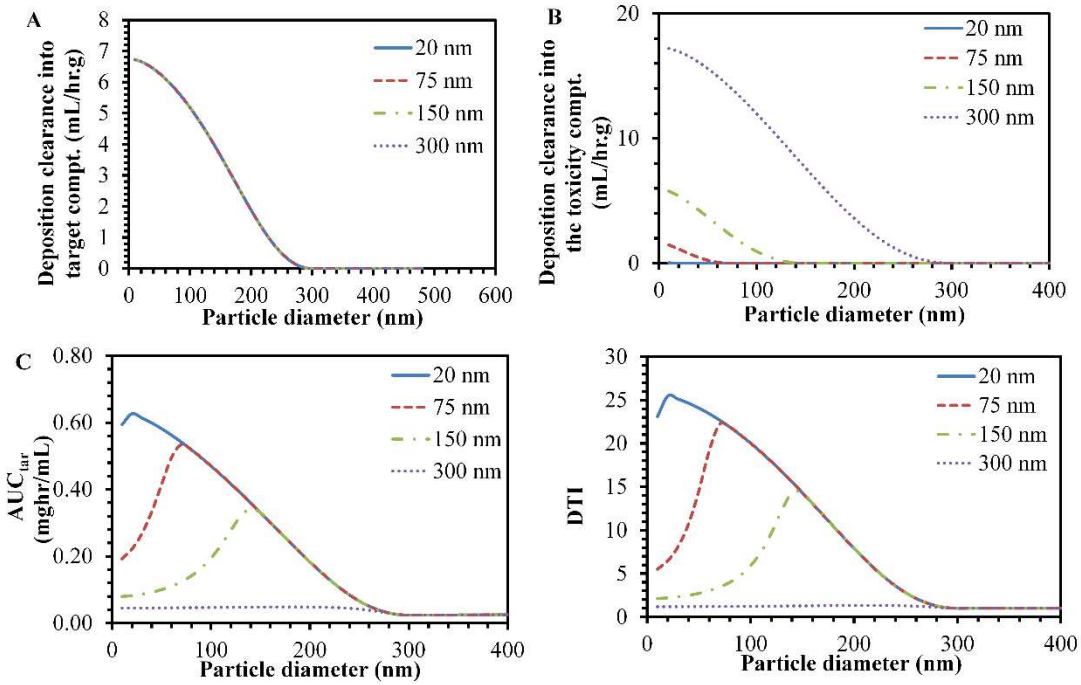

Figure 2-7. Effect of vascular pore size of the toxicity compartment

(A) Deposition clearance of nanoparticles in the target compartment (B) Deposition clearance of nanoparticles in the toxicity compartment (C) AUC of the free drug in the target compartment (D) DTI of various sized nanoparticles. The legends indicate the diameter of the vascular pores of the toxicity compartment.

Both the AUC of the target compartment and the DTI show a maximum at an intermediate particle size, at least in the cases where the pore size of the toxicity compartment is smaller than that of the target compartment (**Figure 2-7 C and D**). The particle size for maximum tumor AUC and DTI shifts with a change in the pore size of the toxicity compartment. These results help confirm that the optimal particle size is indeed a function of the vascular pore size of the toxicity

compartment. When the toxicity compartment has a vascular pore size equal to that of the target compartment, there is minimal effect of particle size on the AUC of the target compartment (**Figure 2-7 C** and **2-8**). These results indicate that a careful consideration of the role of peripheral organs in the distribution of NPs is required.

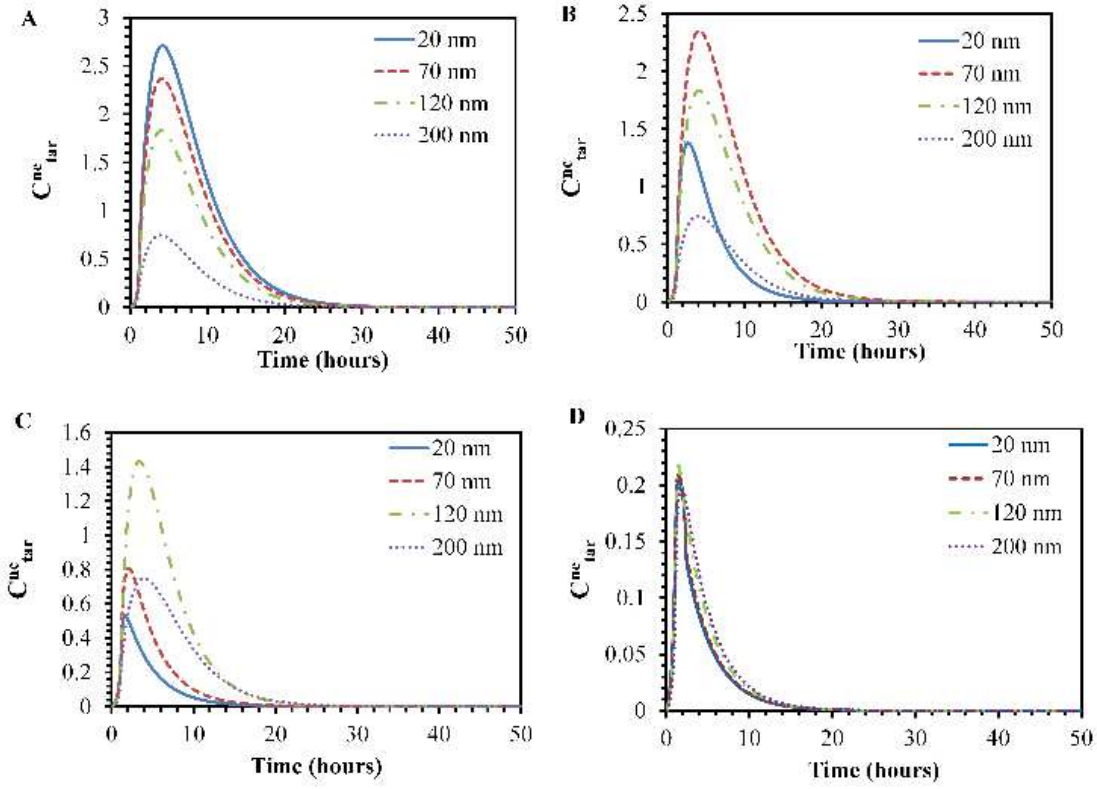

Figure 2-8. Concentration-time profiles of nanoparticles in the target compartment

The toxicity compartment was assumed to have a pore size of (A) 20 nm, (B) 75 nm, (C) 150 nm and (D) 300 nm. The figure legends indicate the diameter of nanoparticles.

2.4.4 Effect of rate of drug release

The rate of drug release from NPs is an important determinant of the performance of nano formulations [456]. An ideal formulation should not release any fraction of the encapsulated drug while in circulation or in the toxicity compartment, and should release the entire drug content once it reaches the target compartment. However, this is seldom possible. Most formulations release the drug irrespective of location. We considered four formulations that release their payload at different rates (first order) independent of their location, and examined the effect of release rate for tumor vascular pore diameters of 300 nm and 100 nm. In both cases, we assumed that the pore fraction is 1%.

The joint effect of NP size and release rate on DTI, when the tumor vasculature pore size is 300 nm, is shown in **Figure 2-9 A**. For particles below the pore cutoff size of the toxicity compartment (<70 nm) and above the pore cutoff size of the target compartment (>280 nm), there is no effect of drug release rate on the DTI. However, at intermediate particle sizes the DTI increases as the release rate decreases. Similar results are obtained when the tumor vascular pore size is assumed to be 100 nm (**Figures 2-9 B**).

We then studied the first case (300 nm pore size) in more detail to develop a mechanistic understanding of this effect. For particle sizes <70 nm, below the cutoffs of both the target and toxicity compartments, NPs are deposited in both compartments. Thus, with a slower release, there is an increase in AUC of the free

drug in both the target and toxicity compartments (**Figures 2-9 C-D)**. Therefore, at very small particle sizes, prolonging drug release may not yield beneficial results.

At an intermediate particle size (between 70 nm and 280 nm), a complex interplay of deposition and elimination processes occurs. When the drug is in the NP form, it has two clearances acting upon it. One of these clearances drives NPs into the target compartment and the other eliminates it from the body. Once the drug is released in the central compartment, it is acted upon by three clearances, one elimination clearance and two distribution clearances, driving it into either the target or toxicity compartments. Based on these clearances, the probability of the drug depositing in the tumor is greater if it is encapsulated in NPs than if it is in the free form (**Figure 2-9 E**). Hence, if a drug is held in the nanoparticulate form for a longer period of time, it has a greater probability to enter the target compartment. This will translate into higher drug deposition into the tumor and an increased AUC. This is in agreement with previous studies that have shown higher tumor concentrations with more sustained drug release [175]. This prolonged confinement in the NP form will also decrease the amount of drug that can be deposited into the toxicity compartment after the drug is released **(Figure 2-9 D)**.

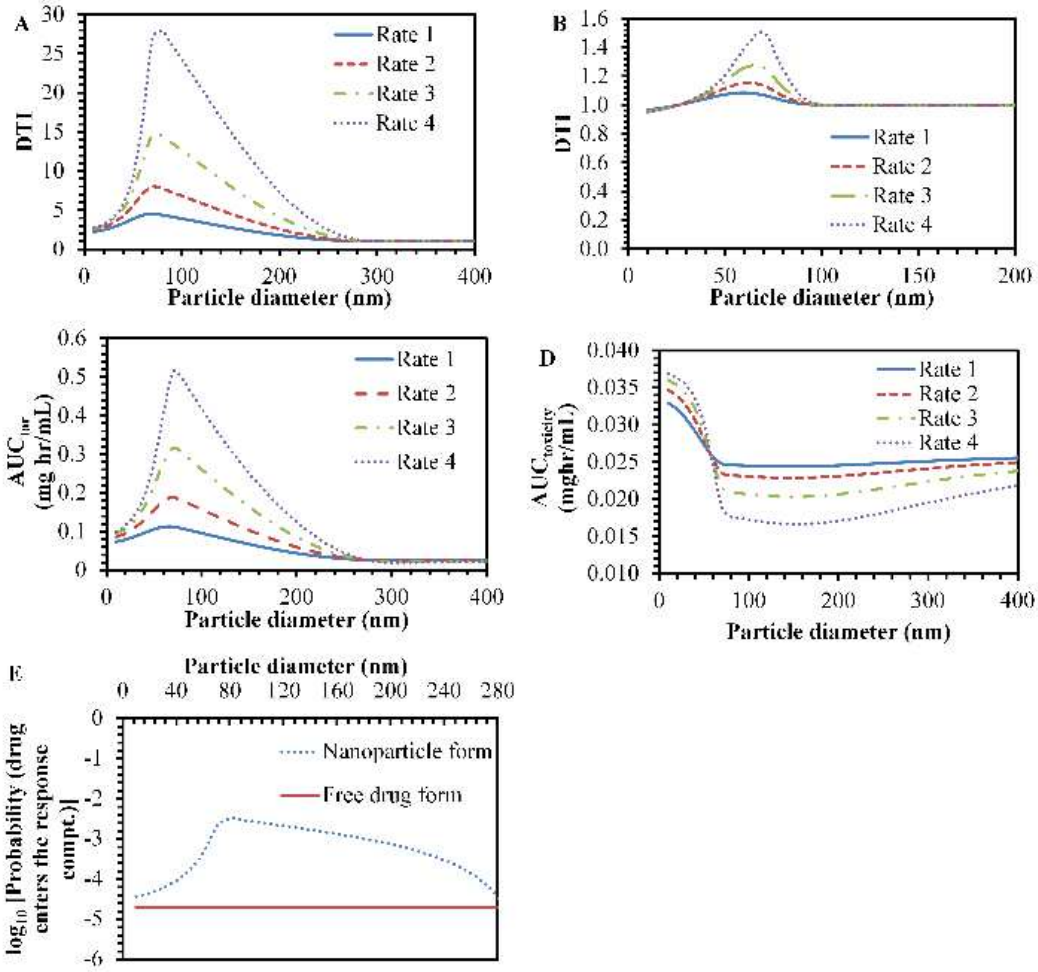

Figure 2-9: Effect of rate of drug release

(A) DTI of various sized nanoparticles in tumors with a vascular pore size of 300 nm (B) DTI of various sized nanoparticles in tumors with a vascular pore size of 100 nm (C) AUC of the target compartment as a function of particle size at various release rates (D) AUC of the toxicity compartment as a function of particle size at various release rates. The legend in A-D indicates rate of drug release. Rate 1 = 16×10^{-5} s^{-1}, Rate 2 = 8×10^{-5} s^{-1}, Rate 3 = 4×10^{-5} s^{-1}, Rate 4 = 2×10^{-5} s^{-1} (E) Probability that the drug enters the target compartment when it is either bound inside the nanoparticles or as free drug.

2.4.5 Comparison of drug targeting index determined using AUCs and average number of visits

One way to view these results is in terms of the average number of visits of the drug molecule into the tumor and toxicity compartments when the drug is administered in its free state or encapsulated in NPs. By avoiding key organs and being in circulation for a longer time, NP-encapsulated drug will more likely deposit in the tumor, and therefore will have a greater average number of visits into the tumor as compared to the free drug. Thus, confining the drug in NPs for a longer period of time increases the average number of visits of the drug molecule to the tumor.

We solved for DTI using AUCs of the drug in the target and toxicity compartment (Eq. 1) and compared it to DTI obtained by using average number of visits of the drug to various compartments (Eq 29). Solutions for DTI obtained using Eqs. (1) and (29) are identical (**Figure 2-10**). More complicated expressions obtained after relaxing these two assumptions will be published elsewhere.

2.4.6 Key findings of the model and future directions

Our results highlight several important points. First, it is necessary to understand the key sites of toxicity for a given drug. Subsequently, these organ sites need to be carefully analyzed for their possible vulnerability to NP deposition. If these organs welcome NP deposition, then particle size can be an important variable that can be tuned to mitigate toxicity. The smallest NPs may not always be optimal.

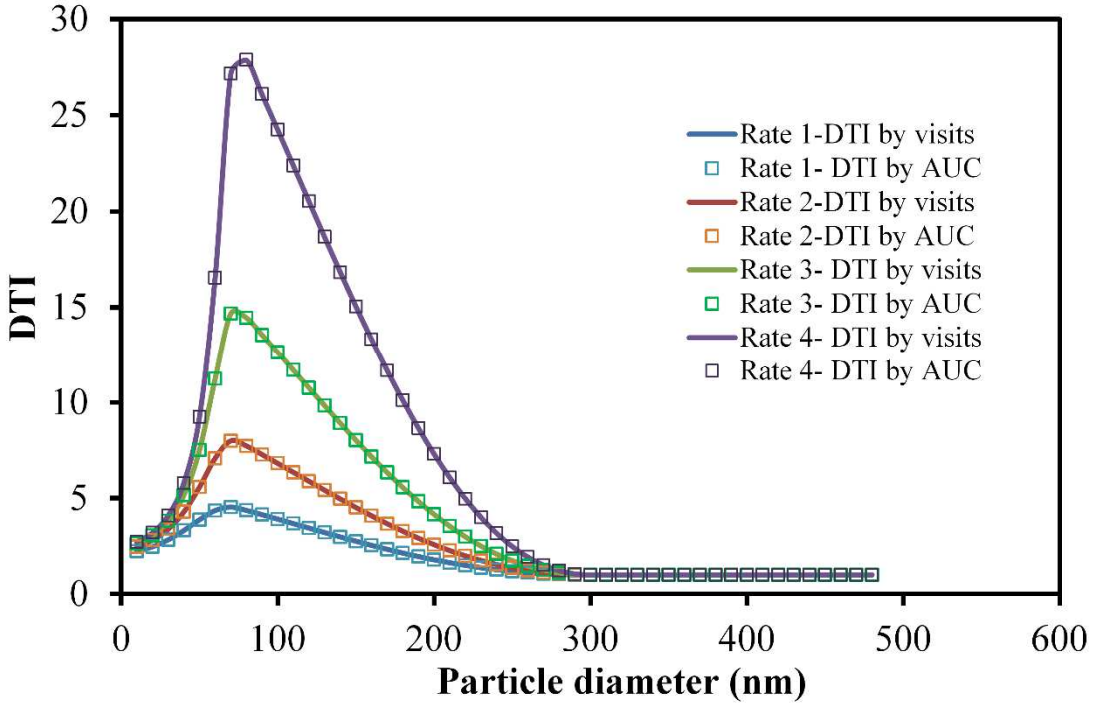

Figure 2-10. Comparison of DTI of various NP formulations determined using the AUC method and 'average number of visits' method

DTI was calculated as the ratio of AUCs and based on the average number of visits to each compartment. Drug encapsulated in intermediate sized particles have the highest number of average visits into the tumor. Legend indicates rate of drug release from nanoparticles. Rate 1 > Rate 2 > Rate 3 > Rate 4.

Much effort has been focused on achieving sustained drug release from NPs, a nontrivial task [330, 457]. However, our results show that altering the rate of drug release may not always be advantageous. NPs that deposit in both the target and toxicity compartments are likely to cause changes in both efficacy and toxicity

that depend on drug release rate. NPs large enough to avoid the toxicity compartment but small enough to deposit in the target compartment will benefit the most from sustained drug release.

Our results also suggest that it is essential to classify drugs based on their suitability for nano drug delivery. This classification system can likely predict and limit the failures of nanotherapeutics earlier in the development pipeline. The site of toxicity of the drug can be the basis of such a classification system. For example, a drug that causes toxicity in a non-fenestrated organ is a good candidate for delivery using NPs. Conversely, NP-form of a drug should be used to treat only those tumors that have a larger pore size than that of the toxicity compartment.

The EPR effect has been the key inspiration for using NPs to deliver anticancer agents [173]. EPR theory suggests that NPs can accumulate to a greater extent in tumors than in normal tissues. However, if the major site of drug toxicity is an organ with fenestrated capillaries similar to those found in tumor tissues then the permeability component of the EPR effect may also apply to the toxicity site. Whether or not the EPR effect is operational and beneficial may depend on the particle size, the location and properties of the tumor, and properties of the site(s) of toxic action. The DTI statistic offers a means to evaluate the relative EPR effects in tumor and toxicity site.

In this report, we used AUC of the drug in the tumor and toxicity compartments as a measure of its efficacy and toxicity. However, time courses of concentrations of the drug in the various compartments may be a better determinant [175]. Prolonged exposure to low drug concentrations may yield high AUCs, but may not

translate into increased efficacy or toxicity. Secondly, in our model we assumed that the tumor is a single well-stirred compartment. Impaired interstitial transport in the tumor and differences in drug activity against a heterogeneous tumor cell population may challenge this assumption [94, 458-460]. Thirdly, we have assumed that elimination of free drug and NPs is carried out only in the central compartment. This may not be true, as drug metabolism and excretion, or NP elimination could occur in either tumor or toxicity related organs, especially the liver. Incorporating these processes provides no analytical difficulties, but would require more kinetic parameters.

An important assumption in our model is that macrophage uptake of NPs results in the elimination of both NPs as well as the encapsulated drug. However, upon phagocytosis, the encapsulated drug can be released in the organ harboring the macrophages, or can cause toxicity to the macrophages. Our model does not consider either of these cases, because quantification of the extent of these processes is difficult. However, some specific effects of macrophage clearance can be speculated. Since larger NPs are taken up by macrophages more efficiently, our model would underestimate the toxicity caused by these NPs. Hence, the ideal particle size may shift to a smaller value based on the extent of toxicity caused by the phagocytosed NPs.

While the model is more general, we specialize it here by assigning the “Target” compartment to tumor and the “Toxicity” compartment to liver. Both tumor and liver contain rather large fenestrae in their capillaries [186, 461], allowing significant NP deposition and accumulation [447]. It must be noted here that the

liver may not be the major site of toxicity for all chemotherapeutic drugs. However, in this special case, we have considered the liver as the toxicity organ because it is highly vascularized and shows porous capillaries. Such an organ can have a significant impact on the overall pharmacokinetics of NPs and the released drug.

We have also assumed that the rate of drug release is the same in all compartments. This need not be so, as drug release can be enhanced, for example, in the relatively acidic tumor environment [340]. With some effort, and with advances in synthetic chemistry and physicochemical understanding of release rates from NPs in different tissue environments, the present model can be extended to include these effects. Additionally, particle size can have a significant impact on the rate of drug release. The large surface area to volume ratio of smaller NPs may result in rapid release of the encapsulated drug. However, in the current case, we assumed that the rate of drug release was independent of particle size. This was done to delineate the effects of the individual parameters. Finally, release rates from NPs have been assumed to obey first order, decaying exponential kinetics. Expressions are possible for DTI for more general release profiles, many of which can be decomposed with good accuracy to polyexponential forms.

2.5 Conclusion

The physicochemical properties of nano drug delivery systems can have a significant impact on their *in vivo* performance. We presented here a pharmacokinetic model to explain the effects of particle size, rate of drug release and vascular physiology on the effectiveness of nano delivery. We found that the optimal particle size and/or drug release rate is strongly dictated by vascular

characteristics of the tumor and toxicity compartments. Additionally, the model identified key factors that may help in selecting these formulation parameters for an individual patient. The use of pharmacokinetic modeling to understand the behavior of nanoparticulate systems *in vivo* has tremendous potential to impact the field of cancer therapy.

Table 2-1. Table of constants and symbols

Symbol	Parameter	Value	Units
a	Radius of NPs	(5-240) x 10^{-7}	cm
R	Radius of pore in blood capillary	(50-300) x10^{-7} (target) 37.5x10^{-7} (toxicity)[455]	cm
λ	Ratio of particle size to pore size	Calculated	
H	Hindrance factor to diffusion	Calculated	
W	Hindrance factor to convection	Calculated	
σ	Reflection co-efficient	Calculated	
k_B	Boltzmann constant	1.38 x10^{-16}	$cm^2g/ s^2 K$
T	Absolute temperature	310	K
μ	Viscosity of blood	3.5 x 10^{-2} [462]	g/cm.s
D	Diffusivity	Calculated	
L	Thickness of blood capillary wall	5 x10^{-4}	cm
γ	Pore fraction	0.01-0.2 (target) 0.075 (toxicity)[455]	%
P	Permeability	Calculated	cm/s
L_p	Hydraulic conductivity	Calculated	cm^2s/g
P_{cap}	Capillary pressure	2.6664 x 10^4 [13]	$g/cm.s^2$
P_{if}	Interstitial fluid pressure	1.9998x10^4 (target)[13] 2.6664x 10^3 (toxicity)[13]	$g/cm.s^2$
Pe	Peclet number	Calculated	
S	Blood vessel surface area	16 (target)[463] 5.2 (toxicity)[464][a]	cm^2/g
i	Used as a subscript to designate the compartment	c (central) tar (target) tox (toxicity)	
$Cl_{dep,i}^{int}$	Intrinsic clearance of NPs into compartment *i* (*i* = tar or tox)	Calculated	mL/s

$Cl_{ex,i}^{int}$	Intrinsic clearance of NPs out of compartment *i* (*i* = tar or tox)	Calculated	mL/s
Q_i	Blood flow to compartment *i* (*i* = tar or tox)	$3.33x10^{-3}$(target)[463] $1.33x10^{-2}$(toxicity)	mL/s.g
$Cl_{dep,i}^{nc}$	Total clearance of NPs into compartment *i* (*i* = tar or tox)	Calculated	mL/s
$Cl_{ex,i}^{nc}$	Total clearance of NPs out of compartment *i* (*i* = tar or tox)	Calculated	mL/s
Cl_{elim}^{nc}	Elimination clearance of NPs from the central compartment	Calculated[1]	mL/s
Cl_{elim}^{f}	Elimination clearance of free drug from the central compartment	10.59	mL/s
k_{rel}	Rate constant for drug release	$2x10^{-5}$ – $16x10^{-5}$	1/s
V_i^{nc}	Volume of distribution of NPs in compartment *i*	3000 (Central) 0.2 (target) 1650 (toxicity)	mL
V_i^{f}	Volume of distribution of free drug in compartment *i*	42000 (Central) 0.2 (target) 1650 (toxicity)	mL
C_i^{nc}	Concentration of drug in NP form in compartment *i*	Calculated	g/mL
C_i^{f}	Concentration of drug in free form in compartment *i*	Calculated	g/mL
AUC_i	Area under the curve for drug in compartment *i*	Calculated	g.s/mL

Chapter 3 Fibrinolytic Enzyme Therapy to Improve Tumor Perfusion and Chemotherapeutic Efficacy of Nanoparticles

3.1 Summary

Elevated interstitial fluid pressure and a high degree of solid stress within tumors contribute to poor intratumoral distribution of nanomedicine and inadequate drug delivery. We hypothesized that the presence of fibrin in tumors contributes to hindered intratumoral distribution of nanocarriers, and that this can be overcome with the use of a fibrinolytic enzyme such as tissue plasminogen activator (tPA). We first conducted a systematic analysis of fibrin(ogen) expression in human tumor biopsies. Fibrin staining was found to be heterogeneous across and within tumor types. On an average, ~20-90% of the tumor area was stained for fibrin. Further analysis in lung carcinomas revealed that a high degree of staining was observed regardless of disease stage or type. We then studied the influence of fibrin degradation on the *in vitro* and *in vivo* performance of a model formulation of paclitaxel nanoparticles. Using Transwell® studies, we found that the diffusivity of nanoparticles in fibrin matrices was poor. However, the resistance offered by the fibrin gel was dramatically reduced in the presence of tPA. We further characterized the efficacy of a combination therapy of tPA and paclitaxel nanoparticles in an orthotopic model of human lung cancer and a syngeneic mouse melanoma model. In both models, co-administration of tPA led to a significant improvement in the activity of paclitaxel nanoparticles. We then used immunohistochemistry and ultrasound analyses to probe into the anatomical and physiological ramifications of tPA treatment on tumor blood vessels. These studies showed that tPA treatment led to an increase in median blood vessel diameter and improved perfusion. In summary, we show here that treatment with tPA improves

tumor perfusion and anticancer efficacy of nanoparticle-encapsulated chemotherapeutic drugs.

3.2 Introduction

Poor intratumoral distribution of the drug carrier and inadequate drug delivery to tumors are significant challenges in chemotherapy [98]. Prolonging circulation times [465, 466] or altering particle size, shape, charge and other physicochemical properties of the drug carrier address these challenges [424, 440, 467, 468] but only to a limited extent. The benefits of these approaches are limited by the erratic blood supply often observed in tumors.

Several peculiar characteristics of tumor blood vessels render them suboptimal for drug delivery. These include inadequate coverage of the tumor, lack of transvascular pressure gradients, and their collapsed nature [181, 202, 468, 469]. Blood vessels in the core of the tumor are compressed under solid stress exerted by fast-dividing cells [470] and large amounts of extracellular matrix (ECM) [202]. Treatment with enzymes that degrade ECM components such as collagen [419] and hyaluronic acid [418] improves vascular characteristics and enhances blood supply to tumors. However, the ubiquitous expression of collagen and hyaluronic acid in the body may limit the systemic use of these enzymes.

Due to the leaky nature of tumor blood vessels, fibrinogen, a soluble vascular protein, is deposited in the tumor matrix. The prothrombogenic activity of tumor cells leads to the conversion of fibrinogen to cross-linked fibrin, the principle ingredient of blood clot [127, 130]. In fact, due to the constitutive activity of coagulation factors in tumors, they are often considered ‘overhealing wounds’ [141]. We hypothesized that the presence of significant amounts of fibrin in the tumor matrix contributes to increased solid stress often observed in tumors.

Additionally, the tumor specific presence of fibrin makes it an excellent target for therapeutic interventions. However, the role of fibrin in limiting the transport of drug carriers has not been previously studied.

We show here that administration of a fibrinolytic enzyme improves tumor perfusion by decompressing blood vessels. This leads to an increase in chemotherapeutic activity of paclitaxel encapsulated in polymeric nanoparticles (NPs). These results were observed in both a syngeneic mouse model of melanoma and an orthotopic human lung cancer model.

3.3 Materials and Methods

3.3.1 Materials

Tissue microarrays of various human tumor biopsies were obtained from Folio Biosciences (Ohio, USA). Anti-human fibrin(ogen) antibody was purchased from Dako (California, USA). Poly(lactide-co-glycolide) (PLGA) was purchased from Lactel (Alabama, USA). L-lactide, bovine fibrinogen, and thrombin were obtained from Sigma Aldrich (Missouri, USA). Tissue plasminogen activator (tPA) was obtained from Abcam (Massachusetts, USA). Poly(ethylene glycol) was purchased from Laysan Bio Inc. (Alabama, USA). Potassium salt of D-luciferin was purchased from Gold Biotechnology, Inc. (Missouri, USA).

3.3.2 Staining, microscopy and analysis of human tissue microarrays

Tissue microarrays were digested with Proteinase K and stained with a polyclonal rabbit anti-human fibrin(ogen) antibody at a dilution of 1:1000.

Representative images were acquired using an Eclipse TS100 microscope (Nikon instruments, New York, USA) under 400X magnification. Fraction of the area stained for fibrin(ogen) was quantified using ImageJ v1.48 software.

3.3.3 Synthesis and characterization of paclitaxel loaded PLGA nanoparticles

A block copolymer of poly(lactide) and poly(ethylene glycol) was synthesized via ring opening polymerization reaction as described before [210]. The block copolymer was characterized using ^{1}H-NMR (Varian 400 MHz) [210].

PLGA NPs loaded with paclitaxel were synthesized by a single emulsion technique as described before [210]. Briefly, PLGA (32 mg) and paclitaxel (5 mg) were dissolved in 1 mL of chloroform. The chloroform solution was added to 8 mL of 2.5 %w/v poly(vinyl alcohol). The mixture was sonicated on an ice bath at an output of 18-21 W for 5 minutes (Sonicator XL, Misonix, New York, USA). The emulsion was then stirred using a magnetic stir plate. The block co-polymer (8 mg) of poly(lactide) and poly(ethylene glycol) was dissolved in 0.2 mL chloroform and added to the emulsion while being stirred. The mixture was stirred overnight under ambient conditions and then for 2 h under vacuum. NPs were then washed thrice with deionized water by ultracentrifugation, and lyophilized. PLGA NPs loaded with fluorescent dye (coumarin 6) were synthesized similarly [33].

To determine particle size and zeta potential, NPs were dispersed in deionized water and analyzed using dynamic light scattering (Delsa Nano C, Beckmann Coulter, California, USA).

To determine drug loading, NPs were dispersed in methanol (~1 mg/mL) and the drug was extracted overnight. NPs were separated from free drug by centrifugation (14000 RPM, 15 minutes). Drug concentration in the extract was analyzed using HPLC (Beckmann Coulter, California, USA) [9].

3.3.4 Migration across fibrin matrix

A Transwell® assay was used to determine the rate of migration of NPs across fibrin matrices. In these studies, fibrin matrix was formed *in situ* in the upper insert of a Transwell® plate (12 mm diameter, 0.4 μm pore size, polycarbonate membrane). Fibrinogen (3 mg/mL) was dissolved in 0.9% w/v saline at 37°C. Plasminogen (0.1 U/mL) and thrombin (1 U/mL) were added to the fibrinogen solution. A 750-μL aliquot of the solution was quickly transferred to the inserts. The plate was placed in a cell culture incubator overnight to allow fibrin gel formation.

At the beginning of the experiment, the bottom well was filled with 1 mL of 0.15 mM phosphate buffered saline (pH 7.4, 1X PBS). The tPA stock solution was diluted in 1X PBS, mixed with NPs (0.5 mg NPs dispersed in 0.1 mL deionized water), and added on top of the fibrin matrices. At various time points, contents of the bottom well were collected and lyophilized. The bottom well was replenished with fresh 1X PBS. The lyophilized samples were extracted overnight with methanol. Concentration of paclitaxel in the extract was determined using HPLC.

To determine the lag time for the appearance of drug in the bottom chamber, a curve given by the following equation was used to fit the data:

$$A = A_0[1 - e^{-k(t-t_{lag})}]$$

where A is the cumulative amount of drug in the bottom chamber, $A_0$is the amount of drug added to the top chamber, k is the rate constant for transport across the insert and t_{lag} is the lag time. Model fitting was performed using Matlab software (Mathworks, Massachusetts, USA).

3.3.5 Cell culture

B16F10 murine melanoma cells, J774 murine macrophages, and A549 human lung cancer cells transfected with firefly luciferase gene (A549-luc) were used in these studies. All cells were cultured in Roswell Park Memorial Institute (RPMI) 1640 medium supplemented with 10% v/v fetal bovine serum and 1% v/v penicillin and streptomycin under humidified atmosphere with 5% CO_2 at 37°C.

3.3.6 Cell uptake across fibrin matrix

Cell uptake of NPs across fibrin matrices was determined using a Transwell® assay. Fibrin matrices were formed in the upper inserts of the Transwell® plate as described before. B16F10 cells were seeded in the bottom well ($1X10^6$ cells/well) and allowed to adhere overnight. On the day of the experiment, media was replaced with serum free media (1 mL/well). Coumarin 6 loaded NPs (0.25 mg dispersed in 0.05 mL deionized water) were mixed with increasing amounts of tPA and added on top of the fibrin matrix. After 4 h, cells were trypsinized, collected in

flow tubes and centrifuged at 1000 RPM for 5 minutes. The supernatant was removed and cells were suspended in cold 1X PBS. Cellular fluorescence was analyzed using flow cytometry (BDCalibur flow cytometer).

3.3.7 Assessing the safety and tolerability of combination therapy

We determined the safety of the combination treatment consisting of tPA and paclitaxel NPs in a mouse model. Female C57Bl/6 mice, 4-6 weeks old, (Charles River laboratories, USA) were randomized in three groups and treated with paclitaxel solution (20 or 40 mg/kg), paclitaxel NPs, or combination of paclitaxel NPs and tPA (218 or 436 μg/kg). Animals received three doses of each treatment at 96 h interval intravenously. Animal weights were monitored throughout the study.

Paclitaxel solution (40mg/mL) was prepared by dissolving paclitaxel in a mixture of Cremophor® EL and ethanol (1:1 v/v). This solution was diluted to 2-4 mg/mL with 1X PBS immediately prior to injection.

The dispersion of paclitaxel NPs was prepared by adding 1X PBS to NPs. The dispersion was probe sonicated thrice (18 W for 30 s each) on an ice bath. The dispersion was used immediately after sonication. For combination treatment, tPA was added to the dispersion immediately before injection.

One week after the final dose, animals were sacrificed using CO_2 asphyxiation. Blood was collected using cardiac stick and transferred to heparinized tubes. Blood cells were separated by centrifugation. Serum concentrations of various markers of liver function were analyzed.

3.3.8 Anti-cancer efficacy of combination therapy in orthotopic lung cancer model

The efficacy of the combination therapy was evaluated in a xenograft mouse model of lung cancer. The lung tumor model was set up as described before [228], with some changes. A549-luc cells (~$6X10^5$ cells/mouse) were dispersed in 1X PBS and injected in 4-6 week old, female severe compromised immunodeficient (SCID) mice (Charles River Laboratories, USA) via the lateral tail vein. Tumor growth in the lungs was monitored by measuring bioluminescence using IVIS spectrum *in vivo* imaging system.

Treatment was initiated 4-5 weeks after cell injection. Animals were intravenously treated with saline or paclitaxel (40 mg/kg) or a combination of paclitaxel and tPA (436 μg/kg). The treatments were administered thrice every 96 h. Tumor bioluminescence was monitored every 3-4 days.

3.3.9 Anti-cancer efficacy of combination therapy in syngeneic melanoma model

B16F10 cells ($1x10^6$ cells dispersed in 0.05 mL 1X PBS) were injected subcutaneously in 4-6 week old female C57Bl/6 mice. Tumor dimensions were measured daily using a digital caliper. Tumor volume was calculated as 0.5 x length x $width^2$. Treatment was initiated when the tumor volume reached ~100 mm^3. Animals were treated intravenously with saline or various formulations of paclitaxel (40 mg/kg) or a combination of paclitaxel and tPA (436 μg/kg). Animals were treated with three doses administered 96 h apart.

Formulations of paclitaxel solution and paclitaxel NPs were prepared as described in the safety study. A dispersion of Abraxane® was prepared by adding 1X PBS. The dispersion was sonicated in a water bath for 5-10 minutes. The dispersion was stored on ice and was used within 1 h.

3.3.10 Immunohistochemistry analysis of $CD31^+$ blood vessels

Tumors from the B16F10 efficacy study were collected and fixed in 5% formalin in PBS for 48 h. After 48 h, formalin was removed and the fixed tumors were washed thrice with 1X PBS. The tumors were then stored in 70% ethanol until further processing. Tumor sections were stained with a goat anti-mouse CD31 antibody (Santa Cruz Biotechnology, TX, USA).

Fifty random images of each tumor section were obtained using an optical microscope at 400X magnification. Diameters of the $CD31^+$ blood vessels were measured using ProgRes® Capture software (Jenoptik AG, Germany). On average, each image contained 2-3 blood vessels. Six sections from each treatment group were analyzed. Hence, results represent ~600-900 blood vessels/treatment group.

3.3.11 Ultrasound imaging of B16F10 tumors

C57Bl/6 mice were shaved and inoculated with B16F10 cells as described in the efficacy study. When tumors reached a volume of ~100 mm^3, animals were randomly assigned to two groups and treated with three doses of either saline or

tPA every 96 h. About 1 h after treatment, tumor perfusion was analyzed using ultrasound imaging.

Ultrasound imaging was performed using a Vevo® 2100 system (FujiFilm VisualSonics Inc.). Animals were anesthetized using isoflurane, and were maintained on the gas throughout the imaging. Any hair on the tumor was removed using Nair (Church and Dwight Co Inc.). Using a motorized stage, an MS550 probe was placed on top of the tumor. Exact position of the tumor was determined by monitoring tumor boundary and location in B-mode. Perfusion area was visualized by switching to the Power Doppler mode. Power Doppler images were analyzed using the ImageJ v1.48 software.

3.3.12 Synthesis and characterization of tPA functionalized polymeric nanoparticles

PLGA NPs loaded with paclitaxel and surface functionalized with tPA were synthesized using maleimide-thiol chemistry as described before [218]. Briefly, NPs (~25 mg) functionalized with maleimide-terminated poly(ethylene glycol) were dispersed in ~1.5 mL deionized water. tPA (1.9 μg/mg NPs) was added to the NP dispersion, and the reaction mixture was incubated on a shaker overnight. On the next day, unbound tPA was separated from the NPs by ultracentrifugation. NPs were lyophilized and stored at -20°C until further use.

Particle size, zeta potential and drug loading were determined as described before. The amount of tPA on the NP surface was measured using bicinchoninic acid (BCA) assay. Activity of tPA was determined using an enzymatic assay kit

that measures plasmin generation (Sigma Aldrich Co., MO, USA, product #0882). Different concentrations of tPA were used to prepare the calibration curve, and the assay was run according to the manufacturer's instructions.

The migration of tPA functionalized NPs across fibrin matrix was determined using a Transwell® assay as described before.

3.3.13 Anti-cancer efficacy of tPA functionalized nanoparticles

Tumor inhibition of tPA functionalized NPs was determined in an orthotopic lung cancer model and a syngeneic melanoma model as described before. Animals were treated with 3 doses of tPA functionalized paclitaxel NPs (40 mg paclitaxel/kg) every 4 days.

3.3.14 Accumulation of paclitaxel in lung tumors

Orthotopic lung tumors were established in SCID mice as described in the efficacy study. After 4-5 weeks of cell injection, animals were randomly assigned to various treatment groups. Different formulations of paclitaxel (20 mg/kg) were administered via the lateral tail vein. Animals were sacrificed 2 h or 6 h after treatment administration. Lungs, liver and spleen were collected and weighed. The organs were homogenized in ~1 mL deionized water and lyophilized. Paclitaxel was extracted overnight from the lyophilized organs using methyl tert-butyl ether. The ether was separated from the tissue homogenate by centrifugation and evaporated to dryness under nitrogen. The dried samples were reconstituted in

methanol, centrifuged (14000 RPM, 15 min), and transferred to HPLC vials. Paclitaxel concentration was analyzed using LC-MS/MS as described before [215].

3.3.15 Effect of tPA on macrophage uptake of nanoparticles

J774 murine macrophage cells were seeded in a 24-well plate (50000 cells/well) and allowed to adhere overnight. On the next day, cells were treated with tPA (10 nM) or saline. After 4 h, coumarin-6 loaded nanoparticles were added to all cells. At different time points, treatments were removed, and the cells were washed thrice with cold 1X PBS. Cells were lysed by incubating with RIPA buffer at 37°C for 15 minutes. The cell lysate was divided into two parts. One part was extracted overnight with methanol, and coumarin 6 concentration in the extract was analyzed using HPLC. The other part was used to determine cell protein concentration using BCA assay.

3.4 Results

3.4.1 Extensive fibrin(ogen) deposition in various tumors

Several solid tumors have leaky blood vessels. This leads to the deposition of vascular proteins in the tumor matrix. We were particularly interested in analyzing the deposition of fibrin, an important vascular protein involved in blood clotting.

We examined the occurrence of fibrin in an array of human tumor biopsies. We found that all tumors considered in our studies showed significant fibrin deposition (**Figure 3-1A-H**). Fraction of the tumor area stained for fibrin ranged from ~20-90% (**Figure 3-1I**). To address the question of whether fibrin levels were affected by the

stage of the disease, metastatic status or type of cancer, we focused on lung carcinomas. We found that all lung carcinomas (adenocarcinoma, non-small cell lung carcinoma and squamous cell carcinomas) had comparable amounts of fibrin (**Figure 3-1J**). These levels were unaffected by stage of the disease (**Figure 3-1K**) or the presence of lymph node metastasis (**Figure 3-1L**).

We also analyzed expression of fibrin in several human and murine tumors grown in mice. Similar to our results with the human tumor samples, high levels of fibrin were found in these tumors as well (**Figure 3-2**). These results corroborated well with previous work that showed that fibrin is an important component of the tumor ECM [131, 471].

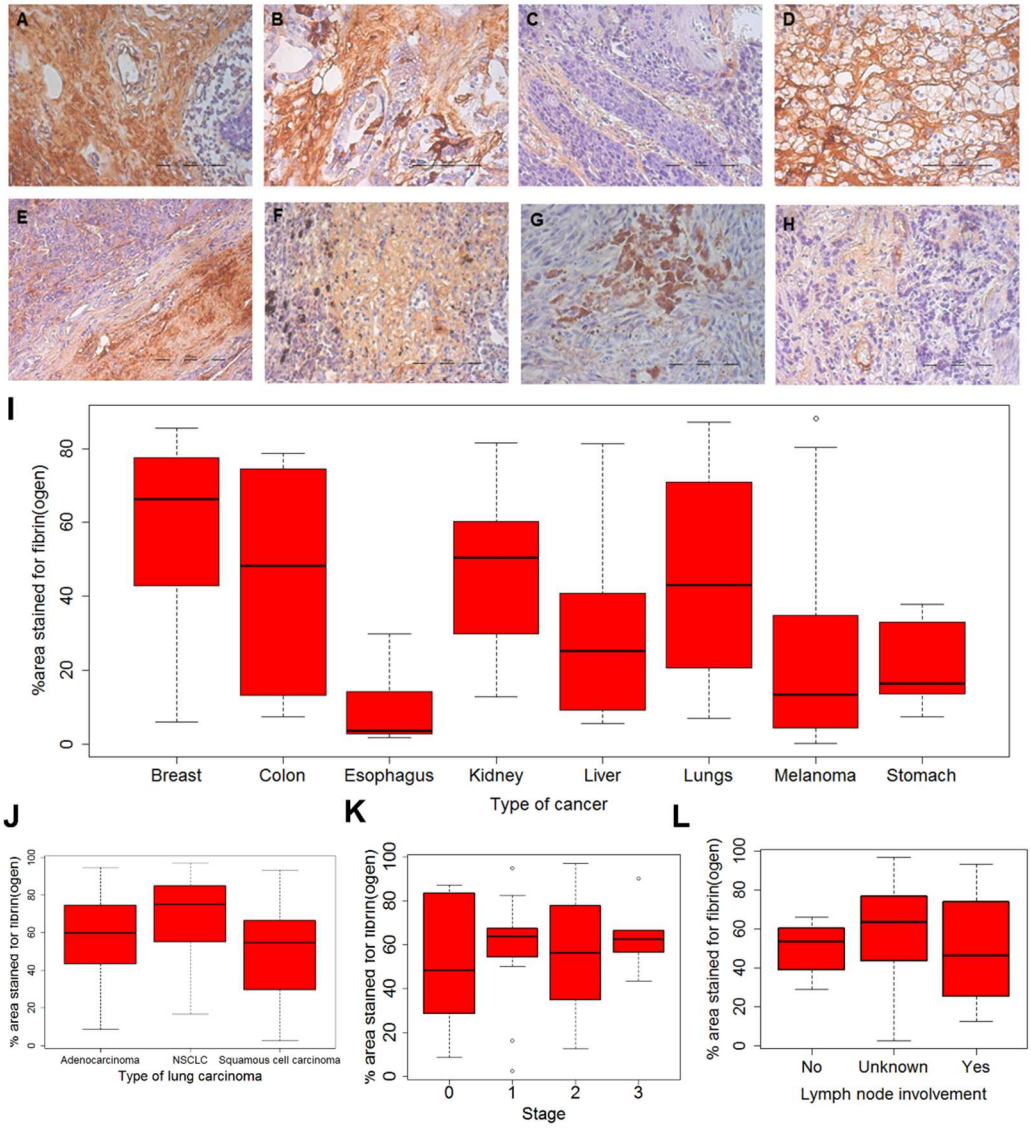

Figure 3-1. Fibrin(ogen) staining in human tumor biopsies

Tissue microarrays of human tumors were stained for fibrin(ogen). Shown here are representative images of fibrin(ogen) staining in cancers of (**A**) breast (**B**) colon (**C**) esophagus (**D**) kidney (**E**) liver (**F**) lungs (**G**) melanoma and (**H**) stomach. (**I**) shows fraction of area stained for fibrin(ogen). (**J-L**) show fibrin(ogen) staining in lung carcinomas as a function of type, stage and lymph node involvement.

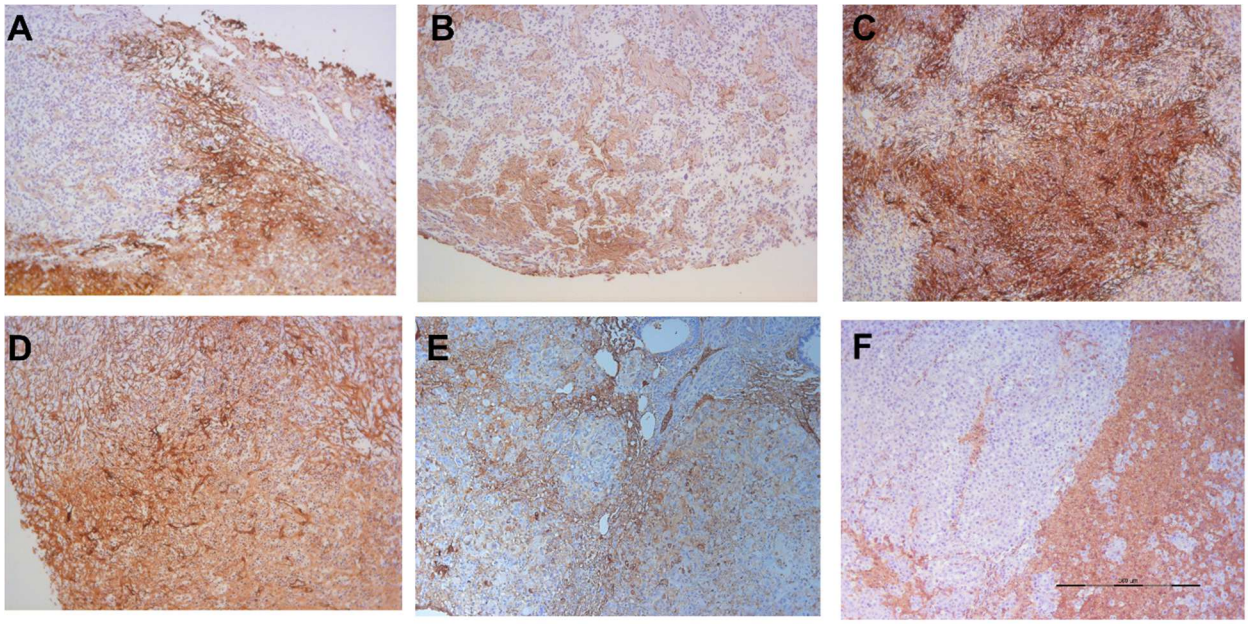

Figure 3-2. Fibrin(ogen) staining in tumors grown in mice

Various tumors grown in mice were excised and fixed in 10% formalin. Tumors were sectioned and stained for fibrin(ogen) expression. Figure shows (A) MIA PaCa (B) H2009 (C) 4T1 (D) MDA-MB-231 (E) A549 and (F) B16F10 tumors

3.4.2 tPA improves diffusivity of nanocarriers *in vitro*

Previous reports have shown that degrading the components of tumor ECM (such as hyaluronic acid and collagen) can improve delivery of drugs to tumors. This result is manifested as both improved intratumoral distribution of the drug as well as improved tumor perfusion [417, 418, 472]. We determined whether degrading fibrin in tumors had a similar effect. To degrade fibrin within tumors we used tPA, an enzyme that is used clinically to treat patients with myocardial infarction and stroke.

PLGA NPs loaded with paclitaxel and surface-functionalized with a block co-polymer of poly(lactide) and poly(ethylene glycol) were used as model drug carriers. The results of the physicochemical characterization of block copolymer and NPs are summarized in **Figure 3-3** and **Table 3-1**.

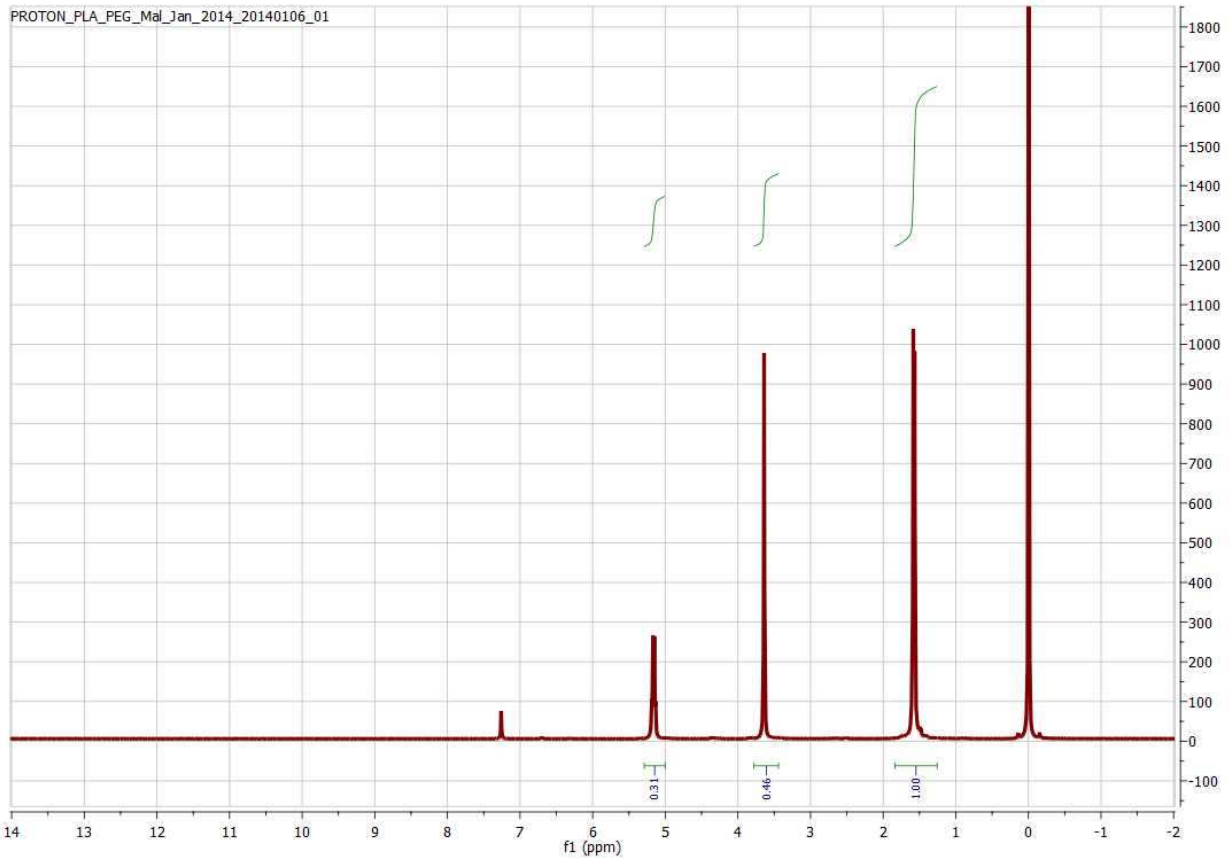

Figure 3-3.^{1}H-NMR of block copolymer of poly(lactide) and poly(ethylene glycol)

Block copolymer of poly(lactide) and poly(ethylene glycol) was dissolved in $CDCl_3$ and analyzed by ^{1}H-NMR. Conjugation of lactide was confirmed by peaks detected at δ= 1.6 and 5.2 ppm.

Table 3-1. Physicochemical characterization of paclitaxel nanoparticles
Data represented as mean ± S.E.M

Particle size (nm)	217.8 ± 15.6
Polydispersity index	0.17 ± 0.02
Zeta potential (mV)	-19.7 ± 1.7
Drug loading (% w/w)	10.9 ± 1.1

To study the diffusion of NPs in fibrin matrices, we used a Transwell® assay. We found that the mobility of NPs across the Transwell® inserts was significantly compromised by the presence of the fibrin matrix. No detectable drug levels could be found in the receiver chamber through the time course of the experiment (**Figure 3-4A**). However, addition of tPA significantly improved the movement of NPs. With an increase in the amount of tPA, the lag time (t_{lag}) for the appearance of drug in the receiver chamber decreased significantly (**Figure 3-4B**). After $t=t_{lag}$, the rate of migration of NPs was unaffected by the concentration of tPA.

In another study, we analyzed the cell uptake of NPs across fibrin gels. In these studies, NPs were separated from a monolayer of B16F10 cells by fibrin matrix. As a positive control, we added NPs directly to the cells. This resulted in a rapid uptake of NPs. However, in the presence of fibrin matrix, NP uptake was significantly reduced (**Figure 3-4C**). Addition of tPA resulted in a dose-dependent increase in cell uptake (**Figure 3-4C-D**). tPA had no effect on cell uptake in the absence of the fibrin matrix (**Figure 3-5**).

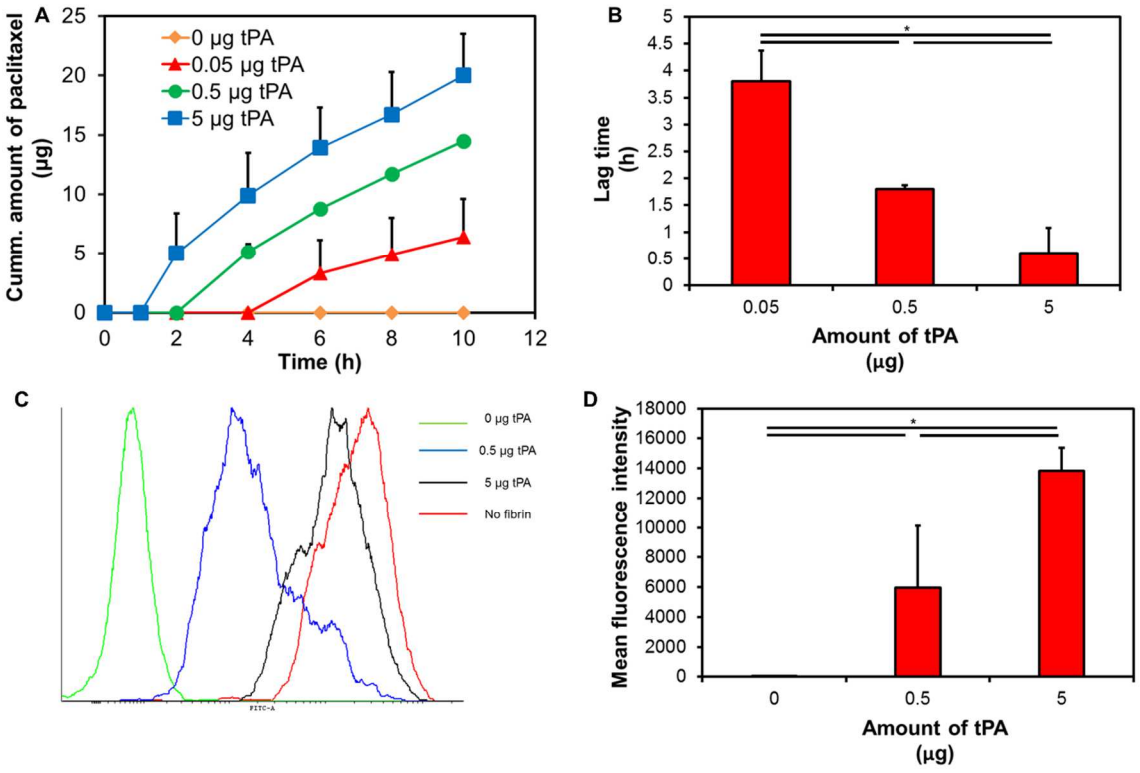

Figure 3-4. Effect of tPA on *in vitro* mobility of nanoparticles in fibrin gels

A Transwell® study was used to analyze the migration of NPs (with or without tPA) across a fibrin matrix. (**A**) Cumulative amount of paclitaxel in the bottom chamber as a function of time (**B**) Lag time for first appearance of paclitaxel in the bottom chamber with increasing amounts of tPA. Results are represented as mean ± S.D., n=3, *p<0.05, one-way ANOVA. Cell uptake of NPs across fibrin gels was determined in Transwell® study. (**C**) Representative histograms indicating cell uptake of fluorescently labeled NPs (**D**) Average results of cell uptake of NPs as function of tPA concentration. Results are represented as mean ± S.D., n=4, *p<0.05, one-way ANOVA.

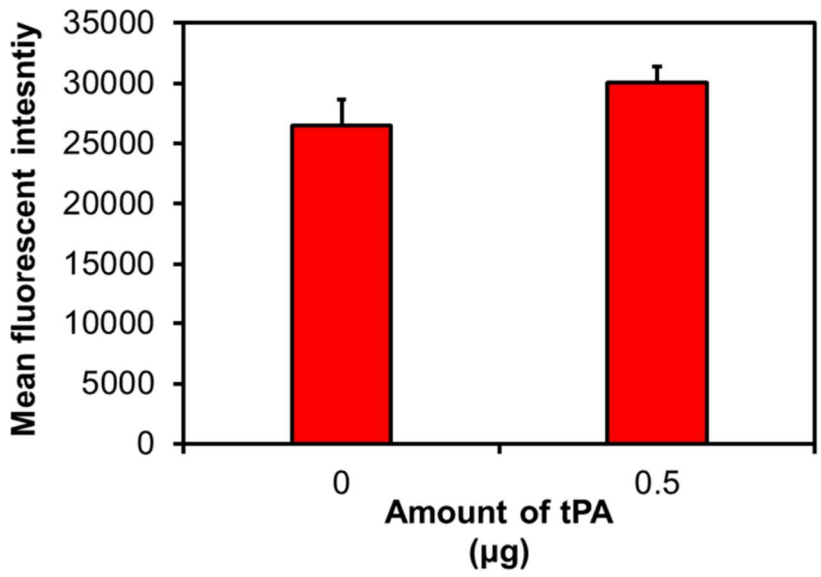

Figure 3-5. Effect of tPA on cell uptake of nanoparticles in B16F10 cells

NPs, with or without tPA, were incubated with B16F10 cells for 4 h. Cell uptake was measured by determining cellular fluorescence using flow cytometry. NP uptake was unaffected by the presence of tPA.

These experiments showed that the fibrin matrix could significantly retard the movement of polymeric NPs, and this effect could be reversed, at least partially, by co-treatment with tPA.

3.4.3 Safety and efficacy of combination therapy of paclitaxel nanoparticles and tPA

We determined the safety and tolerability of a combination of paclitaxel NPs and tPA. Treatment with paclitaxel (as single therapy or in combination) led to a slight loss in body weight (~5%), which was recovered within 48 h (**Figure 3-6 A-B**). The levels of all the markers of liver function were elevated in response to

paclitaxel therapy. Co-administration of tPA did not have a significant impact on the level of these markers (**Figure 3-6C-D**).

We then tested the efficacy of the combination of tPA and paclitaxel NPs in a mouse orthotopic model of human lung cancer. Animals treated with paclitaxel in solution had a slower tumor growth rate as compared to saline treated animals. Paclitaxel in NPs reduced the tumor growth rate even further. However, greatest tumor growth inhibition was seen when paclitaxel NPs were administered in combination with tPA (**Figure 3-6E**).

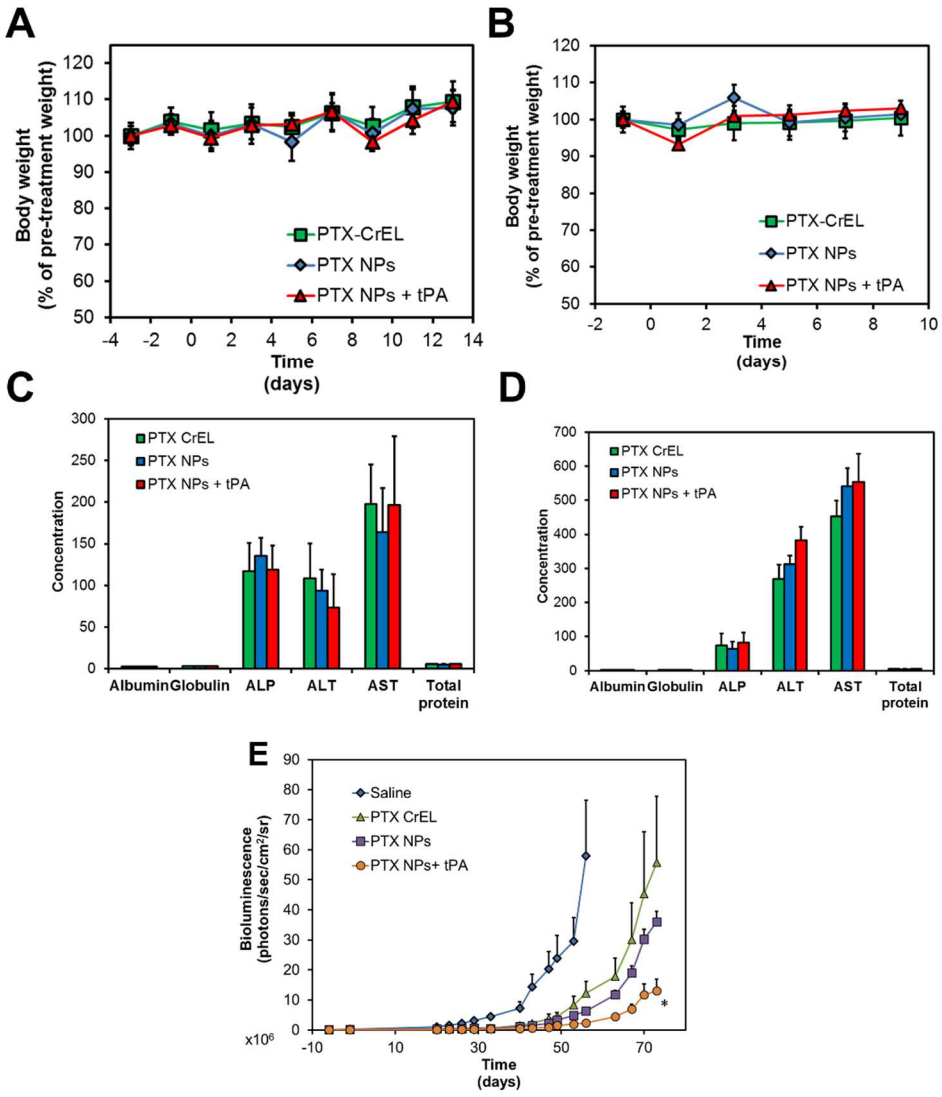

Figure 3-6. Safety and efficacy of paclitaxel nanoparticles-tPA combination therapy

Body weights of animals treated with (**A**) paclitaxel (20 mg/kg) and tPA (218 μg/kg) and (**B**) paclitaxel (40 mg/kg) and tPA (436 μg/kg). Biochemical tests for liver function tests in animals treated with (**C**) paclitaxel (20 mg/kg) and tPA (218 μg/kg) and (**D**) paclitaxel (40 mg/kg) and tPA (436 μg/kg). Concentrations of albumin, globulin and total protein expressed in units of g/dL. Concentrations of hepatic enzymes expressed in units of U/mL. Data shown as mean ± S.E.M., n=5. (**E**) Tumor growth kinetics of A549 lung tumors in animals treated with various formulations. Results shown as mean ± S.E.M, n=6, *$p<0.05$ compared to paclitaxel NPs, Student's t test

3.4.4 tPA improves the anti-cancer efficacy of large nanoparticles in a murine melanoma model

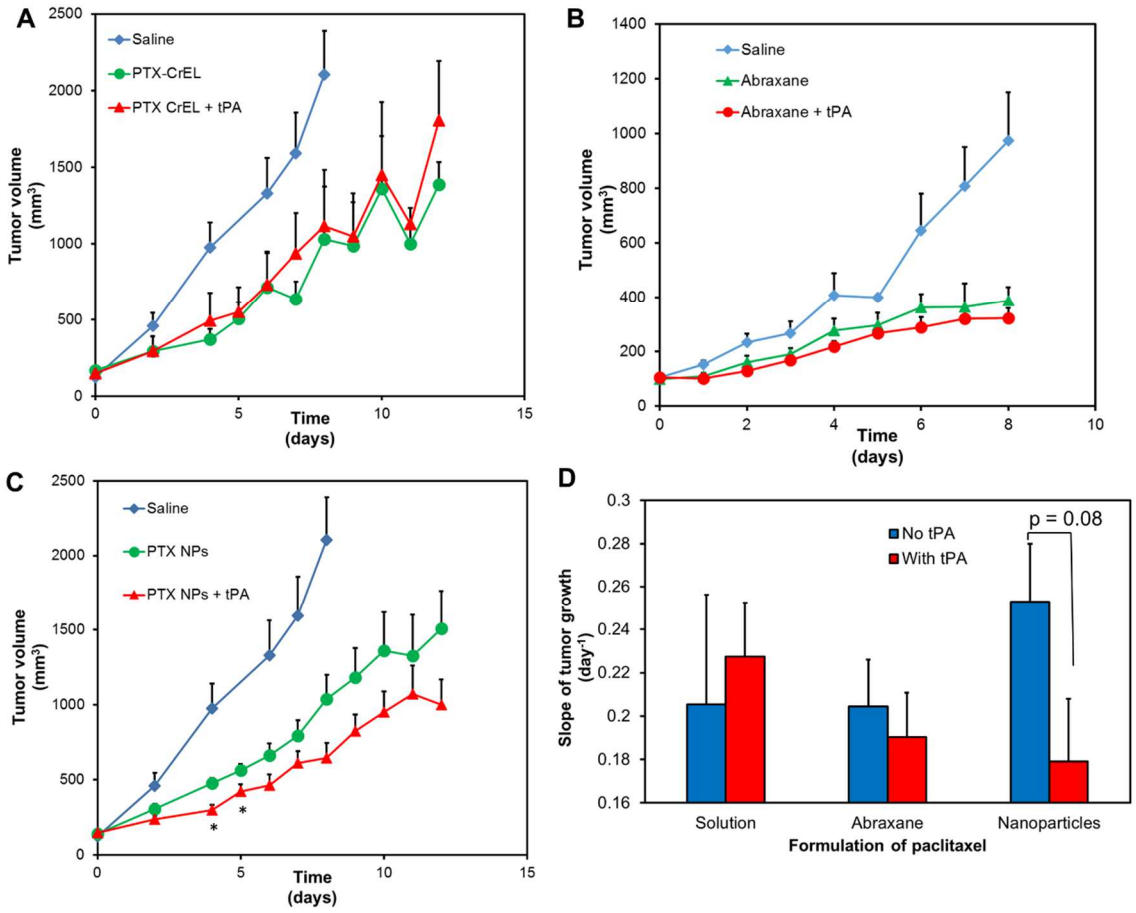

Figure 3-7. Effect of co-administration of tPA on the anti-cancer efficacy of various formulations of paclitaxel

C57Bl/6 mice bearing B16F10 tumors were treated with (**A**) paclitaxel in solution (**B**) Abraxane® or (**C**) paclitaxel NPs with or without tPA. Tumor growth was monitored as a function of time. (**D**) shows slopes of log transformed tumor growth profiles. Results represented as mean ± S.E.M., n=6-9. *indicates $p<0.05$ compared to paclitaxel NPs, Student's t-test.

To determine whether co-administration of tPA affected the anti-cancer efficacy of other paclitaxel formulations, we used three different formulations of paclitaxel viz. paclitaxel in a micellar/cosolvent solution, Abraxane® and PLGA NPs. The three formulations used in our studies differed significantly in their particle size and hence their efficiency and mechanisms of transvascular and intratumoral transport.

We found that administration of paclitaxel in any of the three formulations significantly decreased tumor growth rate in the aggressive B16F10 model of mouse melanoma. Co-administration of tPA with paclitaxel in solution (~800 Da) did not improve its efficacy (**Figure 3-7A**). When co-administered with Abraxane® (particle size ~5 nm), there was a small improvement (*not statistically significant*) in its anti-cancer efficacy (**Figure 3-7B**). However, when administered in conjunction of PLGA NPs (particle size ~200 nm), there was a significant improvement in anti-tumor efficacy (**Figure 3-7C**). Slopes of the log-transformed tumor growth profiles are shown in **Figure 3-7D**. Administration of tPA reduced the rate of tumor growth for both colloidal formulations of paclitaxel (Abraxane® and PLGA NPs). However, the advantage was more pronounced for the formulation with the larger particle size.

3.4.5 Administration of tPA increases blood vessel diameter and tumor perfusion

Blood vessels in solid tumors are compressed due to the presence of copious amounts of ECM components and a fast growing cell population. Previous experiments have shown that administration of cytotoxic therapies [470, 473] or

ECM degrading enzymes [418] can decrease solid stress and restore vascular function. We were interested in determining if tPA had such an effect on B16F10 tumors.

Like other solid tumors, we found that B16F10 tumors showed a significant number of collapsed blood vessels (**Figures 3-8A, C and D**). Most blood vessels were <10 μm in diameter. After treatment with paclitaxel NPs, there was an increase in median blood vessel diameter. When treated with a combination of paclitaxel NPs and tPA, the median vessel diameter was found to increase even further (**Figure 3-8B, C and F**). It is interesting to note that regardless of treatment, the diameter of most blood vessels was <10 μm. However, treatment with paclitaxel alone or in combination with tPA led to the appearance of blood vessels in the 10-20 μm diameter range (**Figures 3-8E-F**).

We were further interested in obtaining real-time physiological information regarding blood perfusion in response to fibrinolytic therapy. Ultrasound imaging was used to track blood vessels in subcutaneous B16F10 tumors.

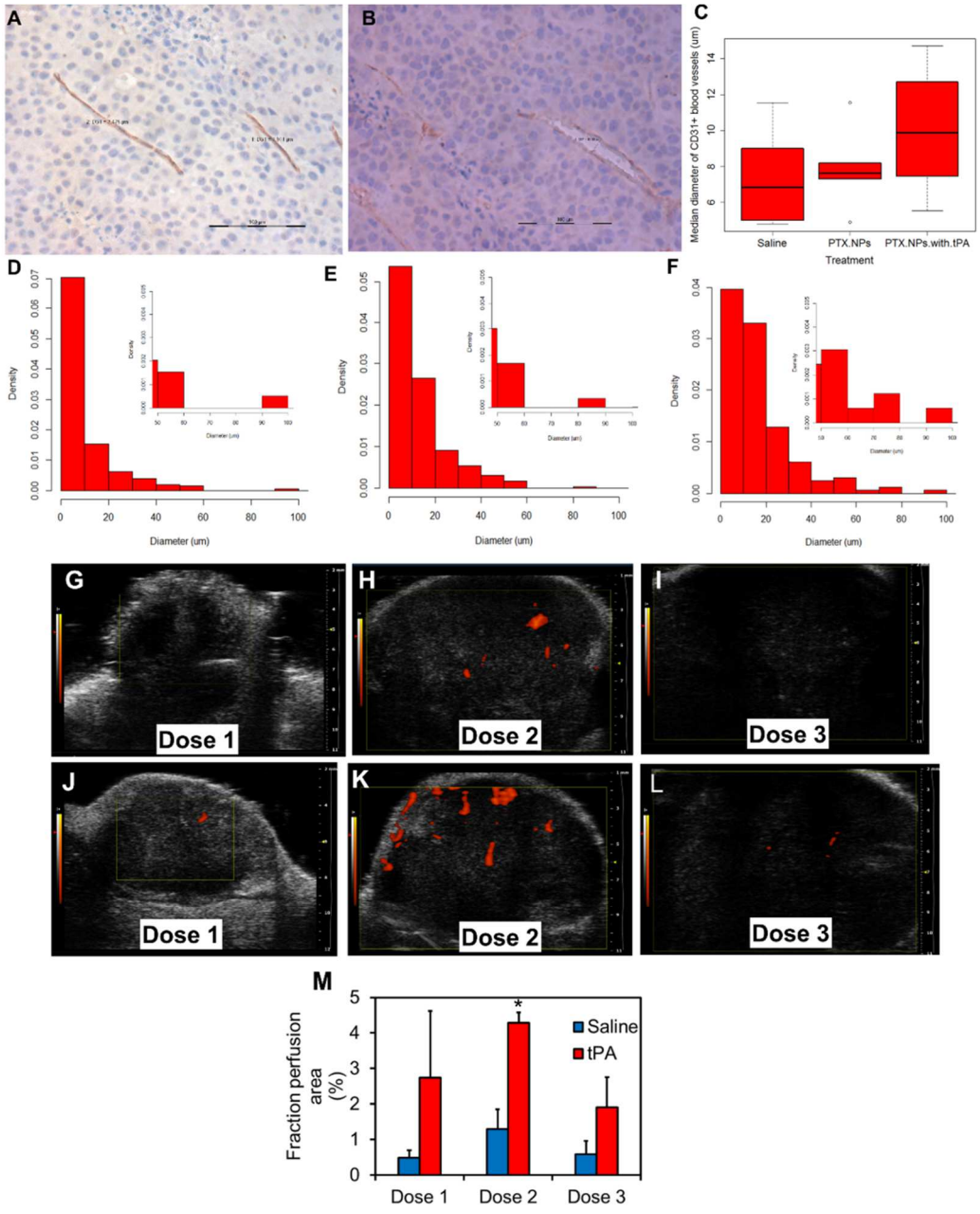

Figure 3-8. Effect of tPA treatment on tumor blood vessel diameter and tumor perfusion

(**A**) Compressed blood vessel in saline-treated tumor (**B**) Decompressed blood vessel in tumor treated with combination therapy (**C**) shows median blood vessel diameter in animals treated with different treatments Representative histograms showing blood vessel diameter in animals treated with (**D**) saline (**E**) paclitaxel NPs and (**F**) paclitaxel NPs and tPA. Representative sonograms of B16F10 tumors treated with three doses of (**G-I**) saline and (**J-L**) tPA (**M**) mean perfusion area in saline and tPA treated tumors. Data represented as mean ± S.E.M., n=3-5, *p<0.05, Student's t-test.

In saline treated animals, tumor perfusion area reached a maximum of ~1% after the second dose (**Figure 3-8G-I**). At all time points analyzed, tPA-treated tumors displayed a greater perfusion area (~3-4 fold higher) as compared to saline treated animals. In animals treated with tPA, tumor perfusion area was maximal after the second dose (~4% of tumor area) (**Figure 3-8J-M**). Difference in perfusion area was statistically significant after the second dose ($p<0.05$).

3.4.6 Migration of tPA functionalized nanoparticles across fibrin matrix

In an effort to co-localize the enzyme and NPs, we surface functionalized PLGA NPs with tPA. tPA functionalized NPs had a particle size of ~250 nm and a net negative zeta potential. The conjugation efficiency of the reaction was found to be ~50-60% (**Table 3-2**). Additionally, 94% of the enzyme was found to be active after the conjugation procedure.

Table 3-2. Physicochemical characterization of tPA functionalized nanoparticles
Data represented as mean ± S.E.M

Particle size (nm)	225.3 ± 15.6
Polydispersity index	0.18 ± 0.03
Zeta potential (mV)	-11.9 ± 1.6
Drug loading (% w/w)	12.1 ± 1.3
tPA conjugation efficiency (%)	54 ± 6.6

We determined the ability of tPA functionalized NPs to migrate across a fibrin matrix using a Transwell® assay. Enzyme functionalized NPs were able to migrate

across fibrin gels more efficiently than non-functionalized NPs (**Figure 3-9**). After an initial lag time, tPA functionalized NPs accumulated in the bottom chamber.

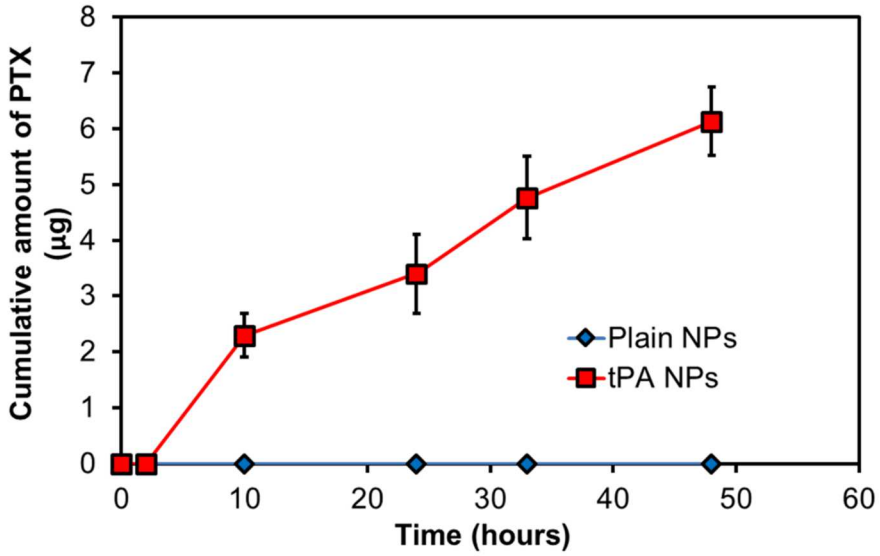

Figure 3-9. *In vitro* mobility of tPA functionalized nanoparticles

Mobility of tPA functionalized NPs was measured in a Transwell® study as described before. The mobility of enzyme functionalized NPs was significantly improved as compared to non-functionalized NPs. Results represented as mean ± S.D., n=3.

3.4.7 Anti-cancer efficacy of tPA functionalized nanoparticles

We determined the anti-cancer activity of tPA functionalized NPs in an orthotopic lung cancer model (**Figure 3-10A**) and in a syngeneic mouse model of melanoma (**Figure 3-10B**). tPA functionalized NPs successfully inhibited tumor growth in both models. However, the treatment efficacy was comparable to that of

non-functionalized NPs. Thus, surface functionalization with tPA did not result in any improvement in anti-cancer activity.

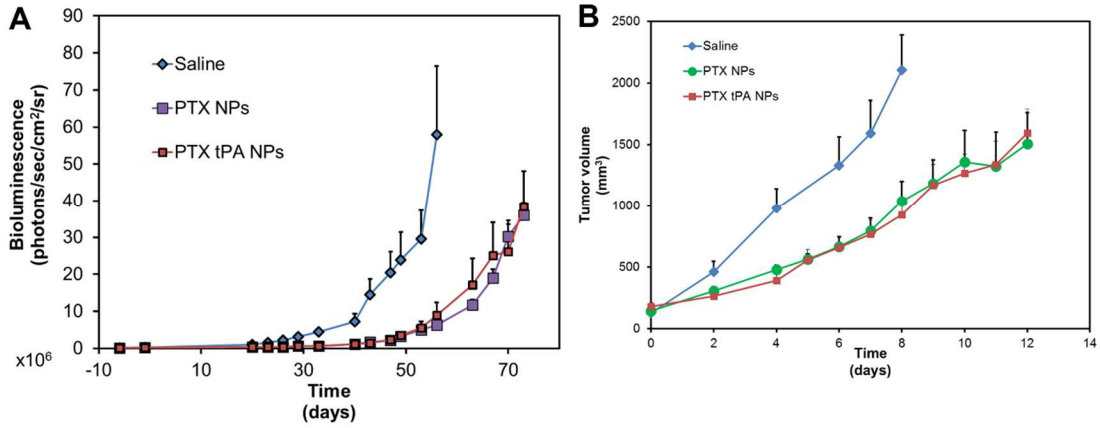

Figure 3-10. Anti-cancer activity of tPA functionalized nanoparticles

The anti-cancer efficacy of tPA functionalized NPs was determined in (**A**) orthotopic lung cancer model and (**B**) syngeneic melanoma model. The anti-cancer efficacy of enzyme functionalized NPs was comparable to that of non-functionalized NPs. Results represented as mean ± S.E.M., n=6-10 animals/group. Tumor inhibition of tPA functionalized nanoparticles was determined with other treatment groups reported in Figures 3-6 and 3-7. Data for saline and paclitaxel nanoparticle treated groups from Figures 3-6 and 3-7 are plotted here again.

3.4.8 Accumulation of paclitaxel in lung tumors

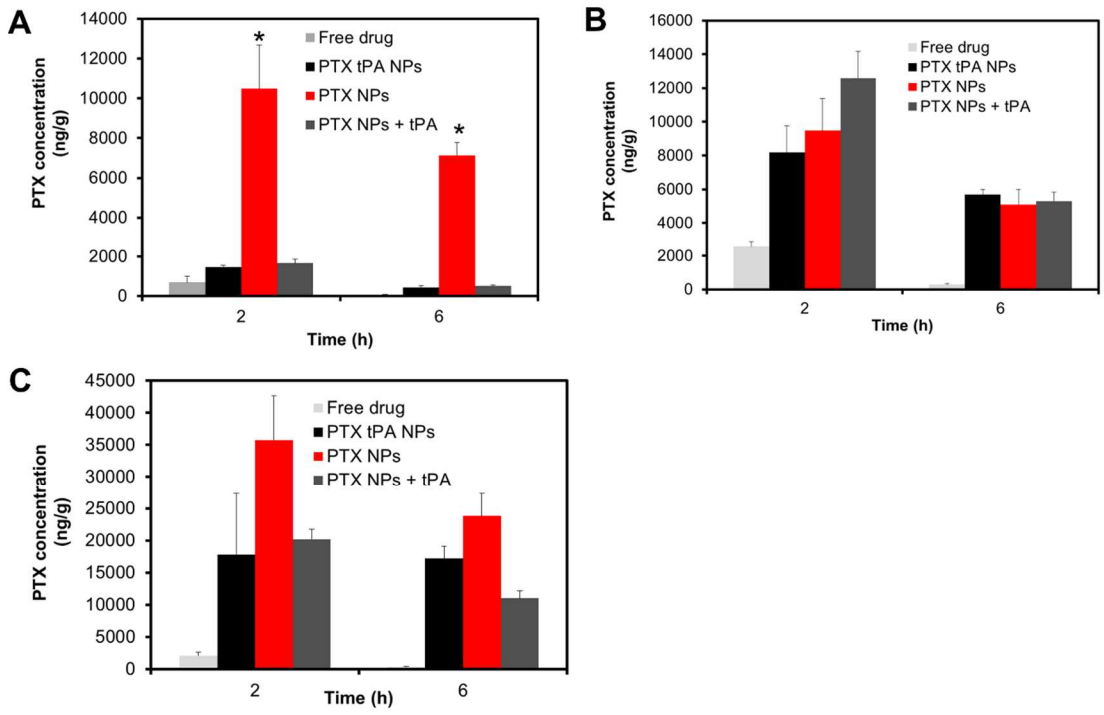

Figure 3-11. Lung tumor accumulation of paclitaxel

SCID animals bearing lung tumors were treated with various formulations of paclitaxel. Animals were sacrificed 2 h and 6 h after treatment administration. Paclitaxel concentrations in the (**A**) lungs (**B**) liver and (**C**) spleen were measured using LC-MS/MS. Results reported as mean ± S.E.M., n=3 animals/group. *indicates $p<0.05$ vs. PTX-tPA- NPs and PTX NPs + tPA, one-way ANOVA, post-hoc Tukey.

We determined the lung tumor accumulation of various formulations of paclitaxel. Treatment with NP formulations led to higher lung concentration than treatment with drug solution. Animals treated with a combination of paclitaxel NPs

and tPA or tPA functionalized NPs had a ~10-fold lower accumulation of paclitaxel in the lungs as compared to those treated with paclitaxel NPs alone (**Figure 3-11A**). Accumulation of the NPs in the liver and spleen was comparable (**Figure 3-11B** and **C**).

3.4.9 Effect of tPA on macrophage uptake of nanoparticles

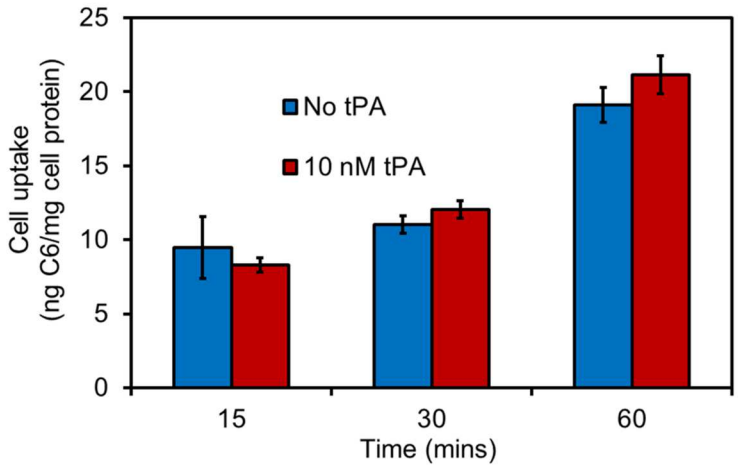

Figure 3-12. Effect of tPA on macrophage uptake of nanoparticles

Coumarin-6 loaded NPs were incubated with J774 cells in the presence or absence of tPA. NP uptake in the cells was determined using HPLC and cell protein content was determined using BCA. Results represented as mean ± S.D., n=4.

Previous reports suggest that tPA can affect macrophage function. These include polarization of macrophages to a M1 phenotype and production of NF-kB [46, 474]. We were interested in determining if the decreased lung accumulation of tPA conjugated NPs was mediated via an increased macrophage uptake. We

measured the macrophage uptake of NPs in the presence and absence of tPA. Macrophage uptake of NPs with or without tPA was similar (**Figure 3-12**).

3.5 Discussion

Incomplete elimination of tumor cells and disease recurrence are important limitations of current anticancer therapies. There are several factors responsible for this. These include overexpression of efflux transporters on the tumor cell surface, acidity of the tumor microenvironment, instability or lack of drug activity in hypoxic or reducing microenvironment of the tumor [460]. An under-studied yet significant factor responsible for poor efficacy is limited drug delivery to large regions within the tumor [92, 460]. Parts of the tumor that receive low drug concentrations also receive low concentrations of oxygen [93]. These hypoxic regions harbor more aggressive and resistant tumor cells [475]. Hence, it is even more important to deliver high drug concentrations to these under-supplied regions of the tumor.

Tumor blood vessels are formed in response to pro-angiogenic factors secreted by tumor cells [110]. An imbalance in pro- and anti-angiogenic factors within the tumor tissue results in the formation of blood vessels that are abnormal and porous [111]. Fluid from these porous blood vessels leaks out into the tumor microenvironment. Due to the lack of functional lymphatics in the core of the tumor, fluid accumulates in the tumor [13]. This results in diminished transvascular pressure gradient in certain regions of the tumor [13]. Additionally, because of fast dividing cells in a limited area and a highly dense ECM, blood vessels in the core of the tumor are compressed and non-functional [202]. Consequently, drug

exchange through convection is highly compromised [181]. Improving fluid dynamics in the tumor is therefore likely to have a significant impact on the delivery of drugs to tumors and can progress the state of chemotherapy.

Several strategies have been used for improving drug transport within the tumor[460]. Anti-angiogenics have been used to modify the faulty vascular architecture in the tumor. The use of anti-angiogenics results in the normalization of blood vessels, leading to a reduced fluid leakage out of the blood vessels, and a decrease in interstitial fluid pressure [111]. Consequently, convectional transport across blood vessels increases. On the other hand, decreasing the production or degrading the ECM in the tumor has also been shown to improve drug delivery. Decreasing the density of ECM can improve the diffusivity of the carrier/drug in the tumor matrix. Moreover, it can lead to decompression of the collapsed blood vessels in the tumor. This increases the perfusion area within the tumor and improves the efficiency of drug delivery [418, 419].

Due to the leaky nature of tumor blood vessels, there is significant fibrinogen deposition within the tumor. The prothrombogenic activity of the tumor microenvironment leads to the activation of fibrinogen to fibrin. The role of fibrin in tumor growth and metastasis has been well studied [476-479]. During the initial stages of tumor growth, fibrin provides a scaffold for the growth of tumor cells. Fibrin also plays an important role in the angiogenesis, modulating the influx macrophages and in the storage of growth factors [126, 480]. Depletion of fibrinogen has also been shown to reduce formation of pulmonary metastatic foci.

This effect is likely due to the loss of fibrinogen mediated protection of tumor cells against NK cells [478].

However, the role of fibrin in limiting drug delivery to tumors has not been studied previously. In the current study, we hypothesized that degrading fibrin within the tumor ECM may reduce solid stress within the tumor and improve the intratumoral distribution of drug carriers. Through immunohistochemistry studies, we found that treatment with tPA led to an increased blood vessel diameter. This data was supported by increased tumor perfusion as noted by ultrasound imaging. Importantly, co-administration of tPA led to an improved chemotherapeutic activity of paclitaxel nanoparticles in a syngeneic model of mouse melanoma and orthotopic human lung cancer model.

Fibrin expression in tumors has been a topic of considerable interest. Consequently several studies have analyzed the expression of fibrin in different animal tumor models [131, 471]. However, a systematic analysis of fibrin expression in human tumors has not been conducted. We examined the level of fibrin expression in several human tumor biopsies. Fibrin levels were found to be variable, with no tumor type showing either a complete lack or consistently high level of fibrin. There are several reasons cited for this heterogeneity in fibrin expression. Current immunohistochemistry techniques cannot distinguish between fibrinogen and cross-linked fibrin. Additionally, bleeding during the collection of the tumor biopsy can also significantly affect the results [126]. Accurately quantifying fibrin levels in tumors is important to successfully advance adjuvant fibrinolytic therapy. Novel peptides that specifically identify fibrin may be useful [481, 482].

The clinical use of anti-coagulants and fibrinolytic therapies in cancer patients has been reported before [483-487]. These studies have shown that administration of anti-coagulants such as heparin and warfarin improve mean survival in patients with small cell lung cancer. The rationale presented for the use of anti-coagulants is that it reduces the occurrence of spontaneous thromboembolism and tumor cell dissemination [486, 488]. Some studies have reported the beneficial effects of using urokinase in conjunction with chemotherapy [483]. The mechanism for the improved response to chemotherapy was not explored.

In our studies, the benefit of tPA on the anti-cancer activity of paclitaxel manifested itself in a particle-size dependent manner. The greatest improvement in anti-cancer activity was observed at the largest particle size. This effect may be dependent on the tumor model used in our studies. Though highly compressed, the blood vessels in B16F10 tumors may be permissive to the entry of paclitaxel in solution and Abraxane®. Thus, the distance between functional blood vessels for these formulations in this tumor model is not large. A low diffusion distance coupled with moderately high diffusivity of the drug in these formulations may enable efficient intratumoral distribution. Hence, improving the vascularity of the tumor any further does not impact the chemotherapeutic activity of these formulations. On the other hand, the blood vessels in B16F10 tumors may not be permissive to the entry of large nanoparticles. Additionally, the diffusivity of large NPs would be orders of magnitude lower than that of the other formulations. Previous work shows that decrease in diffusivity of large NPs in tumor matrices is greater than what would be expected by Stokes-Einstein law [489]. Hence,

improving vascular function and decreasing intra-vessel distance in the tumor will likely affect the chemotherapeutic activity of larger NPs. Studies in tumors with a lower degree of vascularity may help address the mechanism further.

The time course of change in perfusion area with tumor volume is also interesting. Perfusion area in untreated tumors and tPA treated tumors was highest after the second dose of treatment. The perfused area in tPA treated tumors was found to be ~3-4 fold higher than saline treated tumors at each time point. Previous work has shown that blood flow generally decreases with an increase in tumor volume [490]. The disparity in results may be due to different techniques used for measurement of blood flow. Lack of sensitivity of the ultrasound technique may have limited our ability to detect blood vessels in small tumors.

Studies with anti-angiogenic therapy have shown that there is a time window associated with the normalization of blood vessels [402, 491, 492]. In other words, the decrease in interstitial fluid pressure is transient. The improvement in drug delivery is maximal in this time window. It is conceivable that a similar phenomenon may occur with tPA treatment as well. Modeling reports suggest that an increased perfusion in leaky blood vessels can result in a rapid increase in interstitial fluid pressure [493]. This would quickly neutralize the advantage obtained with increased perfusion. Moreover, tPA has a short half-life. If the deposition of fibrin in tumors is rapid, the decrease in fibrin content of the tumor will likely be observed only for a short period of time. The pharmacokinetics of NP and tPA accumulation in the tumor may also be different. Additional studies are needed to determine the optimal frequency of tPA dosing and the time window following tPA dosing when

the improvement in drug delivery is maximal. Further, we have only considered Abraxane and PLGA NPs in this study. The effect of tPA co-delivery on other nanoparticulate systems of intermediate sizes would be of interest as well. A careful consideration of all these aspects can help maximize benefits obtained from this strategy.

An important difference between collagen or hyaluronic acid and fibrin is the mechanism of deposition into the tumor matrix. Both collagen and hyaluronic acid are synthesized by the tumor cells. On the other hand, fibrin is deposited into tumors due to the leaky tumor blood vessels. This indicates that the leakiness of tumor blood vessels is a prerequisite for fibrin occurrence in tumors. As mentioned previously, tumors with leaky blood vessels are less likely to benefit from improved perfusion due to a rapid increase in interstitial fluid pressure. It might be of interest to combine anti-angiogenic therapy with fibrinolytic therapy to improve tumor perfusion for prolonged time intervals.

We successfully conjugated tPA on the surface of NPs and found it to be active after the conjugation procedure. We hypothesized that conjugating tPA on the NPs may help co-localize the NPs with enzyme, potentially increase its half-life and tumor accumulation. All these effects could, in turn, improve the adjuvant activity of tPA. Unfortunately, tPA functionalized NPs had comparable activity to non-functionalized NPs. The current study did not analyze the mechanism for the loss of activity. One possible reason could be the decrease in mobility of tPA due to its conjugation to the NPs.

The results of the lung tumor accumulation study are difficult to explain. Co-treatment with tPA, either as free enzyme or conjugated on the NP surface, decreased the lung accumulation of NPs. One of the major organs that can influence the biodistribution of NPs is the liver. The accumulation of the different formulations in the liver was comparable. It is however possible that the current analysis may not be able to detect a difference in liver accumulation due to the rapid metabolism of paclitaxel. Given that there is some evidence in literature of tPA-mediated activation of macrophages [474], we measured the macrophage uptake of NPs in response to co-incubation with tPA. We did not find any effect of tPA on the uptake of NPs. Other evidence suggests that tPA is rapidly taken up by the hepatic cells and endothelial cells in the liver [494-497]. Uptake of tPA in the endothelial cells occurs through mannose receptors [494]. Alternately, uptake of tPA in liver parenchyma occurs via a receptor that binds a complex of tPA and plasminogen activator inhibitor, which is abundantly expressed in the liver [495]. While these results may partly explain the decreased lung accumulation of tPA conjugated NPs, the reason for the decreased lung accumulation of paclitaxel in combination therapy is still unclear. A detailed understanding of this phenomenon may prove useful for advancing this therapy.

3.6 Conclusion

Poor vascular architecture and lack of tumor perfusion limits the overall efficacy of chemotherapy. Fibrin deposition within the tumor can be an important cause for the compression of tumor blood vessels. Administration of tPA improved blood

supply to solid tumors and enhanced chemotherapeutic activity of paclitaxel in polymeric NPs.

Chapter 4 Reformulating Tylocrebrine in EGFR Targeted Polymeric Nanoparticles Improves its Therapeutic Index[3]

[3] This chapter is published elsewhere [293]. Reproduced with permission.

4.1 Summary

Several promising anti-cancer drug candidates have been sidelined owing to their poor physicochemical properties or unfavorable pharmacokinetics, resulting in high overall cost of drug discovery and development. Using alternative formulation strategies that alleviate these issues can help advance new molecules to the clinic at a significantly lower cost. Tylocrebrine is a natural product with potent anti-cancer activity. Its clinical trial was discontinued following the discovery of severe central nervous system toxicities. To improve the safety and potency of tylocrebrine, we formulated the drug in polymeric nanoparticles targeted to the epidermal growth factor receptor (EGFR) overexpressed on several types of tumors. Through *in vitro* studies in different cancer cell lines, we found that EGFR targeted nanoparticles were significantly more effective in killing tumor cells than the free drug. *In vivo* pharmacokinetic studies revealed that encapsulation in nanoparticles resulted in lower brain penetration and enhanced tumor accumulation of the drug. Further, targeted nanoparticles were characterized by significantly enhanced tumor growth inhibitory activity in a mouse xenograft model of epidermoid cancer. These results suggest that the therapeutic index of drugs that were previously considered unusable could be significantly improved by reformulation. Applying novel formulation strategies to previously abandoned drugs provides an opportunity to advance new molecules to the clinic at a lower cost. This can significantly increase the repertoire of treatment options available to cancer patients.

4.2 Introduction

Much of current cancer research is focused on exploring novel targets and discovering new anticancer drugs. While the availability of new molecules certainly offers hope to patients who do not respond to existing drugs, development of each new molecule is associated with tremendous costs [498, 499]. Many highly active drug candidates have been shelved because of poor physicochemical and/or pharmacokinetic characteristics [500-502]. Re-formulation of such molecules can overcome their unfavorable biological behavior, and would offer a less expensive approach to anticancer drug development [501, 503, 504].

Tylocrebrine, a phenanthropiperidine alkaloid, is an example of a drug with potent anti-cancer activity and whose clinical trial was discontinued following the discovery of severe central nervous system (CNS) toxicities. The CNS toxicities of the drug were likely caused by its extensive penetration into the brain [505, 506]. We hypothesized that encapsulation of tylocrebrine in poly(lactide-*co*-glycolide) (PLGA)-based polymeric NPs will limit the distribution of the drug to the CNS, potentially decreasing its neurological toxicities. Additionally, NPs are known to passively accumulate in the tumor tissue through the enhanced permeability and retention (EPR) effect [507, 508]. The combination of these properties should result in significantly improved therapeutic index. To further enhance the tumor cell uptake and retention of NPs, we functionalized the NP surface with a peptide capable of targeting the epidermal growth factor receptor (EGFR) [227, 228], which is over-expressed on the cell membrane of multiple solid tumors [386]. Using *in vitro* and *in vivo* models of EGFR-overexpressing tumors, we evaluated the therapeutic benefit of encapsulating tylocrebrine in NPs. Our studies show that this

reformulation strategy significantly improved the anti-tumor efficacy while reducing the brain penetration of tylocrebrine.

4.3 Materials and methods

4.3.1 Materials

Amine terminated poly(ethylene glycol) (molecular weight: 3400 Da) was purchased from Laysan Bio Inc. (Arab, AL). PLGA (50:50 molar ratio of lactide-glycolide, molecular weight ~40 kDa) was purchased from Lactel (Birmingham, AL). Poly(vinyl alcohol) (molecular weight 30-70 kDa) and lactic acid were obtained from Sigma-Aldrich Co. (St. Louis, MO). EGFR targeting peptide (YHWYGYTPQNVI) and scrambled peptide (HWPYAHPTHPSW) were obtained from Peptide 2.0, Inc. (Chantilly, VA). Radioimmunoprecipiation (RIPA) buffer and bicinchoninic acid (BCA) assay kit were obtained from Thermo Scientific (Rockford, IL). All other chemicals were obtained from Sigma-Aldrich Co. (St. Louis, MO). Tylocrebrine was synthesized as described previously [509].

4.3.2 Cell culture

A549 human lung cancer cell line was obtained from ATCC. A431 human epidermoid cancer cells were obtained from Dr. Benjamin Hackel (University of Minnesota). A549 cells were cultured in Dulbecco's Minimum Essential Media (DMEM) while A431 cells were grown in Roswell Park Memorial Institute media (RPMI-1640). Both media were supplemented with 10%v/v fetal bovine serum and

1%v/v penicillin-streptomycin. The cells were grown in a humidified environment consisting of 5% CO_2/95% air and maintained at 37 °C.

4.3.3 Effect of extracellular pH on cell uptake of tylocrebrine

We determined the effect of extracellular pH on the cell accumulation of tylocrebrine. For low pH conditions, serum free RPMI was acidified with 9.1 %v/v 0.1M HCl. The pH of acidified RPMI was maintained between 6.3-6.7 for 6 h when placed under routine cell culture conditions.

A431 cells were seeded in a 24-well plate ($5x10^4$ cells/well) and allowed to adhere overnight. Tylocrebrine was first dissolved in 1 M HCl (1:1 molar ratio) and then diluted in serum-free RPMI to prepare a stock solution of 1 mg/mL. The stock solution was then diluted to 5 µg/mL in neutral or acidic serum-free RPMI and added to the cells. Treatments were removed 1 h later, and the cells were washed with cold 0.15 mM phosphate buffered saline (pH 7.4, henceforth referred to as 1X PBS). Cells were digested with RIPA buffer (0.1 mL) for 15 min and the cell lysate was divided into two parts. One part (20 µL) was analyzed by BCA assay to determine cell protein concentration (ELx800 absorbance microplate reader, Biotek Inc., Winooski, VT). The other part (80 µL) was extracted overnight with methanol and tylocrebrine concentration in the methanol extract was analyzed using HPLC. HPLC was performed on a Beckman Coulter HPLC system equipped with a System Gold 508 autosampler was used. A Beckman Coulter C18 column (4.6 mm x 250 mm, 5 µm) was used as the stationary phase. The mobile phase

consisted of 80:20 mix of acetonitrile and 87 mM ammonium acetate (pH 4.2), run isocratically at a flow rate of 1 mL/min. Tylocrebrine was analyzed by measuring absorbance at 265 nm using a System Gold UV detector.

4.3.4 Synthesis of carboxyl terminated block co-polymer of poly(lactide) and poly(ethylene glycol)

A block co-polymer of poly(lactide) (PLA) and carboxyl terminated poly(ethylene glycol) (PEG-COOH) was synthesized in a two-step process. In the first step, lactic acid was reacted with amine-terminated PEG to generate an amine-terminated block co-polymer (PLA-PEG-NH_2) [510]. In the second step, the terminal amino group was reacted with succinic anhydride to produce PLA-PEG-COOH [228].

All glassware were rinsed with toluene and dried overnight at 100°C prior to both reactions. For step 1, amine-terminated PEG (400-500 mg) was dissolved in ~80 mL dichloromethane and added to a round bottom flask. The mixture was stirred in the presence of N_2 gas for 10 minutes. Lactic acid (2 g) was added to this mixture and stirred for 10 minutes. About 20 µL of 1, 8 diazabicyclo [5,4,0] undec-7-ene was added as a catalyst and the reaction was allowed to proceed for 1 hour. After 1 h, the solvent was reduced to ~20 mL using a rotovap. The solution was added drop-wise to chilled diethyl ether to precipitate the amine terminated block co-polymer. The suspension was filtered and the solid was dried at 25°C in a vacuum oven. The product was dissolved in deuterated chloroform and characterized using ^{1}H-NMR (Varian 400 MHz).

For step 2, the amine terminated block co-polymer (1 g) was dissolved in 50 mL tetrahydrofuran and 5 mL triethyl amine in a round bottom flask. The mixture was stirred under N_2 gas for 10 minutes. Succinic anhydride (molar ratio of succinic anhydride to block co-polymer was 1.1:1) was added to this solution. The reaction was allowed to proceed at 50°C for 2 h. The reaction mixture was then concentrated using a rotavap and added to cold diethyl ether to precipitate the polymer. The polymer was filtered and dried in a vacuum oven at 25°C. The product was dissolved in deuterated chloroform and characterized by ^{1}H NMR.

4.3.5 Synthesis, optimization and physicochemical characterization of nanoparticles

PLGA NPs loaded with tylocrebrine and surface functionalized with carboxyl-terminated PEG were synthesized by the interfacial activity assisted surface functionalization (IAASF) technique developed by our lab [33, 210].

Briefly, PLGA (30-35 mg) and tylocrebrine (5 mg) were dissolved in 1 mL chloroform. An aqueous solution of 2%w/v poly(vinyl alcohol) in 1X PBS was prepared. The polymer-drug mixture was added to the aqueous surfactant to form an o/w emulsion. The emulsion was probe sonicated at an output of 18-21 W for 5 minutes over an ice bath (Sonicator XL, Misonix, NY) and then stirred at 650 rpm on a magnetic stir plate. PLA-PEG-COOH (8 mg) dissolved in 0.2 mL chloroform was added drop-wise to the emulsion. The organic solvent was evaporated overnight under ambient conditions and then for 2 hours under vacuum. The NP dispersion was washed twice with 30 mL 1X PBS by ultracentrifugation (35000

rpm, 35 min, 4°C) (Beckman, Palo Alto, CA). After the second wash, NPs were dispersed in 1.5 mL 1X PBS. To this dispersion, 0.7 mg N-hydroxysuccinimide (NHS), 1.14 mg 1-ethyl-3-[3-dimethylaminopropyl] carbodiimide hydrochloride (EDC) and 1.8 mg targeting or control peptide were added, and the reaction was allowed to proceed for 3, 5 or 8 hours. Following the conjugation reaction, NPs were dispersed in 30 mL deionized water and centrifuged (35000 rpm, 35 min, 4°C) to remove unconjugated peptide. The NP pellet was redispersed in ~10 mL deionized water, frozen below -50°C for 2 h, and lyophilized (Labconco FreeZone 4.5, Kansas city, MO). The lyophilized formulation was stored at -20°C.

To determine particle size and zeta potential, a dispersion of NPs (~1 mg/mL) was analyzed by dynamic light scattering (Delsa^{TM} Nano C, Beckman Coulter, Fullerton, CA).

To determine drug loading, NPs were dispersed in a mixture of methanol and acetic acid (95:5 v/v). Drug was extracted overnight at room temperature. NPs were separated from the extract by centrifugation (14000 rpm, 15 min, 4°C). The supernatant was analyzed by HPLC.

The amount of peptide on the surface of NPs was determined using BCA. NPs were dispersed in deionized water and incubated with the BCA reagent for 20 minutes at 37°C. The NP dispersion and standards were then centrifuged (14000 rpm, 15 minutes, 25°C), and the absorbance of the supernatant was measured at 562 nm (ELx800 absorbance microplate reader, Biotek Inc., Winooski, VT).

Drug release kinetics was assessed in pH 7.4 and 6.5 buffers. NPs were dispersed in a sufficient volume of 1X PBS (pH 7.4 or 6.5) to maintain sink conditions. The dispersions were kept on a shaker at 37°C and 100 RPM [C24 incubator shaker, New Brunswick Scientific (now Eppendorf Inc. Enfield, CT)]. At various time points, the released drug was separated from NPs using a MicroKros® filter module (Spectrum Labs, Rancho Dominguez, CA). The NP concentrate was retrieved and redispersed in the buffer. Drug solution was lyophilized, dissolved in a mixture of methanol and acetic acid (95:5 v/v), and analyzed by HPLC.

4.3.6 Cellular uptake of EGFR-targeted and non-targeted nanoparticles

We first determined whether cellular uptake of EGFR targeted NPs was higher than non-targeted NPs, and if their uptake was mediated by EGFR. A549 cells were seeded in a 24-well plate at a seeding density of 5 x 10^4 cells/well and allowed to adhere overnight. On the next day, NPs loaded with a fluorescent dye (coumarin 6), in the presence or absence of excess free targeting peptide, were added to the cells. Cells were incubated with the treatments at 4°C for 1 h, washed twice with 1X PBS, and incubated with fresh media at 37°C. After 1 h, the media was aspirated, cells were washed with 1X PBS, and lysed with RIPA buffer. One part of the lysed cells was extracted with methanol and coumarin 6 content was determined using HPLC [210]. The other part was analyzed by BCA assay to determine the amount of cell protein.

We also compared the cell uptake of targeted and non-targeted NPs loaded with tylocrebrine. A431 cells were seeded in a 24-well plate as described above.

On the day of the experiment, tylocrebrine loaded NPs, dispersed in serum-free media, were added to the cells (100 µg NPs/mL). After 1 h, the media was aspirated and the cells were washed thrice with cold 1X PBS. The cells were then lysed with 0.1 mL RIPA buffer for 15 minutes. The cell lysate was divided into two parts. One part (20 µL) was analyzed by BCA assay to determine the amount of cell protein. The other part (80 µL) was extracted with a mixture of methanol and acetic acid (95:5 v/v). Tylocrebrine concentration in the methanolic extract was determined using HPLC.

4.3.7 *In vitro* efficacy of various formulations of tylocrebrine

We compared the tumor cell kill efficacy of free drug, non-targeted and targeted NPs in both neutral and acidic media. A549 cells or A431 cells were seeded in a 96-well plate ($8x10^3$ cells/well) and allowed to attach overnight. NPs or free drug were dispersed in serum-free RPMI media to form a stock solution. This stock solution was then diluted with either neutral or acidified serum-free media and added to the cells at various dilutions. The treatments were removed 6 h later, and the cells were washed with cold 1X PBS. The cells were then incubated with serum containing media for further 90 h. Cell viability was measured using CellTiter 96® AQ_{ueous} One Solution Cell Proliferation Assay kit (Promega, Madison, WI) according to the supplier's protocol.

4.3.8 Pharmacokinetics and biodistribution of various formulations of tylocrebrine

All the animal studies described here were approved by the University of Minnesota's institutional animal care and use committee.

We determined the pharmacokinetics of tylocrebrine in a mouse tumor model. A431 cells (1-2x10^6) were dispersed in 0.05 mL 1X PBS and injected subcutaneously in female athymic nude mice (4-6 weeks old, Taconic Biosciences, Hudson, NY). The tumors were allowed to grow to a volume of ~300 mm^3. Mice were lightly anesthetized using isofluorane and treated with various formulations of tylocrebrine (dose: 12 mg/kg; dosing volume: 10 mL/kg) via retroorbital injection.

The free drug formulation was prepared by dissolving the drug in 1M HCl (1:1 molar ratio), and diluting the solution with saline. Excess acid was neutralized with 1M NaOH to obtain a final drug concentration of 1.2 mg/mL. To prepare NP treatments, NPs were dispersed in saline and probe sonicated at an output of 18-21 W thrice for 30 sec each on an ice bath. The NP dispersion was centrifuged (1000 rpm, 5 min) to remove any large aggregates and the supernatant was used.

At various time points, cohorts of mice were sacrificed and blood was collected by cardiac stick. Key organs and the tumor were excised. Tissues were homogenized in ~1 mL deionized water and lyophilized. The dry organs were then extracted overnight with a mixture of methanol and acetic acid (95:5). The extract was separated by centrifugation and dried under N_2 gas. The dried residue was redispersed in a mixture of acetonitrile and acetic acid (95:5). The resulting

suspension was centrifuged (14000 rpm, 15 min, 4°C), and the supernatant was used for LC-MS/MS analysis.

LC-MS/MS was performed using an Acquity UPLC system equipped with a Waters/Micromass Quattro^{TM} Ultima mass spectrometer. Liquid chromatography was performed using Agilent XDB-C18 column (4.6 mm x 50 mm, 1.8 µm) as the stationary phase. A mixture of 10 mM ammonium acetate with 0.06%v/v acetic acid and acetonitrile (55:45 v/v) was used as the mobile phase. The flow rate was 0.4 mL/min, and the run time was set to 6 minutes. The mass spectrometer was run in the electrospray positive mode. The mass spectrometer conditions were as follows: cone voltage, 50 V; collision voltage, 20 V; dwell time, 0.4 seconds. Tylocrebrine was detected by monitoring the m/z transition of 394→324.9.

Concentration of tylocrebrine was normalized to tissue weight and injected dose, and was represented as % injected dose (ID)/g of organ weight. Drug exposure in each tissue was determined by calculating the area under the concentration curve (AUC). AUC was calculated using the trapezoidal rule. The relative benefit of using the nanoparticulate formulation over the free drug was determined using the drug targeting index (DTI) [450]. The DTI was calculated as shown below:

$$DTI = \frac{\left(\frac{AUC_{tumor}}{AUC_{brain}}\right)_{nanoparticle}}{\left(\frac{AUC_{tumor}}{AUC_{brain}}\right)_{free\ drug}}$$

4.3.9 Tumor inhibition studies

The therapeutic efficacy of various formulations of tylocrebrine was determined in a mouse model of epidermoid cancer. About $1x10^6$ A431 cells, suspended in 50 µL 1X PBS, were injected subcutaneously in female nude mice. The dimensions of the tumor were measured periodically using a digital caliper. Tumor volume was calculated as $0.5 * length * width^2$. When tumor volume reached ~75 mm^3, animals were treated with saline, free drug, non-targeted NPs or EGFR targeted NPs (3 doses, every 96 h, 12 mg/kg). The treatments were prepared and administered as described in the biodistribution study.

At the end of the study, animals were sacrificed and the tumors were excised. The tumors were fixed using 5% formalin solution in 1X PBS for 24 hours. After the initial fixation, tumors were preserved in 70% ethanol. Microtome sectioning was performed on the fixed and mounted tumor samples, and the sections were stained for cleaved caspase 3 (to determine apoptosis) and Ki67 (as a marker of proliferation). Staining of tumor sections was quantified using ImageJ 1.48v software. To determine apoptotic and proliferative indices, the fraction of the total cellular area that stained positive for the individual markers was determined and presented as apoptotic and proliferative indices.

4.3.10 Statistical analysis

All statistical analyses were performed using One-way ANOVA and post-hoc Tukey test. For the efficacy study, a linear model was fit to log transformed tumor values. Slopes of the tumor growth profile were analyzed at each time point for

each animal. One-way ANOVA and post-hoc Tukey test was performed to determine if the differences in various treatments were statistically significant. A P value < 0.05 was considered statistically significant.

4.4 Results

4.4.1 Effect of extracellular pH on the cell uptake of tylocrebrine

Tumors are often characterized by increased production of lactic acid due to the Warburg effect [511]. Impaired drainage of the acid from the tumor microenvironment leads to low extracellular pH in the tumor [512]. Tylocrebrine is a weak base and is ionized under acidic conditions. Ionization of the drug molecule can decrease its diffusion across the cell membrane and hence lead to decreased intracellular drug availability [513]. We measured the effect of extracellular pH on drug accumulation in A431 cells (**Figure 4-1**). Decreasing the pH of the media from 7.4 (physiologic) to 6.3-6.7 (to mimic tumor microenvironment) resulted in reduced drug uptake (~60% reduction). This is likely due to the protonation of the indolizidine nitrogen, leading to a positive charge on the molecule [514].

To overcome this unfavorable ionization of tylocrebrine and reduced availability inside the cells, we formulated the drug in EGFR-targeted polymeric NPs. NPs loaded with tylocrebrine and surface functionalized with PEG-COOH were first fabricated using the IAASF technique. These NPs were then conjugated to either the EGFR-targeting peptide or a control, non-targeting peptide.

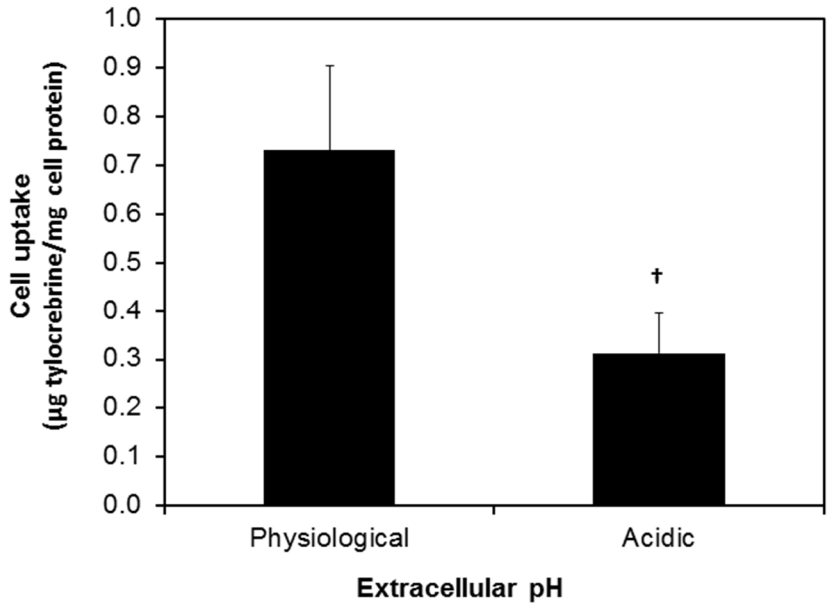

Figure 4-1. Effect of extracellular pH on cellular accumulation of tylocrebrine

Tylocrebrine (as free drug) was incubated with A431 cells at an extracellular pH of 7.4 (physiological) or ~6.5 (acidic). Cellular accumulation was measured by determining intracellular tylocrebrine concentration using HPLC. Tylocrebrine concentration was normalized to cell protein content. Data represented as mean ± S.D., n=6, † indicates $p<0.005$.

4.4.2 Synthesis and NMR analysis of block-copolymer

PLA-PEG-COOH block copolymer was used to incorporate carboxyl groups on the surface of PLGA NPs. We synthesized PLA-PEG-COOH through a two-step

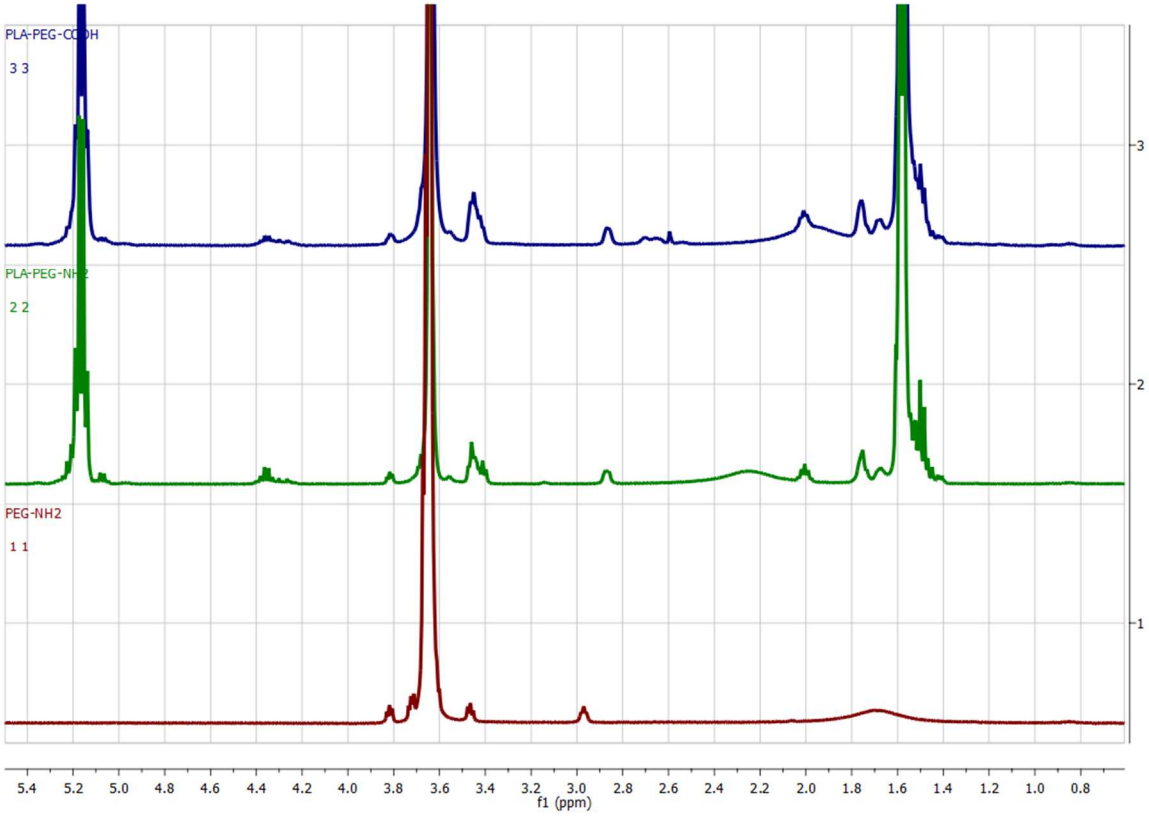

Figure 4-2. ^{1}H-NMR spectra of PLA-PEG block co-polymers

Block co-polymer of PLA and carboxyl terminated PEG was synthesized by a two-step procedure. The starting material (PEG), intermediate product (PLA-PEG-NH_2) and final product (PLA-PEG-COOH) were dissolved in deuterated chloroform and analyzed by ^{1}H-NMR. Conjugation of lactide to PEG was confirmed by the appearance of peak at 1.6 and 5.2 ppm. Conjugation of succinate to the terminal amine group in PEG was confirmed by appearance of peak at 2.6 ppm.

reaction, involving the generation of PLA-PEG-NH_2 from PEG-NH_2, followed by the reaction of the terminal amino group with succinic anhydride. The NMR spectra of PEG-NH_2, PLA-PEG-NH_2, and PLA-PEG-COOH are shown in **Figure 4-2**. Conjugation of lactide to PEG was confirmed by the appearance of peaks at δ=5.3 ppm and δ=1.6 ppm [515]. Conjugation of succinate moiety to PLA-PEG-NH_2 was confirmed by the appearance of a peak at δ=2.6 ppm [228]. Based on the AUC of the peaks, the molecular weight of PLA was estimated to be ~15 kDa.

4.4.3 Physicochemical characterization of nanoparticles

We initially determined the effect of reaction time on drug loading in NPs and efficiency of targeting peptide conjugation to the surface of NPs. Increasing the

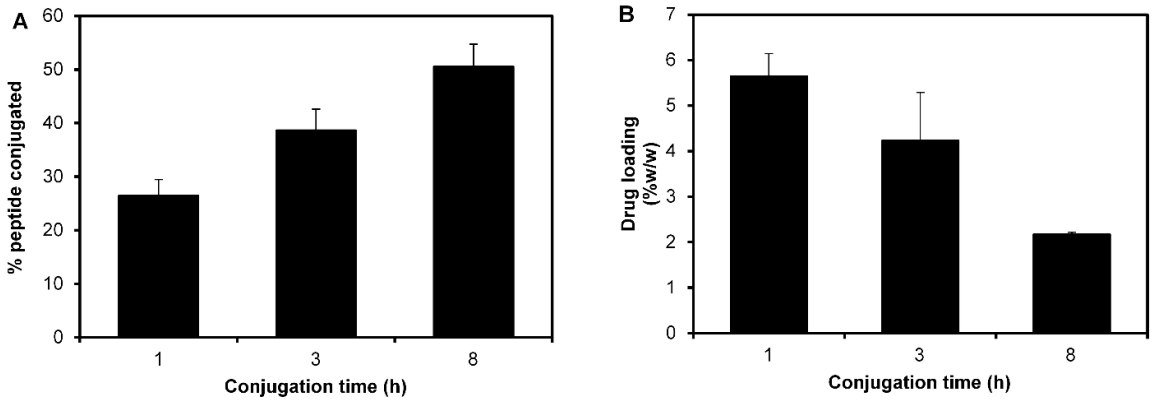

Figure 4-3. Effect of conjugation time on targeting peptide conjugation efficiency and drug loading

EGFR targeting peptide was conjugated to the surface of nanoparticles using NHS-EDC chemistry. The influence of reaction time on **(A)** conjugation efficiency of the peptide and **(B)** drug loading is shown. Data represented as mean ± S.D., n=3.

reaction time resulted in an increase in peptide conjugation efficiency but resulted in decreased drug loading (**Figure 4-3**). Particle size and zeta potential were unaffected by the duration of the reaction time. In general, the particle size was found to be in the range of 300-400 nm and the particles had a net negative zeta potential (**Table 4-1**). We used an intermediate reaction time (5 h) for achieving optimum drug loading and conjugation efficiency. The drug and peptide loading for NPs used in the rest of the studies are summarized in **Table 4-1**.

The drug release profile from NPs at physiological pH is shown in **Figure 4-4 A**. Both targeted and non-targeted NP formulations showed a characteristic initial burst release, followed by sustained release over a period of 48 h. Drug release profiles were comparable for both targeted and non-targeted NPs.

Table 4-1. Physicochemical characterization of nanoparticles
Data represented as mean ± S.E.M., n=3-6

	Non-targeted nanoparticles	Targeted nanoparticles
Particle size (nm)	322.6 ± 34.6	365.3 ± 18.8
Polydispersity index	0.17 ± 0.01	0.17 ± 0.01
Zeta potential (mV)	-15.78 ± 1.15	-14.87 ± 3.46
Drug loading (% w/w)	5.65 ± 0.59	5.78 ± 0.55
Peptide loading (µg protein/mg nanoparticle)	9.2 ± 0.8	16.6 ± 1.4

Drug release from NPs was also determined at pH 6.5 (**Figure 4-4 B**). Drug release profiles were comparable to those obtained at physiological pH. However, the extent of burst release in acidic pH was higher than that at physiologic pH (~25% Vs ~50%).

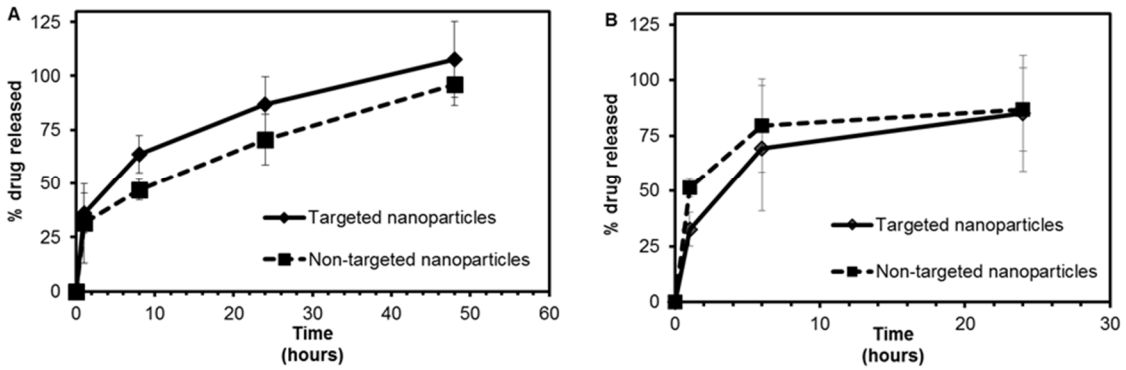

Figure 4-4. Drug release kinetics from tylocrebrine nanoparticles

Nanoparticles were dispersed in (**A**) 1X PBS (pH 7.4) or (B) 1X PBS (pH 6.5) and incubated at 37°C and 100 rpm. Drug release from nanoparticles was monitored by analyzing tylocrebrine concentration in the release buffer using HPLC. Data represented as mean ± S.D., n=3.

4.4.4 Cellular uptake of tylocrebrine loaded nanoparticles

Using fluorescent dye labeled particles, we first determined if cellular uptake of targeted NPs was greater than that of non-targeted NPs. We found that targeted NPs resulted in ~2-3 fold higher uptake than non-targeted NPs. Additionally, uptake of targeted NPs was reduced (not statistically significant) in the presence of excess free targeting peptide (**Figure 4-5 A**). This indicated that the enhanced uptake of targeted NPs could be mediated via EGFR. Additional experiments investigating uptake in EGFR knockout cells are needed to confirm this finding.

We determined the uptake of targeted and non-targeted tylocrebrine NPs in A431 cells (**Figure 4-5 B**). We found that encapsulation of tylocrebrine in targeted NPs increased the cellular drug uptake by ~3-fold ($p<0.05$).

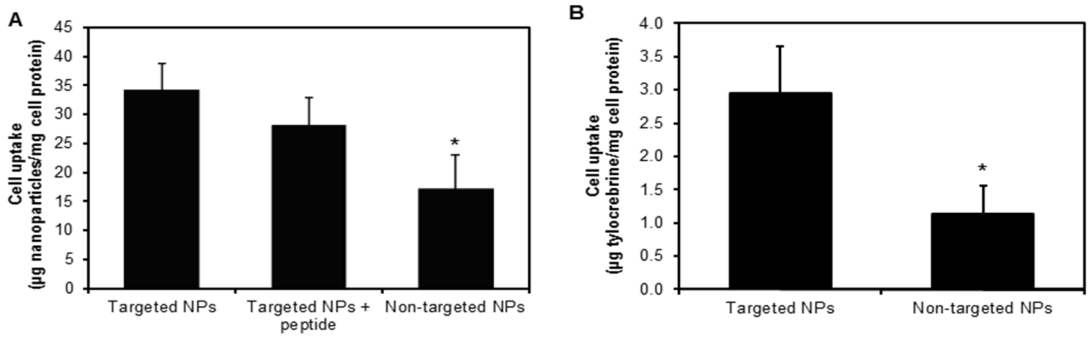

Figure 4-5. Cell uptake of EGFR-targeted and non-targeted nanoparticles

(A) A549 cells were incubated with coumarin 6 loaded targeted nanoparticles with or without excess peptide, or non-targeted nanoparticles for 1 h at 4°C. Treatments were removed and the cells were incubated in fresh media at 37°C for 1h. Intracellular levels of coumarin 6 were estimated using HPLC. (B) A431 cells were incubated with tylocrebrine loaded nanoparticles. After 1 h, treatments were removed and the cells were washed. Intracellular tylocrebrine concentration was measured using HPLC and normalized to cell protein. Data represented as mean ± S.D., n=6, * indicates $p<0.05$

4.4.5 *In vitro* efficacy of various formulations of tylocrebrine

We compared the *in vitro* efficacy of various formulations of tylocrebrine in both A549 and A431 cells. As our previous results showed that acidic pH led to a decreased intracellular accumulation of tylocrebrine, we performed these studies under both physiologic as well as acidic pH conditions. The free drug was found to be potent in both cell lines under neutral conditions, with an IC50 of 210 and 37 nM (**Figure 4-6 A and C**). However, there was a dramatic decrease in the efficacy of tylocrebrine under acidic conditions (compare **Figures 4-6 A and B**, and **4-6 C and D**). The IC50 of tylocrebrine increased from 210 nM and 37 nM to 432 nM and 361 nM, respectively. At physiological pH the efficacy of non-targeted tylocrebrine NPs was comparable to that of the free drug, while targeted tylocrebrine NPs were more effective than the free drug. With a decrease in extracellular pH, IC50 of NP formulations remained unchanged in A431 cells, while there was a small increase in IC50 for the NP formulations in A549 cells. As a result, both non-targeted and targeted tylocrebrine NPs showed superior efficacy than the free drug under acidic conditions. The IC50 values estimated from the efficacy studies are summarized in **Table 4-2**.

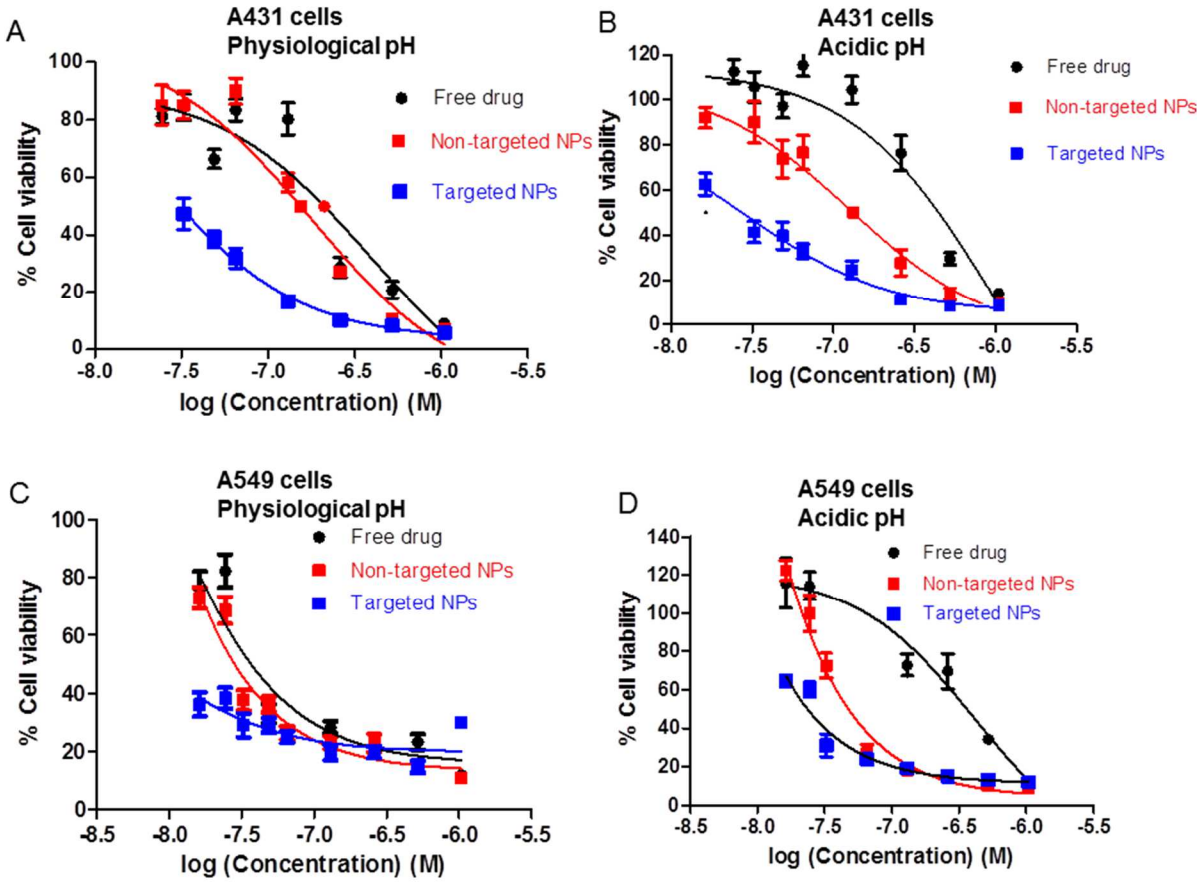

Figure 4-6. *In vitro* cytotoxicity of tylocrebrine

A431 and A549 cells were treated with different formulations of tylocrebrine at physiological and acidic extracellular pH. Cell viability was measured using MTS assay and normalized to untreated controls. Data represented as mean ± S.D., n=4.

Table 4-2. IC50 values of various formulations of tylocrebrine in A431 and A549 cells

A431 cells	IC50 at physiological pH (nM)	IC50 at acidic pH (nM)
Free drug	210	432
Non-targeted nanoparticles	154	132
Targeted nanoparticles	31	28

A549 cells	IC50 at physiological pH (nM)	IC50 at acidic pH (nM)
Free drug	37	361
Non-targeted nanoparticles	28	47
Targeted nanoparticles	7	24

4.4.6 Pharmacokinetics of various formulations of tylocrebrine

Concentration-time profile of the drug in the tumor is shown in **Figure 4-7 A**. Accumulation of the drug and targeted NPs in the tumor was rapid and reached a peak at 0.5 hours. When encapsulated in non-targeted NPs, tumor accumulation was slower, reaching a peak at ~2 hours. At 0.5, 2, 4 and 6 h post dose, tumor tylocrebrine concentrations in targeted NP treated group were 2-4-fold higher than free drug group. Tumor concentration of tylocrebrine in animals treated with non-targeted NPs was 2-fold higher than the free drug-treated animals only at 2 and 4 hours post-dose; the concentrations were similar to the free drug treatment group at later time points. AUCs of the free drug and non-targeted NPs in the tumor were comparable. The AUC of targeted NPs was ~3 fold higher than that of the other formulations (**Table 4-3**).

The concentration-time profile of the drug in the brain (the major site of toxicity) is shown in **Figure 4-7 B**. Similar to that in the tumor, there was a rapid accumulation of the drug in the brain. However, encapsulation in NPs resulted in a 5-fold decrease in brain concentration of the drug at the first time point. Drug concentrations in the brain declined rapidly. Overall, animals treated with free drug had a 2-fold higher drug exposure in the brain as compared to those treated with the NP formulations (**Table 4-3**). Targeted NPs had a DTI of ~5 because of the reduced brain exposure and enhanced tumor exposure.

The concentration time profile of the drug in the blood is shown in **Figure 4-7 C**. NPs resulted in higher blood concentration of the drug relative to that achieved after the administration of the free drug. Concentration-time profiles of the drug in other key organs are summarized in **Figure 4-8**.

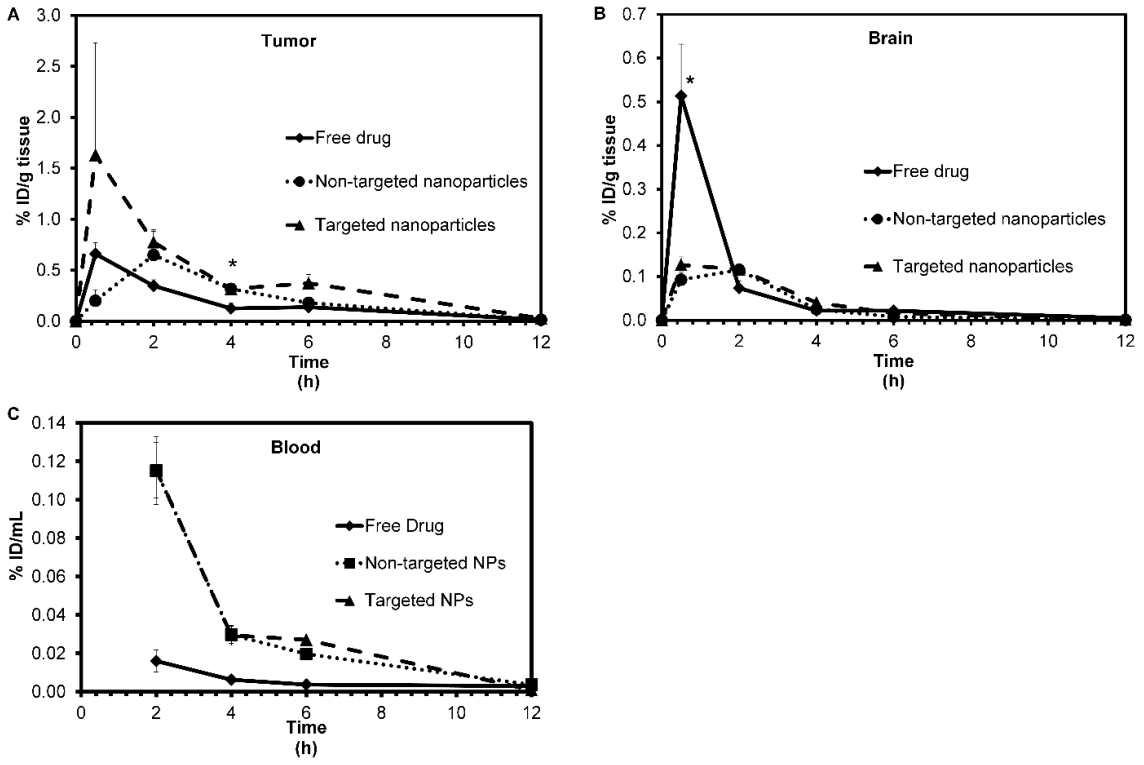

Figure 4-7. Pharmacokinetics of tylocrebrine

A431 tumor bearing mice were treated intravenously with tylocrebrine in solution or encapsulated in nanoparticles. At various time points, concentration of tylocrebrine in (**A**) tumor, (**B**) brain and (**C**) blood was measured using LC-MS/MS. Data represented as mean ± S.E.M, n=3-4, * indicates $p<0.05$.

Table 4-3. On-target AUC, off-target AUC, and DTI of tylocrebrine

	Free drug	Non-targeted nanoparticles	Targeted nanoparticles
AUC_{tumor} ($\mu g\ h\ mL^{-1}$)	5.5	6.8	17.7
AUC_{brain} ($\mu g\ h\ mL^{-1}$)	2.1	1.0	1.3
DTI	---	2.6	5.2

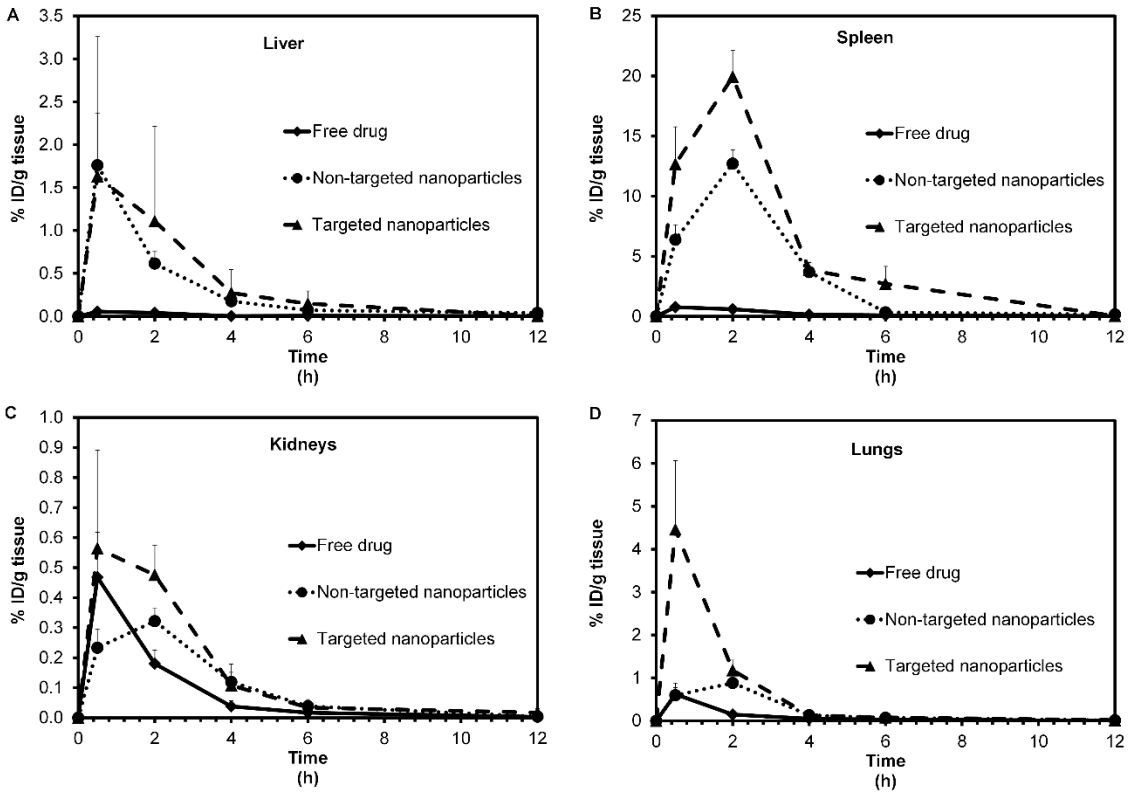

Figure 4-8. Biodistribution of tylocrebrine in key organs

A431 tumor bearing mice were treated with various formulations of tylocrebrine. At different time points, animals were sacrificed and key organs were excised. Tylocrebrine concentration in these organs were determined using LC-MS/MS.

4.4.7 Tumor inhibition studies

We determined the anti-tumor efficacy of the different formulations of tylocrebrine in A431 tumor model (**Figure 4-9**). There was a reduction in tumor growth rate in animals treated with tylocrebrine solution and non-targeted NPs relative to that in the saline treated animals. Treatment with non-targeted tylocrebrine NPs and tylocrebrine in solution resulted in comparable activities. In

agreement with our pharmacokinetic studies, treatment with EGFR targeted tylocrebrine NPs resulted in greater tumor growth inhibition than that with the other

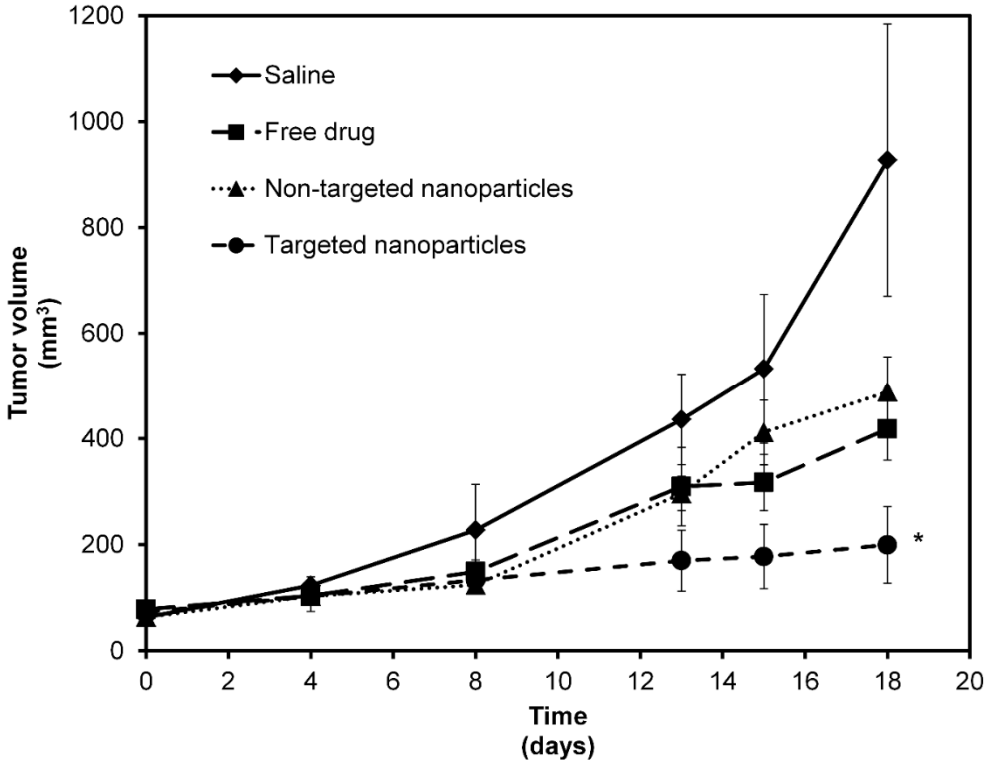

Figure 4-9. *In vivo* tumor inhibition studies

Anti-tumor efficacy of various formulations of tylocrebrine was determined in mouse A431 tumor model. Tumor bearing mice were treated with three doses of tylocrebrine (12 mg/kg) administered at 96 h intervals. Tumor volume was measured using a digital caliper. Data represented as mean ± S.E.M., n= 3-4. * indicates $p<0.05$ for saline vs. targeted nanoparticles and non-targeted nanoparticles vs. targeted nanoparticles

formulations.

Tumor samples were stained for Ki67 and cleaved caspase 3 to determine the proliferative and apoptotic indices, respectively. Representative micrographs of Ki67 staining are shown in **Figure 4-10**. Saline treated animals had significantly higher $Ki67^{+}$ cells as compared to the other treatment groups. There was no significant difference in the staining profile of free drug and non-targeted NP treated tumors. Tumors treated with targeted NPs had the lowest Ki67 staining. An opposite profile was observed for cleaved caspase 3 expression (**Figure 4-11**). Cleaved caspase 3 staining was lowest in saline treated animals and highest in animals treated with targeted NPs. Taken together, this data suggests that treatment with tylocrebrine inhibited tumor cell proliferation and induced apoptosis, with targeted NPs resulting in the greatest decrease in tumor cell viability.

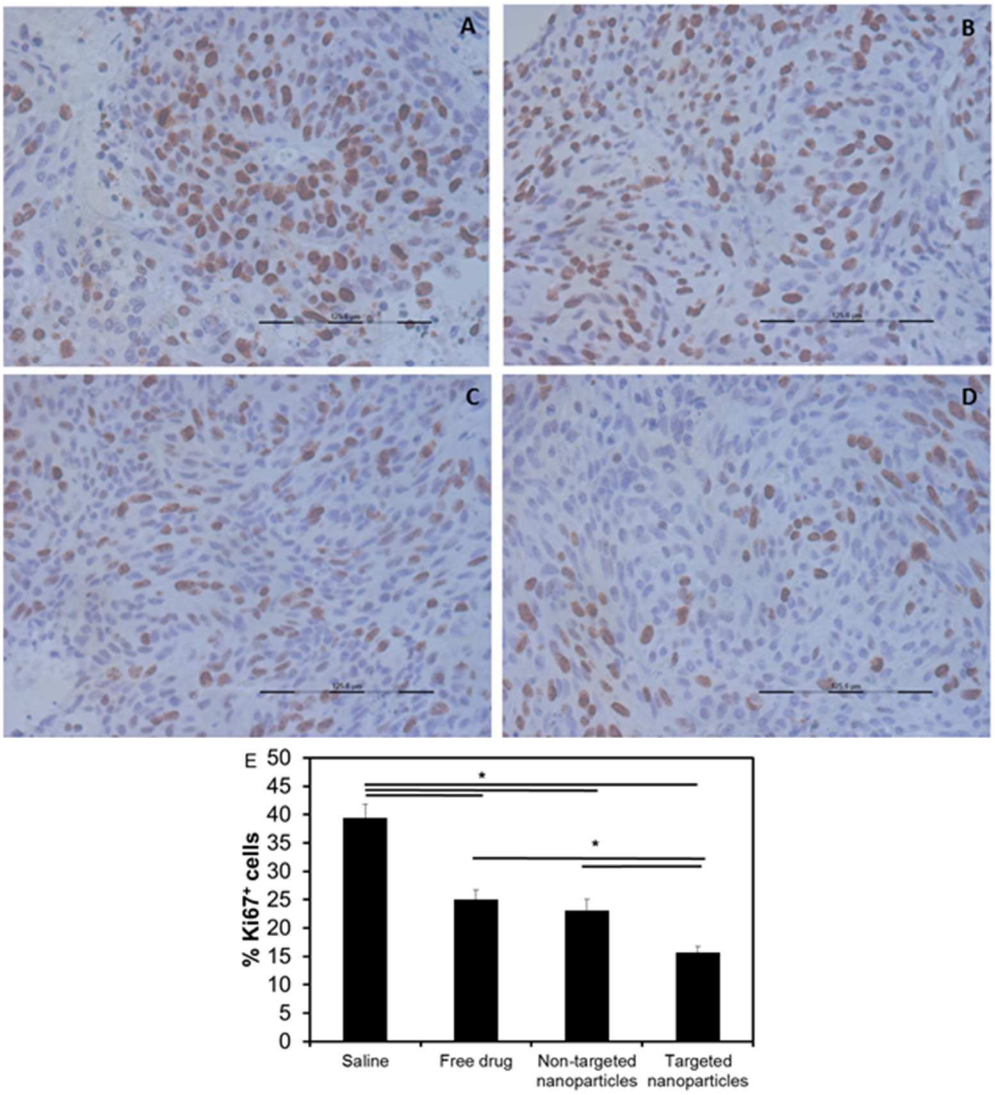

Figure 4-10. Ki67 staining in tumor sections

Tumors were excised at the end of the efficacy study and stained for Ki67. Representative micrographs of tumor from animals treated with (**A**) saline (**B**) free drug (**C**) non-targeted nanoparticles and (**D**) targeted nanoparticles are shown. (**E**) shows quantification of Ki67 staining. Data represented as mean ± S.E.M, n= 6 sections x 3 images/ section. * indicates $p<0.05$.

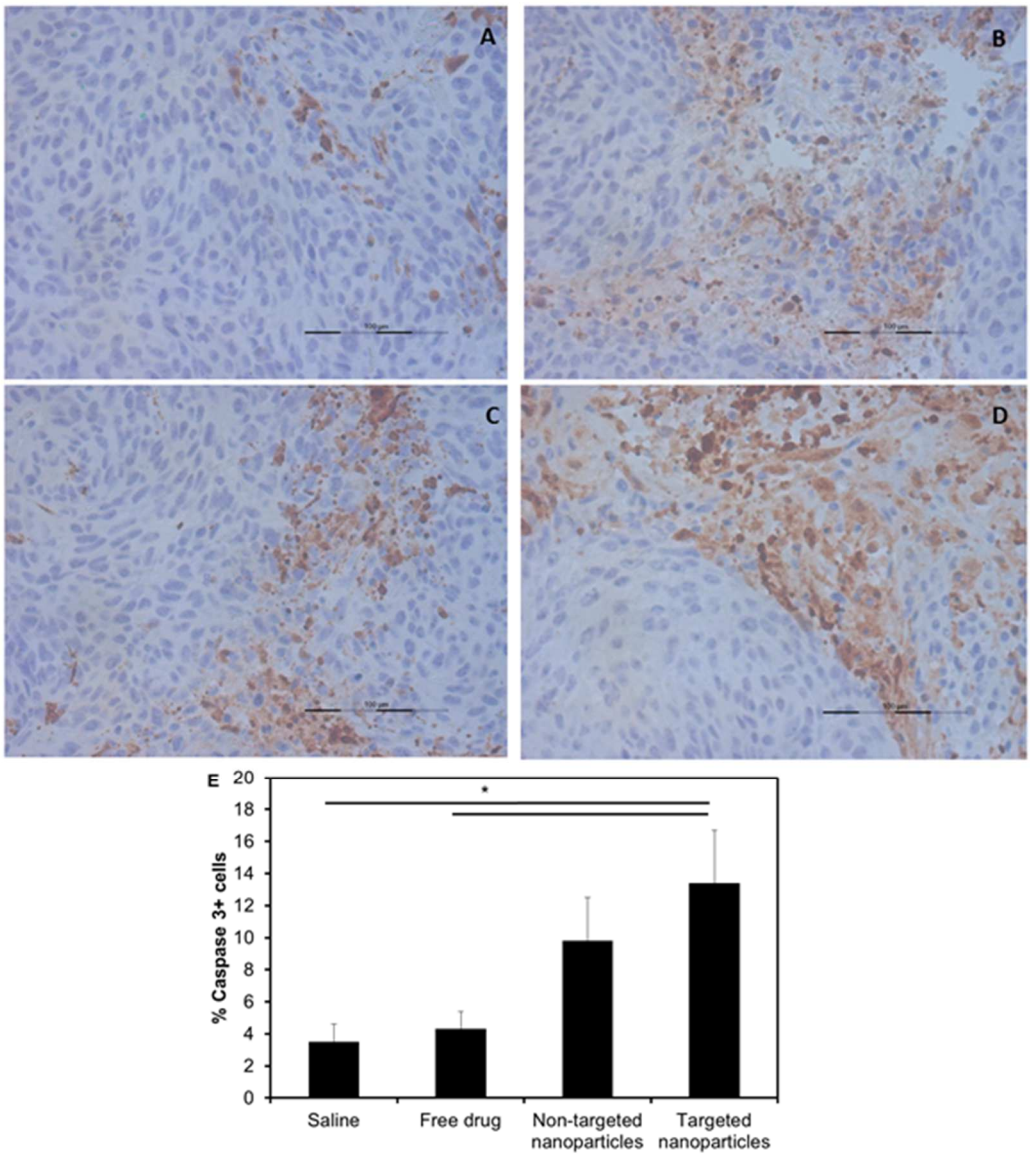

Figure 4-11. Cleaved caspase 3 staining in tumor sections

Micrographs of cleaved caspase 3 staining in tumors from animals treated with (**A**) saline (**B**) free drug (**C**) non-targeted nanoparticles and (**D**) targeted nanoparticles are shown. Quantification of staining is shown in (**E**). Data represented as mean ± S.E.M, n= 6 sections x 3 images/ section. * indicates $p<0.05$.

4.5 Discussion

Tylocrebrine was originally isolated in 1962 from the North Queensland vine, *T. crebriflora* [516]. With accumulating evidence that this family of phenanthropiperidine alkaloids had anti-cancer properties, tylocrebrine was tested and found to be effective in several cancer models [506]. Unfortunately, there were unforeseen problems with the drug and clinical trials were terminated before tylocrebrine's therapeutic efficacy could be established in the clinic [505]. CNS toxicity, as evidenced by ataxia and disorientation, was considered the major reason for abandoning clinical trials. In the decades that followed tylocrebrine's failure in the clinic, medical interest in tylocrebrine and other members of its class waned. Recently, however, there has been a resurgence of activity with regard to these natural products and their analogs. Many of these alkaloids have been found to possess potent and broad spectrum cytotoxicity. Several members of this class, including tylocrebrine, were found to inhibit tumor cell growth with GI50 values in the low nanomolar to sub-nanomolar range across the NCI 60 cell line panel [517].

A major barrier to the clinical use of tylocrebrine and other members of its class is their neurological side effects [518]. In a review [519], Hitchcock and Pennington show that the degree of passive diffusion across the blood-brain barrier (BBB) correlates with a molecule's polar surface area (PSA), number of H-bond donors (HBD), cLogP, cLogD and molecular weight [519]. A calculation of these properties for tylocrebrine reveals that each of these values is well within the suggested parameters for CNS penetrant drugs (**Table 4-4**). Increasing the hydrophilicity of tylocrebrine can potentially decrease its diffusion across the blood-brain barrier.

To this effect, Lee and colleagues recently reported water-soluble phenanthrene based tylophorine derivatives [520-522]. These molecules showed promising anti-cancer activity *in vivo*, with minimal gross toxicity [523]. However, brain penetration of these molecules needs further investigation.

Table 4-4. Physicochemical characteristics of CNS penetrant drugs and tylocrebrine

Mean values and suggested limits adapted with permission from [519] © 2006 American Chemical Society

Property	Top 25 CNS drugs mean values	Suggested limits	Tylocrebrine
PSA ($Å^2$)	47	< 90	40
HBD	0.8	< 3	0
cLogP	2.8	2-5	4.3
MW	293	< 500	394

Tylocrebrine's anticancer activity is mediated through inhibition of protein synthesis. This effect is facilitated through binding of the drug to the 40S and 80S ribosomal subunits [524]. Hence, cellular internalization is required for its anti-cancer activity. Tylocrebrine is a weak base, and is mainly un-ionized at physiological pH. Due to its neutral charge and high hydrophobicity, tylocrebrine can cross cell membranes efficiently under physiological conditions (for example, the blood-brain barrier). However, under acidic conditions (such as those found in

the tumor), tylocrebrine is ionized. This is likely to reduce its diffusion across the tumor cell membrane and its anti-cancer activity.

In order to address these twin problems of high CNS penetration and limited tumor cell uptake, we encapsulated tylocrebrine in PLGA NPs surface functionalized with a peptide targeting the EGFR. PLGA NPs, likely due to their colloidal size range, do not cross the intact blood-brain barrier. Additionally, PLGA NPs are rapidly taken up by cells through endocytosis [287], a process augmented by the presence of targeting ligands [215, 360].

Our *in vitro* studies showed that tylocrebrine had potent activity with IC50 values in the nanomolar range. Encapsulation in EGFR targeted NPs further increased its potency. Under acidic conditions, there was a dramatic decrease in the potency of the free drug while the activity of the NP formulations showed a minor decrease. This suggested that the issue of drug delivery into the tumor cells could be addressed through NP-encapsulation. The minor decrease in the efficacy of the NP formulations can be attributed to the increase in the burst release observed in acidic pH.

Upon IV administration, we found that there was rapid accumulation of tylocrebrine in both the target tissue (tumor) and the site of toxicity (brain). Encapsulation of tylocrebrine in non-targeted NPs reduced the brain exposure but did not significantly improve the tumor exposure. On the other hand, delivering tylocrebrine in targeted NPs resulted in both reduced brain exposure and improved tumor exposure. Our studies highlight a few important points. Using a targeting moiety on the NP surface merely improves their accumulation at the target site

without affecting their accumulation at non-target sites [177]. Usually, the target site has negligible influence on the overall pharmacokinetics of the drug or drug carrier. There is still some debate in literature regarding whether targeting ligands improve the tumor accumulation of NPs or merely increase their tumor cell uptake [525]. Bartlett *et al*. and Choi *et al.* have shown that transferrin receptor targeted NPs have similar tumor accumulation to non-targeted NPs [265, 526]. However, owing to improved tumor cell uptake, these NPs resulted in better efficacy. On the other hand, studies from our and other labs have shown that NPs targeting folic acid receptor, biotin receptor or EGFR improved tumor accumulation of encapsulated drug relative to that with non-targeted NPs [215, 216, 224, 227]. Differences in tumor models, receptor expression levels, and recycling rates of different receptors, and affinities of targeting moieties could contribute to these discrepancies. Other variables such as choice of the drug, drug release kinetics and mechanisms, and plasma kinetics of drug and drug carrier also make comparison between studies difficult. Finally, current characterization techniques cannot distinguish between NP-encapsulated and free drug. Additional, in-depth characterization studies are needed to draw strong mechanistic conclusions. Blood concentrations of NP-encapsulated tylocrebrine were significantly higher than the free drug (~6-fold higher). This indicates that the driving force for accumulation of tylocrebrine in tumors is much higher when administered in the form of NPs. However, the increase in tumor levels of tylocrebrine was less dramatic (only ~3-fold with targeted NPs). This may be attributed to the favorable partition coefficient of the free drug into the tumor, as illustrated by a high tumor to

blood concentration ratio (>10). Thus, the advantage gained by nano-encapsulation strongly depends on the drug being investigated [450, 527]. Additionally, A431 tumors were found to be fluid-filled (not shown), suggesting that the interstitial fluid pressure (IFP) in these tumors is high, as previously reported [528, 529]. High IFP is likely to affect the intratumoral transport of NPs more significantly than that of free drug molecules [460, 493]. The relatively large hydrodynamic particle size of the NPs used in our studies may also decrease their tumor penetration. Decreasing the particle size can potentially increase the delivery of NPs into the tumor [424, 527]. Alternately, tumors with a low IFP may prove to be better candidates for treatment with these formulations.

The *in vivo* tumor growth inhibition studies show that free drug inhibited tumor growth even at the low dose used. While treatment efficacy did not improve with non-targeted NPs, targeted NPs resulted in a considerably greater tumor growth inhibition than other treatments. This effect may be a manifestation of both the higher tumor tissue accumulation and higher cytotoxicity of targeted NPs.

The dose of tylocrebrine used in our studies was relatively low (12 mg/kg). This dose was effective only if the treatment was started before the tumors reached a volume of ~75 mm^3. Larger tumors did not respond to this dose of tylocrebrine in any formulation *(data not shown)*. The overall dose of tylocrebrine that could be administered was limited by its loading in NPs. Additionally, burst release of drug from NPs may limit the overall efficiency of targeting and chemotherapeutic efficacy of NPs. Strategies that enable higher drug loading and prolonged drug release will allow for larger doses to be administered and this could further

enhance the anti-tumor efficacy of the drug. Using polymers that have greater interaction with the drug can help achieve this goal. To this end, micelles formed from polymers consisting of aromatic rings have been shown to improve drug loading and stability as compared to micelles formed from aliphatic polymers [530, 531]. This has been attributed to the formation of π-π stacks between the drug and polymer. Future studies could investigate the use of such polymers for improving the therapeutic index of tylocrebrine.

4.6 Conclusion

Tylocrebrine is a potent anti-cancer agent but significant penetration into the brain and low tumor cell uptake limits its use. Encapsulation of the drug in PLGA NPs significantly limited its CNS penetration. Moreover, surface functionalizing NPs with an EGFR targeting peptide led to enhanced tumor cell uptake, tumor tissue accumulation and *in vivo* anti-tumor efficacy. We expect that the re-formulation approach presented here will enable further clinical testing of a number of previously abandoned drug candidates while potentially minimizing drug development costs.

Chapter 5 Summary

There is tremendous interest in the targeted delivery of drugs to solid tumors. This can be achieved by delivering drugs in nano-sized drug carriers. Consequently, in the past two decades, there has been an exponential growth in the amount of pre-clinical research involving nano-drug delivery systems. In spite of the progress made in this field, these systems deliver only a small fraction of the dose to the tumor. Poor drug delivery to the tumor and extensive distribution to normal tissues compromises the overall efficacy of chemotherapy. In an effort to improve the chemotherapeutic efficacy of nano-sized drug carriers, we studied their transport from the site of administration to the site of action. We particularly examined three processes: systemic distribution, intratumoral distribution, and cell uptake. In this chapter, we summarize our major findings. We also critically review the techniques and results presented in this thesis. This could provide future directions to further improve the state of nanomedicine.

In Chapter 2, we analyzed the systemic distribution and transvascular transport of nanoparticles (NPs). A semi-physiologically based pharmacokinetic model was constructed to describe the systemic distribution of drug delivered in NPs. Since NPs and drug have distinct pharmacokinetics, the model consisted of separate compartments for NP-encapsulated drug and the released drug. The distributional clearance of NPs across compartments was modeled using equations describing convection and diffusion. The performance of NP formulations was characterized using a metric called the drug targeting index (DTI). DTI compares drug exposure of two different formulations (NP and free drug) in the target and toxicity compartments.

We analyzed the influence of particle size and tumor vascular pore size on the DTI of NPs. Using our model, we found that the maximal targeting efficiency was observed in a limited particle size range. The ideal particle size range for drug targeting was dictated by the vascular pore size of the toxicity and target compartments. Prolonging the duration of drug release also improved the efficiency of drug targeting. However, this effect was also observed in a limited particle size range. Some important conclusions can be drawn from these modeling efforts. First, though distributional clearance provides strong mechanistic information about the deposition of NPs in the target compartment, whole body pharmacokinetics are a better indicator of formulation performance. Second, the enhanced permeability and retention (EPR) effect is likely a special occurrence. The magnitude of the EPR effect strongly depends on the physicochemical properties of the NP platform and drug as well as on the physiological properties of the tumor blood vessels.

There are several limitations to the current model. First, we considered the tumor to be a well-stirred compartment with homogeneous vascular pore size. The intratumoral distribution of NPs, differences in transvascular pressure gradients and vascular pore size in tumors are known to be highly heterogeneous. Hence, describing NP or drug transport in tumors using singular values for these parameters is not accurate. Moreover the effects of particle shape, charge, degree of aggregation etc. were not considered in this model. The performance of NPs was measured in terms of pharmacokinetic parameters such as AUC. This can prove erroneous especially when dealing with controlled release systems such as

NPs. Applying a pharmacodynamic model that uses concentration of drug to determine cell kill may prove to be more useful. Several parameters affecting cell uptake, such as effect of NP size and expression of efflux transporters, were not considered. These processes can have a significant impact on the efficacy of chemotherapy. Finally, the model only determined the effect of NP properties on drug targeting. Drugs with different pharmacokinetic behaviors will benefit to different extents with nano-encapsulation.

In Chapter 3, we studied the influence of fibrinolytic enzymes on the intratumoral distribution and chemotherapeutic efficacy of NPs. Poor intratumoral distribution of NPs and inadequate delivery to certain tumor cell niches is an important yet overlooked cause of drug resistance. Fibrinogen, a soluble blood protein, deposits in the tumor ECM due to leaky blood vessels. It is converted to cross-linked fibrin due to the prothrombogenic activity of tumor cells. Presence of fibrin in the tumor matrix can be an important cause of solid stress in tumors and result in the compression of blood vessels. Degrading fibrin in the tumor matrix can lead to decompression of blood vessels and improvement in drug delivery to tumors.

We used a fibrinolytic enzyme, tissue plasminogen activator (tPA), to degrade fibrin inside tumors. We found that co-administration of tPA resulted in an enhanced anti-cancer activity of paclitaxel NPs in an orthotopic lung cancer model and a syngeneic mouse model of melanoma. Interestingly, co-administration of tPA with paclitaxel solution did not have any significant impact on its efficacy in the syngeneic model. We then analyzed the mechanism for the favorable activity of

tPA. Using immunohistochemistry, we determined that treatment with tPA led to an increase in the mean vascular diameter of angiogenic blood vessels. This result was further corroborated with ultrasound imaging. tPA treated tumors showed a higher perfusion area as compared to saline treated tumors.

There are several mechanistic and translational questions that have not been addressed in this study. tPA mediates several pharmacological effects other than fibrin degradation. It is not clear if the improved chemotherapeutic efficacy of NPs or improved perfusion is mediated solely through fibrin degradation. Conducting these studies in transgenic fibrinogen deficient mice may provide insight into this question. It will also be interesting to determine if co-administration of tPA enables the NPs to access hypoxic regions within the tumor. We are currently probing into this question using confocal microscopy to analyze the intratumoral distribution of Doxil®. Our studies also showed that fibrin expression in tumors is highly variable. Pre-selecting tumors with high fibrin expression may help maximize chances of success with this therapy (if the effect of tPA is fibrin-mediated). Due to its short half-life, using tPA in its current form is not ideal. Conjugating tPA to hydrophilic polymers such as poly(ethylene glycol) may improve its circulation half-life, and tumor accumulation. We attempted to achieve this goal by conjugating tPA to the surface of NPs. This approach was not successful, likely due to the liver accumulation of NPs and the reduced mobility of tPA. Encapsulating tPA in fast releasing NPs may help overcome both these issues.

The goal of our studies in Chapter 4 was to improve the therapeutic index of an abandoned chemotherapeutic drug, tylocrebrine. Due to significant central

nervous system (CNS) side-effects, such as ataxia, its clinical development was discontinued. Additionally, we found that the cell uptake of tylocrebrine is reduced under the acidic tumor microenvironment. We hypothesized that encapsulating the drug in polymeric NPs may address both issues of enhanced CNS penetration and reduced tumor cell uptake. To improve their tumor cell uptake, we surface functionalized the NPs with a peptide that binds the epidermal growth factor receptor (EGFR).

We first compared the cytotoxicity of the free drug, non-targeted NPs and targeted NPs *in vitro*. Under acidic conditions, both NP formulations were more potent than the drug. However, targeted NPs had a higher cell uptake and potency than non-targeted NPs. Through pharmacokinetic studies, we found that treatment with targeted NPs resulted in higher drug exposure in the tumor and lower drug exposure in the brain as compared to the free drug. We then determined the chemotherapeutic efficacy of various formulations of tylocrebrine in a mouse model of xenografted human epidermoid cancer. Treatment with tylocrebrine solution or non-targeted NPs resulted in comparable tumor inhibition. Treatment with targeted NPs led to the greatest inhibition of tumor growth.

The studies presented here show great promise for the future development of tylocrebrine. However some limitations still remain. Drug loading in poly(latide-*co*-glycolide) (PLGA) NPs was moderate, and drug release was rapid. Altering the molecular weight of PLGA and the lactide: glycolide ratio did not have any influence on the loading of the drug. Low drug loading limited the dose of drug. Drug release was also rather rapid, which may be responsible for some of the drug

accumulation in the brain. It may be valuable to investigate a different polymer to enhance drug loading of tylocrebrine. It is currently not known if tylocrebrine is a substrate for efflux transporters. However, previous clinical reports of CNS toxicity, and our pharmacokinetic studies suggest that the drug accumulates in the brain. This may suggest that it is not a substrate to efflux transporters. If this is indeed true, tylocrebrine holds great promise for treating multidrug resistant tumors. Investigating the activity of tylocrebrine in multidrug resistant tumors will be valuable.

In summary, this thesis analyzed the various steps of NP transport from the site of administration to its uptake by tumor cells. Loss of NPs at various steps of the transport decreases the overall efficacy of chemotherapy. Approaches described here may help to further improve the delivery of NPs to solid tumors.

Bibliography

[1] V.P. Chauhan, T. Stylianopoulos, J.D. Martin, Z. Popovic, O. Chen, W.S. Kamoun, M.G. Bawendi, D. Fukumura, R.K. Jain, Normalization of tumour blood vessels improves the delivery of nanomedicines in a size-dependent manner, Nat Nanotechnol, 7 (2012) 383-388.
[2] T.A. Yap, C.P. Carden, S.B. Kaye, Beyond chemotherapy: targeted therapies in ovarian cancer, Nat Rev Cancer, 9 (2009) 167-181.
[3] N. Takebe, P.J. Harris, R.Q. Warren, S.P. Ivy, Targeting cancer stem cells by inhibiting Wnt, Notch, and Hedgehog pathways, Nat Rev Clin Oncol, 8 (2011) 97-106.
[4] G. Szakacs, J.K. Paterson, J.A. Ludwig, C. Booth-Genthe, M.M. Gottesman, Targeting multidrug resistance in cancer, Nat Rev Drug Discov, 5 (2006) 219-234.
[5] A.L. Harris, D. Hochhauser, Mechanisms of multidrug resistance in cancer treatment, Acta Oncol, 31 (1992) 205-213.
[6] J.A. Shabbits, R. Krishna, L.D. Mayer, Molecular and pharmacological strategies to overcome multidrug resistance, Expert Rev Anticancer Ther, 1 (2001) 585-594.
[7] P.M. Fracasso, M.F. Brady, D.H. Moore, J.L. Walker, P.G. Rose, L. Letvak, T.M. Grogan, W.P. McGuire, Phase II study of paclitaxel and valspodar (PSC 833) in refractory ovarian carcinoma: a gynecologic oncology group study, J Clin Oncol, 19 (2001) 2975-2982.
[8] M.K. Ma, H.L. McLeod, P. Westervelt, P.M. Fracasso, Pharmacokinetic study of infusional valspodar, J Clin Pharmacol, 42 (2002) 412-418.
[9] Y. Patil, T. Sadhukha, L. Ma, J. Panyam, Nanoparticle-mediated simultaneous and targeted delivery of paclitaxel and tariquidar overcomes tumor drug resistance, J Control Release, 136 (2009) 21-29.
[10] A.V. Kabanov, E.V. Batrakova, V.Y. Alakhov, Pluronic block copolymers for overcoming drug resistance in cancer, Adv Drug Deliv Rev, 54 (2002) 759-779.
[11] R.K. Jain, T. Stylianopoulos, Delivering nanomedicine to solid tumors, Nat Rev Clin Oncol, 7 (2010) 653-664.
[12] A.S. Chung, J. Lee, N. Ferrara, Targeting the tumour vasculature: insights from physiological angiogenesis, Nat Rev Cancer, 10 (2010) 505-514.
[13] C.H. Heldin, K. Rubin, K. Pietras, A. Ostman, High interstitial fluid pressure - an obstacle in cancer therapy, Nat Rev Cancer, 4 (2004) 806-813.
[14] J.I. Fletcher, M. Haber, M.J. Henderson, M.D. Norris, ABC transporters in cancer: more than just drug efflux pumps, Nat Rev Cancer, 10 (2010) 147-156.
[15] G.D. Kruh, M.G. Belinsky, The MRP family of drug efflux pumps, Oncogene, 22 (2003) 7537-7552.
[16] M. Dean, A. Rzhetsky, R. Allikmets, The human ATP-binding cassette (ABC) transporter superfamily, Genome Res, 11 (2001) 1156-1166.
[17] R.L. Juliano, V. Ling, A surface glycoprotein modulating drug permeability in Chinese hamster ovary cell mutants, Biochim Biophys Acta, 455 (1976) 152-162.
[18] K. Dano, Active outward transport of daunomycin in resistant Ehrlich ascites tumor cells, Biochim Biophys Acta, 323 (1973) 466-483.

[19] N. Kartner, J.R. Riordan, V. Ling, Cell surface P-glycoprotein associated with multidrug resistance in mammalian cell lines, Science, 221 (1983) 1285-1288.
[20] C.J. Chen, J.E. Chin, K. Ueda, D.P. Clark, I. Pastan, M.M. Gottesman, I.B. Roninson, Internal duplication and homology with bacterial transport proteins in the mdr1 (P-glycoprotein) gene from multidrug-resistant human cells, Cell, 47 (1986) 381-389.
[21] K. Ueda, C. Cardarelli, M.M. Gottesman, I. Pastan, Expression of a full-length cDNA for the human "MDR1" gene confers resistance to colchicine, doxorubicin, and vinblastine, Proc Natl Acad Sci U S A, 84 (1987) 3004-3008.
[22] T. McGrath, M.S. Center, Mechanisms of multidrug resistance in HL60 cells: evidence that a surface membrane protein distinct from P-glycoprotein contributes to reduced cellular accumulation of drug, Cancer Res, 48 (1988) 3959-3963.
[23] M.M. Gottesman, Mechanisms of cancer drug resistance, Annu Rev Med, 53 (2002) 615-627.
[24] E.M. Leslie, R.G. Deeley, S.P. Cole, Multidrug resistance proteins: role of P-glycoprotein, MRP1, MRP2, and BCRP (ABCG2) in tissue defense, Toxicol Appl Pharmacol, 204 (2005) 216-237.
[25] S.R. Wright, A.H. Boag, G. Valdimarsson, D.R. Hipfner, B.G. Campling, S.P. Cole, R.G. Deeley, Immunohistochemical detection of multidrug resistance protein in human lung cancer and normal lung, Clin Cancer Res, 4 (1998) 2279-2289.
[26] G.L. Scheffer, A.C. Pijnenborg, E.F. Smit, M. Muller, D.S. Postma, W. Timens, P. van der Valk, E.G. de Vries, R.J. Scheper, Multidrug resistance related molecules in human and murine lung, J Clin Pathol, 55 (2002) 332-339.
[27] K.C. Peng, F. Cluzeaud, M. Bens, J.P. Duong Van Huyen, M.A. Wioland, R. Lacave, A. Vandewalle, Tissue and cell distribution of the multidrug resistance-associated protein (MRP) in mouse intestine and kidney, J Histochem Cytochem, 47 (1999) 757-768.
[28] P. Chandra, K.L. Brouwer, The complexities of hepatic drug transport: current knowledge and emerging concepts, Pharm Res, 21 (2004) 719-735.
[29] M. Maliepaard, G.L. Scheffer, I.F. Faneyte, M.A. van Gastelen, A.C. Pijnenborg, A.H. Schinkel, M.J. van De Vijver, R.J. Scheper, J.H. Schellens, Subcellular localization and distribution of the breast cancer resistance protein transporter in normal human tissues, Cancer Res, 61 (2001) 3458-3464.
[30] C. Cordon-Cardo, J.P. O'Brien, J. Boccia, D. Casals, J.R. Bertino, M.R. Melamed, Expression of the multidrug resistance gene product (P-glycoprotein) in human normal and tumor tissues, J Histochem Cytochem, 38 (1990) 1277-1287.
[31] A.H. Schinkel, The physiological function of drug-transporting P-glycoproteins, Semin Cancer Biol, 8 (1997) 161-170.
[32] A.H. Schinkel, J.J. Smit, O. van Tellingen, J.H. Beijnen, E. Wagenaar, L. van Deemter, C.A. Mol, M.A. van der Valk, E.C. Robanus-Maandag, H.P. te Riele, et al., Disruption of the mouse mdr1a P-glycoprotein gene leads to a deficiency in the blood-brain barrier and to increased sensitivity to drugs, Cell, 77 (1994) 491-502.
[33] E. Roger, S. Kalscheuer, A. Kirtane, B.R. Guru, A.E. Grill, J. Whittum-Hudson, J. Panyam, Folic Acid Functionalized Nanoparticles for Enhanced Oral Drug Delivery, Mol Pharm, 9 (2012) 2103-2110.

[34] S.G. Aller, J. Yu, A. Ward, Y. Weng, S. Chittaboina, R. Zhuo, P.M. Harrell, Y.T. Trinh, Q. Zhang, I.L. Urbatsch, G. Chang, Structure of P-glycoprotein reveals a molecular basis for poly-specific drug binding, Science, 323 (2009) 1718-1722.
[35] A.H. Schinkel, J.W. Jonker, Mammalian drug efflux transporters of the ATP binding cassette (ABC) family: an overview, Adv Drug Deliv Rev, 55 (2003) 3-29.
[36] Z.E. Sauna, M.M. Smith, M. Muller, K.M. Kerr, S.V. Ambudkar, The mechanism of action of multidrug-resistance-linked P-glycoprotein, J Bioenerg Biomembr, 33 (2001) 481-491.
[37] Z.E. Sauna, S.V. Ambudkar, Evidence for a requirement for ATP hydrolysis at two distinct steps during a single turnover of the catalytic cycle of human P-glycoprotein, Proc Natl Acad Sci U S A, 97 (2000) 2515-2520.
[38] Z.E. Sauna, S.V. Ambudkar, Characterization of the catalytic cycle of ATP hydrolysis by human P-glycoprotein. The two ATP hydrolysis events in a single catalytic cycle are kinetically similar but affect different functional outcomes, J Biol Chem, 276 (2001) 11653-11661.
[39] G.A. Altenberg, C.G. Vanoye, J.K. Horton, L. Reuss, Unidirectional Fluxes of Rhodamine 123 in Multidrug-Resistant Cells: Evidence Against Direct Drug Extrusion From the Plasma Membrane, PNAS, 91 (1994) 4654-4657.
[40] T.W. Loo, D.M. Clarke, Do drug substrates enter the common drug-binding pocket of P-glycoprotein through "gates"?, Biochem Biophys Res Commun, 329 (2005) 419-422.
[41] M.R. Lugo, F.J. Sharom, Interaction of LDS-751 with P-Glycoprotein and Mapping of the Location of the R Drug Binding Site, Biochemistry, 44 (2005) 643-655.
[42] M.D. Chavanpatil, Y. Patil, J. Panyam, Susceptibility of nanoparticle-encapsulated paclitaxel to P-glycoprotein-mediated drug efflux, Int J Pharm, 320 (2006) 150-156.
[43] J.H. Weisburg, M. Curcio, P.C. Caron, G. Raghu, E.B. Mechetner, P.D. Roepe, D.A. Scheinberg, The multidrug resistance phenotype confers immunological resistance, J Exp Med, 183 (1996) 2699-2704.
[44] J.H. Weisburg, P.D. Roepe, S. Dzekunov, D.A. Scheinberg, Intracellular pH and multidrug resistance regulate complement-mediated cytotoxicity of nucleated human cells, J Biol Chem, 274 (1999) 10877-10888.
[45] A.A. Ruefli, K.M. Tainton, P.K. Darcy, M.J. Smyth, R.W. Johnstone, P-glycoprotein inhibits caspase-8 activation but not formation of the death inducing signal complex (disc) following Fas ligation, Cell Death Differ, 9 (2002) 1266-1272.
[46] L.J. Robinson, W.K. Roberts, T.T. Ling, D. Lamming, S.S. Sternberg, P.D. Roepe, Human MDR 1 protein overexpression delays the apoptotic cascade in Chinese hamster ovary fibroblasts, Biochemistry, 36 (1997) 11169-11178.
[47] M.A. Sognier, Y. Zhang, R.L. Eberle, K.M. Sweet, G.A. Altenberg, J.A. Belli, Sequestration of doxorubicin in vesicles in a multidrug-resistant cell line (LZ-100), Biochem Pharmacol, 48 (1994) 391-401.
[48] V.M. Wasenius, A. Jekunen, O. Monni, H. Joensuu, S. Aebi, S.B. Howell, S. Knuutila, Comparative genomic hybridization analysis of chromosomal changes occurring during development of acquired resistance to cisplatin in human ovarian carcinoma cells, Genes Chromosomes Cancer, 18 (1997) 286-291.

[49] P.H. Rao, J. Houldsworth, N. Palanisamy, V.V. Murty, V.E. Reuter, R.J. Motzer, G.J. Bosl, R.S. Chaganti, Chromosomal amplification is associated with cisplatin resistance of human male germ cell tumors, Cancer Res, 58 (1998) 4260-4263.
[50] P.H. Rooney, D.A. Stevenson, S. Marsh, P.G. Johnston, N.E. Haites, J. Cassidy, H.L. McLeod, Comparative genomic hybridization analysis of chromosomal alterations induced by the development of resistance to thymidylate synthase inhibitors, Cancer Res, 58 (1998) 5042-5045.
[51] K.V. Chin, S.S. Chauhan, I. Pastan, M.M. Gottesman, Regulation of mdr RNA levels in response to cytotoxic drugs in rodent cells, Cell Growth Differ, 1 (1990) 361-365.
[52] T.M. Grogan, C.M. Spier, S.E. Salmon, M. Matzner, J. Rybski, R.S. Weinstein, R.J. Scheper, W.S. Dalton, P-glycoprotein expression in human plasma cell myeloma: correlation with prior chemotherapy, Blood, 81 (1993) 490-495.
[53] A. Abolhoda, A.E. Wilson, H. Ross, P.V. Danenberg, M. Burt, K.W. Scotto, Rapid activation of MDR1 gene expression in human metastatic sarcoma after in vivo exposure to doxorubicin, Clin Cancer Res, 5 (1999) 3352-3356.
[54] A. Levchenko, B.M. Mehta, X. Niu, G. Kang, L. Villafania, D. Way, D. Polycarpe, M. Sadelain, S.M. Larson, Intercellular transfer of P-glycoprotein mediates acquired multidrug resistance in tumor cells, Proc Natl Acad Sci U S A, 102 (2005) 1933-1938.
[55] W. Loscher, H. Potschka, Blood-brain barrier active efflux transporters: ATP-binding cassette gene family, NeuroRx, 2 (2005) 86-98.
[56] A. Seelig, X.L. Blatter, F. Wohnsland, Substrate recognition by P-glycoprotein and the multidrug resistance-associated protein MRP1: a comparison, Int J Clin Pharmacol Ther, 38 (2000) 111-121.
[57] S. Baltes, A.M. Gastens, M. Fedrowitz, H. Potschka, V. Kaever, W. Loscher, Differences in the transport of the antiepileptic drugs phenytoin, levetiracetam and carbamazepine by human and mouse P-glycoprotein, Neuropharmacology, 52 (2007) 333-346.
[58] D. de Graaf, R.C. Sharma, E.B. Mechetner, R.T. Schimke, I.B. Roninson, P-glycoprotein confers methotrexate resistance in 3T6 cells with deficient carrier-mediated methotrexate uptake, Proc Natl Acad Sci U S A, 93 (1996) 1238-1242.
[59] L.M. Ellis, D.J. Hicklin, Resistance to Targeted Therapies: Refining Anticancer Therapy in the Era of Molecular Oncology, Clin Cancer Res, 15 (2009) 7471-7478.
[60] M. Ono, M. Kuwano, Molecular mechanisms of epidermal growth factor receptor (EGFR) activation and response to gefitinib and other EGFR-targeting drugs, Clin Cancer Res, 12 (2006) 7242-7251.
[61] R. Bianco, T. Troiani, G. Tortora, F. Ciardiello, Intrinsic and acquired resistance to EGFR inhibitors in human cancer therapy, Endocr Relat Cancer, 12 Suppl 1 (2005) S159-171.
[62] K.E. Ware, M.E. Marshall, L.R. Heasley, L. Marek, T.K. Hinz, P. Hercule, B.A. Helfrich, R.C. Doebele, L.E. Heasley, Rapidly acquired resistance to EGFR tyrosine kinase inhibitors in NSCLC cell lines through de-repression of FGFR2 and FGFR3 expression, PLoS One, 5 e14117.

[63] G.K. Balendiran, R. Dabur, D. Fraser, The role of glutathione in cancer, Cell Biochem Funct, 22 (2004) 343-352.
[64] K.D. Tew, Glutathione-associated enzymes in anticancer drug resistance, Cancer Res, 54 (1994) 4313-4320.
[65] D.M. Townsend, K.D. Tew, The role of glutathione-S-transferase in anti-cancer drug resistance, Oncogene, 22 (2003) 7369-7375.
[66] K.J. Mellish, L.R. Kelland, K.R. Harrap, In vitro platinum drug chemosensitivity of human cervical squamous cell carcinoma cell lines with intrinsic and acquired resistance to cisplatin, Br J Cancer, 68 (1993) 240-250.
[67] D.B. Zamble, S.J. Lippard, Cisplatin and DNA repair in cancer chemotherapy, Trends Biochem Sci, 20 (1995) 435-439.
[68] L.P. Martin, T.C. Hamilton, R.J. Schilder, Platinum resistance: the role of DNA repair pathways, Clin Cancer Res, 14 (2008) 1291-1295.
[69] B. Kaina, M. Christmann, DNA repair in resistance to alkylating anticancer drugs, Int J Clin Pharmacol Ther, 40 (2002) 354-367.
[70] M.F. Clarke, J.E. Dick, P.B. Dirks, C.J. Eaves, C.H. Jamieson, D.L. Jones, J. Visvader, I.L. Weissman, G.M. Wahl, Cancer stem cells--perspectives on current status and future directions: AACR Workshop on cancer stem cells, Cancer Res, 66 (2006) 9339-9344.
[71] M. Dean, T. Fojo, S. Bates, Tumour stem cells and drug resistance, Nat Rev Cancer, 5 (2005) 275-284.
[72] A. Trumpp, O.D. Wiestler, Mechanisms of Disease: cancer stem cells--targeting the evil twin, Nat Clin Pract Oncol, 5 (2008) 337-347.
[73] C.X. Pan, W. Zhu, L. Cheng, Implications of cancer stem cells in the treatment of cancer, Future Oncol, 2 (2006) 723-731.
[74] L. Moserle, S. Indraccolo, M. Ghisi, C. Frasson, E. Fortunato, S. Canevari, S. Miotti, V. Tosello, R. Zamarchi, A. Corradin, S. Minuzzo, E. Rossi, G. Basso, A. Amadori, The side population of ovarian cancer cells is a primary target of IFN-alpha antitumor effects, Cancer Res, 68 (2008) 5658-5668.
[75] K. Abubaker, A. Latifi, R. Luwor, S. Nazaretian, H. Zhu, M.A. Quinn, E.W. Thompson, J.K. Findlay, N. Ahmed, Short-term single treatment of chemotherapy results in the enrichment of ovarian cancer stem cell-like cells leading to an increased tumor burden, Mol Cancer, 12 (2013) 24.
[76] P.B. Gupta, T.T. Onder, G. Jiang, K. Tao, C. Kuperwasser, R.A. Weinberg, E.S. Lander, Identification of selective inhibitors of cancer stem cells by high-throughput screening, Cell, 138 (2009) 645-659.
[77] L. Li, R. Bhatia, Stem cell quiescence, Clin Cancer Res, 17 (2011) 4936-4941.
[78] N. Baldini, K. Scotlandi, G. Barbanti-Brodano, M.C. Manara, D. Maurici, G. Bacci, F. Bertoni, P. Picci, S. Sottili, M. Campanacci, et al., Expression of P-glycoprotein in high-grade osteosarcomas in relation to clinical outcome, N Engl J Med, 333 (1995) 1380-1385.
[79] S. Gregorcyk, Y. Kang, D. Brandt, P. Kolm, G. Singer, R.R. Perry, p-Glycoprotein expression as a predictor of breast cancer recurrence, Ann Surg Oncol, 3 (1996) 8-14.

[80] B.J. Trock, F. Leonessa, R. Clarke, Multidrug resistance in breast cancer: a meta-analysis of MDR1/gp170 expression and its possible functional significance, J Natl Cancer Inst, 89 (1997) 917-931.
[81] R. Agarwal, S.B. Kaye, Ovarian cancer: strategies for overcoming resistance to chemotherapy, Nat Rev Cancer, 3 (2003) 502-516.
[82] A. Persidis, Cancer multidrug resistance, Nat Biotechnol, 17 (1999) 94-95.
[83] Chintamani, J. Singh, M. Mittal, S. Saxena, A. Bansal, A. Bhatia, P. Kulshreshtha, Role of p-glycoprotein expression in predicting response to neoadjuvant chemotherapy in breast cancer-a prospective clinical study, World Journal of Surgical Oncology, 3 (2005) 61.
[84] E. Karaszi, K. Jakab, L. Homolya, G. Szakacs, Z. Hollo, B. Telek, A. Kiss, L. Rejto, S. Nahajevszky, B. Sarkadi, J. Kappelmayer, Calcein assay for multidrug resistance reliably predicts therapy response and survival rate in acute myeloid leukaemia, Br J Haematol, 112 (2001) 308-314.
[85] C.P. Leith, K.J. Kopecky, J. Godwin, T. McConnell, M.L. Slovak, I.M. Chen, D.R. Head, F.R. Appelbaum, C.L. Willman, Acute myeloid leukemia in the elderly: assessment of multidrug resistance (MDR1) and cytogenetics distinguishes biologic subgroups with remarkably distinct responses to standard chemotherapy. A Southwest Oncology Group study, Blood, 89 (1997) 3323-3329.
[86] I. Cleary, G. Doherty, E. Moran, M. Clynes, The multidrug-resistant human lung tumour cell line, DLKP-A10, expresses novel drug accumulation and sequestration systems, Biochem Pharmacol, 53 (1997) 1493-1502.
[87] L.M. Breuninger, S. Paul, K. Gaughan, T. Miki, A. Chan, S.A. Aaronson, G.D. Kruh, Expression of multidrug resistance-associated protein in NIH/3T3 cells confers multidrug resistance associated with increased drug efflux and altered intracellular drug distribution, Cancer Res, 55 (1995) 5342-5347.
[88] L. Ma, M.S. Center, The gene encoding vacuolar H(+)-ATPase subunit C is overexpressed in multidrug-resistant HL60 cells, Biochem Biophys Res Commun, 182 (1992) 675-681.
[89] R. Martinez-Zaguilan, N. Raghunand, R.M. Lynch, W. Bellamy, G.M. Martinez, B. Rojas, D. Smith, W.S. Dalton, R.J. Gillies, pH and drug resistance. I. Functional expression of plasmalemmal V-type H+-ATPase in drug-resistant human breast carcinoma cell lines, Biochem Pharmacol, 57 (1999) 1037-1046.
[90] N. Raghunand, R. Martinez-Zaguilan, S.H. Wright, R.J. Gillies, pH and drug resistance. II. Turnover of acidic vesicles and resistance to weakly basic chemotherapeutic drugs, Biochem Pharmacol, 57 (1999) 1047-1058.
[91] R.K. Jain, The next frontier of molecular medicine: delivery of therapeutics, Nat Med, 4 (1998) 655-657.
[92] O. Tredan, C.M. Galmarini, K. Patel, I.F. Tannock, Drug resistance and the solid tumor microenvironment, J Natl Cancer Inst, 99 (2007) 1441-1454.
[93] A.J. Primeau, A. Rendon, D. Hedley, L. Lilge, I.F. Tannock, The distribution of the anticancer drug Doxorubicin in relation to blood vessels in solid tumors, Clin Cancer Res, 11 (2005) 8782-8788.
[94] L. Milane, Z. Duan, M. Amiji, Role of hypoxia and glycolysis in the development of multi-drug resistance in human tumor cells and the establishment of an

orthotopic multi-drug resistant tumor model in nude mice using hypoxic pre-conditioning, Cancer Cell Int, 11 (2011) 3.
[95] E.H. Starling, On the Absorption of Fluids from the Connective Tissue Spaces, J Physiol, 19 (1896) 312-326.
[96] K. Aukland, R.K. Reed, Interstitial-lymphatic mechanisms in the control of extracellular fluid volume, Physiol Rev, 73 (1993) 1-78.
[97] H. Wiig, K. Rubin, R.K. Reed, New and active role of the interstitium in control of interstitial fluid pressure: potential therapeutic consequences, Acta Anaesthesiol Scand, 47 (2003) 111-121.
[98] A.I. Minchinton, I.F. Tannock, Drug penetration in solid tumours, Nat Rev Cancer, 6 (2006) 583-592.
[99] R.K. Jain, Transport of molecules across tumor vasculature, Cancer Metastasis Rev, 6 (1987) 559-593.
[100] R.K. Jain, Transport of molecules in the tumor interstitium: a review, Cancer Res, 47 (1987) 3039-3051.
[101] M. Stanczyk, W.L. Olszewski, M. Gewartowska, A. Domaszewska-Szostek, Lack of functioning lymphatics and accumulation of tissue fluid/lymph in interstitial "lakes" in colon cancer tissue, Lymphology, 43 (2010) 158-167.
[102] Y. Boucher, L.T. Baxter, R.K. Jain, Interstitial pressure gradients in tissue-isolated and subcutaneous tumors: implications for therapy, Cancer Res, 50 (1990) 4478-4484.
[103] W.L. Olszewski, M. Stanczyk, M. Gewartowska, A. Domaszewska-Szostek, M. Durlik, Lack of functioning intratumoral lymphatics in colon and pancreas cancer tissue, Lymphat Res Biol, 10 (2012) 112-117.
[104] D. Gullino, E. Masenti, G. Trotti-Maina, [Primary tumors of the pleura. II. Submesothelial tumors. (Anatomo-clinical considerations on 21 cases)], Arch Chir Torac Cardiovasc, 25 (1968) 83-115.
[105] J. Hagendoorn, R. Tong, D. Fukumura, Q. Lin, J. Lobo, T.P. Padera, L. Xu, R. Kucherlapati, R.K. Jain, Onset of abnormal blood and lymphatic vessel function and interstitial hypertension in early stages of carcinogenesis, Cancer Res, 66 (2006) 3360-3364.
[106] S. Goel, D.G. Duda, L. Xu, L.L. Munn, Y. Boucher, D. Fukumura, R.K. Jain, Normalization of the vasculature for treatment of cancer and other diseases, Physiol Rev, 91 (2011) 1071-1121.
[107] R.K. Jain, Transport of molecules, particles, and cells in solid tumors, Annu Rev Biomed Eng, 1 (1999) 241-263.
[108] L. Brannon-Peppas, J.O. Blanchette, Nanoparticle and targeted systems for cancer therapy, Adv Drug Deliv Rev, 56 (2004) 1649-1659.
[109] A.S. Narang, S. Varia, Role of tumor vascular architecture in drug delivery, Adv Drug Deliv Rev, 63 (2011) 640-658.
[110] P. Carmeliet, R.K. Jain, Angiogenesis in cancer and other diseases, Nature, 407 (2000) 249-257.
[111] R.K. Jain, Normalization of tumor vasculature: an emerging concept in antiangiogenic therapy, Science, 307 (2005) 58-62.
[112] D. Hanahan, J. Folkman, Patterns and emerging mechanisms of the angiogenic switch during tumorigenesis, Cell, 86 (1996) 353-364.

[113] J.S. Young, C.E. Lumsden, A.L. Stalker, The significance of the tissue pressure of normal testicular and of neoplastic (Brown-Pearce carcinoma) tissue in the rabbit, J Pathol Bacteriol, 62 (1950) 313-333.
[114] H.D. Roh, Y. Boucher, S. Kalnicki, R. Buchsbaum, W.D. Bloomer, R.K. Jain, Interstitial hypertension in carcinoma of uterine cervix in patients: possible correlation with tumor oxygenation and radiation response, Cancer Res, 51 (1991) 6695-6698.
[115] Y. Boucher, J.M. Kirkwood, D. Opacic, M. Desantis, R.K. Jain, Interstitial hypertension in superficial metastatic melanomas in humans, Cancer Res, 51 (1991) 6691-6694.
[116] Y. Boucher, R.K. Jain, Microvascular pressure is the principal driving force for interstitial hypertension in solid tumors: implications for vascular collapse, Cancer Res, 52 (1992) 5110-5114.
[117] B.D. Curti, W.J. Urba, W.G. Alvord, J.E. Janik, J.W. Smith, 2nd, K. Madara, D.L. Longo, Interstitial pressure of subcutaneous nodules in melanoma and lymphoma patients: changes during treatment, Cancer Res, 53 (1993) 2204-2207.
[118] K.R. Levental, H. Yu, L. Kass, J.N. Lakins, M. Egeblad, J.T. Erler, S.F. Fong, K. Csiszar, A. Giaccia, W. Weninger, M. Yamauchi, D.L. Gasser, V.M. Weaver, Matrix crosslinking forces tumor progression by enhancing integrin signaling, Cell, 139 (2009) 891-906.
[119] H. Holback, Y. Yeo, Intratumoral drug delivery with nanoparticulate carriers, Pharm Res, 28 (2011) 1819-1830.
[120] B. Hinz, The myofibroblast: paradigm for a mechanically active cell, J Biomech, 43 (2010) 146-155.
[121] M. Larsen, V.V. Artym, J.A. Green, K.M. Yamada, The matrix reorganized: extracellular matrix remodeling and integrin signaling, Curr Opin Cell Biol, 18 (2006) 463-471.
[122] P. Lu, V.M. Weaver, Z. Werb, The extracellular matrix: a dynamic niche in cancer progression, J Cell Biol, 196 (2012) 395-406.
[123] F. Sabeh, R. Shimizu-Hirota, S.J. Weiss, Protease-dependent versus -independent cancer cell invasion programs: three-dimensional amoeboid movement revisited, J Cell Biol, 185 (2009) 11-19.
[124] C.E. Green, T. Liu, V. Montel, G. Hsiao, R.D. Lester, S. Subramaniam, S.L. Gonias, R.L. Klemke, Chemoattractant signaling between tumor cells and macrophages regulates cancer cell migration, metastasis and neovascularization, PLoS One, 4 (2009) e6713.
[125] A.S. Wolberg, Thrombin generation and fibrin clot structure, Blood Rev, 21 (2007) 131-142.
[126] J.A. Nagy, L.F. Brown, D.R. Senger, N. Lanir, L. Van de Water, A.M. Dvorak, H.F. Dvorak, Pathogenesis of tumor stroma generation: a critical role for leaky blood vessels and fibrin deposition, Biochim Biophys Acta, 948 (1989) 305-326.
[127] L.F. Brown, A.M. Dvorak, H.F. Dvorak, Leaky vessels, fibrin deposition, and fibrosis: a sequence of events common to solid tumors and to many other types of disease, Am Rev Respir Dis, 140 (1989) 1104-1107.
[128] F.R. Rickles, S. Patierno, P.M. Fernandez, Tissue factor, thrombin, and cancer, Chest, 124 (2003) 58S-68S.

[129] R. Hiramoto, J. Bernecky, J. Jurandowski, D. Pressman, Fibrin in human tumors, Cancer Res, 20 (1960) 592-593.
[130] L.F. Brown, L. Van de Water, V.S. Harvey, H.F. Dvorak, Fibrinogen influx and accumulation of cross-linked fibrin in healing wounds and in tumor stroma, Am J Pathol, 130 (1988) 455-465.
[131] L.F. Brown, B. Asch, V.S. Harvey, B. Buchinski, H.F. Dvorak, Fibrinogen influx and accumulation of cross-linked fibrin in mouse carcinomas, Cancer Res, 48 (1988) 1920-1925.
[132] H.F. Dvorak, D.R. Senger, A.M. Dvorak, V.S. Harvey, J. McDonagh, Regulation of extravascular coagulation by microvascular permeability, Science, 227 (1985) 1059-1061.
[133] H.M. Verheul, K. van Erp, M.Y. Homs, G.S. Yoon, P. van der Groep, C. Rogers, D.E. Hansel, G.J. Netto, R. Pili, The relationship of vascular endothelial growth factor and coagulation factor (fibrin and fibrinogen) expression in clear cell renal cell carcinoma, Urology, 75 608-614.
[134] H.F. Dvorak, A.M. Dvorak, E.J. Manseau, L. Wiberg, W.H. Churchill, Fibrin gel investment associated with line 1 and line 10 solid tumor growth, angiogenesis, and fibroplasia in guinea pigs. Role of cellular immunity, myofibroblasts, microvascular damage, and infarction in line 1 tumor regression, J Natl Cancer Inst, 62 (1979) 1459-1472.
[135] H.F. Dvorak, N.S. Orenstein, A.C. Carvalho, W.H. Churchill, A.M. Dvorak, S.J. Galli, J. Feder, A.M. Bitzer, J. Rypysc, P. Giovinco, Induction of a fibrin-gel investment: an early event in line 10 hepatocarcinoma growth mediated by tumor-secreted products, J Immunol, 122 (1979) 166-174.
[136] H.F. Dvorak, Tumors: wounds that do not heal. Similarities between tumor stroma generation and wound healing, N Engl J Med, 315 (1986) 1650-1659.
[137] L.F. Brown, N. Lanir, J. McDonagh, K. Tognazzi, A.M. Dvorak, H.F. Dvorak, Fibroblast migration in fibrin gel matrices, Am J Pathol, 142 (1993) 273-283.
[138] N. Lanir, P.S. Ciano, L. Van de Water, J. McDonagh, A.M. Dvorak, H.F. Dvorak, Macrophage migration in fibrin gel matrices. II. Effects of clotting factor XIII, fibronectin, and glycosaminoglycan content on cell migration, J Immunol, 140 (1988) 2340-2349.
[139] R. Kalluri, M. Zeisberg, Fibroblasts in cancer, Nat Rev Cancer, 6 (2006) 392-401.
[140] J.B. Hibbs, Jr., R.R. Taintor, H.A. Chapman, Jr., J.B. Weinberg, Macrophage tumor killing: influence of the local environment, Science, 197 (1977) 279-282.
[141] M. Schafer, S. Werner, Cancer as an overhealing wound: an old hypothesis revisited, Nat Rev Mol Cell Biol, 9 (2008) 628-638.
[142] N.S. Orenstein, A. Buczynski, H.F. Dvorak, Cryptic and active plasminogen activators secreted by line 10 tumor cells in culture, Cancer Res, 43 (1983) 1783-1789.
[143] W.D. Thompson, R. Campbell, T. Evans, Fibrin degradation and angiogenesis: quantitative analysis of the angiogenic response in the chick chorioallantoic membrane, J Pathol, 145 (1985) 27-37.
[144] W.F. Bale, I.L. Spar, R.L. Goodland, Experimental radiation therapy of tumors with I-131-carrying antibodies to fibrin, Cancer Res, 20 (1960) 1488-1494.

[145] T. Nishikawa, L.Y. Tung, Y. Kaneda, Systemic administration of platelets incorporating inactivated Sendai virus eradicates melanoma in mice, Mol Ther, 22 2046-2055.
[146] D. Simberg, T. Duza, J.H. Park, M. Essler, J. Pilch, L. Zhang, A.M. Derfus, M. Yang, R.M. Hoffman, S. Bhatia, M.J. Sailor, E. Ruoslahti, Biomimetic amplification of nanoparticle homing to tumors, Proc Natl Acad Sci U S A, 104 (2007) 932-936.
[147] G. von Maltzahn, J.H. Park, K.Y. Lin, N. Singh, C. Schwoppe, R. Mesters, W.E. Berdel, E. Ruoslahti, M.J. Sailor, S.N. Bhatia, Nanoparticles that communicate in vivo to amplify tumour targeting, Nat Mater, 10 545-552.
[148] R.G. Bristow, R.P. Hill, Hypoxia and metabolism. Hypoxia, DNA repair and genetic instability, Nat Rev Cancer, 8 (2008) 180-192.
[149] M. Hockel, P. Vaupel, Tumor hypoxia: definitions and current clinical, biologic, and molecular aspects, J Natl Cancer Inst, 93 (2001) 266-276.
[150] A.M. Shannon, D.J. Bouchier-Hayes, C.M. Condron, D. Toomey, Tumour hypoxia, chemotherapeutic resistance and hypoxia-related therapies, Cancer Treat Rev, 29 (2003) 297-307.
[151] M.L. Cunningham, P.S. Ringrose, B.R. Lokesh, Inhibition of the genotoxicity of bleomycin by superoxide dismutase, Mutat Res, 135 (1984) 199-202.
[152] I. Freitas, Role of hypoxia in photodynamic therapy of tumors, Tumori, 71 (1985) 251-259.
[153] O. Amellem, E.O. Pettersen, Cell inactivation and cell cycle inhibition as induced by extreme hypoxia: the possible role of cell cycle arrest as a protection against hypoxia-induced lethal damage, Cell Prolif, 24 (1991) 127-141.
[154] L.E. Huang, Z. Arany, D.M. Livingston, H.F. Bunn, Activation of hypoxia-inducible transcription factor depends primarily upon redox-sensitive stabilization of its alpha subunit, J Biol Chem, 271 (1996) 32253-32259.
[155] L.E. Huang, J. Gu, M. Schau, H.F. Bunn, Regulation of hypoxia-inducible factor 1alpha is mediated by an O2-dependent degradation domain via the ubiquitin-proteasome pathway, Proc Natl Acad Sci U S A, 95 (1998) 7987-7992.
[156] K.M. Comerford, T.J. Wallace, J. Karhausen, N.A. Louis, M.C. Montalto, S.P. Colgan, Hypoxia-inducible factor-1-dependent regulation of the multidrug resistance (MDR1) gene, Cancer Res, 62 (2002) 3387-3394.
[157] W.H. Koppenol, P.L. Bounds, C.V. Dang, Otto Warburg's contributions to current concepts of cancer metabolism, Nat Rev Cancer, 11 (2011) 325-337.
[158] E. Racker, Bioenergetics and the problem of tumor growth, Am Sci, 60 (1972) 56-63.
[159] N. Raghunand, R.J. Gillies, pH and drug resistance in tumors, Drug Resist Updat, 3 (2000) 39-47.
[160] L.S. Jabr-Milane, L.E. van Vlerken, S. Yadav, M.M. Amiji, Multi-functional nanocarriers to overcome tumor drug resistance, Cancer Treat Rev, 34 (2008) 592-602.
[161] P.J. Carter, P.D. Senter, Antibody-drug conjugates for cancer therapy, Cancer J, 14 (2008) 154-169.
[162] S.C. Alley, N.M. Okeley, P.D. Senter, Antibody-drug conjugates: targeted drug delivery for cancer, Curr Opin Chem Biol, 14 529-537.

[163] L. Ducry, B. Stump, Antibody-drug conjugates: linking cytotoxic payloads to monoclonal antibodies, Bioconjug Chem, 21 5-13.
[164] S.M. Wang, J.W. Chern, M.Y. Yeh, J.C. Ng, E. Tung, S.R. Roffler, Specific activation of glucuronide prodrugs by antibody-targeted enzyme conjugates for cancer therapy, Cancer Res, 52 (1992) 4484-4491.
[165] K.D. Bagshawe, C.J. Springer, F. Searle, P. Antoniw, S.K. Sharma, R.G. Melton, R.F. Sherwood, A cytotoxic agent can be generated selectively at cancer sites, Br J Cancer, 58 (1988) 700-703.
[166] P.L. Carl, P.K. Chakravarty, J.A. Katzenellenbogen, M.J. Weber, Protease-activated "prodrugs" for cancer chemotherapy, Proc Natl Acad Sci U S A, 77 (1980) 2224-2228.
[167] F. Greco, M.J. Vicent, Combination therapy: opportunities and challenges for polymer-drug conjugates as anticancer nanomedicines, Adv Drug Deliv Rev, 61 (2009) 1203-1213.
[168] L.W. Seymour, K. Ulbrich, P.S. Steyger, M. Brereton, V. Subr, J. Strohalm, R. Duncan, Tumour tropism and anti-cancer efficacy of polymer-based doxorubicin prodrugs in the treatment of subcutaneous murine B16F10 melanoma, Br J Cancer, 70 (1994) 636-641.
[169] C. Li, S. Wallace, Polymer-drug conjugates: recent development in clinical oncology, Adv Drug Deliv Rev, 60 (2008) 886-898.
[170] K. Cho, X. Wang, S. Nie, Z.G. Chen, D.M. Shin, Therapeutic nanoparticles for drug delivery in cancer, Clin Cancer Res, 14 (2008) 1310-1316.
[171] D. Peer, J.M. Karp, S. Hong, O.C. Farokhzad, R. Margalit, R. Langer, Nanocarriers as an emerging platform for cancer therapy, Nat Nanotechnol, 2 (2007) 751-760.
[172] M. Ferrari, Cancer nanotechnology: opportunities and challenges, Nat Rev Cancer, 5 (2005) 161-171.
[173] H. Maeda, J. Wu, T. Sawa, Y. Matsumura, K. Hori, Tumor vascular permeability and the EPR effect in macromolecular therapeutics: a review, J Control Release, 65 (2000) 271-284.
[174] Y. Matsumura, H. Maeda, A new concept for macromolecular therapeutics in cancer chemotherapy: mechanism of tumoritropic accumulation of proteins and the antitumor agent smancs, Cancer Res, 46 (1986) 6387-6392.
[175] C.C. Lee, J.A. MacKay, J.M. Frechet, F.C. Szoka, Designing dendrimers for biological applications, Nat Biotechnol, 23 (2005) 1517-1526.
[176] M.R. Dreher, W. Liu, C.R. Michelich, M.W. Dewhirst, F. Yuan, A. Chilkoti, Tumor vascular permeability, accumulation, and penetration of macromolecular drug carriers, J Natl Cancer Inst, 98 (2006) 335-344.
[177] Y.H. Bae, K. Park, Targeted drug delivery to tumors: myths, reality and possibility, J Control Release, 153 (2011) 198-205.
[178] I.K. Kwon, S.C. Lee, B. Han, K. Park, Analysis on the current status of targeted drug delivery to tumors, J Control Release, 164 108-114.
[179] D. Hanahan, R.A. Weinberg, Hallmarks of cancer: the next generation, Cell, 144 646-674.
[180] J. Folkman, Role of angiogenesis in tumor growth and metastasis, Semin Oncol, 29 (2002) 15-18.

[181] V.P. Chauhan, T. Stylianopoulos, Y. Boucher, R.K. Jain, Delivery of molecular and nanoscale medicine to tumors: transport barriers and strategies, Annu Rev Chem Biomol Eng, 2 281-298.
[182] R.K. Jain, Delivery of molecular and cellular medicine to solid tumors, Adv Drug Deliv Rev, 46 (2001) 149-168.
[183] P.A. Netti, L.M. Hamberg, J.W. Babich, D. Kierstead, W. Graham, G.J. Hunter, G.L. Wolf, A. Fischman, Y. Boucher, R.K. Jain, Enhancement of fluid filtration across tumor vessels: implication for delivery of macromolecules, Proc Natl Acad Sci U S A, 96 (1999) 3137-3142.
[184] S.N. Ekdawi, J.M. Stewart, M. Dunne, S. Stapleton, N. Mitsakakis, Y.N. Dou, D.A. Jaffray, C. Allen, Spatial and temporal mapping of heterogeneity in liposome uptake and microvascular distribution in an orthotopic tumor xenograft model, J Control Release, 207 101-111.
[185] F. Yuan, M. Leunig, S.K. Huang, D.A. Berk, D. Papahadjopoulos, R.K. Jain, Microvascular permeability and interstitial penetration of sterically stabilized (stealth) liposomes in a human tumor xenograft, Cancer Res, 54 (1994) 3352-3356.
[186] F. Yuan, M. Dellian, D. Fukumura, M. Leunig, D.A. Berk, V.P. Torchilin, R.K. Jain, Vascular permeability in a human tumor xenograft: molecular size dependence and cutoff size, Cancer Res, 55 (1995) 3752-3756.
[187] K.Y. Win, S.S. Feng, In vitro and in vivo studies on vitamin E TPGS-emulsified poly(D,L-lactic-co-glycolic acid) nanoparticles for paclitaxel formulation, Biomaterials, 27 (2006) 2285-2291.
[188] L.E. van Vlerken, Z. Duan, S.R. Little, M.V. Seiden, M.M. Amiji, Biodistribution and pharmacokinetic analysis of Paclitaxel and ceramide administered in multifunctional polymer-blend nanoparticles in drug resistant breast cancer model, Mol Pharm, 5 (2008) 516-526.
[189] Z. Xu, W. Gu, J. Huang, H. Sui, Z. Zhou, Y. Yang, Z. Yan, Y. Li, In vitro and in vivo evaluation of actively targetable nanoparticles for paclitaxel delivery, Int J Pharm, 288 (2005) 361-368.
[190] M.L. Forrest, J.A. Yanez, C.M. Remsberg, Y. Ohgami, G.S. Kwon, N.M. Davies, Paclitaxel prodrugs with sustained release and high solubility in poly(ethylene glycol)-b-poly(epsilon-caprolactone) micelle nanocarriers: pharmacokinetic disposition, tolerability, and cytotoxicity, Pharm Res, 25 (2008) 194-206.
[191] Y. Dong, S.S. Feng, In vitro and in vivo evaluation of methoxy polyethylene glycol-polylactide (MPEG-PLA) nanoparticles for small-molecule drug chemotherapy, Biomaterials, 28 (2007) 4154-4160.
[192] Z. Zhang, S.H. Lee, C.W. Gan, S.S. Feng, In vitro and in vivo investigation on PLA-TPGS nanoparticles for controlled and sustained small molecule chemotherapy, Pharm Res, 25 (2008) 1925-1935.
[193] G. Gaucher, R.H. Marchessault, J.C. Leroux, Polyester-based micelles and nanoparticles for the parenteral delivery of taxanes, J Control Release, 143 2-12.
[194] K. Alhareth, C. Vauthier, F. Bourasset, C. Gueutin, G. Ponchel, F. Moussa, Conformation of surface-decorating dextran chains affects the pharmacokinetics

and biodistribution of doxorubicin-loaded nanoparticles, Eur J Pharm Biopharm, 81 453-457.
[195] A. Jain, A. Agarwal, S. Majumder, N. Lariya, A. Khaya, H. Agrawal, S. Majumdar, G.P. Agrawal, Mannosylated solid lipid nanoparticles as vectors for site-specific delivery of an anti-cancer drug, J Control Release, 148 359-367.
[196] Y. Yi, J.H. Kim, H.W. Kang, H.S. Oh, S.W. Kim, M.H. Seo, A polymeric nanoparticle consisting of mPEG-PLA-Toco and PLMA-COONa as a drug carrier: improvements in cellular uptake and biodistribution, Pharm Res, 22 (2005) 200-208.
[197] S. Zhu, M. Hong, G. Tang, L. Qian, J. Lin, Y. Jiang, Y. Pei, Partly PEGylated polyamidoamine dendrimer for tumor-selective targeting of doxorubicin: the effects of PEGylation degree and drug conjugation style, Biomaterials, 31 1360-1371.
[198] C. Mamot, D.C. Drummond, C.O. Noble, V. Kallab, Z. Guo, K. Hong, D.B. Kirpotin, J.W. Park, Epidermal growth factor receptor-targeted immunoliposomes significantly enhance the efficacy of multiple anticancer drugs in vivo, Cancer Res, 65 (2005) 11631-11638.
[199] C. Fang, B. Shi, Y.Y. Pei, M.H. Hong, J. Wu, H.Z. Chen, In vivo tumor targeting of tumor necrosis factor-alpha-loaded stealth nanoparticles: effect of MePEG molecular weight and particle size, Eur J Pharm Sci, 27 (2006) 27-36.
[200] S.D. Perrault, C. Walkey, T. Jennings, H.C. Fischer, W.C. Chan, Mediating tumor targeting efficiency of nanoparticles through design, Nano Lett, 9 (2009) 1909-1915.
[201] A.J. Leu, D.A. Berk, A. Lymboussaki, K. Alitalo, R.K. Jain, Absence of functional lymphatics within a murine sarcoma: a molecular and functional evaluation, Cancer Res, 60 (2000) 4324-4327.
[202] T. Stylianopoulos, J.D. Martin, V.P. Chauhan, S.R. Jain, B. Diop-Frimpong, N. Bardeesy, B.L. Smith, C.R. Ferrone, F.J. Hornicek, Y. Boucher, L.L. Munn, R.K. Jain, Causes, consequences, and remedies for growth-induced solid stress in murine and human tumors, Proc Natl Acad Sci U S A, 109 15101-15108.
[203] K.C. Crowder, M.S. Hughes, J.N. Marsh, A.M. Barbieri, R.W. Fuhrhop, G.M. Lanza, S.A. Wickline, Sonic activation of molecularly-targeted nanoparticles accelerates transmembrane lipid delivery to cancer cells through contact-mediated mechanisms: implications for enhanced local drug delivery, Ultrasound Med Biol, 31 (2005) 1693-1700.
[204] M. Benezra, O. Penate-Medina, P.B. Zanzonico, D. Schaer, H. Ow, A. Burns, E. DeStanchina, V. Longo, E. Herz, S. Iyer, J. Wolchok, S.M. Larson, U. Wiesner, M.S. Bradbury, Multimodal silica nanoparticles are effective cancer-targeted probes in a model of human melanoma, J Clin Invest, 121 2768-2780.
[205] H.D. Han, L.S. Mangala, J.W. Lee, M.M. Shahzad, H.S. Kim, D. Shen, E.J. Nam, E.M. Mora, R.L. Stone, C. Lu, S.J. Lee, J.W. Roh, A.M. Nick, G. Lopez-Berestein, A.K. Sood, Targeted gene silencing using RGD-labeled chitosan nanoparticles, Clin Cancer Res, 16 3910-3922.
[206] Y. Wang, X. Wang, Y. Zhang, S. Yang, J. Wang, X. Zhang, Q. Zhang, RGD-modified polymeric micelles as potential carriers for targeted delivery to integrin-overexpressing tumor vasculature and tumor cells, J Drug Target, 17 (2009) 459-467.

[207] N. Nasongkla, E. Bey, J. Ren, H. Ai, C. Khemtong, J.S. Guthi, S.F. Chin, A.D. Sherry, D.A. Boothman, J. Gao, Multifunctional polymeric micelles as cancer-targeted, MRI-ultrasensitive drug delivery systems, Nano Lett, 6 (2006) 2427-2430.
[208] N. Nasongkla, X. Shuai, H. Ai, B.D. Weinberg, J. Pink, D.A. Boothman, J. Gao, cRGD-functionalized polymer micelles for targeted doxorubicin delivery, Angew Chem Int Ed Engl, 43 (2004) 6323-6327.
[209] F. Danhier, B. Vroman, N. Lecouturier, N. Crokart, V. Pourcelle, H. Freichels, C. Jerome, J. Marchand-Brynaert, O. Feron, V. Preat, Targeting of tumor endothelium by RGD-grafted PLGA-nanoparticles loaded with paclitaxel, J Control Release, 140 (2009) 166-173.
[210] U.S. Toti, B.R. Guru, A.E. Grill, J. Panyam, Interfacial activity assisted surface functionalization: a novel approach to incorporate maleimide functional groups and cRGD peptide on polymeric nanoparticles for targeted drug delivery, Mol Pharm, 7 (2010) 1108-1117.
[211] H.S. Choi, W. Liu, F. Liu, K. Nasr, P. Misra, M.G. Bawendi, J.V. Frangioni, Design considerations for tumour-targeted nanoparticles, Nat Nanotechnol, 5 42-47.
[212] J. Xie, K. Chen, H.Y. Lee, C. Xu, A.R. Hsu, S. Peng, X. Chen, S. Sun, Ultrasmall c(RGDyK)-coated Fe3O4 nanoparticles and their specific targeting to integrin alpha(v)beta3-rich tumor cells, J Am Chem Soc, 130 (2008) 7542-7543.
[213] L. Zhang, X. Zhong, L. Wang, H. Chen, Y.A. Wang, J. Yeh, L. Yang, H. Mao, T(1)-weighted ultrashort echo time method for positive contrast imaging of magnetic nanoparticles and cancer cells bound with the targeted nanoparticles, J Magn Reson Imaging, 33 194-202.
[214] P.M. Winter, S.D. Caruthers, A. Kassner, T.D. Harris, L.K. Chinen, J.S. Allen, E.K. Lacy, H. Zhang, J.D. Robertson, S.A. Wickline, G.M. Lanza, Molecular imaging of angiogenesis in nascent Vx-2 rabbit tumors using a novel alpha(nu)beta3-targeted nanoparticle and 1.5 tesla magnetic resonance imaging, Cancer Res, 63 (2003) 5838-5843.
[215] Y.B. Patil, U.S. Toti, A. Khdair, L. Ma, J. Panyam, Single-step surface functionalization of polymeric nanoparticles for targeted drug delivery, Biomaterials, 30 (2009) 859-866.
[216] R.M. Straubinger, N.G. Lopez, R.J. Debs, K. Hong, D. Papahadjopoulos, Liposome-based therapy of human ovarian cancer: parameters determining potency of negatively charged and antibody-targeted liposomes, Cancer Res, 48 (1988) 5237-5245.
[217] Y. Chen, J.J. Wu, L. Huang, Nanoparticles targeted with NGR motif deliver c-myc siRNA and doxorubicin for anticancer therapy, Mol Ther, 18 828-834.
[218] S.K. Swaminathan, E. Roger, U. Toti, L. Niu, J.R. Ohlfest, J. Panyam, CD133-targeted paclitaxel delivery inhibits local tumor recurrence in a mouse model of breast cancer, J Control Release, 171 280-287.
[219] T.M. Allen, D.R. Mumbengegwi, G.J. Charrois, Anti-CD19-targeted liposomal doxorubicin improves the therapeutic efficacy in murine B-cell lymphoma and ameliorates the toxicity of liposomes with varying drug release rates, Clin Cancer Res, 11 (2005) 3567-3573.

[220] A. Cirstoiu-Hapca, L. Bossy-Nobs, F. Buchegger, R. Gurny, F. Delie, Differential tumor cell targeting of anti-HER2 (Herceptin) and anti-CD20 (Mabthera) coupled nanoparticles, Int J Pharm, 331 (2007) 190-196.
[221] N. Dinauer, S. Balthasar, C. Weber, J. Kreuter, K. Langer, H. von Briesen, Selective targeting of antibody-conjugated nanoparticles to leukemic cells and primary T-lymphocytes, Biomaterials, 26 (2005) 5898-5906.
[222] K.Y. Choi, H. Chung, K.H. Min, H.Y. Yoon, K. Kim, J.H. Park, I.C. Kwon, S.Y. Jeong, Self-assembled hyaluronic acid nanoparticles for active tumor targeting, Biomaterials, 31 106-114.
[223] R. Kumar, I. Roy, T.Y. Ohulchanskyy, L.N. Goswami, A.C. Bonoiu, E.J. Bergey, K.M. Tramposch, A. Maitra, P.N. Prasad, Covalently dye-linked, surface-controlled, and bioconjugated organically modified silica nanoparticles as targeted probes for optical imaging, ACS Nano, 2 (2008) 449-456.
[224] X. Qian, X.H. Peng, D.O. Ansari, Q. Yin-Goen, G.Z. Chen, D.M. Shin, L. Yang, A.N. Young, M.D. Wang, S. Nie, In vivo tumor targeting and spectroscopic detection with surface-enhanced Raman nanoparticle tags, Nat Biotechnol, 26 (2008) 83-90.
[225] L. Yang, H. Mao, Y.A. Wang, Z. Cao, X. Peng, X. Wang, H. Duan, C. Ni, Q. Yuan, G. Adams, M.Q. Smith, W.C. Wood, X. Gao, S. Nie, Single chain epidermal growth factor receptor antibody conjugated nanoparticles for in vivo tumor targeting and imaging, Small, 5 (2009) 235-243.
[226] L. Milane, Z. Duan, M. Amiji, Therapeutic efficacy and safety of paclitaxel/lonidamine loaded EGFR-targeted nanoparticles for the treatment of multi-drug resistant cancer, PLoS One, 6 e24075.
[227] L. Milane, Z.F. Duan, M. Amiji, Pharmacokinetics and biodistribution of lonidamine/paclitaxel loaded, EGFR-targeted nanoparticles in an orthotopic animal model of multi-drug resistant breast cancer, Nanomedicine, 7 (2011) 435-444.
[228] T. Sadhukha, T.S. Wiedmann, J. Panyam, Inhalable magnetic nanoparticles for targeted hyperthermia in lung cancer therapy, Biomaterials, 34 (2013) 5163-5174.
[229] J. Chen, D. Wang, J. Xi, L. Au, A. Siekkinen, A. Warsen, Z.Y. Li, H. Zhang, Y. Xia, X. Li, Immuno gold nanocages with tailored optical properties for targeted photothermal destruction of cancer cells, Nano Lett, 7 (2007) 1318-1322.
[230] T. Reuveni, M. Motiei, Z. Romman, A. Popovtzer, R. Popovtzer, Targeted gold nanoparticles enable molecular CT imaging of cancer: an in vivo study, Int J Nanomedicine, 6 2859-2864.
[231] I.H. El-Sayed, X. Huang, M.A. El-Sayed, Selective laser photo-thermal therapy of epithelial carcinoma using anti-EGFR antibody conjugated gold nanoparticles, Cancer Lett, 239 (2006) 129-135.
[232] C.G. Hadjipanayis, R. Machaidze, M. Kaluzova, L. Wang, A.J. Schuette, H. Chen, X. Wu, H. Mao, EGFRvIII antibody-conjugated iron oxide nanoparticles for magnetic resonance imaging-guided convection-enhanced delivery and targeted therapy of glioblastoma, Cancer Res, 70 6303-6312.
[233] D. Artemov, N. Mori, B. Okollie, Z.M. Bhujwalla, MR molecular imaging of the Her-2/neu receptor in breast cancer cells using targeted iron oxide nanoparticles, Magn Reson Med, 49 (2003) 403-408.

[234] K. Cheng, S. Peng, C. Xu, S. Sun, Porous hollow Fe(3)O(4) nanoparticles for targeted delivery and controlled release of cisplatin, J Am Chem Soc, 131 (2009) 10637-10644.
[235] L. Fan, F. Li, H. Zhang, Y. Wang, C. Cheng, X. Li, C.H. Gu, Q. Yang, H. Wu, S. Zhang, Co-delivery of PDTC and doxorubicin by multifunctional micellar nanoparticles to achieve active targeted drug delivery and overcome multidrug resistance, Biomaterials, 31 5634-5642.
[236] Y. Zu, D. Wang, X. Zhao, R. Jiang, Q. Zhang, D. Zhao, Y. Li, B. Zu, Z. Sun, A novel preparation method for camptothecin (CPT) loaded folic acid conjugated dextran tumor-targeted nanoparticles, Int J Mol Sci, 12 4237-4249.
[237] F. Sonvico, S. Mornet, S. Vasseur, C. Dubernet, D. Jaillard, J. Degrouard, J. Hoebeke, E. Duguet, P. Colombo, P. Couvreur, Folate-conjugated iron oxide nanoparticles for solid tumor targeting as potential specific magnetic hyperthermia mediators: synthesis, physicochemical characterization, and in vitro experiments, Bioconjug Chem, 16 (2005) 1181-1188.
[238] J. Kim, S. Park, J.E. Lee, S.M. Jin, J.H. Lee, I.S. Lee, I. Yang, J.S. Kim, S.K. Kim, M.H. Cho, T. Hyeon, Designed fabrication of multifunctional magnetic gold nanoshells and their application to magnetic resonance imaging and photothermal therapy, Angew Chem Int Ed Engl, 45 (2006) 7754-7758.
[239] J.M. Rosenholm, A. Meinander, E. Peuhu, R. Niemi, J.E. Eriksson, C. Sahlgren, M. Linden, Targeting of porous hybrid silica nanoparticles to cancer cells, ACS Nano, 3 (2009) 197-206.
[240] P. Zhao, H. Wang, M. Yu, Z. Liao, X. Wang, F. Zhang, W. Ji, B. Wu, J. Han, H. Zhang, J. Chang, R. Niu, Paclitaxel loaded folic acid targeted nanoparticles of mixed lipid-shell and polymer-core: in vitro and in vivo evaluation, Eur J Pharm Biopharm, 81 248-256.
[241] M.E. Werner, S. Karve, R. Sukumar, N.D. Cummings, J.A. Copp, R.C. Chen, T. Zhang, A.Z. Wang, Folate-targeted nanoparticle delivery of chemo- and radiotherapeutics for the treatment of ovarian cancer peritoneal metastasis, Biomaterials, 32 8548-8554.
[242] J. Pan, S.S. Feng, Targeting and imaging cancer cells by folate-decorated, quantum dots (QDs)- loaded nanoparticles of biodegradable polymers, Biomaterials, 30 (2009) 1176-1183.
[243] H. Lee, A.K. Lytton-Jean, Y. Chen, K.T. Love, A.I. Park, E.D. Karagiannis, A. Sehgal, W. Querbes, C.S. Zurenko, M. Jayaraman, C.G. Peng, K. Charisse, A. Borodovsky, M. Manoharan, J.S. Donahoe, J. Truelove, M. Nahrendorf, R. Langer, D.G. Anderson, Molecularly self-assembled nucleic acid nanoparticles for targeted in vivo siRNA delivery, Nat Nanotechnol, 7 389-393.
[244] D. Goren, A.T. Horowitz, D. Tzemach, M. Tarshish, S. Zalipsky, A. Gabizon, Nuclear delivery of doxorubicin via folate-targeted liposomes with bypass of multidrug-resistance efflux pump, Clin Cancer Res, 6 (2000) 1949-1957.
[245] H.S. Yoo, T.G. Park, Folate receptor targeted biodegradable polymeric doxorubicin micelles, J Control Release, 96 (2004) 273-283.
[246] X. Jiang, H. Xin, Q. Ren, J. Gu, L. Zhu, F. Du, C. Feng, Y. Xie, X. Sha, X. Fang, Nanoparticles of 2-deoxy-D-glucose functionalized poly(ethylene glycol)-co-

poly(trimethylene carbonate) for dual-targeted drug delivery in glioma treatment, Biomaterials, 35 518-529.
[247] A.H. Abouzeid, N.R. Patel, I.M. Rachman, S. Senn, V.P. Torchilin, Anti-cancer activity of anti-GLUT1 antibody-targeted polymeric micelles co-loaded with curcumin and doxorubicin, J Drug Target, 21 994-1000.
[248] F. Said Hassane, B. Frisch, F. Schuber, Targeted liposomes: convenient coupling of ligands to preformed vesicles using "click chemistry", Bioconjug Chem, 17 (2006) 849-854.
[249] A. Taheri, R. Dinarvand, F. Ahadi, M.R. Khorramizadeh, F. Atyabi, The in vivo antitumor activity of LHRH targeted methotrexate-human serum albumin nanoparticles in 4T1 tumor-bearing Balb/c mice, Int J Pharm, 431 183-189.
[250] G. Luo, X. Yu, C. Jin, F. Yang, D. Fu, J. Long, J. Xu, C. Zhan, W. Lu, LyP-1-conjugated nanoparticles for targeting drug delivery to lymphatic metastatic tumors, Int J Pharm, 385 150-156.
[251] G.R. Reddy, M.S. Bhojani, P. McConville, J. Moody, B.A. Moffat, D.E. Hall, G. Kim, Y.E. Koo, M.J. Woolliscroft, J.V. Sugai, T.D. Johnson, M.A. Philbert, R. Kopelman, A. Rehemtulla, B.D. Ross, Vascular targeted nanoparticles for imaging and treatment of brain tumors, Clin Cancer Res, 12 (2006) 6677-6686.
[252] H.J. Hah, G. Kim, Y.E. Lee, D.A. Orringer, O. Sagher, M.A. Philbert, R. Kopelman, Methylene blue-conjugated hydrogel nanoparticles and tumor-cell targeted photodynamic therapy, Macromol Biosci, 11 90-99.
[253] I. Winer, S. Wang, Y.E. Lee, W. Fan, Y. Gong, D. Burgos-Ojeda, G. Spahlinger, R. Kopelman, R.J. Buckanovich, F3-targeted cisplatin-hydrogel nanoparticles as an effective therapeutic that targets both murine and human ovarian tumor endothelial cells in vivo, Cancer Res, 70 8674-8683.
[254] A.N. Lukyanov, T.A. Elbayoumi, A.R. Chakilam, V.P. Torchilin, Tumor-targeted liposomes: doxorubicin-loaded long-circulating liposomes modified with anti-cancer antibody, J Control Release, 100 (2004) 135-144.
[255] X. Gao, Y. Cui, R.M. Levenson, L.W. Chung, S. Nie, In vivo cancer targeting and imaging with semiconductor quantum dots, Nat Biotechnol, 22 (2004) 969-976.
[256] P.M. Valencia, E.M. Pridgen, M. Rhee, R. Langer, O.C. Farokhzad, R. Karnik, Microfluidic platform for combinatorial synthesis and optimization of targeted nanoparticles for cancer therapy, ACS Nano, 7 10671-10680.
[257] S. Dhar, F.X. Gu, R. Langer, O.C. Farokhzad, S.J. Lippard, Targeted delivery of cisplatin to prostate cancer cells by aptamer functionalized Pt(IV) prodrug-PLGA-PEG nanoparticles, Proc Natl Acad Sci U S A, 105 (2008) 17356-17361.
[258] J. Cheng, B.A. Teply, I. Sherifi, J. Sung, G. Luther, F.X. Gu, E. Levy-Nissenbaum, A.F. Radovic-Moreno, R. Langer, O.C. Farokhzad, Formulation of functionalized PLGA-PEG nanoparticles for in vivo targeted drug delivery, Biomaterials, 28 (2007) 869-876.
[259] L. Zhang, J.M. Chan, F.X. Gu, J.W. Rhee, A.Z. Wang, A.F. Radovic-Moreno, F. Alexis, R. Langer, O.C. Farokhzad, Self-assembled lipid--polymer hybrid nanoparticles: a robust drug delivery platform, ACS Nano, 2 (2008) 1696-1702.

[260] W. Xu, I.A. Siddiqui, M. Nihal, S. Pilla, K. Rosenthal, H. Mukhtar, S. Gong, Aptamer-conjugated and doxorubicin-loaded unimolecular micelles for targeted therapy of prostate cancer, Biomaterials, 34 5244-5253.
[261] J. Guo, J.R. Ogier, S. Desgranges, R. Darcy, C. O'Driscoll, Anisamide-targeted cyclodextrin nanoparticles for siRNA delivery to prostate tumours in mice, Biomaterials, 33 7775-7784.
[262] R. Banerjee, P. Tyagi, S. Li, L. Huang, Anisamide-targeted stealth liposomes: a potent carrier for targeting doxorubicin to human prostate cancer cells, Int J Cancer, 112 (2004) 693-700.
[263] Y. Chen, S.R. Bathula, Q. Yang, L. Huang, Targeted nanoparticles deliver siRNA to melanoma, J Invest Dermatol, 130 2790-2798.
[264] S. Thomas, P. Waterman, S. Chen, B. Marinelli, M. Seaman, S. Rodig, R.W. Ross, L. Josephson, R. Weissleder, K.A. Kelly, Development of Secreted Protein and Acidic and Rich in Cysteine (SPARC) Targeted Nanoparticles for the Prognostic Molecular Imaging of Metastatic Prostate Cancer, J Nanomed Nanotechnol, 2.
[265] C.H. Choi, C.A. Alabi, P. Webster, M.E. Davis, Mechanism of active targeting in solid tumors with transferrin-containing gold nanoparticles, Proc Natl Acad Sci U S A, 107 1235-1240.
[266] J.D. Heidel, Z. Yu, J.Y. Liu, S.M. Rele, Y. Liang, R.K. Zeidan, D.J. Kornbrust, M.E. Davis, Administration in non-human primates of escalating intravenous doses of targeted nanoparticles containing ribonucleotide reductase subunit M2 siRNA, Proc Natl Acad Sci U S A, 104 (2007) 5715-5721.
[267] D.W. Bartlett, M.E. Davis, Impact of tumor-specific targeting and dosing schedule on tumor growth inhibition after intravenous administration of siRNA-containing nanoparticles, Biotechnol Bioeng, 99 (2008) 975-985.
[268] C.W. Gan, S.S. Feng, Transferrin-conjugated nanoparticles of poly(lactide)-D-alpha-tocopheryl polyethylene glycol succinate diblock copolymer for targeted drug delivery across the blood-brain barrier, Biomaterials, 31 7748-7757.
[269] S.J. Chiu, S. Liu, D. Perrotti, G. Marcucci, R.J. Lee, Efficient delivery of a Bcl-2-specific antisense oligodeoxyribonucleotide (G3139) via transferrin receptor-targeted liposomes, J Control Release, 112 (2006) 199-207.
[270] L. Yang, H. Mao, Z. Cao, Y.A. Wang, X. Peng, X. Wang, H.K. Sajja, L. Wang, H. Duan, C. Ni, C.A. Staley, W.C. Wood, X. Gao, S. Nie, Molecular imaging of pancreatic cancer in an animal model using targeted multifunctional nanoparticles, Gastroenterology, 136 (2009) 1514-1525 e1512.
[271] L. Yang, X.H. Peng, Y.A. Wang, X. Wang, Z. Cao, C. Ni, P. Karna, X. Zhang, W.C. Wood, X. Gao, S. Nie, H. Mao, Receptor-targeted nanoparticles for in vivo imaging of breast cancer, Clin Cancer Res, 15 (2009) 4722-4732.
[272] D. Hanahan, R.A. Weinberg, The hallmarks of cancer, Cell, 100 (2000) 57-70.
[273] I. Sassoon, V. Blanc, Antibody-drug conjugate (ADC) clinical pipeline: a review, Methods Mol Biol, 1045 1-27.
[274] J.D. Byrne, T. Betancourt, L. Brannon-Peppas, Active targeting schemes for nanoparticle systems in cancer therapeutics, Adv Drug Deliv Rev, 60 (2008) 1615-1626.

[275] R.M. Sawant, J.P. Hurley, S. Salmaso, A. Kale, E. Tolcheva, T.S. Levchenko, V.P. Torchilin, "SMART" drug delivery systems: double-targeted pH-responsive pharmaceutical nanocarriers, Bioconjug Chem, 17 (2006) 943-949.
[276] N. Bertrand, J. Wu, X. Xu, N. Kamaly, O.C. Farokhzad, Cancer nanotechnology: the impact of passive and active targeting in the era of modern cancer biology, Adv Drug Deliv Rev, 66 2-25.
[277] K. Maruyama, O. Ishida, T. Takizawa, K. Moribe, Possibility of active targeting to tumor tissues with liposomes, Adv Drug Deliv Rev, 40 (1999) 89-102.
[278] F. Marcucci, F. Lefoulon, Active targeting with particulate drug carriers in tumor therapy: fundamentals and recent progress, Drug Discov Today, 9 (2004) 219-228.
[279] T.M. Allen, Ligand-targeted therapeutics in anticancer therapy, Nat Rev Cancer, 2 (2002) 750-763.
[280] Z. Cheng, A. Al Zaki, J.Z. Hui, V.R. Muzykantov, A. Tsourkas, Multifunctional nanoparticles: cost versus benefit of adding targeting and imaging capabilities, Science, 338 903-910.
[281] P. Decuzzi, M. Ferrari, The role of specific and non-specific interactions in receptor-mediated endocytosis of nanoparticles, Biomaterials, 28 (2007) 2915-2922.
[282] H. Yuan, C. Huang, S. Zhang, Virus-inspired design principles of nanoparticle-based bioagents, PLoS One, 5 e13495.
[283] H. Gao, Z. Yang, S. Zhang, S. Cao, S. Shen, Z. Pang, X. Jiang, Ligand modified nanoparticles increases cell uptake, alters endocytosis and elevates glioma distribution and internalization, Sci Rep, 3 2534.
[284] A. Albanese, A.K. Lam, E.A. Sykes, J.V. Rocheleau, W.C. Chan, Tumour-on-a-chip provides an optical window into nanoparticle tissue transport, Nat Commun, 4 2718.
[285] S.K. Sahoo, V. Labhasetwar, Enhanced antiproliferative activity of transferrin-conjugated paclitaxel-loaded nanoparticles is mediated via sustained intracellular drug retention, Mol Pharm, 2 (2005) 373-383.
[286] Y.H. Bae, Interview with Dr You Han Bae: ligand-mediated versus 'passive' targeting approaches in nanoparticle oncology research, Ther Deliv, 3 933-936.
[287] J. Panyam, W.Z. Zhou, S. Prabha, S.K. Sahoo, V. Labhasetwar, Rapid endo-lysosomal escape of poly(DL-lactide-co-glycolide) nanoparticles: implications for drug and gene delivery, FASEB J, 16 (2002) 1217-1226.
[288] R.M. Schiffelers, A. Ansari, J. Xu, Q. Zhou, Q. Tang, G. Storm, G. Molema, P.Y. Lu, P.V. Scaria, M.C. Woodle, Cancer siRNA therapy by tumor selective delivery with ligand-targeted sterically stabilized nanoparticle, Nucleic Acids Res, 32 (2004) e149.
[289] K. Shroff, E. Kokkoli, PEGylated liposomal doxorubicin targeted to alpha5beta1-expressing MDA-MB-231 breast cancer cells, Langmuir, 28 4729-4736.
[290] D.B. Kirpotin, D.C. Drummond, Y. Shao, M.R. Shalaby, K. Hong, U.B. Nielsen, J.D. Marks, C.C. Benz, J.W. Park, Antibody targeting of long-circulating lipidic nanoparticles does not increase tumor localization but does increase internalization in animal models, Cancer Res, 66 (2006) 6732-6740.

[291] O.C. Farokhzad, J. Cheng, B.A. Teply, I. Sherifi, S. Jon, P.W. Kantoff, J.P. Richie, R. Langer, Targeted nanoparticle-aptamer bioconjugates for cancer chemotherapy in vivo, Proc Natl Acad Sci U S A, 103 (2006) 6315-6320.
[292] J.F. Kukowska-Latallo, K.A. Candido, Z. Cao, S.S. Nigavekar, I.J. Majoros, T.P. Thomas, L.P. Balogh, M.K. Khan, J.R. Baker, Jr., Nanoparticle targeting of anticancer drug improves therapeutic response in animal model of human epithelial cancer, Cancer Res, 65 (2005) 5317-5324.
[293] A.R. Kirtane, H.L. Wong, B.R. Guru, L.G. Lis, G.I. Georg, V.J. Gurvich, J. Panyam, Reformulating Tylocrebrine in Epidermal Growth Factor Receptor Targeted Polymeric Nanoparticles Improves Its Therapeutic Index, Mol Pharm.
[294] D. Papahadjopoulos, A. Gabizon, Targeting of liposomes to tumor cells in vivo, Ann N Y Acad Sci, 507 (1987) 64-74.
[295] H. Tang, X. Chen, M. Rui, W. Sun, J. Chen, J. Peng, Y. Xu, Effects of surface displayed targeting ligand GE11 on liposome distribution and extravasation in tumor, Mol Pharm, 11 3242-3250.
[296] K. Kataoka, A. Harada, Y. Nagasaki, Block copolymer micelles for drug delivery: design, characterization and biological significance, Adv Drug Deliv Rev, 47 (2001) 113-131.
[297] S.K. Sahoo, J. Panyam, S. Prabha, V. Labhasetwar, Residual polyvinyl alcohol associated with poly (D,L-lactide-co-glycolide) nanoparticles affects their physical properties and cellular uptake, J Control Release, 82 (2002) 105-114.
[298] M.D. Chavanpatil, A. Khdair, J. Panyam, Surfactant-polymer nanoparticles: a novel platform for sustained and enhanced cellular delivery of water-soluble molecules, Pharm Res, 24 (2007) 803-810.
[299] M.J. Lawrence, Surfactant systems: microemulsions and vesicles as vehicles for drug delivery, Eur J Drug Metab Pharmacokinet, 19 (1994) 257-269.
[300] V.P. Torchilin, Structure and design of polymeric surfactant-based drug delivery systems, J Control Release, 73 (2001) 137-172.
[301] H. Riehm, J.L. Biedler, Potentiation of drug effect by Tween 80 in Chinese hamster cells resistant to actinomycin D and daunomycin, Cancer Res, 32 (1972) 1195-1200.
[302] X. Dong, R.J. Mumper, Nanomedicinal strategies to treat multidrug-resistant tumors: current progress, Nanomedicine (Lond), 5 (2010) 597-615.
[303] D.M. Woodcock, S. Jefferson, M.E. Linsenmeyer, P.J. Crowther, G.M. Chojnowski, B. Williams, I. Bertoncello, Reversal of the multidrug resistance phenotype with cremophor EL, a common vehicle for water-insoluble vitamins and drugs, Cancer Res, 50 (1990) 4199-4203.
[304] D.M. Woodcock, M.E. Linsenmeyer, G. Chojnowski, A.B. Kriegler, V. Nink, L.K. Webster, W.H. Sawyer, Reversal of multidrug resistance by surfactants, Br J Cancer, 66 (1992) 62-68.
[305] H. Gelderblom, J. Verweij, K. Nooter, A. Sparreboom, Cremophor EL: the drawbacks and advantages of vehicle selection for drug formulation, Eur J Cancer, 37 (2001) 1590-1598.
[306] T. Sakai, P. Alexandridis, Single-step synthesis and stabilization of metal nanoparticles in aqueous pluronic block copolymer solutions at ambient temperature, Langmuir, 20 (2004) 8426-8430.

[307] K.S. Oh, J.Y. Song, S.H. Cho, B.S. Lee, S.Y. Kim, K. Kim, H. Jeon, I.C. Kwon, S.H. Yuk, Paclitaxel-loaded Pluronic nanoparticles formed by a temperature-induced phase transition for cancer therapy, J Control Release, 148 (2010) 344-350.
[308] A.V. Kabanov, V.Y. Alakhov, Pluronic block copolymers in drug delivery: from micellar nanocontainers to biological response modifiers, Crit Rev Ther Drug Carrier Syst, 19 (2002) 1-72.
[309] E.V. Batrakova, S. Li, W.F. Elmquist, D.W. Miller, V.Y. Alakhov, A.V. Kabanov, Mechanism of sensitization of MDR cancer cells by Pluronic block copolymers: Selective energy depletion, Br J Cancer, 85 (2001) 1987-1997.
[310] E.V. Batrakova, S. Li, S.V. Vinogradov, V.Y. Alakhov, D.W. Miller, A.V. Kabanov, Mechanism of pluronic effect on P-glycoprotein efflux system in blood-brain barrier: contributions of energy depletion and membrane fluidization, J Pharmacol Exp Ther, 299 (2001) 483-493.
[311] J.W. Valle, A. Armstrong, C. Newman, V. Alakhov, G. Pietrzynski, J. Brewer, S. Campbell, P. Corrie, E.K. Rowinsky, M. Ranson, A phase 2 study of SP1049C, doxorubicin in P-glycoprotein-targeting pluronics, in patients with advanced adenocarcinoma of the esophagus and gastroesophageal junction, Invest New Drugs, 29 (2011) 1029-1037.
[312] J.S. Coon, W. Knudson, K. Clodfelter, B. Lu, R.S. Weinstein, Solutol HS 15, nontoxic polyoxyethylene esters of 12-hydroxystearic acid, reverses multidrug resistance, Cancer Res, 51 (1991) 897-902.
[313] J.M. Koziara, T.R. Whisman, M.T. Tseng, R.J. Mumper, In-vivo efficacy of novel paclitaxel nanoparticles in paclitaxel-resistant human colorectal tumors, J Control Release, 112 (2006) 312-319.
[314] J.M. Koziara, P.R. Lockman, D.D. Allen, R.J. Mumper, Paclitaxel nanoparticles for the potential treatment of brain tumors, J Control Release, 99 (2004) 259-269.
[315] X. Dong, C.A. Mattingly, M.T. Tseng, M.J. Cho, Y. Liu, V.R. Adams, R.J. Mumper, Doxorubicin and paclitaxel-loaded lipid-based nanoparticles overcome multidrug resistance by inhibiting P-glycoprotein and depleting ATP, Cancer Res, 69 (2009) 3918-3926.
[316] K. Bogman, F. Erne-Brand, J. Alsenz, J. Drewe, The role of surfactants in the reversal of active transport mediated by multidrug resistance proteins, J Pharm Sci, 92 (2003) 1250-1261.
[317] L.E. Buckingham, M. Balasubramanian, R.M. Emanuele, K.E. Clodfelter, J.S. Coon, Comparison of solutol HS 15, Cremophor EL and novel ethoxylated fatty acid surfactants as multidrug resistance modification agents, Int J Cancer, 62 (1995) 436-442.
[318] Y.L. Lo, Relationships between the hydrophilic-lipophilic balance values of pharmaceutical excipients and their multidrug resistance modulating effect in Caco-2 cells and rat intestines, J Control Release, 90 (2003) 37-48.
[319] C. Vauthier, C. Dubernet, C. Chauvierre, I. Brigger, P. Couvreur, Drug delivery to resistant tumors: the potential of poly(alkyl cyanoacrylate) nanoparticles, J Control Release, 93 (2003) 151-160.

[320] C. Cuvier, L. Roblot-Treupel, J.M. Millot, G. Lizard, S. Chevillard, M. Manfait, P. Couvreur, M.F. Poupon, Doxorubicin-loaded nanospheres bypass tumor cell multidrug resistance, Biochem Pharmacol, 44 (1992) 509-517.
[321] L. Treupel, M.F. Poupon, P. Couvreur, F. Puisieux, [Vectorisation of doxorubicin in nanospheres and reversion of pleiotropic resistance of tumor cells], C R Acad Sci III, 313 (1991) 171-174.
[322] A.C. de Verdiere, C. Dubernet, F. Nemati, E. Soma, M. Appel, J. Ferte, S. Bernard, F. Puisieux, P. Couvreur, Reversion of multidrug resistance with polyalkylcyanoacrylate nanoparticles: towards a mechanism of action, Br J Cancer, 76 (1997) 198-205.
[323] L. Barraud, P. Merle, E. Soma, L. Lefrancois, S. Guerret, M. Chevallier, C. Dubernet, P. Couvreur, C. Trepo, L. Vitvitski, Increase of doxorubicin sensitivity by doxorubicin-loading into nanoparticles for hepatocellular carcinoma cells in vitro and in vivo, J Hepatol, 42 (2005) 736-743.
[324] E.D. Hugger, K.L. Audus, R.T. Borchardt, Effects of poly(ethylene glycol) on efflux transporter activity in Caco-2 cell monolayers, J Pharm Sci, 91 (2002) 1980-1990.
[325] J. Wang, H. Qu, L. Jin, W. Zeng, L. Qin, F. Zhang, X. Wei, W. Lu, C. Zhang, W. Liang, Pegylated phosphotidylethanolamine inhibiting P-glycoprotein expression and enhancing retention of doxorubicin in MCF7/ADR cells, J Pharm Sci, 100 (2011) 2267-2277.
[326] B.M. Johnson, W.N. Charman, C.J. Porter, An in vitro examination of the impact of polyethylene glycol 400, Pluronic P85, and vitamin E d-alpha-tocopheryl polyethylene glycol 1000 succinate on P-glycoprotein efflux and enterocyte-based metabolism in excised rat intestine, AAPS PharmSci, 4 (2002) E40.
[327] J.M. Harris, R.B. Chess, Effect of pegylation on pharmaceuticals, Nat Rev Drug Discov, 2 (2003) 214-221.
[328] Q. Shen, Y. Lin, T. Handa, M. Doi, M. Sugie, K. Wakayama, N. Okada, T. Fujita, A. Yamamoto, Modulation of intestinal P-glycoprotein function by polyethylene glycols and their derivatives by in vitro transport and in situ absorption studies, Int J Pharm, 313 (2006) 49-56.
[329] J. Kopecek, P. Kopeckova, T. Minko, Z.R. Lu, C.M. Peterson, Water soluble polymers in tumor targeted delivery, J Control Release, 74 (2001) 147-158.
[330] J. Panyam, V. Labhasetwar, Biodegradable nanoparticles for drug and gene delivery to cells and tissue, Adv Drug Deliv Rev, 55 (2003) 329-347.
[331] M. Murakami, H. Cabral, Y. Matsumoto, S. Wu, M.R. Kano, T. Yamori, N. Nishiyama, K. Kataoka, Improving drug potency and efficacy by nanocarrier-mediated subcellular targeting, Sci Transl Med, 3 (2011) 64ra62.
[332] L.M. Bareford, P.W. Swaan, Endocytic mechanisms for targeted drug delivery, Adv Drug Deliv Rev, 59 (2007) 748-758.
[333] F. Wang, Y.C. Wang, S. Dou, M.H. Xiong, T.M. Sun, J. Wang, Doxorubicin-tethered responsive gold nanoparticles facilitate intracellular drug delivery for overcoming multidrug resistance in cancer cells, ACS Nano, 5 (2011) 3679-3692.
[334] A.R. Thierry, D. Vige, S.S. Coughlin, J.A. Belli, A. Dritschilo, A. Rahman, Modulation of doxorubicin resistance in multidrug-resistant cells by liposomes, FASEB J, 7 (1993) 572-579.

[335] A. Colin de Verdiere, C. Dubernet, F. Nemati, M.F. Poupon, F. Puisieux, P. Couvreur, Uptake of doxorubicin from loaded nanoparticles in multidrug-resistant leukemic murine cells, Cancer Chemother Pharmacol, 33 (1994) 504-508.
[336] H.L. Wong, R. Bendayan, A.M. Rauth, H.Y. Xue, K. Babakhanian, X.Y. Wu, A mechanistic study of enhanced doxorubicin uptake and retention in multidrug resistant breast cancer cells using a polymer-lipid hybrid nanoparticle system, J Pharmacol Exp Ther, 317 (2006) 1372-1381.
[337] H.L. Wong, A.M. Rauth, R. Bendayan, J.L. Manias, M. Ramaswamy, Z. Liu, S.Z. Erhan, X.Y. Wu, A new polymer-lipid hybrid nanoparticle system increases cytotoxicity of doxorubicin against multidrug-resistant human breast cancer cells, Pharm Res, 23 (2006) 1574-1585.
[338] M.D. Chavanpatil, A. Khdair, B. Gerard, C. Bachmeier, D.W. Miller, M.P. Shekhar, J. Panyam, Surfactant-polymer nanoparticles overcome P-glycoprotein-mediated drug efflux, Mol Pharm, 4 (2007) 730-738.
[339] V. Omelyanenko, P. Kopeckova, C. Gentry, J. Kopecek, Targetable HPMA copolymer-adriamycin conjugates. Recognition, internalization, and subcellular fate, J Control Release, 53 (1998) 25-37.
[340] Y. Chan, T. Wong, F. Byrne, M. Kavallaris, V. Bulmus, Acid-labile core cross-linked micelles for pH-triggered release of antitumor drugs, Biomacromolecules, 9 (2008) 1826-1836.
[341] E.S. Lee, K. Na, Y.H. Bae, Doxorubicin loaded pH-sensitive polymeric micelles for reversal of resistant MCF-7 tumor, J Control Release, 103 (2005) 405-418.
[342] F. Ahmed, R.I. Pakunlu, G. Srinivas, A. Brannan, F. Bates, M.L. Klein, T. Minko, D.E. Discher, Shrinkage of a rapidly growing tumor by drug-loaded polymersomes: pH-triggered release through copolymer degradation, Mol Pharm, 3 (2006) 340-350.
[343] X. Guo, F.C. Szoka, Jr., Steric stabilization of fusogenic liposomes by a low-pH sensitive PEG--diortho ester--lipid conjugate, Bioconjug Chem, 12 (2001) 291-300.
[344] F.M. Kievit, F.Y. Wang, C. Fang, H. Mok, K. Wang, J.R. Silber, R.G. Ellenbogen, M. Zhang, Doxorubicin loaded iron oxide nanoparticles overcome multidrug resistance in cancer in vitro, J Control Release, 152 (2011) 76-83.
[345] Y. Wang, L. Chen, Y. Ding, W. Yan, Oxidized phospholipid based pH sensitive micelles for delivery of anthracyclines to resistant leukemia cells in vitro, Int J Pharm, 422 409-417.
[346] O.V. Gerasimov, J.A. Boomer, M.M. Qualls, D.H. Thompson, Cytosolic drug delivery using pH- and light-sensitive liposomes, Adv Drug Deliv Rev, 38 (1999) 317-338.
[347] Y. Gao, Y. Chen, X. Ji, X. He, Q. Yin, Z. Zhang, J. Shi, Y. Li, Controlled intracellular release of doxorubicin in multidrug-resistant cancer cells by tuning the shell-pore sizes of mesoporous silica nanoparticles, ACS Nano, 5 (2011) 9788-9798.
[348] D.R. Ferry, H. Traunecker, D.J. Kerr, Clinical trials of P-glycoprotein reversal in solid tumours, Eur J Cancer, 32A (1996) 1070-1081.

[349] G.D. Leonard, T. Fojo, S.E. Bates, The role of ABC transporters in clinical practice, Oncologist, 8 (2003) 411-424.
[350] A.F. List, K.J. Kopecky, C.L. Willman, D.R. Head, D.L. Persons, M.L. Slovak, R. Dorr, C. Karanes, H.E. Hynes, J.H. Doroshow, M. Shurafa, F.R. Appelbaum, Benefit of cyclosporine modulation of drug resistance in patients with poor-risk acute myeloid leukemia: a Southwest Oncology Group study, Blood, 98 (2001) 3212-3220.
[351] P.R. Twentyman, N.M. Bleehen, Resistance modification by PSC-833, a novel non-immunosuppressive cyclosporin [corrected], Eur J Cancer, 27 (1991) 1639-1642.
[352] A.M. Oza, Clinical development of P glycoprotein modulators in oncology, Novartis Found Symp, 243 (2002) 103-115; discussion 115-108, 180-105.
[353] M. Hubensack, C. Muller, P. Hocherl, S. Fellner, T. Spruss, G. Bernhardt, A. Buschauer, Effect of the ABCB1 modulators elacridar and tariquidar on the distribution of paclitaxel in nude mice, J Cancer Res Clin Oncol, 134 (2008) 597-607.
[354] I. Cascorbi, Role of pharmacogenetics of ATP-binding cassette transporters in the pharmacokinetics of drugs, Pharmacol Ther, 112 (2006) 457-473.
[355] X.R. Song, Y. Zheng, G. He, L. Yang, Y.F. Luo, Z.Y. He, S.Z. Li, J.M. Li, S. Yu, X. Luo, S.X. Hou, Y.Q. Wei, Development of PLGA nanoparticles simultaneously loaded with vincristine and verapamil for treatment of hepatocellular carcinoma, J Pharm Sci, 99 (2010) 4874-4879.
[356] X.R. Song, Z. Cai, Y. Zheng, G. He, F.Y. Cui, D.Q. Gong, S.X. Hou, S.J. Xiong, X.J. Lei, Y.Q. Wei, Reversion of multidrug resistance by co-encapsulation of vincristine and verapamil in PLGA nanoparticles, Eur J Pharm Sci, 37 (2009) 300-305.
[357] H.L. Wong, R. Bendayan, A.M. Rauth, X.Y. Wu, Simultaneous delivery of doxorubicin and GG918 (Elacridar) by new polymer-lipid hybrid nanoparticles (PLN) for enhanced treatment of multidrug-resistant breast cancer, J Control Release, 116 (2006) 275-284.
[358] H. Meng, W.X. Mai, H. Zhang, M. Xue, T. Xia, S. Lin, X. Wang, Y. Zhao, Z. Ji, J.I. Zink, A.E. Nel, Codelivery of an optimal drug/siRNA combination using mesoporous silica nanoparticles to overcome drug resistance in breast cancer in vitro and in vivo, ACS Nano, 7 (2013) 994-1005.
[359] S. Yadav, L.E. van Vlerken, S.R. Little, M.M. Amiji, Evaluations of combination MDR-1 gene silencing and paclitaxel administration in biodegradable polymeric nanoparticle formulations to overcome multidrug resistance in cancer cells, Cancer Chemother Pharmacol, 63 (2009) 711-722.
[360] Y.B. Patil, S.K. Swaminathan, T. Sadhukha, L. Ma, J. Panyam, The use of nanoparticle-mediated targeted gene silencing and drug delivery to overcome tumor drug resistance, Biomaterials, 31 (2010) 358-365.
[361] S.D. Li, L. Huang, Pharmacokinetics and biodistribution of nanoparticles, Mol Pharm, 5 (2008) 496-504.
[362] A.A. Van der Veldt, M. Lubberink, I. Bahce, M. Walraven, M.P. de Boer, H.N. Greuter, N.H. Hendrikse, J. Eriksson, A.D. Windhorst, P.E. Postmus, H.M. Verheul, E.H. Serne, A.A. Lammertsma, E.F. Smit, Rapid decrease in delivery of

chemotherapy to tumors after anti-VEGF therapy: implications for scheduling of anti-angiogenic drugs, Cancer Cell, 21 (2012) 82-91.
[363] P.V. Dickson, J.B. Hamner, T.L. Sims, C.H. Fraga, C.Y. Ng, S. Rajasekeran, N.L. Hagedorn, M.B. McCarville, C.F. Stewart, A.M. Davidoff, Bevacizumab-induced transient remodeling of the vasculature in neuroblastoma xenografts results in improved delivery and efficacy of systemically administered chemotherapy, Clin Cancer Res, 13 (2007) 3942-3950.
[364] L.M. Ellis, D.J. Hicklin, VEGF-targeted therapy: mechanisms of anti-tumour activity, Nat Rev Cancer, 8 (2008) 579-591.
[365] C.G. Willett, Y. Boucher, E. di Tomaso, D.G. Duda, L.L. Munn, R.T. Tong, D.C. Chung, D.V. Sahani, S.P. Kalva, S.V. Kozin, M. Mino, K.S. Cohen, D.T. Scadden, A.C. Hartford, A.J. Fischman, J.W. Clark, D.P. Ryan, A.X. Zhu, L.S. Blaszkowsky, H.X. Chen, P.C. Shellito, G.Y. Lauwers, R.K. Jain, Direct evidence that the VEGF-specific antibody bevacizumab has antivascular effects in human rectal cancer, Nat Med, 10 (2004) 145-147.
[366] H. Wildiers, G. Guetens, G. De Boeck, E. Verbeken, B. Landuyt, W. Landuyt, E.A. de Bruijn, A.T. van Oosterom, Effect of antivascular endothelial growth factor treatment on the intratumoral uptake of CPT-11, Br J Cancer, 88 (2003) 1979-1986.
[367] W.L. Monsky, D. Fukumura, T. Gohongi, M. Ancukiewcz, H.A. Weich, V.P. Torchilin, F. Yuan, R.K. Jain, Augmentation of transvascular transport of macromolecules and nanoparticles in tumors using vascular endothelial growth factor, Cancer Res, 59 (1999) 4129-4135.
[368] H. Maeda, The enhanced permeability and retention (EPR) effect in tumor vasculature: the key role of tumor-selective macromolecular drug targeting, Adv Enzyme Regul, 41 (2001) 189-207.
[369] F. Yuan, Y. Chen, M. Dellian, N. Safabakhsh, N. Ferrara, R.K. Jain, Time-dependent vascular regression and permeability changes in established human tumor xenografts induced by an anti-vascular endothelial growth factor/vascular permeability factor antibody, Proc Natl Acad Sci U S A, 93 (1996) 14765-14770.
[370] D.W. Miles, A. Chan, L.Y. Dirix, J. Cortes, X. Pivot, P. Tomczak, T. Delozier, J.H. Sohn, L. Provencher, F. Puglisi, N. Harbeck, G.G. Steger, A. Schneeweiss, A.M. Wardley, A. Chlistalla, G. Romieu, Phase III study of bevacizumab plus docetaxel compared with placebo plus docetaxel for the first-line treatment of human epidermal growth factor receptor 2-negative metastatic breast cancer, J Clin Oncol, 28 (2010) 3239-3247.
[371] G. McMahon, VEGF receptor signaling in tumor angiogenesis, Oncologist, 5 Suppl 1 (2000) 3-10.
[372] M. Shibuya, Structure and function of VEGF/VEGF-receptor system involved in angiogenesis, Cell Struct Funct, 26 (2001) 25-35.
[373] O. Casanovas, D.J. Hicklin, G. Bergers, D. Hanahan, Drug resistance by evasion of antiangiogenic targeting of VEGF signaling in late-stage pancreatic islet tumors, Cancer Cell, 8 (2005) 299-309.
[374] N. Ferrara, K.J. Hillan, H.P. Gerber, W. Novotny, Discovery and development of bevacizumab, an anti-VEGF antibody for treating cancer, Nat Rev Drug Discov, 3 (2004) 391-400.

[375] H.I. Hurwitz, L. Fehrenbacher, J.D. Hainsworth, W. Heim, J. Berlin, E. Holmgren, J. Hambleton, W.F. Novotny, F. Kabbinavar, Bevacizumab in combination with fluorouracil and leucovorin: an active regimen for first-line metastatic colorectal cancer, J Clin Oncol, 23 (2005) 3502-3508.
[376] A. Zakarija, G. Soff, Update on angiogenesis inhibitors, Curr Opin Oncol, 17 (2005) 578-583.
[377] A.R. Quesada, R. Munoz-Chapuli, M.A. Medina, Anti-angiogenic drugs: from bench to clinical trials, Med Res Rev, 26 (2006) 483-530.
[378] R.K. Jain, D.G. Duda, J.W. Clark, J.S. Loeffler, Lessons from phase III clinical trials on anti-VEGF therapy for cancer, Nat Clin Pract Oncol, 3 (2006) 24-40.
[379] J. Folkman, Tumor angiogenesis: therapeutic implications, N Engl J Med, 285 (1971) 1182-1186.
[380] M.A. Gimbrone, Jr., S.B. Leapman, R.S. Cotran, J. Folkman, Tumor dormancy in vivo by prevention of neovascularization, J Exp Med, 136 (1972) 261-276.
[381] N. Ferrara, R.S. Kerbel, Angiogenesis as a therapeutic target, Nature, 438 (2005) 967-974.
[382] R. Kerbel, J. Folkman, Clinical translation of angiogenesis inhibitors, Nat Rev Cancer, 2 (2002) 727-739.
[383] A.W. Le Serve, K. Hellmann, Metastases and the normalization of tumour blood vessels by ICRF 159: a new type of drug action, Br Med J, 1 (1972) 597-601.
[384] R.T. Tong, Y. Boucher, S.V. Kozin, F. Winkler, D.J. Hicklin, R.K. Jain, Vascular normalization by vascular endothelial growth factor receptor 2 blockade induces a pressure gradient across the vasculature and improves drug penetration in tumors, Cancer Res, 64 (2004) 3731-3736.
[385] R. Cairns, I. Papandreou, N. Denko, Overcoming physiologic barriers to cancer treatment by molecularly targeting the tumor microenvironment, Mol Cancer Res, 4 (2006) 61-70.
[386] R.I. Nicholson, J.M. Gee, M.E. Harper, EGFR and cancer prognosis, Eur J Cancer, 37 Suppl 4 (2001) S9-15.
[387] A. Maity, N. Pore, J. Lee, D. Solomon, D.M. O'Rourke, Epidermal growth factor receptor transcriptionally up-regulates vascular endothelial growth factor expression in human glioblastoma cells via a pathway involving phosphatidylinositol 3'-kinase and distinct from that induced by hypoxia, Cancer Res, 60 (2000) 5879-5886.
[388] C.K. Goldman, J. Kim, W.L. Wong, V. King, T. Brock, G.Y. Gillespie, Epidermal growth factor stimulates vascular endothelial growth factor production by human malignant glioma cells: a model of glioblastoma multiforme pathophysiology, Mol Biol Cell, 4 (1993) 121-133.
[389] G.J. Cerniglia, N. Pore, J.H. Tsai, S. Schultz, R. Mick, R. Choe, X. Xing, T. Durduran, A.G. Yodh, S.M. Evans, C.J. Koch, S.M. Hahn, H. Quon, C.M. Sehgal, W.M. Lee, A. Maity, Epidermal growth factor receptor inhibition modulates the microenvironment by vascular normalization to improve chemotherapy and radiotherapy efficacy, PLoS One, 4 (2009) e6539.

[390] M.J. Moore, D. Goldstein, J. Hamm, A. Figer, J.R. Hecht, S. Gallinger, H.J. Au, P. Murawa, D. Walde, R.A. Wolff, D. Campos, R. Lim, K. Ding, G. Clark, T. Voskoglou-Nomikos, M. Ptasynski, W. Parulekar, Erlotinib plus gemcitabine compared with gemcitabine alone in patients with advanced pancreatic cancer: a phase III trial of the National Cancer Institute of Canada Clinical Trials Group, J Clin Oncol, 25 (2007) 1960-1966.
[391] M. Krause, M. Baumann, Clinical biomarkers of kinase activity: examples from EGFR inhibition trials, Cancer Metastasis Rev, 27 (2008) 387-402.
[392] Z. Fan, J. Baselga, H. Masui, J. Mendelsohn, Antitumor effect of anti-epidermal growth factor receptor monoclonal antibodies plus cis-diamminedichloroplatinum on well established A431 cell xenografts, Cancer Res, 53 (1993) 4637-4642.
[393] F. Ciardiello, R. Bianco, V. Damiano, S. De Lorenzo, S. Pepe, S. De Placido, Z. Fan, J. Mendelsohn, A.R. Bianco, G. Tortora, Antitumor activity of sequential treatment with topotecan and anti-epidermal growth factor receptor monoclonal antibody C225, Clin Cancer Res, 5 (1999) 909-916.
[394] J. Baselga, L. Norton, H. Masui, A. Pandiella, K. Coplan, W.H. Miller, Jr., J. Mendelsohn, Antitumor effects of doxorubicin in combination with anti-epidermal growth factor receptor monoclonal antibodies, J Natl Cancer Inst, 85 (1993) 1327-1333.
[395] N. Qayum, J. Im, M.R. Stratford, E.J. Bernhard, W.G. McKenna, R.J. Muschel, Modulation of the tumor microvasculature by phosphoinositide-3 kinase inhibition increases doxorubicin delivery in vivo, Clin Cancer Res, 18 (2012) 161-169.
[396] M.B. Yin, Z.R. Li, K. Toth, S. Cao, F.A. Durrani, G. Hapke, A. Bhattacharya, R.G. Azrak, C. Frank, Y.M. Rustum, Potentiation of irinotecan sensitivity by Se-methylselenocysteine in an in vivo tumor model is associated with downregulation of cyclooxygenase-2, inducible nitric oxide synthase, and hypoxia-inducible factor 1alpha expression, resulting in reduced angiogenesis, Oncogene, 25 (2006) 2509-2519.
[397] M.G. Fakih, L. Pendyala, P.F. Smith, P.J. Creaven, M.E. Reid, V. Badmaev, R.G. Azrak, J.D. Prey, D. Lawrence, Y.M. Rustum, A phase I and pharmacokinetic study of fixed-dose selenomethionine and irinotecan in solid tumors, Clin Cancer Res, 12 (2006) 1237-1244.
[398] S. Cao, F.A. Durrani, Y.M. Rustum, Selective modulation of the therapeutic efficacy of anticancer drugs by selenium containing compounds against human tumor xenografts, Clin Cancer Res, 10 (2004) 2561-2569.
[399] A. Bhattacharya, M. Seshadri, S.D. Oven, K. Toth, M.M. Vaughan, Y.M. Rustum, Tumor vascular maturation and improved drug delivery induced by methylselenocysteine leads to therapeutic synergy with anticancer drugs, Clin Cancer Res, 14 (2008) 3926-3932.
[400] F.E. Escorcia, E. Henke, M.R. McDevitt, C.H. Villa, P. Smith-Jones, R.G. Blasberg, R. Benezra, D.A. Scheinberg, Selective killing of tumor neovasculature paradoxically improves chemotherapy delivery to tumors, Cancer Res, 70 (2010) 9277-9286.

[401] A.G. Sorensen, K.E. Emblem, P. Polaskova, D. Jennings, H. Kim, M. Ancukiewicz, M. Wang, P.Y. Wen, P. Ivy, T.T. Batchelor, R.K. Jain, Increased survival of glioblastoma patients who respond to antiangiogenic therapy with elevated blood perfusion, Cancer Res, 72 (2012) 402-407.
[402] F. Winkler, S.V. Kozin, R.T. Tong, S.S. Chae, M.F. Booth, I. Garkavtsev, L. Xu, D.J. Hicklin, D. Fukumura, E. di Tomaso, L.L. Munn, R.K. Jain, Kinetics of vascular normalization by VEGFR2 blockade governs brain tumor response to radiation: role of oxygenation, angiopoietin-1, and matrix metalloproteinases, Cancer Cell, 6 (2004) 553-563.
[403] C. Rolny, M. Mazzone, S. Tugues, D. Laoui, I. Johansson, C. Coulon, M.L. Squadrito, I. Segura, X. Li, E. Knevels, S. Costa, S. Vinckier, T. Dresselaer, P. Akerud, M. De Mol, H. Salomaki, M. Phillipson, S. Wyns, E. Larsson, I. Buysschaert, J. Botling, U. Himmelreich, J.A. Van Ginderachter, M. De Palma, M. Dewerchin, L. Claesson-Welsh, P. Carmeliet, HRG inhibits tumor growth and metastasis by inducing macrophage polarization and vessel normalization through downregulation of PlGF, Cancer Cell, 19 (2011) 31-44.
[404] Y. Huang, M. Snuderl, R.K. Jain, Polarization of tumor-associated macrophages: a novel strategy for vascular normalization and antitumor immunity, Cancer Cell, 19 (2011) 1-2.
[405] R.K. Jain, L.T. Baxter, Mechanisms of heterogeneous distribution of monoclonal antibodies and other macromolecules in tumors: significance of elevated interstitial pressure, Cancer Res, 48 (1988) 7022-7032.
[406] G. Vlahovic, A.M. Ponce, Z. Rabbani, F.K. Salahuddin, L. Zgonjanin, I. Spasojevic, Z. Vujaskovic, M.W. Dewhirst, Treatment with imatinib improves drug delivery and efficacy in NSCLC xenografts, Br J Cancer, 97 (2007) 735-740.
[407] T.D. Tailor, G. Hanna, P.S. Yarmolenko, M.R. Dreher, A.S. Betof, A.B. Nixon, I. Spasojevic, M.W. Dewhirst, Effect of pazopanib on tumor microenvironment and liposome delivery, Mol Cancer Ther, 9 (2010) 1798-1808.
[408] U. Prabhakar, H. Maeda, R.K. Jain, E.M. Sevick-Muraca, W. Zamboni, O.C. Farokhzad, S.T. Barry, A. Gabizon, P. Grodzinski, D.C. Blakey, Challenges and Key Considerations of the Enhanced Permeability and Retention Effect for Nanomedicine Drug Delivery in Oncology, Cancer Res, 73 2412-2417.
[409] D.J. Burgess, Microenvironment: A dense danger, Nat Rev Cancer, 12 (2012) 656-657.
[410] U. Maier, G. Baumgartner, Metaphylactic effect of mitomycin C with and without hyaluronidase after transurethral resection of bladder cancer: randomized trial, J Urol, 141 (1989) 529-530.
[411] K.J. Smith, H.G. Skelton, G. Turiansky, K.F. Wagner, Hyaluronidase enhances the therapeutic effect of vinblastine in intralesional treatment of Kaposi's sarcoma. Military Medical Consortium for the Advancement of Retroviral Research (MMCARR), J Am Acad Dermatol, 36 (1997) 239-242.
[412] J. Schumer, J. Klocker, J. Tidstrand, B. Rab, H. Allmayer, [Cisplatin, vindesine and hyaluronidase combined with simultaneous radiotherapy of advanced head and neck tumors], Onkologie, 13 (1990) 310-312.

[413] N. Kohno, T. Ohnuma, P. Truog, Effects of hyaluronidase on doxorubicin penetration into squamous carcinoma multicellular tumor spheroids and its cell lethality, J Cancer Res Clin Oncol, 120 (1994) 293-297.
[414] C. Farr, J. Menzel, J. Seeberger, B. Schweigle, [Clinical pharmacology and possible applications of hyaluronidase with reference to Hylase "Dessau"], Wien Med Wochenschr, 147 (1997) 347-355.
[415] C. Brekken, C. de Lange Davies, Hyaluronidase reduces the interstitial fluid pressure in solid tumours in a non-linear concentration-dependent manner, Cancer Lett, 131 (1998) 65-70.
[416] C. Brekken, M.H. Hjelstuen, O.S. Bruland, C. de Lange Davies, Hyaluronidase-induced periodic modulation of the interstitial fluid pressure increases selective antibody uptake in human osteosarcoma xenografts, Anticancer Res, 20 (2000) 3513-3519.
[417] L. Eikenes, M. Tari, I. Tufto, O.S. Bruland, C. de Lange Davies, Hyaluronidase induces a transcapillary pressure gradient and improves the distribution and uptake of liposomal doxorubicin (Caelyx) in human osteosarcoma xenografts, Br J Cancer, 93 (2005) 81-88.
[418] P.P. Provenzano, C. Cuevas, A.E. Chang, V.K. Goel, D.D. Von Hoff, S.R. Hingorani, Enzymatic targeting of the stroma ablates physical barriers to treatment of pancreatic ductal adenocarcinoma, Cancer Cell, 21 (2012) 418-429.
[419] L. Eikenes, O.S. Bruland, C. Brekken, L. Davies Cde, Collagenase increases the transcapillary pressure gradient and improves the uptake and distribution of monoclonal antibodies in human osteosarcoma xenografts, Cancer Res, 64 (2004) 4768-4773.
[420] T.D. McKee, P. Grandi, W. Mok, G. Alexandrakis, N. Insin, J.P. Zimmer, M.G. Bawendi, Y. Boucher, X.O. Breakefield, R.K. Jain, Degradation of fibrillar collagen in a human melanoma xenograft improves the efficacy of an oncolytic herpes simplex virus vector, Cancer Res, 66 (2006) 2509-2513.
[421] X. Zheng, B.A. Goins, I.L. Cameron, C. Santoyo, A. Bao, V.C. Frohlich, G.D. Fullerton, Ultrasound-guided intratumoral administration of collagenase-2 improved liposome drug accumulation in solid tumor xenografts, Cancer Chemother Pharmacol, 67 (2011) 173-182.
[422] I. Muckenschnabel, G. Bernhardt, T. Spruss, A. Buschauer, Pharmacokinetics and tissue distribution of bovine testicular hyaluronidase and vinblastine in mice: an attempt to optimize the mode of adjuvant hyaluronidase administration in cancer chemotherapy, Cancer Lett, 131 (1998) 71-84.
[423] C. Wong, T. Stylianopoulos, J. Cui, J. Martin, V.P. Chauhan, W. Jiang, Z. Popovic, R.K. Jain, M.G. Bawendi, D. Fukumura, Multistage nanoparticle delivery system for deep penetration into tumor tissue, Proc Natl Acad Sci U S A, 108 (2011) 2426-2431.
[424] H. Cabral, Y. Matsumoto, K. Mizuno, Q. Chen, M. Murakami, M. Kimura, Y. Terada, M.R. Kano, K. Miyazono, M. Uesaka, N. Nishiyama, K. Kataoka, Accumulation of sub-100 nm polymeric micelles in poorly permeable tumours depends on size, Nat Nanotechnol, 6 (2011) 815-823.

[425] T.T. Goodman, P.L. Olive, S.H. Pun, Increased nanoparticle penetration in collagenase-treated multicellular spheroids, Int J Nanomedicine, 2 (2007) 265-274.
[426] S.J. Kuhn, S.K. Finch, D.E. Hallahan, T.D. Giorgio, Proteolytic surface functionalization enhances in vitro magnetic nanoparticle mobility through extracellular matrix, Nano Lett, 6 (2006) 306-312.
[427] M. Magzoub, S. Jin, A.S. Verkman, Enhanced macromolecule diffusion deep in tumors after enzymatic digestion of extracellular matrix collagen and its associated proteoglycan decorin, FASEB J, 22 (2008) 276-284.
[428] P.A. Netti, D.A. Berk, M.A. Swartz, A.J. Grodzinsky, R.K. Jain, Role of extracellular matrix assembly in interstitial transport in solid tumors, Cancer Res, 60 (2000) 2497-2503.
[429] K.P. Olive, M.A. Jacobetz, C.J. Davidson, A. Gopinathan, D. McIntyre, D. Honess, B. Madhu, M.A. Goldgraben, M.E. Caldwell, D. Allard, K.K. Frese, G. Denicola, C. Feig, C. Combs, S.P. Winter, H. Ireland-Zecchini, S. Reichelt, W.J. Howat, A. Chang, M. Dhara, L. Wang, F. Ruckert, R. Grutzmann, C. Pilarsky, K. Izeradjene, S.R. Hingorani, P. Huang, S.E. Davies, W. Plunkett, M. Egorin, R.H. Hruban, N. Whitebread, K. McGovern, J. Adams, C. Iacobuzio-Donahue, J. Griffiths, D.A. Tuveson, Inhibition of Hedgehog signaling enhances delivery of chemotherapy in a mouse model of pancreatic cancer, Science, 324 (2009) 1457-1461.
[430] A. Jimeno, G.J. Weiss, W.H. Miller, Jr., S.N. Gettinger, B. Eigl, A.L. Chang, J. Dunbar, S. Devens, K. Faia, G. Skliris, J.L. Kutok, K.D. Lewis, R. Tibes, W.H. Sharfman, R.W. Ross, C.M. Rudin, Phase 1 Study of the Hedgehog Pathway Inhibitor IPI-926 in Adult Patients with Solid Tumors, Clin Cancer Res, (2013).
[431] B. Diop-Frimpong, V.P. Chauhan, S. Krane, Y. Boucher, R.K. Jain, Losartan inhibits collagen I synthesis and improves the distribution and efficacy of nanotherapeutics in tumors, Proc Natl Acad Sci U S A, 108 (2011) 2909-2914.
[432] T. Lammers, F. Kiessling, W.E. Hennink, G. Storm, Drug targeting to tumors: principles, pitfalls and (pre-) clinical progress, J Control Release, 161 175-187.
[433] H. Maeda, K. Greish, J. Fang, The EPR effect and polymeric drugs: a paradigm shift for cancer chemotherapy in the 21st century, in: Polymer Therapeutics II, Springer, 2006, pp. 103-121.
[434] M. Dowsett, A.K. Dunbier, Emerging biomarkers and new understanding of traditional markers in personalized therapy for breast cancer, Clin Cancer Res, 14 (2008) 8019-8026.
[435] R.S. Herbst, S.M. Lippman, Molecular signatures of lung cancer--toward personalized therapy, N Engl J Med, 356 (2007) 76-78.
[436] V.P. Chauhan, R.K. Jain, Strategies for advancing cancer nanomedicine, Nat Mater, 12 (2013) 958-962.
[437] T. Lammers, L.Y. Rizzo, G. Storm, F. Kiessling, Personalized nanomedicine, Clin Cancer Res, 18 4889-4894.
[438] F. Thorsen, B. Fite, L.M. Mahakian, J.W. Seo, S. Qin, V. Harrison, S. Johnson, E. Ingham, C. Caskey, T. Sundstrom, T.J. Meade, P.N. Harter, K.O. Skaftnesmo, K.W. Ferrara, Multimodal imaging enables early detection and

characterization of changes in tumor permeability of brain metastases, J Control Release, 172 (2013) 812-822.
[439] B.J. Vakoc, D. Fukumura, R.K. Jain, B.E. Bouma, Cancer imaging by optical coherence tomography: preclinical progress and clinical potential, Nat Rev Cancer, 12 (2012) 363-368.
[440] P.M. Valencia, E.M. Pridgen, M. Rhee, R. Langer, O.C. Farokhzad, R. Karnik, Microfluidic Platform for Combinatorial Synthesis and Optimization of Targeted Nanoparticles for Cancer Therapy, ACS Nano, (2013).
[441] J. Hrkach, D. Von Hoff, M. Mukkaram Ali, E. Andrianova, J. Auer, T. Campbell, D. De Witt, M. Figa, M. Figueiredo, A. Horhota, S. Low, K. McDonnell, E. Peeke, B. Retnarajan, A. Sabnis, E. Schnipper, J.J. Song, Y.H. Song, J. Summa, D. Tompsett, G. Troiano, T. Van Geen Hoven, J. Wright, P. LoRusso, P.W. Kantoff, N.H. Bander, C. Sweeney, O.C. Farokhzad, R. Langer, S. Zale, Preclinical development and clinical translation of a PSMA-targeted docetaxel nanoparticle with a differentiated pharmacological profile, Sci Transl Med, 4 (2012) 128ra139.
[442] L. Zhang, F.X. Gu, J.M. Chan, A.Z. Wang, R.S. Langer, O.C. Farokhzad, Nanoparticles in medicine: therapeutic applications and developments, Clin Pharmacol Ther, 83 (2008) 761-769.
[443] S. Ait-Oudhia, R.M. Straubinger, D.E. Mager, Meta-analysis of nanoparticulate paclitaxel delivery system pharmacokinetics and model prediction of associated neutropenia, Pharm Res, 29 (2012) 2833-2844.
[444] T. Hara, S. Iriyama, K. Makino, H. Terada, M. Ohya, Mathematical description of drug movement into tumor with EPR effect and estimation of its configuration for DDS, Colloids Surf B Biointerfaces, 75 (2010) 42-46.
[445] S. Stapleton, M. Milosevic, C. Allen, J. Zheng, M. Dunne, I. Yeung, D.A. Jaffray, A mathematical model of the enhanced permeability and retention effect for liposome transport in solid tumors, PLoS One, 8 (2013) e81157.
[446] M.M. Schmidt, K.D. Wittrup, A modeling analysis of the effects of molecular size and binding affinity on tumor targeting, Mol Cancer Ther, 8 (2009) 2861-2871.
[447] D. Liu, A. Mori, L. Huang, Role of liposome size and RES blockade in controlling biodistribution and tumor uptake of GM1-containing liposomes, Biochim Biophys Acta, 1104 (1992) 95-101.
[448] M.J. Ernsting, M. Murakami, A. Roy, S.D. Li, Factors controlling the pharmacokinetics, biodistribution and intratumoral penetration of nanoparticles, J Control Release, 172 (2013) 782-794.
[449] Y. Liu, Y. Hu, L. Huang, Influence of polyethylene glycol density and surface lipid on pharmacokinetics and biodistribution of lipid-calcium-phosphate nanoparticles, Biomaterials.
[450] C.A. Hunt, R. MacGregor, R. Siegel, Engineering Targeted In Vivo Drug Delivery. I. The Physiological and Physicochemical Principles Governing Opportunities and Limitations, Pharmaceutical Research, 3 (1986) 333-344.
[451] K.S. Pang, M. Rowland, Hepatic clearance of drugs. I. Theoretical considerations of a "well-stirred" model and a "parallel tube" model. Influence of hepatic blood flow, plasma and blood cell binding, and the hepatocellular

enzymatic activity on hepatic drug clearance, J Pharmacokinet Biopharm, 5 (1977) 625-653.
[452] P. Dechadilok, W.M. Deen, Hindrance Factors for Diffusion and Convection in Pores, Industrial & Engineering Chemistry Research, 45 (2006) 6953-6959.
[453] H.S. Choi, W. Liu, P. Misra, E. Tanaka, J.P. Zimmer, B. Itty Ipe, M.G. Bawendi, J.V. Frangioni, Renal clearance of quantum dots, Nat Biotechnol, 25 (2007) 1165-1170.
[454] S.K. Hobbs, W.L. Monsky, F. Yuan, W.G. Roberts, L. Griffith, V.P. Torchilin, R.K. Jain, Regulation of transport pathways in tumor vessels: role of tumor type and microenvironment, Proc Natl Acad Sci U S A, 95 (1998) 4607-4612.
[455] F. Braet, E. Wisse, Structural and functional aspects of liver sinusoidal endothelial cell fenestrae: a review, Comp Hepatol, 1 (2002) 1.
[456] P. Chytil, S. Hoffmann, L. Schindler, L. Kostka, K. Ulbrich, H. Caysa, T. Mueller, K. Mader, T. Etrych, Dual fluorescent HPMA copolymers for passive tumor targeting with pH-sensitive drug release II: Impact of release rate on biodistribution, J Control Release, 172 (2013) 504-512.
[457] R.H. Muller, K. Mader, S. Gohla, Solid lipid nanoparticles (SLN) for controlled drug delivery - a review of the state of the art, Eur J Pharm Biopharm, 50 (2000) 161-177.
[458] G.M. Thurber, K. Dane Wittrup, A mechanistic compartmental model for total antibody uptake in tumors, J Theor Biol, 314 (2012) 57-68.
[459] J. Sharma, H. Lv, J.M. Gallo, Intratumoral modeling of gefitinib pharmacokinetics and pharmacodynamics in an orthotopic mouse model of glioblastoma, Cancer Res, 73 (2013) 5242-5252.
[460] A.R. Kirtane, S.M. Kalscheuer, J. Panyam, Exploiting nanotechnology to overcome tumor drug resistance: Challenges and opportunities, Adv Drug Deliv Rev, 65 (2013) 1731-1747.
[461] H. Sarin, Physiologic upper limits of pore size of different blood capillary types and another perspective on the dual pore theory of microvascular permeability, J Angiogenes Res, 2 (2010) 14.
[462] G.D. Lowe, A.J. Lee, A. Rumley, J.F. Price, F.G. Fowkes, Blood viscosity and risk of cardiovascular events: the Edinburgh Artery Study, Br J Haematol, 96 (1997) 168-173.
[463] R.K. Jain, Determinants of tumor blood flow: a review, Cancer Res, 48 (1988) 2641-2658.
[464] N.K. Devaraj, E.J. Keliher, G.M. Thurber, M. Nahrendorf, R. Weissleder, 18F labeled nanoparticles for in vivo PET-CT imaging, Bioconjug Chem, 20 (2009) 397-401.
[465] S.M. Moghimi, A.C. Hunter, J.C. Murray, Long-circulating and target-specific nanoparticles: theory to practice, Pharmacol Rev, 53 (2001) 283-318.
[466] V.P. Torchilin, Polymer-coated long-circulating microparticulate pharmaceuticals, J Microencapsul, 15 (1998) 1-19.
[467] A. Albanese, P.S. Tang, W.C. Chan, The effect of nanoparticle size, shape, and surface chemistry on biological systems, Annu Rev Biomed Eng, 14 1-16.
[468] E.A. Simone, T.D. Dziubla, V.R. Muzykantov, Polymeric carriers: role of geometry in drug delivery, Expert Opin Drug Deliv, 5 (2008) 1283-1300.

[469] D. Fukumura, R.K. Jain, Tumor microvasculature and microenvironment: targets for anti-angiogenesis and normalization, Microvasc Res, 74 (2007) 72-84.
[470] T.P. Padera, B.R. Stoll, J.B. Tooredman, D. Capen, E. di Tomaso, R.K. Jain, Pathology: cancer cells compress intratumour vessels, Nature, 427 (2004) 695.
[471] H.F. Dvorak, D.R. Senger, A.M. Dvorak, Fibrin as a component of the tumor stroma: origins and biological significance, Cancer Metastasis Rev, 2 (1983) 41-73.
[472] L. Eikenes, I. Tufto, E.A. Schnell, A. Bjorkoy, C. De Lange Davies, Effect of collagenase and hyaluronidase on free and anomalous diffusion in multicellular spheroids and xenografts, Anticancer Res, 30 359-368.
[473] G. Griffon-Etienne, Y. Boucher, C. Brekken, H.D. Suit, R.K. Jain, Taxane-induced apoptosis decompresses blood vessels and lowers interstitial fluid pressure in solid tumors: clinical implications, Cancer Res, 59 (1999) 3776-3782.
[474] L. Lin, C. Wu, K. Hu, Tissue plasminogen activator activates NF-kappaB through a pathway involving annexin A2/CD11b and integrin-linked kinase, J Am Soc Nephrol, 23 1329-1338.
[475] B.A. Teicher, Hypoxia and drug resistance, Cancer Metastasis Rev, 13 (1994) 139-168.
[476] V. Costantini, L.R. Zacharski, The role of fibrin in tumor metastasis, Cancer Metastasis Rev, 11 (1992) 283-290.
[477] J.S. Palumbo, J.M. Potter, L.S. Kaplan, K. Talmage, D.G. Jackson, J.L. Degen, Spontaneous hematogenous and lymphatic metastasis, but not primary tumor growth or angiogenesis, is diminished in fibrinogen-deficient mice, Cancer Res, 62 (2002) 6966-6972.
[478] J.S. Palumbo, K.E. Talmage, J.V. Massari, C.M. La Jeunesse, M.J. Flick, K.W. Kombrinck, M. Jirouskova, J.L. Degen, Platelets and fibrin(ogen) increase metastatic potential by impeding natural killer cell-mediated elimination of tumor cells, Blood, 105 (2005) 178-185.
[479] J.S. Palumbo, K.W. Kombrinck, A.F. Drew, T.S. Grimes, J.H. Kiser, J.L. Degen, T.H. Bugge, Fibrinogen is an important determinant of the metastatic potential of circulating tumor cells, Blood, 96 (2000) 3302-3309.
[480] Y. Lu da, X.L. Chen, J. Ding, Treatment of solid tumors and metastases by fibrinogen-targeted anticancer drug therapy, Med Hypotheses, 68 (2007) 188-193.
[481] L.W. Starmans, T. van Mourik, R. Rossin, I. Verel, K. Nicolay, H. Grull, Noninvasive visualization of tumoral fibrin deposition using a peptidic fibrin-binding single photon emission computed tomography tracer, Mol Pharm, 12 1921-1928.
[482] Y.T. Tsai, J. Zhou, H. Weng, E.N. Tang, D.W. Baker, L. Tang, Optical imaging of fibrin deposition to elucidate participation of mast cells in foreign body responses, Biomaterials, 35 2089-2096.
[483] F.A. Calvo, O.F. Hidalgo, F. Gonzalez, J. Rebollo, S. Martin Algarra, D. Ortiz de Urbina, A. Brugarolas, Urokinase combination chemotherapy in small cell lung cancer. A phase II study, Cancer, 70 (1992) 2624-2630.
[484] E.G. Elias, A. Brugarolas, The role of heparin in the chemotherapy of solid tumors: preliminary clinical trial in carcinoma of the lung, Cancer Chemother Rep, 56 (1972) 783-785.

[485] E.G. Elias, S.K. Shukla, I.B. Mink, Heparin and chemotherapy in the management of inoperable lung carcinoma, Cancer, 36 (1975) 129-136.
[486] L.R. Zacharski, W.G. Henderson, F.R. Rickles, W.B. Forman, C.J. Cornell, Jr., R.J. Forcier, R. Edwards, E. Headley, S.H. Kim, J.R. O'Donnell, R. O'Dell, K. Tornyos, H.C. Kwaan, Effect of warfarin on survival in small cell carcinoma of the lung. Veterans Administration Study No. 75, JAMA, 245 (1981) 831-835.
[487] M. Altinbas, H.S. Coskun, O. Er, M. Ozkan, B. Eser, A. Unal, M. Cetin, S. Soyuer, A randomized clinical trial of combination chemotherapy with and without low-molecular-weight heparin in small cell lung cancer, J Thromb Haemost, 2 (2004) 1266-1271.
[488] G. Agnelli, D.J. George, A.K. Kakkar, W. Fisher, M.R. Lassen, P. Mismetti, P. Mouret, U. Chaudhari, F. Lawson, A.G. Turpie, Semuloparin for thromboprophylaxis in patients receiving chemotherapy for cancer, N Engl J Med, 366 601-609.
[489] A. Pluen, Y. Boucher, S. Ramanujan, T.D. McKee, T. Gohongi, E. di Tomaso, E.B. Brown, Y. Izumi, R.B. Campbell, D.A. Berk, R.K. Jain, Role of tumor-host interactions in interstitial diffusion of macromolecules: cranial vs. subcutaneous tumors, Proc Natl Acad Sci U S A, 98 (2001) 4628-4633.
[490] F. Kallinowski, K.H. Schlenger, S. Runkel, M. Kloes, M. Stohrer, P. Okunieff, P. Vaupel, Blood flow, metabolism, cellular microenvironment, and growth rate of human tumor xenografts, Cancer Res, 49 (1989) 3759-3764.
[491] R.K. Jain, Normalizing tumor vasculature with anti-angiogenic therapy: a new paradigm for combination therapy, Nat Med, 7 (2001) 987-989.
[492] M.I. Lin, W.C. Sessa, Antiangiogenic therapy: creating a unique "window" of opportunity, Cancer Cell, 6 (2004) 529-531.
[493] T. Stylianopoulos, R.K. Jain, Combining two strategies to improve perfusion and drug delivery in solid tumors, Proc Natl Acad Sci U S A, 110 (2013) 18632-18637.
[494] J. Kuiper, M. Otter, D.C. Rijken, T.J. van Berkel, Characterization of the interaction in vivo of tissue-type plasminogen activator with liver cells, J Biol Chem, 263 (1988) 18220-18224.
[495] L.R. Wing, B. Bennett, N.A. Booth, The receptor for tissue plasminogen activator (t-PA) in complex with its inhibitor, PAI-1, on human hepatocytes, FEBS Lett, 278 (1991) 95-97.
[496] B. Smedsrod, M. Einarsson, H. Pertoft, Tissue plasminogen activator is endocytosed by mannose and galactose receptors of rat liver cells, Thromb Haemost, 59 (1988) 480-484.
[497] B. Smedsrod, M. Einarsson, Clearance of tissue plasminogen activator by mannose and galactose receptors in the liver, Thromb Haemost, 63 (1990) 60-66.
[498] S. Niraula, E. Amir, F. Vera-Badillo, B. Seruga, A. Ocana, I.F. Tannock, Risk of incremental toxicities and associated costs of new anticancer drugs: a meta-analysis, J Clin Oncol, 32 (2014) 3634-3642.
[499] K.I. Kaitin, Deconstructing the drug development process: the new face of innovation, Clin Pharmacol Ther, 87 (2010) 356-361.
[500] J.H. Grossman, McNeil, S.E., Preclinical Efficacy and Toxicity of Engineered Nanomaterials, Karger, Basel, 2011.

[501] A.Z. Wang, Nanoparticle drug delivery: focusing on the therapeutic cargo, Nanomedicine (Lond), 7 (2012) 1463-1465.
[502] P. Kirkpatrick, Pressures in the pipeline, Nat Rev Drug Discov, 2 (2003) 337-337.
[503] E. Kwong, Advancing Drug Discovery: A Pharmaceutics Perspective, J Pharm Sci, (2014).
[504] S. Karve, M.E. Werner, R. Sukumar, N.D. Cummings, J.A. Copp, E.C. Wang, C. Li, M. Sethi, R.C. Chen, M.E. Pacold, A.Z. Wang, Revival of the abandoned therapeutic wortmannin by nanoparticle drug delivery, Proc Natl Acad Sci U S A, 109 (2012) 8230-8235.
[505] G.A.C. M. Suffnes, The Alkaloids, Academic Press, Orlando, FL, 1985.
[506] E. Gellert, R. Rudzats, The Antileukemia Activity of Tylocrebrine, J Med Chem, 7 (1964) 361-362.
[507] A.K. Iyer, G. Khaled, J. Fang, H. Maeda, Exploiting the enhanced permeability and retention effect for tumor targeting, Drug Discov Today, 11 (2006) 812-818.
[508] H. Maeda, H. Nakamura, J. Fang, The EPR effect for macromolecular drug delivery to solid tumors: Improvement of tumor uptake, lowering of systemic toxicity, and distinct tumor imaging in vivo, Adv Drug Deliv Rev, 65 (2013) 71-79.
[509] M.J. Niphakis, G.I. Georg, Synthesis of tylocrebrine and related phenanthroindolizidines by VOF3-mediated oxidative aryl-alkene coupling, Org Lett, 13 (2011) 196-199.
[510] H. Qian, A.R. Wohl, J.T. Crow, C.W. Macosko, T.R. Hoye, A Strategy for Control of "Random" Copolymerization of Lactide and Glycolide: Application to Synthesis of PEG-b-PLGA Block Polymers Having Narrow Dispersity, Macromolecules, 44 7132-7140.
[511] M.G. Vander Heiden, L.C. Cantley, C.B. Thompson, Understanding the Warburg effect: the metabolic requirements of cell proliferation, Science, 324 (2009) 1029-1033.
[512] I.F. Tannock, D. Rotin, Acid pH in tumors and its potential for therapeutic exploitation, Cancer Res, 49 (1989) 4373-4384.
[513] N. Raghunand, B.P. Mahoney, R.J. Gillies, Tumor acidity, ion trapping and chemotherapeutics. II. pH-dependent partition coefficients predict importance of ion trapping on pharmacokinetics of weakly basic chemotherapeutic agents, Biochem Pharmacol, 66 (2003) 1219-1229.
[514] S.R. Chemler, Phenanthroindolizidines and Phenanthroquinolizidines: Promising Alkaloids for Anti-Cancer Therapy, Curr Bioact Compd, 5 (2009) 2-19.
[515] N. Ignjatovic, S. Tomic, M. Dakic, M. Miljkovic, M. Plavsic, D. Uskokovic, Synthesis and properties of hydroxyapatite/poly-L-lactide composite biomaterials, Biomaterials, 20 (1999) 809-816.
[516] E. Gellert, T.R. Govindachari, M.V. Lakshmikantham, I.S. Ragade, R. Rudzats, N. Viswanathan, 189. The alkaloids of Tylophora crebriflora: structure and synthesis of tylocrebrine, a new phenanthroindolizidine alkaloid, Journal of the Chemical Society (Resumed), (1962) 1008-1014.
[517] J.-C. Lin, S.-C. Yang, T.-M. Hong, S.-L. Yu, Q. Shi, L. Wei, H.-Y. Chen, P.-C. Yang, K.-H. Lee, Phenanthrene-Based Tylophorine-1 (PBT-1) Inhibits Lung

Cancer Cell Growth through the Akt and NF-ÎºB Pathways, Journal of Medicinal Chemistry, 52 (2009) 1903-1911.
[518] S.D. Gopalakrishnan C., Kameswaran L., Natarajan S., Pharmacological investigations of tylophorine, the major alkaloid of Tylophora indica., Indian J Med Res, 69 (1979) 513-520.
[519] S.A. Hitchcock, L.D. Pennington, Structure-brain exposure relationships, J Med Chem, 49 (2006) 7559-7583.
[520] S. Zhang, L. Wei, K. Bastow, W. Zheng, A. Brossi, K.H. Lee, A. Tropsha, Antitumor agents 252. Application of validated QSAR models to database mining: discovery of novel tylophorine derivatives as potential anticancer agents, J Comput Aided Mol Des, 21 (2007) 97-112.
[521] X. Yang, Q. Shi, Y.N. Liu, G. Zhao, K.F. Bastow, J.C. Lin, S.C. Yang, P.C. Yang, K.H. Lee, Antitumor agents 268. Design, synthesis, and mechanistic studies of new 9-substituted phenanthrene-based tylophorine analogues as potent cytotoxic agents, J Med Chem, 52 (2009) 5262-5268.
[522] L. Wei, A. Brossi, R. Kendall, K.F. Bastow, S.L. Morris-Natschke, Q. Shi, K.H. Lee, Antitumor agents 251: synthesis, cytotoxic evaluation, and structure-activity relationship studies of phenanthrene-based tylophorine derivatives (PBTs) as a new class of antitumor agents, Bioorg Med Chem, 14 (2006) 6560-6569.
[523] L. Wei, Q. Shi, K.F. Bastow, A. Brossi, S.L. Morris-Natschke, K. Nakagawa-Goto, T.S. Wu, S.L. Pan, C.M. Teng, K.H. Lee, Antitumor agents 253. Design, synthesis, and antitumor evaluation of novel 9-substituted phenanthrene-based tylophorine derivatives as potential anticancer agents, J Med Chem, 50 (2007) 3674-3680.
[524] M.T. Huang, A.P. Grollman, Mode of action of tylocrebrine: effects on protein and nucleic acid synthesis, Mol Pharmacol, 8 (1972) 538-550.
[525] K.F. Pirollo, E.H. Chang, Does a targeting ligand influence nanoparticle tumor localization or uptake?, Trends Biotechnol, 26 (2008) 552-558.
[526] D.W. Bartlett, H. Su, I.J. Hildebrandt, W.A. Weber, M.E. Davis, Impact of tumor-specific targeting on the biodistribution and efficacy of siRNA nanoparticles measured by multimodality in vivo imaging, Proc Natl Acad Sci U S A, 104 (2007) 15549-15554.
[527] A.R. Kirtane, R.A. Siegel, J. Panyam, A pharmacokinetic model for quantifying the effect of vascular permeability on the choice of drug carrier: a framework for personalized nanomedicine, J Pharm Sci, 104 1174-1186.
[528] M. Hofmann, M. Guschel, A. Bernd, J. Bereiter-Hahn, R. Kaufmann, C. Tandi, H. Wiig, S. Kippenberger, Lowering of tumor interstitial fluid pressure reduces tumor cell proliferation in a xenograft tumor model, Neoplasia, 8 (2006) 89-95.
[529] S. Torosean, B. Flynn, J. Axelsson, J. Gunn, K.S. Samkoe, T. Hasan, M.M. Doyley, B.W. Pogue, Nanoparticle uptake in tumors is mediated by the interplay of vascular and collagen density with interstitial pressure, Nanomedicine, 9 (2013) 151-158.
[530] M. Yokoyama, S. Fukushima, R. Uehara, K. Okamoto, K. Kataoka, Y. Sakurai, T. Okano, Characterization of physical entrapment and chemical

conjugation of adriamycin in polymeric micelles and their design for in vivo delivery to a solid tumor, J Control Release, 50 (1998) 79-92.
[531] Y. Shi, M.J. van Steenbergen, E.A. Teunissen, L. Novo, S. Gradmann, M. Baldus, C.F. van Nostrum, W.E. Hennink, Pi-pi stacking increases the stability and loading capacity of thermosensitive polymeric micelles for chemotherapeutic drugs, Biomacromolecules, 14 1826-1837.